be obtained simply by reading the extensive figure captions. Secondly, the main text describes the principles in more detail, but without deriving the equations in detail. Thirdly, the appendices contain detailed derivations and some necessary mathematical background. It is stressed that only those readers who are specialising in the subject would usually need to study the appendices in detail.

Within the main text, an essentially self-contained guide to the subject is presented. That is, the reader is introduced to the mechanisms of crystal nucleation and growth occurring at the atomic scale (chapter 2) before being shown how the form of an initially planar solid/liquid interface evolves (chapter 3). Subsequently, the most important single-phase (chapter 4) and multi-phase (chapter 5) solid/liquid interface morphologies are presented. Finally, the effect which solidification has upon the redistribution of solute is discussed (chapter 6). One subject which is not covered in detail is convection in the melt. To introduce this complex field properly would require another book! However, the overall effect of the interaction of convection and solidification is described where necessary.

Each chapter includes a bibliography of key references for further study, and exercises which are designed to test the reader's understanding of the contents of the preceding chapter. For certain exercises, it is advisable firstly to work through the corresponding appendices.

The authors hope that, after reading this book, the newcomer will feel confident when delving further into solidification-related subjects, and that the experienced foundryman will also find some thought-provoking points.

W. Kurz, D.J. Fisher

Lausanne,
April 1984

Fundamentals of Solidification
W. Kurz, D.J. Fisher
Trans Tech Publications
1984

ACKNOWLEDGEMENTS

The authors wish to thank Dr. T.W. Clyne, Dr. H. Jones, Dr. J. Lipton, Prof. J. Perepezko, Mr. D. Previero, Dr. M. Rappaz, Prof. P.R. Sahm, Dr. T. Sato, and Dr. M. Wolf, for their helpful discussions and critical comments concerning the manuscript.

The invaluable aid of Mrs. E. Schlosser in preparing the diagrams and arranging the text is also gratefully acknowledged.

CONTENTS

SYMBOLS

Symbol	Meaning	Definition	Units
A	surface or cross-sectional area	-	m^2
	gradient term	$kVG_c/(Vp - Db)$	%/m
A*	parameter in stability analysis	equation A6.13	-
A'	surface area of casting	-	m^2
B	constant	-	-
C	concentration	-	at%, wt%
C_e	eutectic composition	-	at%, wt%
C'	length of eutectic tie-line	-	at%, wt%
C_o	initial alloy concentration	-	at%, wt%
D	diffusion coefficient in liquid	$-J/G_c$	m^2/s
D_o	pre-exponential term (diffusion)	-	m^2/s
D_s	diffusion coefficient in solid	-	m^2/s
E	energy	-	J
	internal energy	-	J/mol
E_1	exponential integral function	equation A7.16	-
F	stability parameter	$(\dot{\epsilon}/\epsilon)(mG_c/V)$	K/m^2
G	Gibbs free energy	-	J/mol
	interface temperature gradient	dT/dz	K/m
G_c	interface concentration gradient	dC/dz	at%/m, wt%/m
H	enthalpy	-	J/mol
I	nucleation rate	equation 2.11	$/m^3s$
J	mass flux	-	%m/s
K	curvature	$1/r_1+1/r_2$	/m
	constant	-	-
L	length	-	m
M	atomic (molecular) weight	-	g/mol
N	number	-	-
N_A	Avogadro's number	6.022×10^{23}	/mol
P	pressure	-	Pa
P'	series term for eutectic growth	equation A9.30	-
P_c	solute Péclet number	VR/2D	-
P_t	thermal Péclet number	VR/2a	-
Q	activation energy for diffusion	-	J/mol
	quantity of heat	-	J
R	gas constant	8.31	J/mol K
	radius	-	m
S	entropy	-	J/mol K
	perturbation term	$\epsilon\sin(\omega y)$	m
$\mathcal{S}$	stability parameter	equation A6.12	-
T	temperature	-	K
$\dot{T}$	cooling rate	dT/dt	K/s
T_f	melting point of pure substance	-	K
T_l	liquidus temperature	-	K

SYMBOLS (continued)

Symbol	Meaning	Definition	Units
T_q	measurable temperature	-	K
T_s	solidus temperature	-	K
T_s'	non-equilibrium solidus	-	K
V	rate of interface movement	-	m/s
V'	rate of crucible movement	-	m/s
X	mole fraction	-	-
Y	partial solution to equation	equation A2.13	-
Z	partial solution to equation	equation A2.10	-
a	thermal diffusivity	κ/c	m^2/s
	separation constant	equation A2.9	m
	half-axis of ellipsoid	-	m
b	half-axis of ellipsoid	-	m
	$(V/2D) + [(V/2D)^2 + \omega^2]^{0.5}$	equation A2.38	/m
c	volumetric specific heat	-	J/m^3K
d	exponent	-	-
	distance	-	m
e	exponent	-	-
f	force	-	N
f[hkl]	crystallographic factor	equation A5.7	-
f_ℓ	liquid fraction	$v_\ell/(v_\ell + v_s)$	-
f_s	solid fraction	$1 - f_\ell$	-
f	volume fraction of α-phase	-	-
h	Planck's constant	6.63×10^{-34}	Js
	heat transfer coefficient	$q/\Delta T_g$	W/m^2K
k	distribution coefficient	C_s/C_ℓ	-
k_B	Boltzmann's constant	1.38×10^{-23}	J/K
m	liquidus slope	dT_ℓ/dC	K/at%, K/wt%
	mass	-	g
	normal to isoconcentrates	-	-
n	number	-	-
	exponent	-	-
	interface normal	-	-
n_s	adsorption site density	equation A4.9	-
o	exponent	-	-
p	probability	-	-
	complementary distribution coeff.	1 - k	-
q	heat flux	-	W/m^2
q'	strength of heat source	-	W/m^3
r	radius	-	m
r^0	critical nucleation radius	-	m
s	position of s/l interface	-	m

SYMBOLS (continued)

Symbol	Meaning	Definition	Units
s_c	solute capillarity length	$\Gamma/mC^*(k - 1)$	m
s_t	thermal capillarity length	$-\Gamma c/\Delta h_f$	m
t	time	-	s
t_f	local solidification time	-	s
u	back-diffusion parameter	$(1 - 2\alpha' k)$	-
v	volume	-	m^3
v'	atomic volume	-	m^3
v_m	molar volume	-	m^3/mol
w	work	-	J
x	coordinate in s/l interface	-	m
y	coordinate in s/l interface	-	m
z	coordinate perpendicular to a planar solid/liquid interface	-	m
z'	system coordinate	-	m
α	dimensionless entropy of fusion	$\Delta S_f/R$	-
	dimensionless coefficient for back-diffusion	$D_s t_f/L^2$	-
α'	dimensionless coefficient for interdendritic back-diffusion	equation 6.10	-
Γ	Gibbs-Thomson coefficient	$\sigma/\Delta s_f$	Km
δ_c	solute boundary layer thickness	2D/V	m
δ_s	solute boundary layer thickness in solid	$2D_s/V$	m
δ_t	thermal boundary layer thickness	2a/V	m
ΔC_o	concentration difference between liquidus and solidus at solidus temperature of alloy	$C_o(1 - k)/k$	at%, wt%
ΔG	total Gibbs free energy	-	J/mol
ΔG_d	activation free energy for diffusion across solid/liquid interface	-	J/mol
ΔG°	standard free energy	-	J/mol
ΔG°	activation energy for the nucleation of the critical cluster radius	-	J
ΔG_n°	activation energy for the nucleation of a critical number of clustered atoms	-	J
ΔG_i	interface free energy	-	J/mol
ΔG_v	Gibbs free energy per mole	-	J/mol
Δg	Gibbs free energy per unit volume	$\Delta G_v/v_m$	J/m^3
ΔH°	standard enthalpy	-	J/mol
ΔH_f	latent heat of fusion per mole	-	J/mol
Δh_f	latent heat of fusion per volume	$\Delta H_f/v_m$	J/m^3

SYMBOLS (continued)

Symbol	Meaning	Definition	Units
ΔH_v	latent heat of vaporisation	-	J/mol
ΔS^*	standard entropy	-	J/mol K
ΔS_f	entropy of fusion per mole	$\Delta H_f/T_f$	J/mol K
Δs_f	entropy of fusion per volume	$\Delta h_f/T_f$	J/m³K
ΔT	undercooling	$T_f - T$	K
$\Delta T'$	dendrite tip-to-root temperature difference	-	K
ΔT_g	temperature drop across gap	equation A1.25	K
ΔT_o	liquidus-solidus range at C_0	$T_l - T_s$	K
ΔT_r	undercooling due to curvature	equation A 3.20	K
ΔT_c	temperature difference due to solute diffusion	-	K
ΔT_t	temperature difference due to heat flow	-	K
γ	surface tension	-	N/m
ϵ	amplitude of perturbation	-	m
$\dot{\epsilon}$	growth rate of amplitude	$d\epsilon/dt$	m/s
η	dynamic viscosity	-	Pas
	shape factor	equation A4.2	-
θ	angle	-	°
κ	thermal conductivity	-	W/Km
λ	wavelength	-	m
	spacing	-	m
μ	chemical potential	-	J/mol
ν	adsorption frequency	equation A4.8	/s
ν_o	atomic frequency	-	/s
υ	kinematic viscosity	-	m²/s
ρ	density	-	kg/m³
σ	solid/liquid interface energy	-	J/m²
Σ	correction term for back-diffusion	equation A11.17	-
τ	reduced temperature	$RT/\Delta H_V$	-
	relaxation time	equation A11.33	s
ϕ	temperature gradient difference	$mG_c - G$	K/m
Φ	reduced coordinate	equation A1.11	-
Ω	dimensionless solutal supersaturation	equation A7.1	-
Ω_t	dimensionless thermal supersaturation	equation A7.5	-
ω	wave number	$2\pi/\lambda$	/m

SYMBOLS (continued)

Superscripts:

- m - maximum value
- ° - critical activation value
- * - interface or tip value
- · - value for pure substance

Subscripts:

- c - solutal
- *l* - liquid or liquidus
- m - minimum value
- s - solid or solidus
- t - thermal

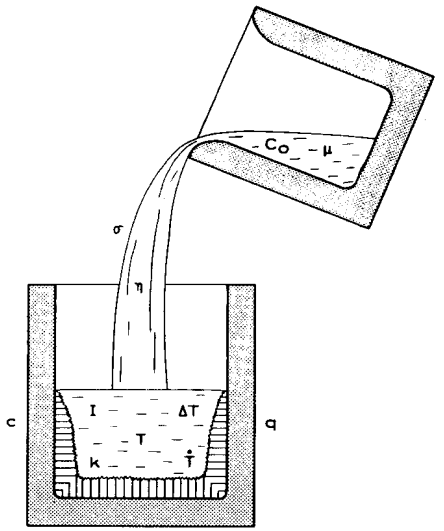

CHAPTER ONE

INTRODUCTION

1.1 The Importance of Solidification

Solidification is a phase transformation which is familiar to everyone, even if the only acquaintance with it involves the making of ice cubes. It is relatively little appreciated that the manufacture of almost every man-made object involves solidification at some stage.

The scope of this book is restricted mainly to a presentation of the theory of solidification as it applies to the most widely-used group of materials, i.e. metallic alloys. Here, solidification is generally accompanied by the formation of crystals; an event which is much rarer during the solidification of glasses or polymers.

Solidificatic. . of such importance simply because one of its major practical applications, namely casting, is a very economic method of forming a component if the melting point of the metal is not too high. Nowadays, cast metal products can be economically produced from alloys having melting points as high as 1660°C (Ti).

In the case of metals, melting is accompanied by an enormous decrease in viscosity, of some twenty orders of magnitude, as illustrated in figure 1.1. Thus, instead of expending energy against the typically high flow stress of a solid metal during forging or similar processes, it is only necessary to contend with the essentially zero shear stress of a liquid. If the properties of castings were easier to control, then

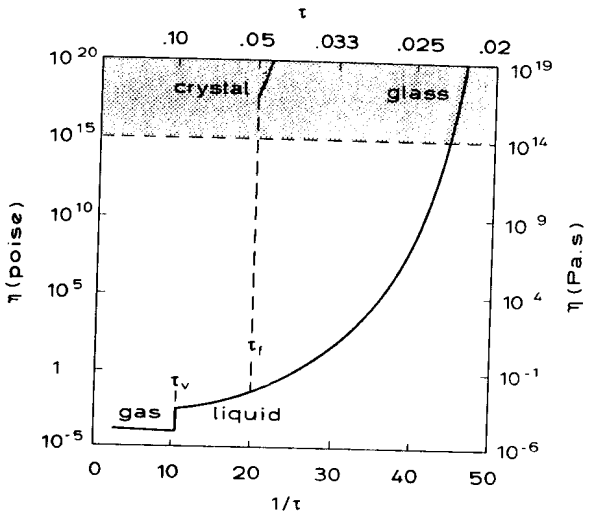

Figure 1.1: DYNAMIC VISCOSITY AS A FUNCTION OF TEMPERATURE. The fundamental advantage of solidification, as a forming operation, is that it permits metal to be shaped with a minimum of effort since the liquid metal offers very little resistance to shear stresses. When the material solidifies due to a decrease in the temperature, τ, its viscosity increases continuously (glass formation) or discontinuously (crystallisation), by over 20 orders of magnitude, to yield a strong solid, the viscosity of which is defined arbitrarily to be greater than 10^{14}Pas. (The reduced temperature, τ, is used here since it leads to a single curve which is applicable to many substances. The suffix, f or v, indicates the melting point or boiling point, respectively.) [D.Turnbull: Transactions of the Metallurgical Society of AIME 221 (1961) 422]

solidification would be an even more important process. In this respect, solidification theory plays a vital role since it forms the basis for influencing the microstructure and hence improving the quality of cast products.

The effect of solidification is most evident when casting is the final operation since the resultant properties can depend markedly upon the position in the casting (figure 1.2). Its influence is also seen in a finished product, even after heavy working, since a solidification structure and its associated defects are difficult to eliminate once they are created. Solidification defects tend to persist throughout subsequent

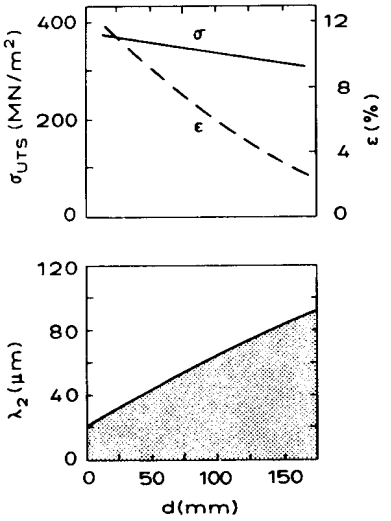

Figure 1.2: ALLOY PROPERTIES AS A FUNCTION OF POSITION IN A CASTING. The use of casting as a production route unfortunately poses its own problems. One of these is the local variation of the microstructure, leading to compositional variations, and this is illustrated for example by the dendrite arm spacing, λ_2, measured as a function of the distance, d, from the surface of the casting. This can lead to a resultant variation in properties such as the ultimate tensile strength and the elongation. Like the weakest link in a chain, the inferior regions of a casting may impair the integrity of the whole. Thus, it is important to understand the factors which influence the microstructure. Finer microstructures generally have superior mechanical properties and finer structures, in turn, generally result from higher solidification rates. Such rates are found at small distances from the surface of the mould, in thin sections, or on remelted surfaces. [M.C.Flemings: Solidification Processing, McGraw-Hill, New York, 1974]

operations (see 1.3). Good control of the solidification process at the outset is therefore of utmost importance.

Some important processes which involve solidification are:

Casting:	continuous- ingot- form- precision- die-
Welding:	arc- resistance- plasma- electron beam- laser- friction- (including the micro-mechanisms of wear)
Soldering/Brazing	
Rapid Solidification Processing:	melt-spinning planar-flow casting atomisation surface remelting
Directional Solidification:	Bridgman liquid metal cooling Czochralski electroslag remelting

In addition, the crystallisation of certain pure substances is of great importance. For example, the preparation of semiconductor-grade silicon crystals is an essential step in modern solid-state physics and technology. The production of integrated circuits, the basis of any new electronic device (radio, watch, computer, etc), requires the preparation of large single crystals of very high perfection, containing a controlled amount of a uniformly distributed dopant. At the moment, such a crystal can only be produced by growth from the melt. Indeed, the requirements of semiconductor physics have enormously influenced solidification theory and practice. Therefore, during the past 30 years solidification has evolved from being a purely technological, empirical field, to become a science.

Figure 1.3: EFFECT OF DEFORMATION UPON A CAST MICROSTRUCTURE. Often, casting is not the final forming operation. However, subsequent deformation is not a very efficient method of modifying the as-cast microstructure since any initial heterogeneity exhibits a strong tendency to persist. Thus, during the rolling of this L-shaped profile which contains a heavily segregated central region, the latter defect survives the many stages between the cast billet and the final product. This example emphasises the fact that any effective control of product quality must be exercised during solidification. [A.J.Pokorny, De Ferri Metallographia, Vol.III, Luxembourg, 1966, p287]

Historically, simple cast objects (in copper) first appeared before about 4000BC and were, no doubt, a natural by-product of the potter's skill in handling the clay used in mould-making. The production of the renowned and highly sophisticated bronze castings of China began in about 1600BC. However, it is probable that the technique had originally been imported from elsewhere. For instance, the lost-wax process was developed in Mesopotamia as long ago as 3000BC. Iron-casting in China began in about 500BC, but in Europe it did not appear until the 16th century, and achieved acceptance as a constructional material, in England in the 18th century, only under the impetus of the industrial revolution.

Much of the delay in exploiting cast materials probably originated from the complete lack of understanding of the nature of solidification phenomena and of the microstructures produced. In particular, the facets of fracture surfaces were invariably taken to indicate the nature of the 'crystals' of which a casting was composed. In the absence of an adequate picture of the solidification process, casting was bound to remain a black art rather than a science, and vestiges of this attitude still remain today.

1.2 Heat Extraction

The various solidification processes mentioned above involve extraction of heat from the melt in a more or less controlled manner. Heat extraction changes the energy of the phases (solid and liquid) in two ways:

1 - There is a decrease in the enthalpy of the liquid or solid, due to cooling, which is given by:
$\Delta H = \int c dT$

2 - There is a decrease in enthalpy, due to the transformation from liquid to solid, which is equal to the latent heat of fusion, ΔH_f; defined to be negative for the liquid-to-solid transformation (exothermic reaction)

Heat extraction is achieved by applying a suitable means of cooling to the melt in order to create an external heat flux, q_e. The resultant cooling rate, dT/dt, can be deduced from a simple heat balance if the metal is isothermal (low cooling rate) and the specific heats of the liquid and the solid are the same. Using the latent heat per unit volume, $\Delta h_f = \Delta H_f / v_m$, in order to conform with the dimensions of the other factors, then:

$$q_e\left(\frac{A'}{v}\right) = -c\left(\frac{dT}{dt}\right) - \Delta h_f\left(\frac{df_s}{dt}\right)$$

so that:

$$\dot{T} = \frac{dT}{dt} = -q_e\left(\frac{A'}{vc}\right) - \left(\frac{df_s}{dt}\right)\left(\frac{\Delta h_f}{c}\right) \qquad [1.1]$$

The first term on the right-hand-side (RHS) of equation 1.1 reflects the effect of casting geometry (ratio of surface area of the casting, A', to its volume, v) upon the extraction of sensible heat, while the second term takes account of the continuing evolution of latent heat of fusion during solidification. It can be seen from this equation that, during solidification, heating will occur if the second term on the RHS of equation 1.1 becomes greater than the first one ($\Delta h_f < 0$). This phenomenon is known as recalescence. For an alloy, where solidification occurs over a range of temperatures, the variation of the fraction of solid as a function of time must be calculated from the relationship:

$$\frac{df_s}{dt} = \left(\frac{dT}{dt}\right)\left(\frac{df_s}{dT}\right)$$

since f_s is a function of temperature. In this case:

$$\dot{T} = \frac{-q_e\left(\frac{A'}{vc}\right)}{1 + \left(\frac{\Delta h_f}{c}\right) \cdot \left(\frac{df_s}{dT}\right)} \qquad [1.2]$$

It is seen that solidification decreases the cooling rate since both df_s/dT and Δh_f are negative.

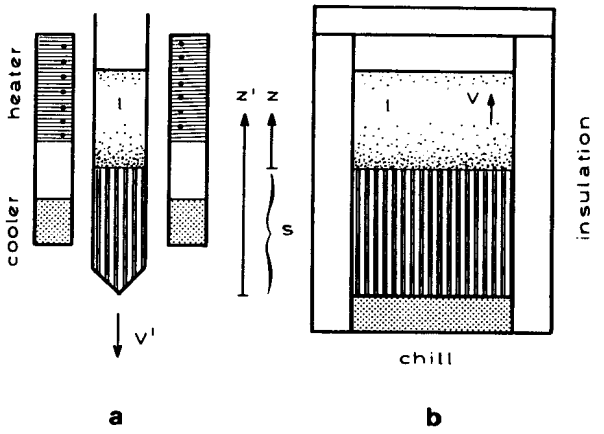

Figure 1.4: BASIC METHODS OF CONTROLLED SOLIDIFICATION. Without heat extraction there is no solidification. The liquid must be cooled to the solidification temperature and then the latent heat of solidification appearing at the growing solid/liquid interface must be extracted. There are several methods of heat extraction. In directional (Bridgman-type) solidification (a): the crucible is drawn downwards through a constant temperature gradient, G, at a uniform rate, V', and therefore the microstructure is highly uniform throughout the specimen. The method is restricted to small specimen diameters and is expensive because it is slow and, paradoxically, heat must be supplied during solidification in order to maintain the imposed positive temperature gradient. For these reasons, it is employed only for research purposes and for the growth of single crystals. In directional casting (b), the benefits of directionality, such as a better control of the properties and an absence of detrimental macrosegregation, are retained but the microstructure is no longer uniform along the specimen because the growth rate, V, and the temperature gradient decrease as the distance from the chill increases. The process is cheaper than that of a) and is used for the directional solidification of gas-turbine blades, for example.

Figure 1.4 illustrates two fundamentally different solidification processes. In figure 1.4a, the heat is extracted in an almost steady manner by moving the crucible at a fixed rate, V', through the temperature profile imposed by the furnace. Such a process is usually used for single crystal growth or directional solidification. It permits the growth rate of the solid, V (which is not necessarily equal to the rate of crucible movement - see exercise 1.9), and the temperature gradient, G, to be separately controlled. If V' is not too high, both the solidification and the heat flux are unidirectional. Therefore, the cooling rate is related to the other constants by:

$$\dot{T} = \left(\frac{dT}{dz'}\right)_{s,t} \left(\frac{ds}{dt}\right)_{z',t} = GV$$

where $s = z' - z$.

Another directional casting process is illustrated by figure 1.4b. Here, heat is extracted via a chill and, as in figure 1.4a, growth occurs in a direction which is parallel, and opposite, to the heat-flux direction. In this situation, the heat-flux decreases with time as do the coupled parameters, G and V. Thus $\dot{T}$ also varies. Heat flow in the mould/metal system leads to an expression for the position, s, of the solid/liquid interface, which is of the type (appendix 1):

$$s = K\sqrt{t} \qquad [1.3]$$

This equation is exact only if the melt is not superheated, if the solid/liquid interface is planar, and if the surface temperature of the casting at the chill drops immediately, at $t = 0$, to a constant value. Upon turning figure 1.4b through 90°, it can be regarded as being a volume element in a conventional casting (figure 1.5). The difference between the figures is the presence of a dendritic morphology at the solid/liquid interface shown schematically in figure 1.5. This morphology depends (chapter 4) upon the alloy composition, and upon G and V. If it is assumed, for simplicity, that the dendrites can be represented by plates (§), then solidification on a microscopic scale again takes place directionally (perpendicular to the primary growth axis of the dendrites, as shown in the upper inset of figure 1.5). This representation permits a simple estimation of interdendritic microsegregation (chapter 6).

§ Plate-like primary crystal morphologies are often observed during solid-state precipitation. When metallic primary crystals grow into a melt, they are always rod-like rather than plate-like in form and possess many branches leading to the characteristic dendrite form.

1.3 Solidification Microstructures

In an ingot or casting, three zones of solidification behaviour can generally be distinguished (figure 1.6). At the mould/metal interface, the cooling rate is at its

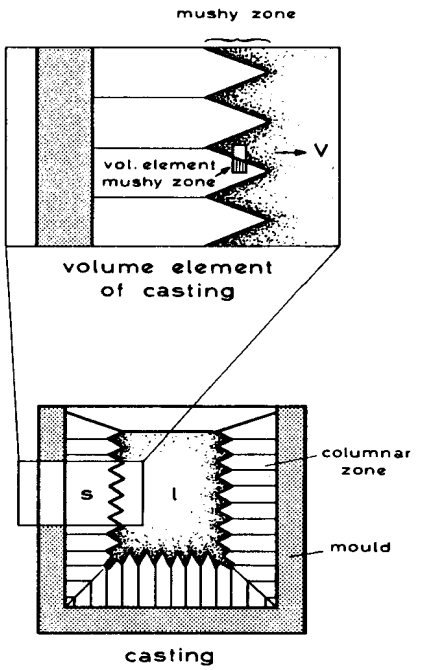

Figure 1.5: SOLIDIFICATION IN CONVENTIONAL CASTINGS AND INGOTS. In the vast majority of castings, no directionality is imposed upon the overall structure, but the local situation can be seen to be equivalent to that occurring in directional casting (figure 1.4b). This is true of the way in which the solid advances inward from the mould wall to form a columnar zone. During the growth of the columnar zone, three regions can be distinguished. These are the liquid, the liquid plus solid (so-called mushy zone), and the solid regions. The mushy zone is the region where all of the microstructural characteristics are determined, e.g. the density, shape, size, and distribution of concentration variations, precipitates, and pores. An infinitesimally narrow volume element which is fixed in the mushy zone and is perpendicular to the overall growth direction permits the description of the microscopic solidification process and therefore of the scale and composition of the microstructure.

highest due to initially low relative temperature of the mould. Consequently, many small grains having random orientations, are nucleated at the mould surface and an 'outer equiaxed' zone is formed. These grains rapidly become dendritic, and develop arms which grow along preferred crystallographic directions (⟨001⟩ in the case of cubic crystals). Competitive growth between the randomly oriented outer equiaxed grains causes those which have a preferred growth direction aligned parallel and opposite to the direction to eliminate the others. This is because their higher growth rate allows them to dominate the solid/liquid interface morphology, thus leading to the formation of the characteristic columnar zone. It is often observed

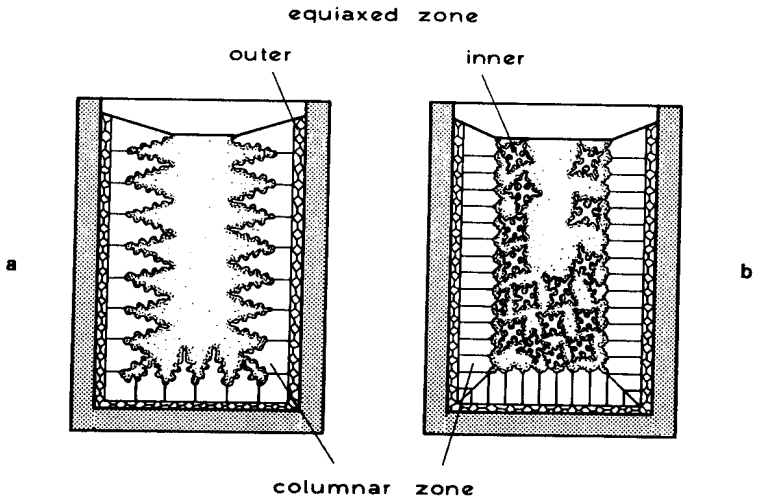

Figure 1.6: STRUCTURAL ZONE FORMATION IN CASTINGS. Firstly, solid nuclei appear at, or close to, the mould wall. For a short time, they increase in size and form the outer equiaxed zone. Then, those crystals (dendrites) which can grow parallel and opposite to the heat flow direction will advance most rapidly. Other orientations tend to be overgrown, due to mutual competition, leading to the formation of a columnar zone (a). Beyond a certain stage in the development of the columnar dendrites, branches which become detached from the latter can grow independently. These tend to take up an equiaxed shape because their latent heat is extracted radially through the undercooled melt. The solidified region containing them is called the inner equiaxed zone (b). The transition from columnar to equiaxed growth is very dependent upon the degree of convection in the liquid. In continuous casting machines, electromagnetic stirring is often used to promote this transition and lead to superior soundness at the ingot centre.

that another equiaxed zone forms in the centre of the casting, mainly as a result of the growth of detached dendrite arms in the remaining, slightly-undercooled liquid.

Figure 1.7 shows the temperature fields of the various cast structures which one might encounter. These are planar interface (columnar grains - a) or thermal dendrites (equiaxed grains - b) in pure materials, and solutal (constitutional) dendrites in alloys (c,d). It can be seen that columnar grains must always grow out from the mould (which is the heat sink) in a direction which is opposite to that of the heat

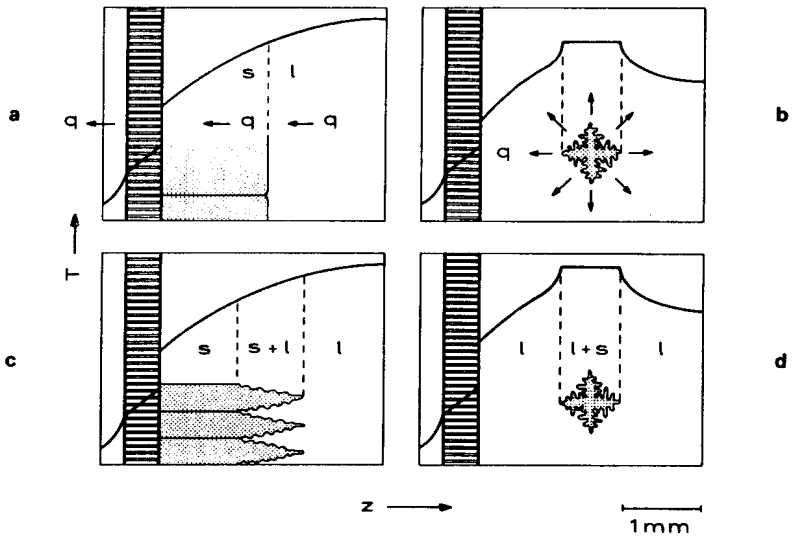

Figure 1.7: SOLID/LIQUID INTERFACE MORPHOLOGY AND TEMPERATURE DISTRIBUTION. In the case of a pure metal (a,b) which is solidifying inwards from the mould wall, the columnar grains (a) possess an essentially planar interface, and grow in a direction which is antiparallel to that of the heat flow. Within the equiaxed region of pure cast metal (b), the crystals are dendritic and grow radially in the same direction as the heat flow. When alloying elements or impurities are present, the morphology of the columnar crystals (c) is generally dendritic. The equiaxed morphology in alloys (d) is almost indistinguishable from that in pure metals, although a difference may exist in the relative scale of the dendrites. This is because the growth in pure metals is heat-flow-controlled, while the growth in alloys is mainly solute-diffusion-controlled. Note that in columnar growth the hottest part of the system is the melt, while in equiaxed solidification the crystals are the hottest part. It follows that the melt must always be cooled to below the melting point (i.e. undercooled) before equiaxed crystals can grow.

flow, while equiaxed grains grow in a supercooled melt which acts as their heat sink. Thus, the growth direction and the heat flow direction are the same in equiaxed growth.

The form of a solidification microstructure depends not only upon the cooling conditions, but also upon the alloy composition (figure 1.8). There are essentially two basic growth morphologies which can exist during alloy solidification. These are the dendritic and eutectic morphologies (peritectic alloys grow in a dendritic form). Generally, a mixture of both morphologies will be present. It is reassuring, in the face of the apparent microstructural complexity, to remember that it is only necessary to understand these two growth forms in order to interpret the solidification microstructure of almost any alloy.

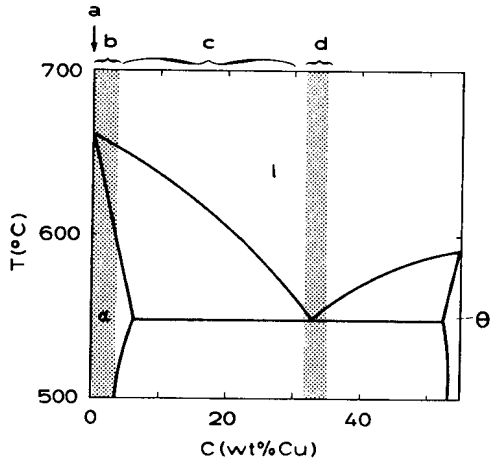

Figure 1.8: PRINCIPAL ALLOY TYPES. It is important to understand how the various microstructures are influenced by the alloy composition and by the solidification conditions. Fortunately, this can usually be reduced to the study of two basic morphological forms: dendritic and eutectic. Thus, one can distinguish: a) pure substances, which solidify in a planar or dendritic manner, b) solid-solution dendrites (with or without interdendritic precipitates), c) dendrites plus interdendritic eutectic, and d) eutectic. The latter group includes the familiar 'cast iron' and 'plumber's solder' type of alloy. In general, the design of casting alloys is governed by the twin aims of obtaining the required properties and good castability (i.e. easy mould filling, low shrinkage, small hot tearing tendency, etc.). Castability is greatest for pure metals and alloys of eutectic composition. The diagram represents the Al-Cu system between Al and the intermetallic (theta) phase, Al_2Cu.

Figure 1.9 illustrates the various stages of equiaxed solidification - from nucleus to grain - for the two major growth morphologies: dendrites and eutectic. Each grain has one nucleus at its origin. (In the literature of cast iron, an eutectic grain is often called an eutectic cell. This definition will not be adopted because the term, cell, is here reserved for another morphology.)

The transformation of liquid into solid involves the creation of curved solid/liquid interfaces (leading to capillarity effects) and to the microscopic flow of heat, and also of solute in the case of alloys.

1.4 Capillarity Effects

With any solid/liquid interface of area, A, is associated an excess (interface) energy which is required for its creation. Therefore, heterogeneous systems or parts of systems which possess a high A/v ratio will be in a state of higher energy and therefore unstable with respect to a system of lower A/v ratio. The relative stability can be expressed by the equilibrium temperature between both phases (melting point). As shown in appendix 3, the change in melting point due to this curvature effect, often called the curvature or Gibbs-Thomson undercooling, is given by:

$$\Delta T_r = \Gamma K \qquad [1.4]$$

Note that the curvature, K, and the Gibbs-Thomson coefficient, Γ, are here defined so that a positive undercooling (decrease in equilibrium melting point) is associated with a portion of solid/liquid interface which is convex towards the liquid phase. The curvature can be expressed as (appendix 3):

$$K = \frac{dA}{dv} = \frac{1}{r_1} + \frac{1}{r_2} \qquad [1.5]$$

where r_1 and r_2 are the principal radii of curvature (§). Thus, the total curvature of a sphere is 2/r and that of a cylindrical surface is 1/r. The Gibbs-Thomson

§ The two principal radii of curvature are the minimum and maximum values for a given surface. It can be shown that they are always perpendicular to each other.

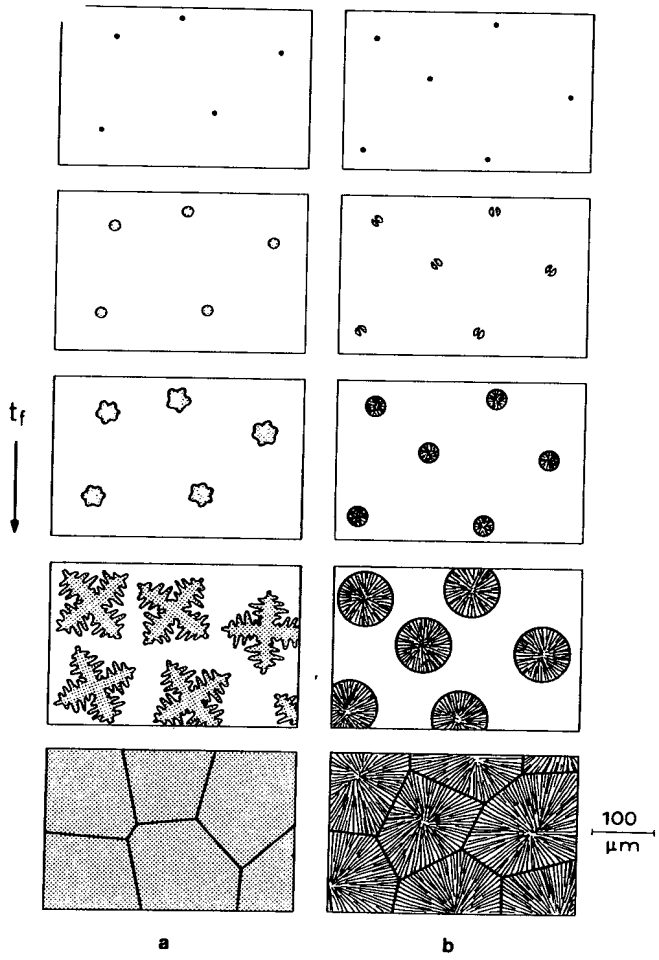

Figure 1.9: PROCESS OF EQUIAXED SOLIDIFICATION OF DENDRITES AND EUTECTIC. In each case, single-phase nuclei form initially. In pure metals or single-phase alloys (a), the nuclei then grow into spherical crystals which rapidly become unstable and dendritic in form. These dendrites grow freely in the melt and finally impinge on one another. In a pure metal after solidification, no trace of the dendrites themselves will remain, although their points of impingement will be visible as the grain boundaries. In an alloy, the dendrites will remain visible after etching due to local composition differences (microsegregation). In an eutectic alloy (b), a second phase will soon nucleate on the initial, single-phase nucleus. The eutectic grains then continue to grow in an essentially spherical form. In a casting, both growth forms, dendritic and eutectic, often develop together. Note that each grain originates from a single nucleus.

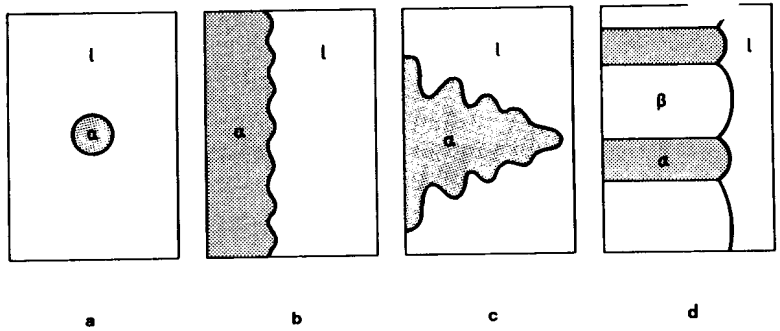

Figure 1.10: THE SCALE OF VARIOUS SOLID/LIQUID INTERFACE MORPHOLOGIES. Solidification morphologies are determined by the interplay of two effects acting at the solid/liquid interface. These are the diffusion of solute (or heat), which tends to minimise the scale of the morphology (maximise curvature), and capillarity effects which tend to maximise the scale. The crystal morphologies actually observed are thus a compromise between these two tendencies, and this can be shown with respect to nucleation (a), interface instability (b), dendritic growth (c), and eutectic growth (d).

coefficient is given by:

$$\Gamma = \frac{\sigma}{\Delta s_f} \qquad [1.6]$$

For most metals, Γ is of the order of 10^{-7}Km. Hence, the effect of the solid/liquid interface energy, σ, only becomes important for morphologies which have a radius which is less than about 10μm. These include nuclei, interface perturbations, dendrites, and eutectic phases (figure 1.10).

1.5 Solute Redistribution

The creation of a crystal from an alloy melt causes a local change in the composition. This is due to the equilibrium condition for a binary system containing two phases:

$$\mu_l^A = \mu_s^A, \quad \mu_l^B = \mu_s^B \qquad [1.7]$$

(appendix 3). The difference in composition at the growing interface, assuming that local (i.e. at the interface) equilibrium exists in metals, can be described by the distribution coefficient under isothermal and isobaric conditions (figure 1.11):

$$k = \left(\frac{C_s}{C_l}\right)_{T,P} \qquad [1.8]$$

In most of the theoretical treatments to be presented later, the solidus and liquidus lines will be assumed to be straight. This means that k and m are then constant. This

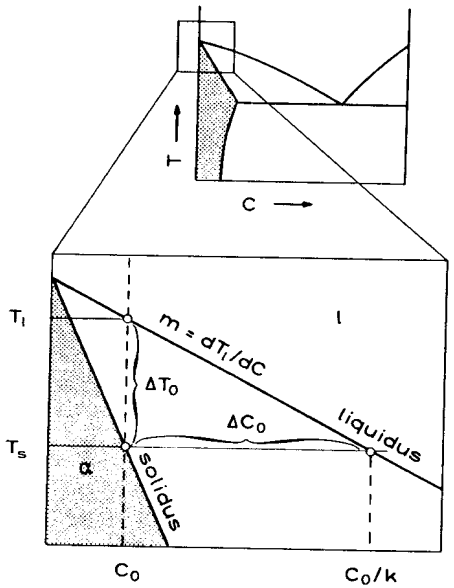

Figure 1.11: SOLID/LIQUID EQUILIBRIUM. In order to simplify the mathematical treatment of solidification processes, it is generally assumed that the liquidus and solidus lines of the phase diagram are straight, and therefore that the distribution coefficient, k, and the liquidus slope, m, are constant. The characteristic properties of the system are defined in the text (equations 1.8 to 1.10).

violates the condition for thermodynamic equilibrium (equation 1.7) but often makes theoretical analyses more tractable without seriously affecting the conclusions. Throughout this book, m is defined so that the product, (k-1)m, is positive. That is, m is defined to be positive when k is greater than unity, and to be negative when k is less than unity. Two other important parameters of an alloy system are shown in figure 1.11. These are the liquidus-solidus temperature interval for an alloy of composition, C_o:

$$\Delta T_o = -m\,\Delta C_o = (T_l - T_s) \qquad [1.9]$$

and the concentration difference between the liquid and solid solute contents at the solidus temperature of the alloy:

$$\Delta C_o = \frac{C_o(1-k)}{k} \qquad [1.10]$$

In later chapters it will be shown how these parameters influence the solidification microstructure. Meanwhile, the starting point of solidification (nucleation) will be considered briefly, and a look will be taken at the mechanisms by which atoms in the melt become part of the growing crystal.

BIBLIOGRAPHY

- Solidification Microstructure and Properties

M.C.Flemings: Solidification Processing, McGraw-Hill, New York, 1974, p328
W.Kurz, P.R.Sahm: Gerichtet erstarrte eutektische Werkstoffe, Springer, Berlin, 1975
G.F.Bolling in Solidification, American Society for Metals, Metals Park, Ohio, 1971, p341
J.F.Burke, M.C.Flemings, A.E.Gorum: Solidification Technology, Brook Hill, 1974

- Analytical Solutions to Heat Flow Problems in Solidification

H.S.Carslaw & J.C.Jaeger: Conduction of Heat in Solids, 2nd Edition, Oxford University Press, London, 1959
G.H.Geiger, D.R.Poirier: Transport Phenomena in Metallurgy, Addison-Wesley, 1973
J.Szekely, N.J.Themelis: Rate Phenomena in Process Metallurgy, Wiley - Interscience, New York, 1971

- Capillarit ects

W.W.Mullins in: Metal Surfaces - Structure, Energetics, and Kinetics, ASM, Metals Park, Ohio, 1963, p17
R.Trivedi in: Lectures on the Theory of Phase Transformations (Edited by H.I.Aaronson), TMS of AIME, New York, 1975, p51

- Thermodynamics of Solidification

J.C.Baker, J.W.Cahn in: Solidification, American Society for Metals, Metals Park, Ohio, 1971, p23
M.C.Flemings: Solidification Processing, McGraw-Hill, 1974, p263
J.S.Kirkaldy in: Energetics in Metallurgical Phenomena - Volume IV, (Edited by W.M.Mueller), Gordon & Breach, New York, 1968, p197
M.Hillert in: Lectures on the Theory of Phase Transformations (Edited by H.I.Aaronson), TMS of AIME, New York, 1975, p1

- Casting Techniques

R.Flinn in: Techniques of Metals Research - Volume I, (Edited by R.F.Bunshah), Wiley, New York, 1968
F.L.Versnyder, M.E.Shank: Materials Science and Engineering 6 (1970) 213
T.F.Bower, D.A.Granger, J.Keverian in: Solidification, American Society for Metals, Metals Park, Ohio, 1971, p385

- Phase Diagrams

M.Hansen: Constitution of Binary Alloys, McGraw-Hill, New York, 1958
W.G.Moffatt: The Handbook of Binary Phase Diagrams, General Electric Company, Schenectady, 1978
Metals Handbook - Volume 8, ASM, Metals Park, Ohio

EXERCISES

1.1 - Discuss the shape of the upper surface of the ingot in figure 1.6. What would happen if the solidifying material was one of the following substances: water, Ge, Si, Bi?

1.2 - From a consideration of the volume element in the mushy zone of figure 1.5 (upper part), define the local solidification time, t_f, in terms of the dendrite growth rate, V, and the length, a, of the mushy zone.

1.3 - Sketch η-τ diagrams for the crystallisation of a pure metal and for an alloy, and comment on their significance in each case.

1.4 - Equiaxed dendrites develop freely in an undercooled melt. Discuss the direction of movement of the equiaxed dendrites in a quiescent melt. Where would most of them be found in solidifying melts of a) steel, b) Bi?

1.5 - Sketch two different phase diagrams having a positive and a negative value of m. Show that the product, m(k-1), is always positive.

1.6 - Using data from "Constitution of Binary Alloys" (M.Hansen and K.Anderko, McGraw-Hill, New York, 1958) or a similar compilation, estimate the distribution coefficient, k, of S in Fe at temperatures between 1530 and 900°C, and of Cu in Ni at temperatures between 1400 and 1300°C. Discuss the validity of the assumption that k is constant in these systems.

1.7 - A molten alloy, like any liquid which exhibits local density variations, will be subject to movements known as natural convection. What is the origin of this convection in a) a pure metal, b) an alloy? Discuss your conclusions with regard to various alternative solidification processes such as upward (as opposed to downward) directional solidification (Bridgman - figure 1.4), and casting (figure 1.5).

1.8 - Give possible reasons for the good mould-filling characteristics which are exhibited by pure metals and eutectic alloys during the casting of small sections. Discuss them with regard to the interface morphology shown in figure 1.7.

1.9 - Figure 1.4 illustrates two directional solidification processes which differ with respect to their heat transfer characteristics. In one case, a steady-state behaviour is established after some transient changes. In the other case, changes continue to occur with the passage of time. One process is not limited with regard to the length of the product, but is limited by its diameter. The other process is not affected by the diameter, but rather by the specimen length. Sketch heat flux lines, and T, G, and V values as a function of z' for various times and discuss the above facts in the light of the sketches. Note that, in directional solidification, the temperature gradient at the solid/liquid interface in the liquid must always be positive, as shown in figure 1.7a,c.

1.10 - Illustrate the changes in the temperature distribution of a casting as a function of time between the moment of pouring of a pure, superheated melt and the establishment of the situation shown in figure 1.7a and b. Discuss the fundamental differences between a and b.

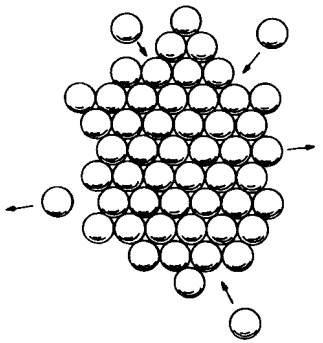

CHAPTER TWO

ATOM TRANSFER AT THE SOLID/LIQUID INTERFACE

From a thermodynamic point of view, solidification requires an outflow of heat which changes the free energies, and therefore the relative thermodynamic stability, of the phases present. From the same point of view, thermodynamically stable phases are more likely to be observed, but the transformation of one phase into another requires rearrangement of the atoms. This may involve a relatively short-range (atomic) rearrangement to form a new crystal structure, as in the case of a pure substance. Alternatively, atomic movement may be required over much larger, but still microscopic, distances as in the case of alloy solidification where mass diffusion controls the transformation. Because of these atomic movements, solidification can never be an equilibrium process and some irreversible departure from equilibrium is always required to drive the process.

Like a chemical reaction, phase transformations are driven by thermal fluctuations and can only oc when the probability of transfer of atoms from the parent phase to the product phase is higher than that for the opposite direction. However, even before this stage is reached, it is necessary that some of the new phase, to which atoms of the parent phase can jump, should already exist. Therefore, stable regions of the new phase have to form. In solid metals, random fluctuations may create minute crystalline regions (clusters, embryoes) even at temperatures greater than the melting point, but these will not be stable. Indeed, they continue to be unstable to some temperature below the melting point because the relatively large excess energy required for surface creation tends to weight the 'energy balance' against their survival when they are small.

Once nucleation has occurred, atom transfer to the crystals has to continue in order to ensure their growth. The mechanisms involved during this second stage are discussed in section 2.3.

2.1 Conditions for Nucleation

It is inherently difficult to observe the process of nucleation because it involves such small clusters of atoms. Consequently, only extremely careful comparison of theoretical models and experimental results can clarify the very first stages of solidification. As demonstrated in figure 2.1, for the case of a hypothetical metal, nucleation begins at some degree of undercooling, $\Delta T = \Delta T_n$ (§), which is generally very small in practical situations. The initially small number of grains which begin to grow does not appreciably modify the cooling rate imposed by the external heat flux, q_e. Increasing the undercooling has the effect of markedly increasing the nucleation rate, I, and also the growth rate, V. The solidification rate approaches a maximum value when the internal heat flux (q_i), which is proportional to the latent heat of fusion and the volume rate of transformation, $\dot{f}_s (= df_s/dt)$, is equal to the external one (q_e) (equation 1.1). Here, $\dot{T} = 0$. During the first stage of equiaxed

§ The undercooling, ΔT, is usually defined as the temperature difference between the equilibrium temperature of a system and its actual temperature. The latter is lower than the equilibrium temperature when the melt is undercooled. In this case, ΔT is greater than zero. The term, supercooling, is often used interchangeably with undercooling in the literature.

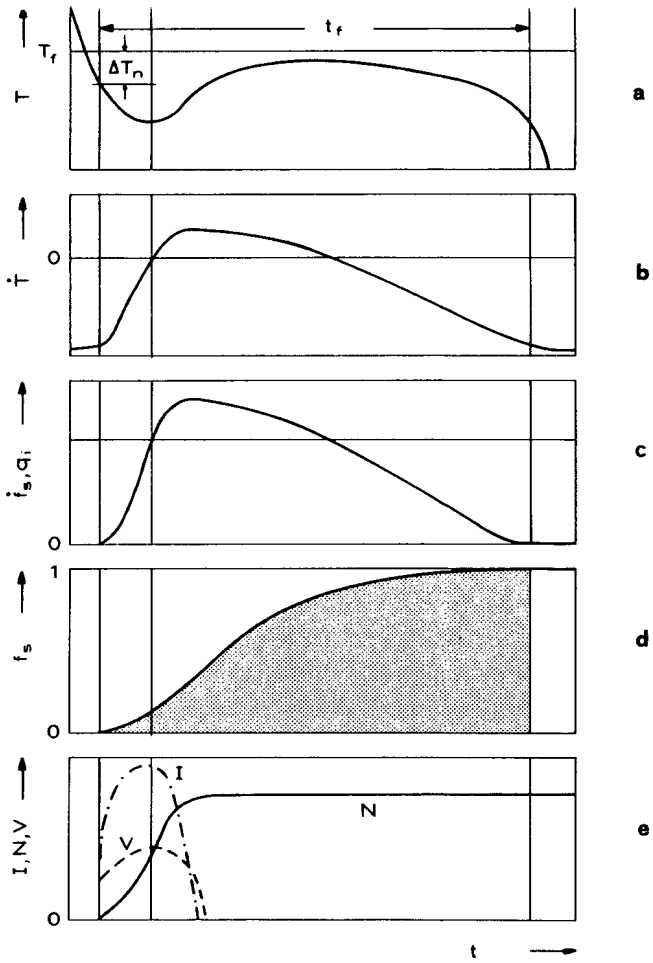

Figure 2.1: THERMAL HISTORY OF EQUIAXED DENDRITIC SOLIDIFICATION. The above temperature-time curve is one which might well be obtained during a solidification sequence such as that pictured in figure 1.9a. The usual cooling curve (a) begins to deviate slightly at the undercooling where nucleation occurs, ΔT_n. At this point, the first fraction of solid, f_s, appears (d). With further cooling, the nucleation rate, I, rapidly increases to a maximum value (e) which corresponds to a minimum in the temperature/time curve (a). At this point, the growth rate, V, of the grains (i.e. of the dendrite tips) is at its highest. The subsequent increase in temperature is due to the high internal heat flux, q_i, arising from the rate of transformation, $\dot{f}_s$ ($= df_s/dt$), and the latent heat released (c). Note that I is much more sensitive to temperature changes than is V (e). The final solidification which takes place after impingement of the grains involves dendrite arm coarsening at a tip growth rate, V, equal to zero. During this time interval, the number of grains, N, remains constant.

solidification, . is essentially nucleation-controlled, the volume fraction of solid is still very small. After some time, the temperature of the system has risen above the nucleation temperature and the second stage of solidification is growth-controlled. The number of grains present thus remains essentially constant and solidification proceeds via the lengthening of dendrites, and dendrite arm thickening.

From this sort of consideration, it is possible to deduce that nucleation is the dominant process at the beginning of solidification and leads very rapidly to the establishment of the final grain population, with each nucleus forming one equiaxed grain of the type shown in figure 1.9b or d. Note that even in the case of columnar solidification, the very first solid in a casting always appears in the form of equiaxed grains (figure 1.6). The conditions leading to nucleation are therefore of utmost importance in determining the characteristics of any cast microstructure.

In phase changes such as solidification, which are discontinuous, the transformation process cannot occur at any arbitrarily small undercooling. The reason for this arises from the large curvature associated with a crystal of atomic dimensions. This curvature markedly lowers the equilibrium temperature (appendix 3) so that, the smaller the crystal, the lower is its melting point. This occurs because the small radius of curvature creates a pressure difference between the two phases which is of the order of 100MPa (1kbar) for a crystal radius of 1nm. The equilibrium melting point of the system is thus lowered by an amount, ΔT_r. The critical size, r^o, of a crystal, i.e. the size which allows equilibrium between the curved crystal and its melt, can be calculated. For a sphere (appendix 3) this is:

$$\Delta T_r = \Gamma K = \frac{2\Gamma}{r^o}$$

and

$$r^o = \frac{2\Gamma}{\Delta T_r} = \frac{2\sigma}{\Delta T_r \Delta s_f} \qquad [2.1]$$

This relationship indicates that, the smaller the difference (undercooling) between the melting point and the temperature of the melt, the larger will be the size of the equilibrium crystal. For nucleation of a spherical crystal of radius, r, to occur, a number of atoms, each of volume, v', given by:

$$n \simeq \frac{4r^3\pi}{3v'} \qquad [2.2]$$

have to arrange themselves on the sites of the corresponding solid crystal lattice. It

is evident that the probability of this event occurring is very small for larg ues of r^o, i.e. at small undercoolings (equation 2.1).

As shown in figure 2.2, the critical condition for nucleation is derived by summing the interface and volume terms for the Gibbs free energy:

$$\Delta G = \Delta G_i + \Delta G_v = \sigma A + \Delta g.v \qquad [2.3]$$

where σ is the solid/liquid interface energy and Δg is the Gibbs free energy difference between the liquid and solid per unit volume. Again assuming a spherical form (minimum A/v ratio) for the nucleus,

$$\Delta G = \sigma 4\pi r^2 + \frac{\Delta g.4\pi r^3}{3} \qquad [2.4]$$

The Gibbs free energy per unit volume, Δg, is proportional to ΔT (appendix 3):

$$\Delta g = \Delta s_f \Delta T \qquad [2.5]$$

The right-hand-side of equation 2.4 is composed of a quadratic and a cubic term. The value of σ is always positive whereas Δg depends upon ΔT, and is negative if ΔT is positive. This behaviour leads to the occurrence of a maximum in the value of ΔG when the melt is undercooled, i.e. when ΔT is positive (figure 2.2c). This maximum can be regarded as being the activation energy which has to be overcome in order to form a crystal nucleus which will continue to grow. The maximum value is given by:

$$\frac{d(\Delta G)}{dr} = 0 \qquad [2.6]$$

and can be regarded as being a condition for equilibrium between liquid, and solid having a curvature such that the driving force for solidification is equal to that for melting. Consequently, it is not surprising that setting the first derivative of equation 2.4 equal to zero should lead to equation 2.1.

Figure 2.2d demonstrates how fluctuations in a melt, corresponding to the conditions of figure 2.2c, will behave. At least one cluster which is as large as the critical nucleus (of radius, r^o) must be formed before solidification can begin. The time which elapses before this occurs will be different (t_1, t_2, ...) at different locations in the melt. In this case, fluctuations spontaneously create a small crystalline volume in an otherwise homogeneous melt (containing no solid phase). This is referred to as homogeneous nucleation because the occurrence of nucleation transforms an initially homogeneous system (consisting only of atoms in the liquid state) into a heterogeneous system (crystals plus liquid). Using equations 2.2 to 2.6, the critical

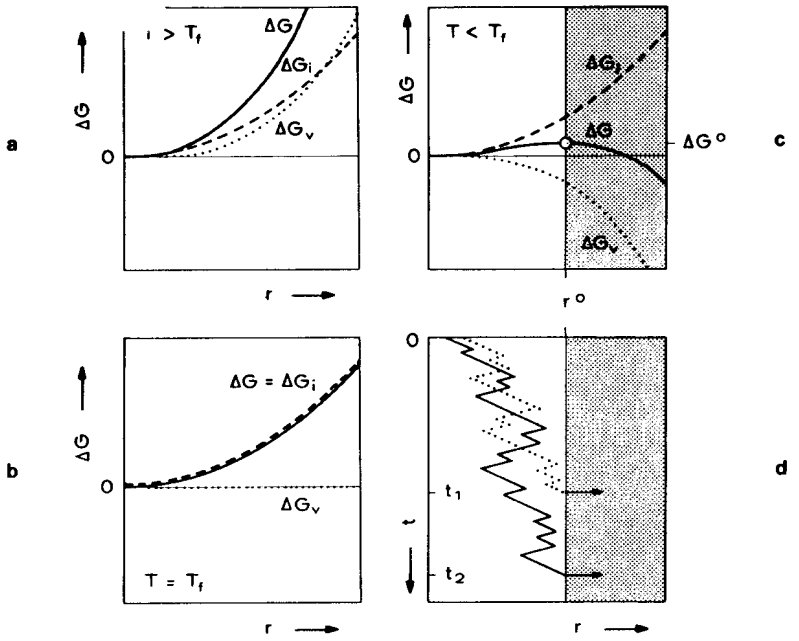

Figure 2.2: FREE ENERGY OF A CRYSTAL-LIKE CLUSTER AS A FUNCTION OF ITS RADIUS. The process of nucleation of a crystal from its melt depends mainly on two processes: thermal fluctuations which lead to the creation of variously sized crystal embryoes (clusters), and creation of an interface between the liquid and the solid. The free energy change, ΔG_v, which is associated with the first process is proportional to the volume transformed. That is, it is proportional to the cube power of the cluster radius. The free energy change, ΔG_i, which is associated with the second process is proportional to the area of solid/liquid interface formed. That is, it is proportional to the square of the cluster radius. At temperatures, T, greater than the melting point (a), both the volume free energy (ΔG_v) and the surface free energy (ΔG_i) increase monotonically with increasing radius, r. Therefore, the total free energy, ΔG, which is their sum, also increases monotonically. At the melting point (b), the value of ΔG_i still increases monotonically since it is only slightly temperature dependent. Because, by definition, thermodynamic equilibrium exists between the solid and liquid at the melting point, the value of ΔG_v is zero. Hence ΔG again increases monotonically with increasing radius. At a temperature below the equilibrium melting point (c), the sign of ΔG_v is reversed because the liquid is now unstable, while the behaviour of ΔG_i is still the same as in (a) and (b). However, ΔG_v has a 3rd power dependence on the radius while ΔG_i has only a 2nd power dependence. Thus, at small values of the radius, the absolute value of ΔG_v is less than that of ΔG_i, while at large values of r the cubic dependence of ΔG_v predominates. The value of ΔG therefore passes through a maximum at a critical radius, r^o. Fluctuations may move the cluster backwards and forwards along the ΔG-r curve (c) due to the effect of random additions or removals of atoms to or from the unstable nucleus. When a fluctuation causes the cluster to become larger than r^o, growth will occur due to the resultant decrease in the total free energy. Thus, an embryo or cluster ($r<r^o$) becomes a nucleus ($r=r^o$) and eventually leads to the formation of a grain ($r \gg r^o$).

parameters can be calculated and are given in table 2.1 where ΔG_n is equivalent to ΔG in equation 2.3, except that n (the number of atoms in the nucleus, equation 2.2) rather than the radius, r, has been used to describe the nucleus size.

As an example, suppose that an undercooling of 230K is required to cause nucleation in small Cu droplets. From this value and the properties of the metal it is estimated that r^o=1nm and n^o=360.

When the melt contains solid particles, or is in contact with a crystalline crucible or oxide layer, nucleation may be facilitated if the number of atoms, or activation energy required for nucleation, are decreased. This is known as heterogeneous nucleation. A purely geometrical calculation shows that when the solid/liquid interface of the substance is partly replaced by an area of low-energy solid/solid interface between the crystal and a foreign solid, nucleation can be greatly facilitated. The magnitude of the effect can be calculated using the result derived in appendix 3:

$$f(\theta) = \frac{(2 + \cos\theta)(1 - \cos\theta)^2}{4} \qquad [2.7]$$

where θ is the wetting angle, in the presence of the melt, between a growing spherical cap of solid (nucleus) and a solid substrate (particle or mould wall). The n^o and $\Delta G_n{}^o$ values are decreased by small values of θ but the r^o value is not.

Numerical values of $f(\theta)$, given by equation 2.7, are listed in table 2.2, and show that, under conditions of good solid/solid wetting (small θ) between the crystal nucleus and the foreign substrate in the melt, a large decrease in n^o and ΔG^o can be expected.

Table 2.1: CRITICAL DIMENSIONS AND ACTIVATION ENERGY FOR THE NUCLEATION OF A SPHERICAL NUCLEUS IN A PURE MELT ($\Delta g = \Delta s_f \Delta T$)

	Homogeneous Nucleation	Heterogeneous Nucleation
critical dimension r^o	$\frac{2\sigma}{\Delta g}$	$\frac{2\sigma}{\Delta g}$
n^o	$(\frac{32\pi}{3v'})(\frac{\sigma}{\Delta g})^3$	$(\frac{32\pi}{3v'})(\frac{\sigma}{\Delta g})^3 f(\theta)$
activation energy $\Delta G_n{}^o$	$(\frac{16\pi}{3})(\frac{\sigma^3}{\Delta g^2})$	$(\frac{16\pi}{3})(\frac{\sigma^3}{\Delta g^2}) f(\theta)$

Table 2.2: VALUES OF THE EXPRESSION:
$f(\theta) = (1/4)(2 + \cos\theta)(1 - \cos\theta)^2$

θ(°)	Type of Nucleation	$f(\theta)$
0 complete wetting	no nucleation barrier (§)	0
10	heterogeneous	0.00017
20		0.0027
30		0.013
40		0.038
50		0.084
70		0.25
90		0.5
110		0.75
130		0.92
150		0.99
170		0.9998
180 no wetting	homogeneous	1

§ immediate growth can occur

This can have a dramatic effect on the nucleation rate and is used daily in foundries in the form of inoculation. Here, substances are added to the melt which are crystalline or form crystals at temperatures greater than the melting point. The effect is usually time-dependent since the added substances tend to dissolve in the melt. In the case of the breaking-off of dendrite branches there is no nucleation problem at all since θ, and therefore ΔT, are zero. In this case, growth can commence immediately.

The above arguments have been developed for pure metals with or without foreign particles. They can also be applied to alloys. In this case, the Gibbs free energy is not only a function of nucleus size (r or n), but also of composition. To a first approximation, the critical size and composition would be found in this case from the conditions, $d(\Delta G)/dn = 0$ and $d(\Delta G)/dC = 0$, which define a saddle point.

2.2 Rate of Nucleus Formation

In order to calculate the number of grains nucleated in a given molten volume and time (called the nucleation rate), the simplest case will be considered. This is an ideal mixture between an ensemble, N_n, of small crystalline clusters, each of which

contain n atoms, and N_l atoms of the liquid. The equilibrium distribution (solubility) of these clusters can be calculated (appendix 4) leading to the result, for n (when $N_n \ll N_l$):

$$\frac{N_n}{N_l} = \exp[-\frac{\Delta G_n}{k_B T}] \qquad [2.8]$$

Equation 2.8 and figure 2.3 show that there are always crystal clusters in a melt, although they are not necessarily stable. Their number increases with decreasing value of ΔG_n. The number of clusters is shown schematically in figure 2.3 as a density of points. If the melt is superheated, $d(\Delta G_n)/dn$ is always positive and the equilibrium concentration of crystal nuclei is zero. In an undercooled melt, a maximum in ΔG_n, as a function of n exists, over which clusters can 'escape' and form the flux of nuclei, I. The maximum value, ΔG_n° (table 2.1), varies with $1/\Delta T^2$. The value of N_n° varies according to equation 2.8 and therefore:

$$N_n^\circ = K_1 \exp[-\frac{K_2}{T\Delta T^2}] \qquad [2.9]$$

where K_1 and K_2 are constants. If it is assumed here that the rate of cluster formation is so high or I is so small that the equilibrium concentration of critical clusters, N_n°/N_l, will not change i.e. the source of nucleation will not be exhausted(§), the steady-state nucleation rate is given by:

$$I = K_3 N_n^\circ$$

$$I = K_3 N_l \exp[-\frac{\Delta G_n^\circ}{k_B T}] \qquad [2.10]$$

where K_3 is a constant.

However, the formation of clusters will require the transfer of atoms from the liquid to the nuclei. An activation energy, ΔG_d, for transfer through the solid/liquid interface must therefore be added to equation 2.10, giving (appendix 4):

$$I = I_o \exp[-\frac{(\Delta G_n^\circ + \Delta G_d)}{k_B T}] \qquad [2.11]$$

where I_o is a pre-exponential factor. This important equation contains two

§ This assumption is a crude but useful simplification. For more details, the reader is referred to J.W.Christian, 'The Theory of Transformations in Metals and Alloys', Pergamon, Oxford, 2nd Edition, 1975, p418.

exponential terms. One of these varies as $-1/T\Delta T^2$ (equation 2.9), while the other varies, like the diffusion coefficient, as $-1/T$. An increase in ΔT, giving more numerous and smaller nuclei of critical size, is accompanied by a decrease in T and fewer atoms are transferred from the liquid to the nuclei. These opposing tendencies

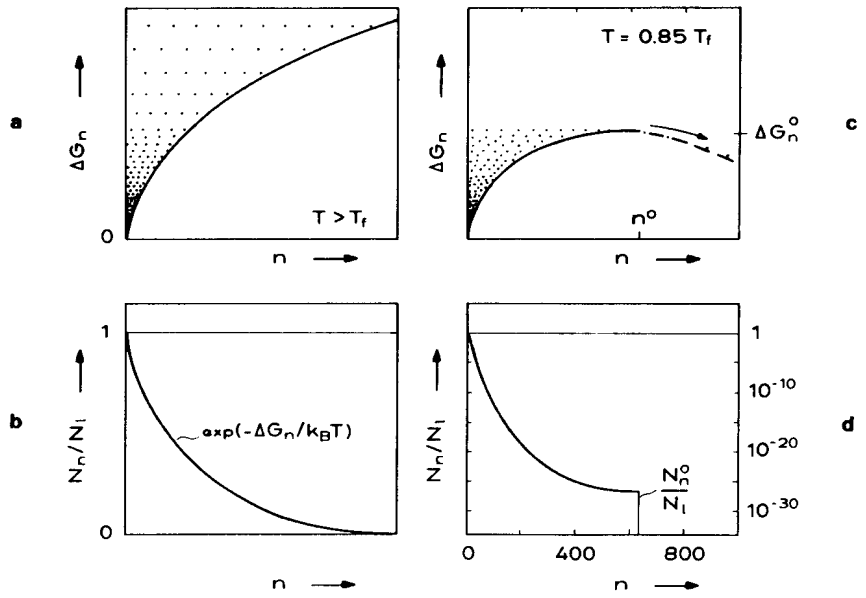

Figure 2.3: DEPENDENCE OF CLUSTER-SIZE DISTRIBUTION UPON TEMPERATURE: a,c: free energy, ΔG_n, of a cluster containing n atoms, at two temperatures. b,d: number of clusters, N_n, containing n atoms, as a fraction of the number of atoms, N_l, in the liquid phase. There is an exponential relationship between ΔG_n and N_n. Thermal fluctuations are always creating small crystalline regions in the liquid, even at temperatures greater than the melting point (a). The number of clusters, N_n, divided by the number of atoms in the liquid, N_l, will be much smaller for large clusters (large r or large number of atoms, n), than for small ones (b). This variation in the distribution of cluster sizes is represented schematically (a) as a varying density of points. At temperatures below T_f (c), there will be a maximum, ΔG_n^o, in the free energy of the fluctuating system as is also shown in figure 2.2. The clusters reaching this critical size (nuclei) will grow. The corresponding cluster-concentration, N_n^o/N_l, and cluster size, n^o (minimum in figure d), are sensitive functions of the undercooling. The nucleation rate will depend on the number of clusters having the critical size, N_n^o/N_l.

lead to a maximum in the nucleation rate at a critical temperature, T_c, which is situated somewhere between the melting point ($\Delta T = 0$) and the point where there is no longer any thermal activation (T=0K). This is illustrated by figure 2.4a. Note that I would exhibit a maximum value even in the absence of the diffusion term. The presence of the latter term increases the temperature at which the maximum occurs. Since, for a unit volume of the melt, the reciprocal of the nucleation rate is time, the I-T diagram can be easily transformed into a TTT-diagram (figure 2.4b) where the curve represents the beginning of the liquid to solid transformation. The effect of decreasing the wetting angle, θ, is mainly felt via its influence on the equilibrium concentration of nuclei and a decrease in ΔT, i.e. nucleation occurs closer to the melting point. At very high cooling rates, such as those encountered in rapid solidification processing, there may be insufficient time for the formation of even one nucleus, and a glassy (amorphous) solid then results (cooling curve 2 in figure 2.4b).

It is interesting to calculate the effect of a slight change in ΔG_n° (due perhaps to a change in $f(\theta)$) upon the nucleation rate. This can easily be done by approximating equation 2.11. At low values of ΔT, the value of $\exp[-\Delta G_d/k_BT]$ is approximately equal to 0.01 and I_o is approximately equal to $10^{41}\,m^{-3}s^{-1}$. The nucleation rate (in units of $m^{-3}s^{-1}$) therefore becomes:

$$I = 10^{39}\exp[-\frac{\Delta G_n^\circ}{k_BT}] \qquad [2.12]$$

A nucleation rate of one nucleus per cm^3 per second ($10^6 m^{-3}s^{-1}$) occurs when the value of $(\Delta G_n^\circ/k_BT)$ is about 76. Close to this value, a change in the exponential term of a factor of two, from 50 to 100 for example, decreases the nucleation rate by a factor of 10^{22}. When $\Delta G_n^\circ/k_BT$ is equal to 50, 10^8 nuclei per litre of melt per microsecond are formed. If the latter term is equal to 100, only one nucleus will be formed per litre of melt over a period of 3.2 years (figure 2.5). This example shows that very slight changes in the solid/liquid interface energy can have striking effects.

By calculating the undercooling, for a constant value ($1/cm^3s$) of I, as a function of θ, another interesting result is revealed. This is illustrated by table 2.3 which gives the change in undercooling in heterogeneous nucleation as a function of the nucleus/substrate contact angle. If the substrate is highly dispersed, as in inoculation, the active surface area of the inoculant must also be taken into account in the pre-exponential factor (I_o), in equation 2.11. This leads to a decrease in the undercooling. This effect is relatively small in comparison with that caused by a change in activation energy, and is therefore usually neglected. However, the grain size will be inversely proportional to the particle density. When a fine grain size is required, it is clear that many finely dispersed particles should be introduced into the

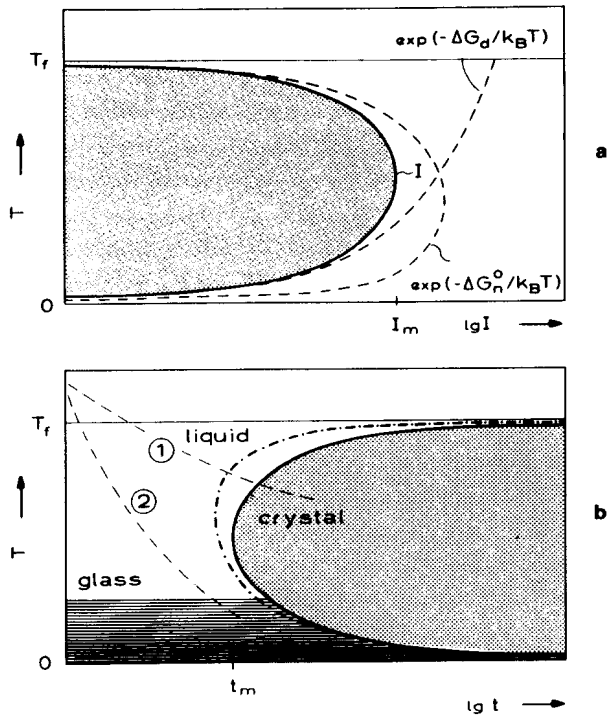

Figure 2.4: NUCLEATION RATE AND NUCLEATION TIME AS A FUNCTION OF ABSOLUTE TEMPERATURE. The overall nucleation rate, I (number of nuclei created per unit volume and time), is influenced both by the rate of cluster formation, depending upon the nucleus concentration (N_n^o), and by the rate of atom transport to the nucleus. At low undercoolings, the energy barrier for nucleus formation is very high and the nucleation rate is very low. As the undercooling increases, the nucleus formation rate increases before again decreasing (a). The decrease in the overall nucleation rate, at large departures from the equilibrium melting point, is due to the decrease in the rate of atomic migration (diffusion) with decreasing temperature. A maximum in the nucleation rate, I_m, is the result. This information can be presented in the form of a TTT (time-temperature- transformation) diagram (b) which gives the time required for nucleation. This time is inversely proportional to the nucleation rate, and diagram (b) is therefore the inverse of diagram (a) for a given alloy volume. The diagram indicates that there is a minimum time for nucleation, t_m (proportional to $1/I_m$). This minimum value can be moved to higher temperatures and shorter times by decreasing the activation energy for nucleation, ΔG_n^o [dash-dot line in (b)]. When liquid metals are cooled by normal means, the cooling curve will generally cross the nucleation curve (curve 1) somewhere close to T_f. However, very high rates of heat removal (curve 2) can cause the cooling curve to miss the nucleation curve completely and an amorphous solid (hatched region, glass) is then formed via a continuous increase in viscosity (figure 1.1). The production and characterisation of metallic glasses is currently the subject of intensive study. Note that this figure relates to nucleation (start of transformation) only. The second curve of a TTT diagram which describes the end of the transformation, after growth has occurred, is not shown.

Table 2.3: ABSOLUTE AND RELATIVE UNDERCOOLINGS, REQUIRED TO GIVE ONE NUCLEUS PER SECOND PER CM^3, AS A FUNCTION OF θ

θ(°)	$\Delta T/T_f$	$\Delta T(T_f = 1500K)$
180	0.33	495
90	0.23	345
60	0.13	195
40	0.064	96
20	0.017	25.5
10	0.004	6.5
5	0.001	1
0	0.0	0

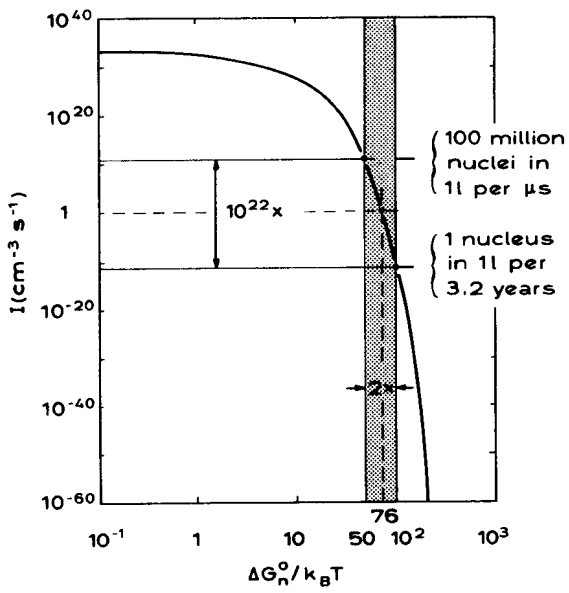

Figure 2.5: NUCLEATION RATE AS A FUNCTION OF ACTIVATION ENERGY, ΔG_n^o. Variations in the value of the term, $\Delta G_n^o/k_BT$, have a remarkable effect upon the rate of nucleation, I, due to the exponential relationship. If, for an observable rate of $I = 1/cm^3s$, $\Delta G_n^o/k_BT$ is changed by a factor of two, the resultant change in the nucleation rate is of the order of 10^{22}. Thus, changing the temperature or changing the value of ΔG_n^o can enormously increase or decrease the nucleation rate. The value of ΔG_n^o can be decreased by adding foreign crystalline particles which 'wet' the growing nucleus to the melt (inoculation), or by increasing the undercooling.

melt. More importantly, these particles should have a low interface energy when in contact with the solid which is to be nucleated. This is most likely to be so when the nuclei and the nucleated solid have similar atomic structures and the same type of bonding. In many casting situations, this is most effectively achieved by the breaking-off of dendrite arms by convection in the melt. This phenomenon is exploited in the continuous casting of steel by electromagnetically stirring the melt. This method is very effective since it produces nuclei (dendrite arms) which are free of any oxide film which might impair wetting. The presence of oxide films on inoculants is often a problem since they inhibit the action of the latter. For this reason, inoculation by chemical reaction or precipitation in the melt is favoured. Peritectic reactions are most effective in pure metals such as Al since precipitates having a higher melting point than that of the melt are formed and can promote nucleation before dissolution occurs.

2.3 Interface Structure

Once a nucleus is formed, it will continue to grow. Such growth will be limited by:

- the kinetics of atom attachment to the interface,
- capillarity,
- diffusion of heat and mass.

The relative importance of each of these factors depends upon the substance in question and upon the solidification conditions. This chapter will consider only the atomic attachment kinetics, and the other processes will be treated in chapters 3 to 5. The kinetics of atomic addition can play an important role in some substances. When the latter exhibits the 'non-faceted' growth morphology typical of a metal, it can be assumed that the kinetics of transfer of atoms from the liquid to the crystal are so rapid that they can be neglected. When the substance exhibits the faceted mode of growth typical of non-metals or intermetallic compounds, a large kinetic term may be involved. However, it is by no means certain that this term will dominate the growth process.

The classification of substances into faceted and non-faceted types is based upon their growth morphology (figure 2.6). Metals, and a special class of molecular compounds (plastic crystals), usually solidify with macroscopically smooth solid/liquid interfaces and exhibit no facets, despite their crystalline nature. This behaviour reflects an independence of the atomic attachment kinetics with respect to the crystal plane involved. A slight tendency to anisotropic growth remains and results from an anisotropy of the interface energy and the atomic attachment kinetics. This

leads to the appearance of crystallographically determined dendrite trunk and arm directions of low-index type. On the other hand, substances exhibiting complex crystal structures and directional bonding form crystals having planar, angular surfaces (facets). Note that the faceted versus non-faceted classification also depends upon the growth process. A substance which exhibits non-faceted crystals when grown from the melt can give faceted crystals when grown from a solution or vapour.

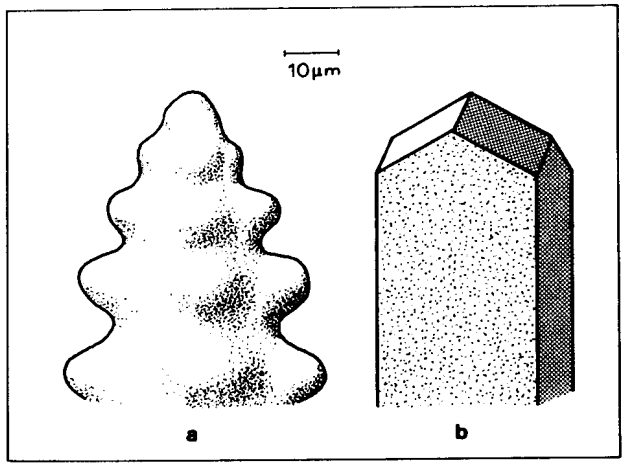

Figure 2.6: NON-FACETED AND FACETED GROWTH MORPHOLOGIES. After nucleation has occurred, further atoms must be added to the crystal in order that growth can continue. During this process, the solid/liquid interface takes on a specific structure at the atomic scale. This structure depends on the difference in crystal structure and bonding between liquid and solid. During the solidification of a non-faceted material, such as a metal (a), atoms can be added easily to any point of the surface and the crystal shape is dictated mainly by the form of the heat and solute diffusion fields. Nevertheless, a remaining slight anisotropy in properties such as the interface energy leads to the growth of dendrite arms along certain crystallographic directions. In faceted materials, such as intermetallic compounds or minerals (b), the inherently rough, high-index planes accept added atoms readily and grow quickly. As a result, these planes disappear and the crystal remains bounded by the more slowly growing facets (low-index planes). The classes of non-faceted and faceted crystals can be distinguished on the basis of the higher entropy of fusion of the latter. This is due to the greater difference in structure and bonding between the solid and liquid phases as compared to metals, which exhibit only very small differences between the two phases.

In the present book, the classification will only be applied to melt-grown crystals. This classification is of practical interest to metallurgists because of the importance of intermetallic phases and compounds in most alloys, and the large-scale industrial use of eutectic alloys (chapter 5) which contain a faceted phase as one component (e.g. Fe-C, Al-Si). From a theoretical point of view, the reason for this marked difference in morphology is worthy of mention here because of the light which it throws on the detailed structure of the solid/liquid interface at the atomic level. Finally, an understanding of atomic attachment kinetics aids the correct choice of transparent model systems which are often used in order to observe solidification phenomena directly (figures 4.3 and 4.16).

The growth rate of a crystal depends upon the net difference between the rates of attachment and detachment of atoms at the interface (appendix 5). The rate of attachment depends upon the rate of diffusion in the liquid, while the rate of detachment depends on the number of nearest neighbours binding the atom to the interface. The number of nearest neighbours depends upon the crystal face considered, i.e. upon the surface roughness at the atomic scale (number of unsaturated bonds). This is the simplest possible situation. In general, reorientation of a complicated molecule in the melt, surface diffusion, and other steps may be required.

Consider the essentially flat interface of a simple cubic crystal. Here, an atom in the bulk crystal has six nearest neighbours represented by the six faces of a cube (figure 2.7). There are five different positions at the interface, characterised by the number of nearest neighbours (1 - 5). In an undercooled system, where the crystal has a lower free energy, it is evident that an atom in position 5 will have a very much higher probability of remaining in the crystal than will an atom in position 1. In order to incorporate atom 1 into the crystal, a very large difference must exist between the force binding it to the crystal, and the force binding it to the liquid. In order to create such a difference, a large undercooling of the melt is required.

An atomically flat interface (figure 2.8a) will maximise the bonding between atoms in the crystal and those in the interface. Thus, such an interface will expose few bonds to atoms arriving via diffusion through the liquid. Such a crystal has a tendency to close up any gap in its solid-liquid interface at the atomic scale. This leads to crystals which are faceted at the microscopic scale and usually exhibit high undercoolings.

An atomically rough interface (figure 2.8b) always exposes a lot of favourable sites for the attachment of atoms from the liquid. Such an interface tends to remain rough and leads to smooth crystals which are non-faceted at the microscopic scale and exhibit low kinetic undercoolings.

Generally, it can be said that the greater the difference in structure and bonding

between the solid and liquid phases, the narrower is the transition region over which these differences have to be accommodated. A sharp transition (i.e. an atomically flat, microscopically faceted interface) exhibits little tendency to incorporate newly arriving atoms into the crystal. Hence growth is more difficult and requires an additional (kinetic) undercooling. Also, because high-index crystallographic planes tend to be inherently rough and to contain many steps, a marked anisotropy in growth rates can develop when the low-index planes are atomically flat. This, in turn, leads to the disappearance of the higher index planes, due to their more rapid growth, and

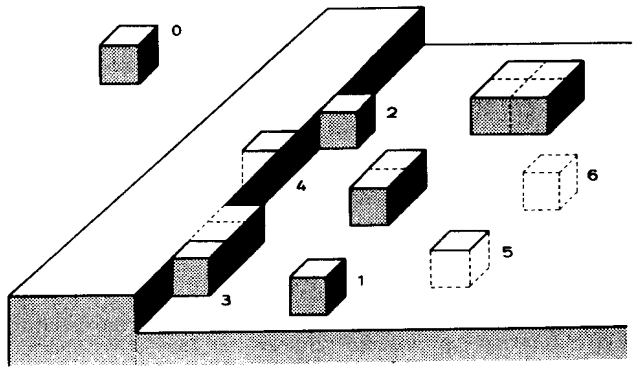

Figure 2.7: VARIATION IN BOND NUMBER AT THE SOLID/LIQUID INTERFACE OF A SIMPLE-CUBIC CRYSTAL. In order to understand the two types of growth shown in figure 2.6, the various ways in which an atom can be adsorbed onto the solid/liquid interface have to be considered. Growth is determined by the probability that an atom will reach the interface and remain adsorbed there until it has been fully incorporated into the crystal. This probability increases with an increasing number of nearest neighbours in the crystal. The possible arrangements of atoms on the crystal interface are indicated here, where the numbers specify the number of neighbouring atoms in the crystal. The atoms of the liquid phase are not shown here. A special role is played by type 3 atoms in the growth of faceted crystals because, having three bonds, they can be considered to be situated half in the solid and half in the liquid (when the crystal coordination number is 6 as in a simple cubic crystal). A likely growth sequence would be: addition of type 3 atoms until a row is complete; addition of a type 2 atom to start a new row; and so on until a layer is complete. Thereupon, nucleation of a new layer by the addition of a type 1 atom would be necessary. This is an unfavourable process and requires a very high undercooling. Therefore, other processes will play a role (figure 2.10).

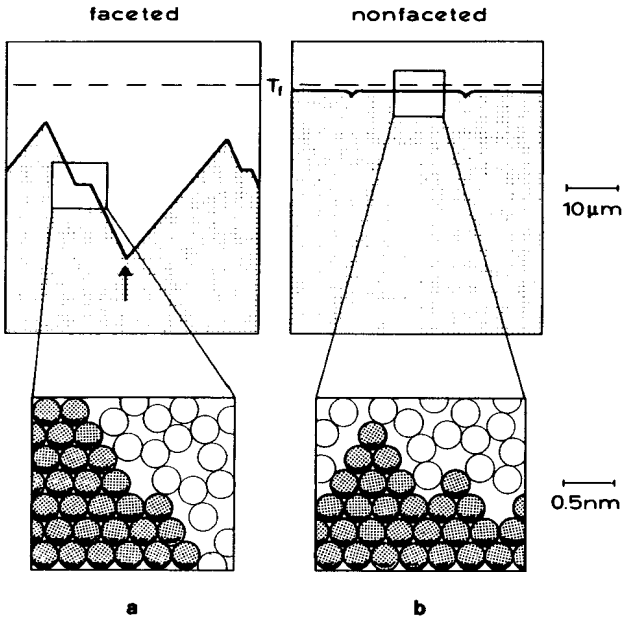

Figure 2.8: FORM OF FACETED (a) AND NON-FACETED (b) INTERFACES. Transparent organic substances, when observed under the microscope during directional solidification (upwards growth), exhibit the forms shown in the upper diagrams (the liquid is uppermost). It is important to note that, during growth, a faceted interface (a) is jagged and faceted at the microscopic scale (upper diagram), but smooth at the atomic scale (lower diagram). On the other hand, a non-faceted interface (b) can be microscopically flat (upper diagram), while at the atomic scale it is rough and uneven (lower diagram). This roughness causes the attachment of atoms to be easy and largely independent of the crystal orientation. Note also that the interface of a non-faceted material will grow at a temperature which is close to the melting point, T_f, while the interface of a faceted material might have a very high local undercooling. Such a point (arrow) is a re-entrant corner (figure 2.10), and is associated with an increased number of nearest neighbours. Thus, growth will tend to spread from here.

leads to a characteristic crystal form which is bounded by the slowest growing faces (right hand side of figure 2.9).

Metals, on the other hand, have a similar structure, density, and bonding in both the liquid and solid states. Hence, the transition from one phase to the other at the interface is very gradual and the interface becomes rough and diffuse (i.e. it exposes

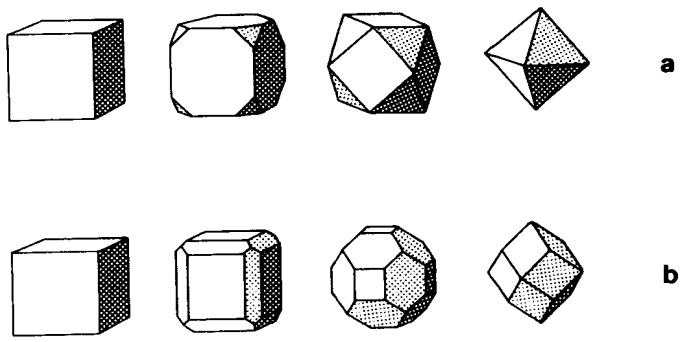

Figure 2.9: DEVELOPMENT OF FACETED CRYSTAL GROWTH MORPHOLOGIES. A growing cubic crystal which is originally bounded only by (100) planes (left hand side) will change its shape to an octahedral form (bounded by (111)) when the (100) planes grow more quickly than the (111) planes (a). Often, impurities change the growth behaviour of specific planes and this results in the appearance of different growth forms for the same crystal structure. If the (110) planes are the slowest-growing, this will lead to a rhombohedral dodecahedron (b). The slowest-growing planes (usually of low-index type) always dictate the growth habit of the crystal. The resultant minimum growth rate form is not the same as the equilibrium (non-growing) form, which is governed by minimisation of the total surface energy. In the above sequences, the crystal size has been kept constant.

Table 2.4: GROWTH MORPHOLOGIES AND CRYSTALLISATION ENTROPIES

Dimensionless Entropy ($\Delta S_f/R$)	Substance	Supersaturated Phase	Morphology
~1	metals	melt	non-faceted
~1	'plastic' crystals	melt	non-faceted
2-3	semiconductors	solution	nf/faceted
2-3	semimetals	solution	nf/faceted
~6	molecular crystals	solution	faceted
~10	metals	vapour	faceted
~20	complex molecules	melt	faceted
~100	polymers	melt	faceted

many suitable growth steps to atoms arriving from the melt).

The melting entropy is a convenient criterion for predicting this aspect of the crystallisation behaviour. Values of α (= $\Delta S_f/R$) which are less than 2 can be taken to imply a tendency to non-faceted crystal growth, while higher α-values imply that faceted growth forms will be produced.

In table 2.4, a list of different substances is presented which compares their growth forms and their dimensionless entropies for crystallisation from various media. The fact that metals and plastic crystals (§) fall into the same group is of great value in the study of solidification. The interior of metals can obviously not be observed using visible light, whereas the transparent, low-melting-point organic crystals can easily be studied in this way. Microscopic study of their interface morphology during growth has provided a good deal of useful information and continues to be an attractive research tool.

A high entropy of fusion increases the disparity in growth rates between the low-index planes and the faster-growing high-index planes. Table 2.5 presents some

Table 2.5: GROWTH RATE COEFFICIENT, K_{hkl}, AS A FUNCTION OF CRYSTALLISATION ENTROPY FOR A SIMPLE-CUBIC TWO-DIMENSIONAL CRYSTAL (Jackson, 1968)

Dimensionless Entropy, α	K_{100}	K_{111}	K_{111}/K_{100}
1	0.2	0.1	0.5
5	0.007	0.01	1.4
10	0.000005	0.0001	20.0

§ Plastic crystals are a special class of molecular substance (organic or inorganic) whose molecular asymmetry is destroyed by rotational motion. That is, the molecules behave like spheres having surfaces defined by the envelope of all of the possible arrangements of the molecule's extremities. Since these 'spheres' no longer exhibit asymmetry or directional bonding, they can arrange themselves into simple crystal structures; particularly cubic ones, and many of their properties are analogous to those of metals. For example, the name, 'plastic', refers to their observed high malleability. In the present context, however, it is interesting to note that they were first recognised as a distinct class due to their low entropies of fusion. This also indicates that their crystallisation behaviour will be analogous to that of metals.

numerical estimates for growth rate coefficients, K_{hkl}, as a function of the dimensionless entropy and crystallographic plane for a simple-cubic, two-dimensional crystal (appendix 5), used as a rough approximation of the behaviour of a real three-dimensional crystal. At small undercoolings, with respect to T_f, the actual growth rate of the faces can be obtained from the expression:

$$V = K_{hkl} \Delta T \qquad [2.13]$$

This expression corresponds to equation A5.7, and assumes that a simple growth mechanism is operating. It can already be seen from this simple example that a very marked anisotropy results in the case of a high melting entropy. That is, the ratio of $V_{[111]}$ to $V_{[100]}$ is increased, and the absolute growth rates are markedly decreased. As a consequence, a crystal of a substance having a large value of α will be bounded by (100) planes.

Observation of primary crystals growing from melts of various composition often permits the relative growth rates of different crystal faces to be deduced.

The widest range of morphologies arising from differences in the growth rates of various faces is probably that exhibited by hexagonal ice crystals growing from the vapour. An example of more practical importance to metallurgists is that of cast iron. The faceted phase (graphite) grows at a different rate in different directions. When $V_{[0001]}$ is less than $V_{[10\bar{1}0]}$, plates delimited by (0001) planes appear, and the morphology is referred to as 'flake graphite'. When $V_{[10\bar{1}0]}$ is less than $V_{[0001]}$, hexagonal prisms form. Often, this is not immediately evident because the prisms tend to grow in a radial direction and the morphology is then called 'spherulitic'. Changes in the growth behaviour of graphite are obtained in practice by controlling the trace element concentration. For example, the presence of S leads to the appearance of flake graphite while the presence of Mg or Ce results in the production of nodular cast iron.

Due to the greater difficulties experienced in attaching atoms to the surfaces of substances possessing a high entropy of fusion, surface defects are of particular importance in this case. Evidently, such defects do not greatly facilitate growth if the attachment of the atoms easily removes them. Therefore, only those defects which cannot be eliminated by growth are effective (figure 2.10). These include screw dislocations which emerge at the growth surface, twin boundaries, and rotation boundaries. Each of these supplies re-entrant corners (steps) which locally increase the number of bonds which an attached atom makes with the crystal (figure 2.7). This reduces the kinetic undercooling and leads to highly anisotropic growth. As a result, the morphology becomes sheet-like (planar defect in b and c) or whisker-like (line defect in a). This phenomenon has a marked effect upon the growth behaviour of the most widely used eutectic alloys, Fe-C and Al-Si (chapter 5).

Finally, it should be noted that under a sufficiently high driving force (e.g. high undercooling) the atomic interface of even a high melting entropy phase may become rough. Its growth behaviour then becomes more isotropic.

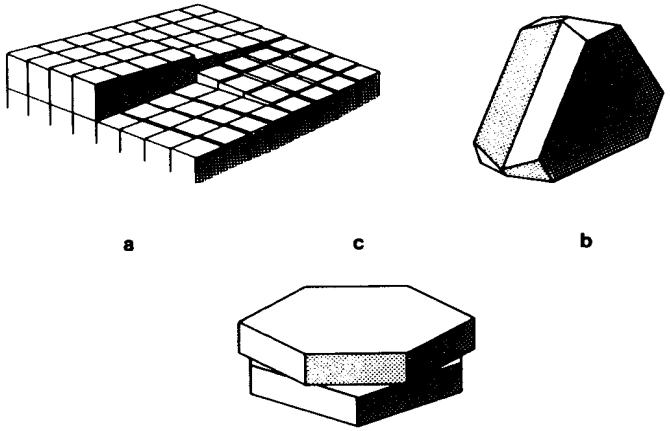

Figure 2.10: REPEATABLE GROWTH DEFECTS IN FACETED CRYSTALS. As pointed out with reference to figure 2.7, steps in rows of atoms are favoured growth sites, but can easily be eliminated by the very growth which they promote. Several types of defect have been shown to provide steps and also to be impossible to eliminate by growth. These are the emergent screw dislocation (a) [F.C.Frank: Discussions of the Faraday Society 5 (1949) 48], which leads to the establishment of a spiral ramp; the re-entrant corner due to twinning (b) [D.R.Hamilton, R.G.Seidensticker: Journal of Applied Physics 31 (1960) 1165] which acts as a macroscopic step; and the twist (rotation) boundary which also provides effective steps (c). Depending upon the type of defect present, the faceted crystal can exhibit various morphologies: needles in the case of line defects (a), or plates in the case of planar defects - e.g. Si in Al-Si alloys (b) or graphite in cast iron (c) [I.Minkoff in: The Solidification of Metals, Iron and Steel Institute Publication 110, London, 1968]. The latter two defects are important in understanding the growth of irregular eutectic microstructures.

BIBLIOGRAPHY

- Nucleation Theory

M.Volmer, A.Weber: Zeitschrift für Physikalische Chemie 119 (1926) 277
R.Becker, W.Döring: Annalen der Physik 24 (1935) 719
D.Turnbull, J.C.Fisher: Journal of Chemical Physics 17 (1949) 71
D.R.Uhlmann, B.Chalmers: Industrial and Engineering Chemistry 57 (1965) 19
B.Cantor, R.D.Doherty: Acta Metallurgica 27 (1979) 33
C.V.Thompson, F.Spaepen: Acta Metallurgica 31 (1983) 2021

- Nucleation Experiments

D.Turnbull, R.E.Cech: Journal of Applied Physics 21 (1950) 804
M.E.Glicksman, W.J.Childs: Acta Metallurgica 10 (1962) 925
J.H.Perepezko, J.S.Paik in: Proceedings of the Materials Research Society Symposium on Rapidly Solidified Amorphous and Crystalline Alloys (edited by B.H.Kear and B.C.Giessen), North-Holland, New York, 1982

- Inoculation

A.Cibula: Grain Control, University of Sussex, Institution of Metallurgists, London, 1969, pp22
I.Maxwell, A.Hellawell: Acta Metallurgica 23 (1975) 229
T.W.Clyne, M.H.Robert: Metals Technology 7 (1980) 177
J.H.Perepezko, S.E.LeBeau in: Proceedings of the 2nd International Symposium on Al-Transformation Technology and its Applications, Buenos Aires, August, 1981.

- Solid/Liquid Interface Structure

K.A.Jackson in: Liquid Metals and Solidification, American Society for Metals, Cleveland, 1958, p174
K.A.Jackson: Journal of Crystal Growth 3/4 (1968) 507
G.H.Gilmer, K.A.Jackson in: Crystal Growth and Materials (edited by E.Kaldis and H.J.Scheel), North-Holland, 1977
D.Camel, G.Lesoult, N.Eustathopoulos: Journal of Crystal Growth 53 (1981) 327

- Crystal Growth Form

H.E.Cline: Journal of Crystal Growth 51 (1981) 97
B.Lux, M.Grages, W.Kurz: Praktische Metallographie 5 (1968) 567
I.Minkoff, S.Myron: Philosophical Magazine 19 (1969) 379
M.Fredriksson, M.Hillert, N.Lange: Journal of the Institute of Metals 101 (1973) 285

EXERCISES

2.1 - Show that setting the first derivative of equation 2.4 equal to zero leads to equation 2.1.

2.2 - Compare the dA/dv ratio of spheres and cylinders with equation 1.5, and the curvature of the critical nucleus.

2.3 - What is the meaning of the expression, $d(\Delta G)/dr = 0$, in terms of the forces acting upon the critical nucleus?

2.4 - Develop an equation for ΔG-n which is analogous to equation 2.4, and calculate ΔG_n° and n°.

2.5 - Derive equation 2.5. What approximations are made? Why must caution be exercised when applying it to cases involving high undercooling?

2.6 - For small undercoolings, the nucleation rate given by equation 2.11 can be written in the form, $I = K_1 \exp[-K_2/\Delta T^2]$. Develop expressions for K_1 and K_2 and explain the origin of the term, ΔT^2. Determine how much K_1 and K_2 must change in order to double the value of ΔT required to produce one nucleus $m^{-3}s^{-1}$ when K_1 is originally equal to $10^{37} m^{-3}s^{-1}$.

2.7 - In his classic experiments, Turnbull divided a melt up into droplets which were only a few microns in diameter in order to measure the temperature at which homogeneous nucleation occurred. Why did he use this method?.

2.8 - By measuring the temperature required for homogeneous nucleation, it is possible to determine the solid/liquid interface energy, which is difficult to measure using other methods. Develop the equations needed for this with the aid of equation 2.11. In order to learn more about this technique, the reader should consult the papers of D.Turnbull: Journal of Applied Physics 21 (1950) 1022 and J.H.Perepezko et al in: Solidification and Casting of Metals, The Metals Society, London, 1979, p169.

2.9 - Show that n° and ΔG° are functions of θ but not r°. Why is this so? (See appendix 3, figure 3.7).

2.10 - Determine the curvature and the melting point of a pure iron crystal in a wetted ($\theta = 30°$) conical pore in the crucible surface, as illustrated below.

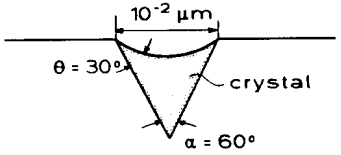

2.11 - What will happen if one stirs 0.1wt% of Ti powder into a pure Al melt at 700C just before casting? (Hint: consult the phase diagram!). For more details, see T.W.Clyne, M.H.Robert: Metals Technology 7 (1980) 177.

2.12 - Water and Bi expand during solidification. From this fact alone, one can make predictions concerning the entropy of melting, and therefore the crystallisation behaviour, in terms of the faceted/non-faceted classification. What reasoning would you employ?

2.13 - Show graphically in two dimensions why rapidly growing planes disappear during crystal growth and leave the slowest growing ones.

2.14 - What is the difference in the shape of an equilibrium crystal, when $V = 0$ and σ is a minimum for $\{111\}$, and the shape arising from growth when $V > 0$ and is a minimum for $\langle 100 \rangle$?

2.15 - Explain why an atomically smooth interface is usually microscopically rough when growing in a temperature gradient (figure 2.8a - top).

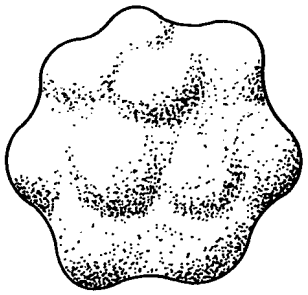

CHAPTER THREE

MORPHOLOGICAL INSTABILITY OF A SOLID/LIQUID INTERFACE

Classical thermodynamic definitions of stability are inapplicable to the determination of the morphology of a growing interface, and current extensions of equilibrium thermodynamics have not yet furnished a fully acceptable alternative. Meanwhile, in order to proceed with theoretical analyses of growth morphologies, it has been found necessary to use heuristically-based stability criteria. The simplest assumption made is that the morphology which appears is the one which has the maximum growth rate or minimum undercooling. An alternative method is the use of stability arguments. These involve perturbing the mathematical function, which describes the solid/liquid interface morphology, in order to determine whether it is likely to change into another one. The interface is then said to be morphologically unstable if the perturbation is amplified with the passage of time and to be morphologically stable if it is damped out (figure 3.1).

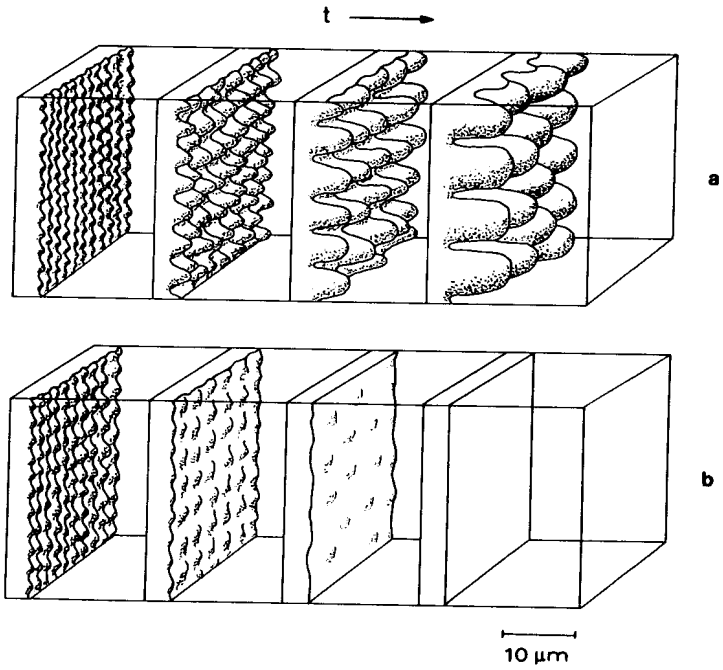

Figure 3.1: INITIAL EVOLUTION OF AN UNSTABLE (a) or STABLE (b) INTERFACE. Such an interface might be observed during light microscopical observation of transparent non-faceted organic substances. During growth, any interface will be subject to random disturbances caused by insoluble particles, temperature fluctuations, or grain boundaries. A stable interface is distinguished from an unstable interface by its response to such disturbances. It is imagined here that the interface is initially slightly distorted by a spatially regular disturbance. If the distorted interface is unstable (a), the projections may find themselves in a more advantageous situation for growth and therefore increase in prominence. In the case of a stable interface (b), the perturbations will be unfavourably situated and tend to disappear. During the casting of alloys, the solid/liquid interface is usually unstable. A stable interface is only obtained in special cases such as columnar solidification of pure metals (figure 1.7a) or directional solidification of alloys in a Bridgman-type furnace (figure 1.4a) under a sufficiently high temperature gradient, G. The indicated scale is typical for alloys under normal casting conditions.

3.1 Interface Instability in Pure Substances

The conditions which lead to instability can easily be understood in the case of a pure substance. Figure 3.2 illustrates, in a schematic manner, the development of a perturbation during columnar and equiaxed growth (see also figure 1.7).

During columnar growth of a pure substance (figure 3.2a), the temperature given by the heat flux, T_q, increases in the z-direction (i.e. G is positive). The interface will be found at the isotherm where the temperature, T_q, imposed by the heat flux is equal to the equilibrium melting point, T_f (§).

If an interface perturbation is to remain at the melting point over its entire surface, and curvature effects are neglected, the temperature field (T_q) must be deformed so that the temperature gradient in the liquid at the tip (along line A-A) increases while the temperature gradient in the solid decreases. According to Fourier's first law this means that the heat flux from the liquid to the tip increases and that the flux in the solid decreases. Therefore, more heat will flow into the tip and less will flow out of it. Meanwhile, the reverse situation occurs in the depressions (line B-B). As a result, the perturbation tends to be damped out. Thus, the interface of a pure substance during columnar growth will always be stable.

Turning now to equiaxed solidification, the situation is completely different (figure 3.2b). In this case, the heat flux does not reach the mould wall via the solid but through the melt. Therefore, the melt must be undercooled in order to establish the necessary temperature gradient at the solid/liquid interface. The temperature gradient in the liquid will therefore be negative, while the gradient in the solid is essentially zero. A perturbation will sense a higher gradient at its tip, leading to an increased heat flux, and a resultant increase in the growth rate of the tip. Thus, the interface of a pure substance (with negligible kinetic undercooling) will always be unstable under equiaxed solidification conditions. The immediate result is that equiaxed grains in a pure metal always adopt a dendritic morphology (figure 1.7b). Because segregation is absent, the dendritic form will not be detectable in a solid, pure metal casting. Fortunately, the characteristics of dendritic growth in this case

§ In general, a growing interface will always require some (kinetic) undercooling below the equilibrium melting point for its advance (figure 2.8 and equation 2.13). In faceted substances, this undercooling may be appreciable (greater than 1K). In non-faceted substances, such as metals, its value will be negligibly small in most cases. Its effect can generally be ignored for these materials under normal solidification conditions.

can be very closely observed in pure organic substances or in pure water.

It can be concluded that the solid-liquid interface of a pure metal will always be stable if the temperature gradient is positive, and unstable if the gradient is negative. Perturbations will grow if the temperature gradient at the interface, given by the heat flux, $G = dT_q/dz$, obeys the relationship:

$$G < 0 \qquad \text{(pure metals)} \qquad [3.1]$$

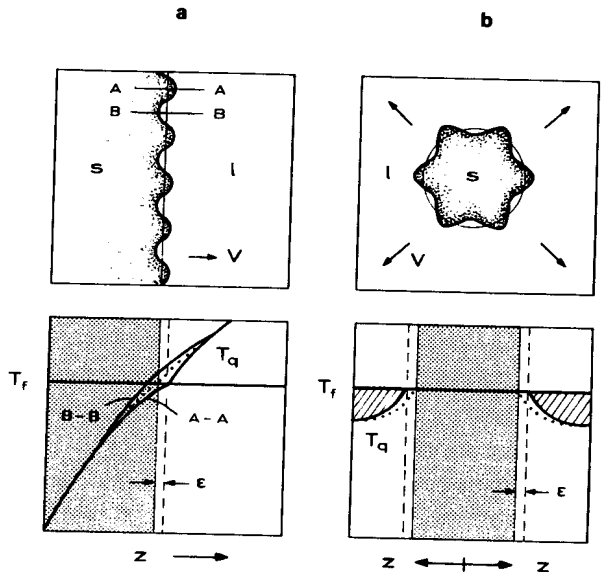

Figure 3.2: COLUMNAR AND EQUIAXED SOLIDIFICATION OF A PURE SUBSTANCE. In a pure substance, stability depends on the direction of heat flow. In directional solidification, as in the columnar zone of a casting, the temperature always increases with distance ahead of the interface (a). Therefore, the heat flow direction is opposite to that of solidification. When a perturbation of amplitude, ϵ, forms at an initially smooth interface (thin line in the above figure), the temperature gradient in the liquid increases while the gradient in the solid decreases (compare full and dotted lines along section, A-A). Since the heat flux is proportional to the gradient, more heat then flows into the tip of the perturbation and less flows out of it into the solid. As a result, the perturbation melts back and the planar interface is stabilised. In equiaxed solidification, the opposite situation is found (b). Here, the free crystals grow into an undercooled melt (cross-hatched region) and the latent heat produced during growth also flows down the negative temperature gradient in the liquid. A perturbation which is formed on the sphere will make this gradient steeper (full line compared to the dotted line) and permit the tip to reject more heat. As a result, the local growth rate is increased and the interface is always morphologically unstable.

3.2 Solute Pile-Up at a Planar Solid/Liquid Interface

In alloys, the criterion for stable/unstable behaviour is more complicated because the local equilibrium melting point can vary along the solid/liquid interface. During the solidification of an alloy, solute will pile up ahead of the interface due to the smaller solubility of the solid when the distribution coefficient is less than unity (figure 1.11). The excess solute rejected from the solid will accumulate in an enriched boundary layer ahead of the interface. The fully developed diffusion boundary layer, which is analogous to the bow wave of a ship, is illustrated in figure 3.3. It is established during a transient period before steady-state (time-independent) growth begins. In this steady-state situation, where all of the concentrations are constant with respect to a reference frame moving with the solid/liquid interface, the solid forms at the solidus temperature. Therefore, the composition of the solid is equal to that, C_o, of the liquid far ahead of the interface (where the effect of the solute pile-up has not yet been felt). The solute concentration in the boundary layer decreases exponentially, from C_o/k to C_o, according to (appendix 2):

$$C_l = C_o + \Delta C_o \exp[-\frac{Vz}{D}] \qquad [3.2]$$

Mathematically, the thickness, δ_c, of the boundary layer is infinite. However, for practical purposes it can be taken to be equal to the 'equivalent boundary layer' (appendix 2):

$$\delta_c = \frac{2D}{V} \qquad [3.3]$$

This length is equal to the base-length of a right-angled triangle having a height which is equal to the excess solute concentration at the interface, and an area which is the same as that under the exponential curve. Equation 3.3 reveals that the equivalent boundary layer thickness is inversely proportional to the growth rate.

A simple flux balance shows that an interface of area, A, rejects J_s atoms per second:

$$J_s = A\,(\frac{dz}{dt})\,(C_l^* - C_s^*) \qquad [3.4]$$

where the term, A(dz/dt), represents the volume of liquid which is transformed to solid per unit time, and the second term represents the difference in the solute concentrations in the liquid and the solid at the interface. Under steady-state

conditions, the resultant flux of rejected solute has to be balanced by an equal flux which takes solute away from the interface by diffusion. The flux in the liquid is:

$$J_l = -AD\left(\frac{dC_l}{dz}\right) \qquad [3.5]$$

Equating the fluxes and noting that, in the steady state, $C_l^* = C_o/k$, gives the important flux balance:

$$G_c = \left(\frac{dC_l}{dz}\right)_{z=0} = -\left(\frac{V}{D}\right)\Delta C_o \qquad [3.6]$$

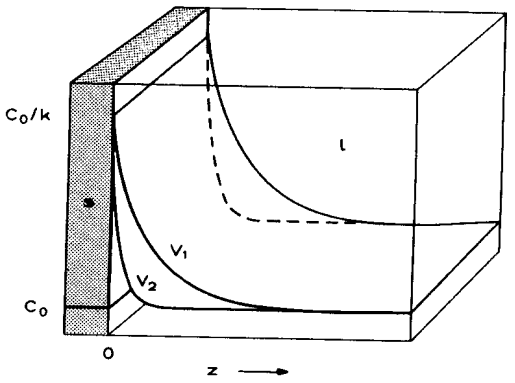

Figure 3.3: STEADY-STATE BOUNDARY LAYER AT A PLANAR SOLID/LIQUID INTERFACE. In the case of an alloy, the stability arguments are similar to those advanced in the caption to figure 3.2, except that solute diffusion as well as heat flow effects must be considered. The former will be considered here. Firstly, as the interface advances, solute is rejected if the solubility of the solute in the solid is lower than that in the liquid (k less than unity). When the interface has been advancing for some time, the concentration distribution becomes time-independent (steady-state). If a planar interface is advancing under steady-state conditions at a rate which permits local equilibrium to be assumed, then the solute concentration in the solid is the same as that of the original melt (appendix 2). Under these circumstances, the concentration in the liquid decreases exponentially from the maximum composition, C_o/k, at the interface to the original composition, C_o, far from the interface. In general, the rate of rejection of solute at the interface is proportional to the growth rate. The rejected solute must be carried away by diffusion down the interfacial concentration gradient, and this therefore becomes steeper with increasing growth rate. In the figure, the boundary layers for two growth rates, $V_2 > V_1$, are shown.

3.3 Interface Instability in Alloys

It is seen from the above that, during the solidification of an alloy, there is a substantial change in the concentration ahead of the interface. This change will affect the local equilibrium solidification temperature, T_l, of the liquid, which is related to the composition by:

$$T_l(C_o) - T_l = m(C_o - C_l) \qquad [3.7]$$

where $T_l(C_o)$ is the liquidus temperature corresponding to the initial alloy composition. This relationship is shown in figure 3.4 and indicates that the concentration boundary layer can be converted, using the phase diagram, into a liquidus-temperature boundary layer. The liquidus temperature increases with increasing z, when the value of k is less than unity, because the value of m is then negative. It represents the local equilibrium temperature for the solidification of a corresponding volume element of the melt. To investigate stability, it is also necessary to determine the temperature, T_q, imposed by the heat flux. Both temperatures must be equal at the interface (see previous footnote). In the steady state growth of a planar interface, this will correspond to the solidus temperature for the composition, C_o, as shown in figure 3.4.
Depending upon the temperature gradient,

$$G = \left(\frac{dT_q}{dz}\right)_{z=0} \qquad [3.8]$$

in the liquid at the solid/liquid interface (which is imposed by the external heat flux) there may, or may not, exist a zone of constitutional undercooling (figure 3.5). This zone is defined to be that volume of melt ahead of the interface within which the actual temperature, T_q, is lower than the local equilibrium solidification temperature, T_l. The melt in this zone is thus undercooled, i.e., in a metastable state. It is quickly seen that the condition required for the existence of such a constitutionally undercooled zone is that the temperature gradient, G, at the interface in the liquid should be lower than the gradient of liquidus temperature change in the melt. The latter gradient is obtained by multiplying the concentration gradient, G_c, by the liquidus slope, m. Therefore, the interface is constitutionally undercooled when:

$$G < mG_c \qquad \text{(alloys)} \qquad [3.9]$$

As before, consider the behaviour of a perturbation arising during directional solidification. Such a protuberance at the solid/liquid interface will increase the local temperature gradient in the melt. In the case of a pure melt (figure 3.2), this led to the disappearance of the perturbation. However, in an alloy melt (figure 3.4), the local concentration gradient will also become steeper and consequently the local gradient of the liquidus temperature will increase. Hence, the region of constitutional supercooling will tend to be preserved.

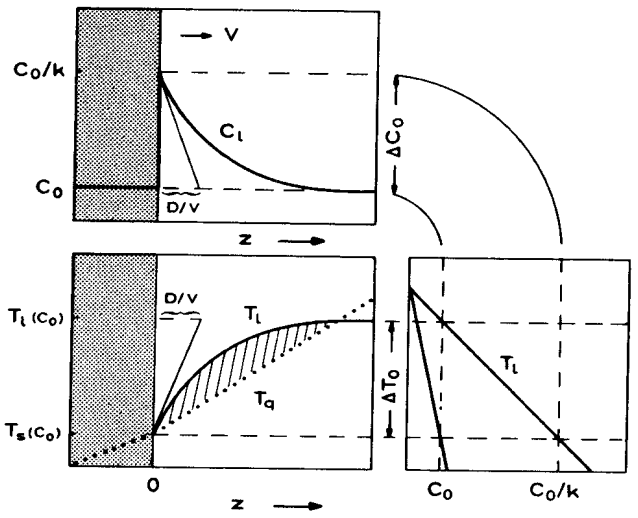

Figure 3.4: CONSTITUTIONAL UNDERCOOLING IN ALLOYS. The steady-state diffusion boundary layer, shown in figure 3.3, is reproduced here (upper diagram) for a given growth rate. As the liquid concentration, C_l, decreases with distance, z, the liquidus temperature, T_l (i.e. the melting point), of the alloy will increase as indicated by the phase diagram. This means that if small volumes of liquid at various distances ahead of the solid/liquid interface were extracted by some means and solidified, their equilibrium freezing points would vary with position in the manner described by the heavy curve in the lower left-hand diagram. However, each volume element finds itself at a temperature, T_q, which is imposed by the temperature gradient arising from the heat flow occurring in the casting. Since, at the solid/liquid interface (z=0), T_q must be less than or equal to T_s in order to drive the atomic addition mechanism, there may exist a volume of liquid which is undercooled when the gradient of T_q is less than the gradient of T_l. This (cross-hatched) region is called the zone of constitutional undercooling. There exists a driving force for the development of perturbations in this volume as in figure 3.2b.

In the introduction to this chapter, it was stated that equilibrium thermodynamics principles could not properly be applied to solidification. However, it is interesting to see how far the use of such classical methods can be pursued in this non-equilibrium situation. In general, growth rates and undercoolings are found to be closely related by functions whose form depends upon the process controlling growth (atomic attachment, mass diffusion, or thermal diffusion). In each case, the growth rate increases with increasing undercooling. An interface perturbation can be imagined to experience a driving force, f', for accelerated growth which is given by the negative value of the first derivative of the Gibbs free energy with respect to distance:

$$f' = -\frac{d(\Delta G)}{dz} \qquad [3.10]$$

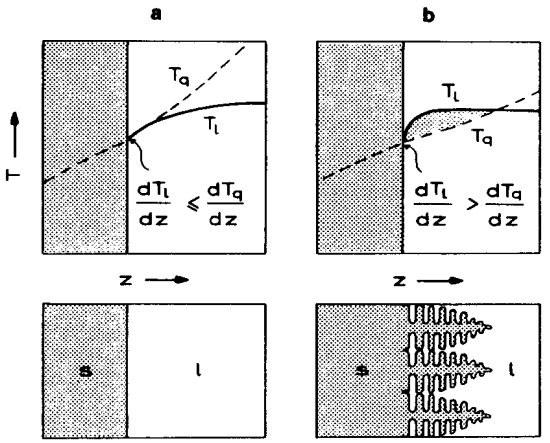

Figure 3.5: CONDITION FOR CONSTITUTIONAL UNDERCOOLING AT THE SOLID/LIQUID INTERFACE, AND THE RESULTANT STRUCTURES. When the temperature gradient due to the heat flux is greater than the liquidus temperature gradient at the solid/liquid interface, the latter is stable (a). On the other hand, it can be seen that a driving force for interface change will be present whenever the slope of the local melting point curve (liquidus temperature) at the interface is greater than the slope of the actual temperature distribution. This is easily understood since the undercooling encountered by the tip of a perturbation advancing into the melt increases and therefore a planar interface is unstable (b). After the dendritic microstructure shown has developed, the region of constitutional undercooling is largely eliminated.

For small undercoolings, $\Delta G = \Delta S_f \Delta T$ and ΔS_f = constant. Thus,

$$f' = -\Delta S_f \left(\frac{d\Delta T}{dz}\right) = -\Delta S_f \phi \qquad [3.11]$$

where $\Delta T = T_l - T_q$, and ϕ is the difference between the liquidus temperature gradient (mG_c) and the heat-flux-imposed temperature gradient at the interface (G):

$$\phi = \left(\frac{d\Delta T}{dz}\right)_{z=0} = \left(\frac{dT_l}{dz} - \frac{dT_q}{dz}\right)_{z=0} = mG_c - G \qquad [3.12]$$

Since ΔS_f is negative for solidification, a positive driving force will exist which causes any perturbation to grow when ϕ is positive, i.e. when a zone of constitutional undercooling exists ahead of the interface. If its value is zero or negative, G is equal to, or greater than, mG_c. The limiting condition for constitutional undercooling is therefore:

$$\phi = 0 \qquad [3.13]$$

Thus, this pseudo-thermodynamic approach gives the same result as that deduced from consideration of the zone of constitutional undercooling. Since the concentration gradient at the interface is known, it is simple to derive the criterion for the existence of constitutional undercooling in another form. The interface will always become unstable if equation 3.9 is satisfied. Using equation 3.6, this can be written:

Table 3.1: SUMMARY OF STABILITY CONDITIONS IN PURE METALS AND ALLOYS

	Growth Conditions	
	Equiaxed ($G < 0$)	Columnar ($G > 0$)
pure metal	-	+
alloy	-	- ($\phi > 0$) + ($\phi < 0$)

(-) interface always unstable, (+) always stable

$$G < -\frac{mV\Delta C_o}{D} \qquad [3.14]$$

Also, because $-m\,\Delta C_o = \Delta T_o$ (equation 1.9), the limit of constitutional undercooling can be expressed in its usual form:

$$\frac{G}{V} = \frac{\Delta T_o}{D} \qquad [3.15]$$

or

$$V_c = \frac{GD}{\Delta T_o}$$

where ΔT_o can be replaced by the expression: $mC_o(k-1)/k$ (equations 1.9, 1.10). If G/V is smaller than $\Delta T_o/D$, instability will result (§).

Table 3.1 summarises the types of interface morphology to be expected under various conditions, and table 3.2 presents typical numerical values involved in constitutional undercooling. It is evident that, even for relatively low solute concentrations, high temperature gradients must be imposed in order to suppress interface instability and cellular or dendritic growth. Note that, in the preparation of single crystals, or in other directional growth processes, a gradient of 20K/mm is considered to be high.

So far, only the limit of stability has been estimated. Nothing has been said about the form and scale of the perturbations which will develop if the interface is unstable.

Table 3.2: MINIMUM STABILISING TEMPERATURE GRADIENT (K/mm) AS A FUNCTION OF PHASE DIAGRAM PARAMETERS ($D = 0.005 mm^2/s$, $V = 0.01 mm/s$, $m = -10 K/wt\%$)

	C_o(wt%)		
k	10	1	0.01
0.5	200	20	0.2
0.1	1800	180	1.8

§ Note that an exact interface stability analysis leads to a slightly modified criterion (appendix 6).

Information concerning the dimensions of the initial, perturbed morphology is very important because this will influence the spacing of the resultant growth morphologies. However, it must be remembered that the morphology which initially develops at the limit of stability is usually only a transient structure which disappears once the steady-state cellular or dendritic morphology is established (see for example, figure 4.3).

3.4 Perturbation Analyses

A drawback of the constitutional undercooling criterion is that it ignores the effect of the surface tension of the interface. It is reasonable to suppose that the latter should have a marked influence upon interface stability. In order to investigate this possibility, and to learn more about the morphological changes occurring near to the limit of stability, it is necessary to suppose that the interface has already been slightly disturbed and to study its development under the constraints of diffusion and capillarity. More details of this procedure are presented in appendix 6, and the present discussion is intended merely to point out some of the physical principles involved.

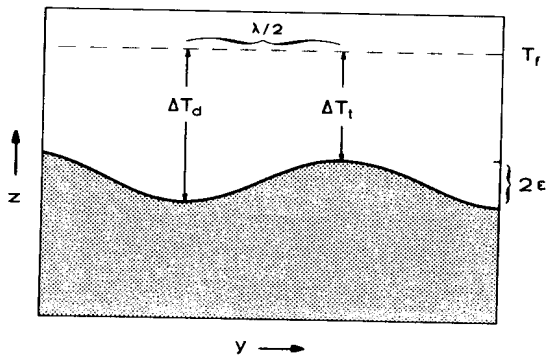

Figure 3.6: INTERFACE PERTURBATIONS AT A SOLID/LIQUID INTERFACE. The existence of a zone of constitutional undercooling implies that a driving force for a change in the morphology is available, but gives no indication of the scale of the morphology which will appear. Experimental observation shows that the initial form of the new morphology is approximately sinusoidal. Perturbation analysis permits the calculation of the wavelength of the instabilities which develop. The result is of great importance in the theory of dendrite and eutectic growth.

Firstly, it is assumed for simplicity that the purely mathematical perturbations (see figure 3.6), which have an infinitesimal amplitude, do not affect the thermal or solutal diffusion fields. The perturbed interface can be described by a simple sine function:

$$z = \epsilon \sin[\omega y] \qquad [3.16]$$

where ϵ is the amplitude, and $\omega (= 2\pi/\lambda)$ is the wave number. The temperature, T*, of the interface can be deduced from the assumption of local equilibrium:

$$T^* = T_f + mC_l^* - \Gamma K^* \qquad [3.17]$$

This equation states that the difference between the melting point, T_f, and the interface temperature, T*, is equal to the sum of the temperature differences due to the local interface composition and local interface curvature. Here, any temperature difference needed to drive atomic processes has been neglected. This is a reasonable assumption in the case of metals and other materials having a low entropy of fusion. Taking just two points, at the tips (t) and depressions (d) of the interface and calculating the temperature difference gives:

$$T_t - T_d = m(C_t - C_d) - \Gamma(K_t - K_d) \qquad [3.18]$$

The curvatures at tips and depressions which are not too accentuated can be determined from the second derivative of the function which describes the interface shape (equation 3.16) at $y = \lambda/4$ and $3\lambda/4$:

$$K_t = -K_d = \frac{4\pi^2\epsilon}{\lambda^2} \qquad [3.19]$$

(Note that K has the opposite sign to that which arises from the mathematical definition - equation 1.4). Since it is assumed that the temperature and concentration fields are unaffected by the presence of a very small perturbation, the temperature and concentration differences between the tips and depressions can be found from the gradients existing at the originally planar interface. Thus:

$$T_t - T_d = 2\epsilon G \qquad [3.20]$$

and

$$C_t - C_d = 2\epsilon G_c \qquad [3.21]$$

Substituting equations 3.19 to 3.21 into equation 3.18 leads to:

$$\lambda_i = 2\pi\sqrt{\frac{\Gamma}{\phi}} \qquad [3.22]$$

where ϕ is the degree of constitutional undercooling as defined in equation 3.12. The wavelength, λ_i (given by equation 3.22), defines a critical perturbation which matches both the thermal and solutal diffusion fields. In this case, the wave-form will be stationary with respect to the unperturbed interface. That is, neither the tip nor the depression will grow.

In order to obtain a relationship between the time dependence of ϵ and λ, one can simplify equation A6.3 by assuming that the solid solubility in the alloy is essentially zero. Thus, k is approximately equal to zero and p is approximately equal to unity. Moreover, the differences in the thermal gradients in the liquid and solid, and the effect of latent heat, can be neglected:

$$\frac{\dot{\epsilon}}{\epsilon} = \left(\frac{V}{mG_c}\right)\left(b - \frac{V}{D}\right)\left(-\omega^2\Gamma - G + mG_c\right) \qquad [3.23]$$

where $\dot{\epsilon} = d\epsilon/dt$. This function ($\dot{\epsilon}/\epsilon - \lambda$) is plotted in figure 3.7 for an Al-Cu alloy, and exhibits a characteristic maximum. At λ values below the maximum, the perturbations develop less quickly or disappear ($\dot{\epsilon}<0$) due to the effect of the high curvature. At λ values above the maximum, the perturbations develop less quickly due to diffusion limitations. The wavelength, λ_i, describes the perturbed morphology which is at the limit of stability ($\dot{\epsilon} = 0$) under conditions of constitutional undercooling. Upon setting equation 3.23 equal to zero and noting that the first of the three terms on the right-hand-side of the equation is not zero, the second term gives, upon substituting for b (see list of symbols):

$$\lambda = \infty$$

The third term gives:

$$\omega^2\Gamma = mG_c - G = \phi$$

or:

$$\lambda_i = 2\pi\sqrt{\frac{\Gamma}{\phi}}$$

This is exactly the same as equation 3.22 which was derived above using a much simpler method. The term, Γ/ϕ, is the ratio of the capillarity force to the driving force for instability. If ϕ tends to zero (the limit of constitutional undercooling), the minimum unstable wavelength approaches infinity. This is to be expected since, at the limit, only the planar interface should be observed. On the other hand, far from the limit of constitutional undercooling in the unstable regime:

$$G \ll mG_c = \frac{\Delta T_o V}{D} \qquad [3.24]$$

Thus, the wavelength becomes, for $V \gg GD/\Delta T_o$:

$$\lambda_i = 2\pi\sqrt{\frac{D\Gamma}{V\Delta T_o}} \qquad [3.25]$$

The latter expression reveals that the wavelength of the unstable morphology is proportional to the geometric mean of a diffusion length (D/V) and a capillarity length ($\Gamma/\Delta T_o$). Increasing D or Γ, and decreasing V or ΔT_o will increase the minimum unstable wavelength.

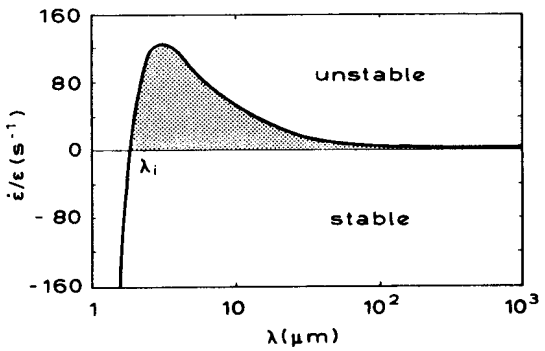

Figure 3.7: RATE OF DEVELOPMENT OF A PERTURBATION AT A CONSTITUTIONALLY UNDERCOOLED INTERFACE (Al-2wt%Cu, V = 0.1mm/s, G = 10K/mm). The parameter, $\dot{\epsilon}/\epsilon$, describes the relative rate of development of the amplitude of a small sinusoidal perturbation. At very short wavelengths, the value of this parameter is negative due to curvature damping and the perturbation will tend to disappear (figure 3.1b). At wavelengths of λ_i and above, the sinusoidal shape will become more accentuated (instability - figure 3.1a). The wavelength having the highest rate of development is likely to become dominant. The reason for the tendency to stability at high λ-values is the difficulty of diffusional mass transfer over large distances. When the interface is completely stable, the curve will remain below the $\dot{\epsilon}/\epsilon = 0$ line for all wavelengths. This implies disappearance of perturbations having any of these wavelengths (appendix 6).

BIBLIOGRAPHY

- Constitutional Undercooling

W.A.Tiller, K.A.Jackson, J.W.Rutter, B.Chalmers: Acta Metallurgica 1 (1953) 428

- Stability Theory

W.W.Mullins, R.F.Sekerka: Journal of Applied Physics 34 (1963) 323
W.W.Mullins, R.F.Sekerka: Journal of Applied Physics 35 (1964) 444
R.F.Sekerka: Journal of Applied Physics 36 (1965) 264
R.F.Sekerka: Journal of Crystal Growth 3 (1968) 71
R.T.Delves in: Crystal Growth (Edited by B.R.Pamplin), Pergamon, Oxford, 1975, p40

- Interface Stability Experiments

S.C.Hardy, S.R.Coriell: Journal of Crystal Growth 7 (1970) 147
R.J.Schaefer, M.E.Glicksman: Metallurgical Transactions 1 (1970) 1973
K.Shibata, T.Sato, G.Ohira: Journal of Crystal Growth 44 (1978) 419

EXERCISES

3.1 - A solid/liquid interface becomes unstable when relation 3.1 (3.9) is obeyed in the case of a pure metal (alloy). Show that relation 3.1 is implied by relation 3.9. Discuss the differences.

3.2 - Indicate why the constitutional undercooling criterion cannot yield the wavelength of the perturbed interface resulting from instability.

3.3 - Discuss the advantage of the Bridgman method (figure 1.4a), over conventional casting processes (figure 1.4b), with respect to the control of interface stability.

3.4 - Determine the phase diagram from the information that the solute distribution ahead of the planar solid/liquid interface of an Al-Cu alloy has been found to be described by:

$$C_l\,[wt\%] = 2(1 + [0.86/0.14]\exp[-Vz/D])$$

under steady-state conditions. It has also been determined that the interface temperature is 624°, and it is known that the melting point of Al is 660°C. Give the values of k, m, ΔT_o, T_l, and ΔC_o.

3.5 - What is the limit of stability, G/V, of the above alloy if it is given that $D = 3 \times 10^{-5} cm^2/s$?

3.6 - Calculate the heat-flux required to produce a value of G which is sufficient to stabilise the planar front in question 3.5 at a growth rate, V, of 10cm/h.

3.7 - By analogy with figure 3.4, draw a diagram for $k>1$ and discuss the constitutional undercooling criterion for this situation. Point out differences between this case and the case where $k<1$.

3.8 - Calculate C_l^*, T*, and the minimum value of G required to stabilise the planar interface of a Cu-10wt%Ni and an Fe-0.01wt%S (see exercise 1.6) alloy during directional growth at a rate of 0.01mm/s. Plot the solute concentration in the boundary layer existing in each case. (See appendix 12 for the data required.)

3.9 - Determine the difference between the critical G/V ratio estimated according to the constitutional undercooling criterion and that estimated according to the Mullins-Sekerka criterion, for Al-2wt%Cu alloy (see appendix 6).

3.10 - Calculate the ratio, λ_m/λ_i, for conditions of high constitutional undercooling and constant V and G values. Here, λ_m is the wavelength which corresponds to the maximum in figure 3.7. Note that b in equation 3.23 is a function of ω and, in appendix 6, is defined as: $b = (V/2D) + \sqrt{[(V/2D)^2 + \omega^2]}$. Under certain conditions, this can be simplified by comparing the relative magnitudes of V/2D and ω. In order to estimate the value of ω, use equation 3.25. Does the value of λ_m/λ_i depend upon the composition of the alloy?

3.11 - Imagine that an experiment is carried out, on the alloy of question 3.4, in which the specimen is solidified using the Bridgman method with a temperature gradient of G = 10K/mm and is maintained at its limit of stability until steady-state conditions are established. The growth rate is then doubled without changing the value of G. Calculate the minimum, and the most probable, wavelength which the resultant perturbation is likely to have.

3.12 - For the case of pure Al at an undercooling of 1K, determine the order of magnitude of the radius of a growing sphere ($R \approx \lambda_i$) at which the spherical crystal will become unstable when growing in its undercooled melt. Assume for the purpose of calculating G that the steady-state solution for the temperature field around a sphere is applicable (appendix 2).

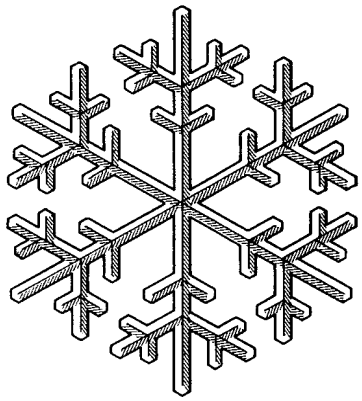

CHAPTER FOUR

SOLIDIFICATION MICROSTRUCTURE: CELLS AND DENDRITES

Nearly all of the solidification microstructures which can be exhibited by a pure metal or an alloy can be divided into two groups: single-phase primary crystals and polyphase structures. The most important growth form, and the one to be discussed in this chapter, is the tree-like primary crystal, i.e. the dendrite. Polyphase structures (eutectics) will be described in the next chapter.

As shown in chapter 1, dendrites, eutectics, or combinations of these, make up the grains of any metallic microstructure after solidification. The growth of both morphologies can be described by analogous theoretical models, the development of which comprises two steps:

1 - derivation of an equation which describes the general relationship between th. scale of the microstructure, the undercooling, and the growth rate,

2 - choice of a criterion which permits the definition of an unique relationship between the scale of the microstructure and the undercooling (in the case of equiaxed growth), or the growth rate (in the case of directional growth)

With regard to the first part of the problem, it is necessary to determine an expression for the heat- and/or solute- distribution and to take account of the effects of capillarity. In the absence of a suitable non-equilibrium thermodynamic criterion, step 2 above can be satisfied by using one of two alternative growth criteria. These are:

i - growth at the extremum - i.e. at the maximum growth rate or minimum undercooling. This assumption can be justified on the basis of non-equilibrium thermodynamic concepts such as minimum entropy production.

ii - growth at the limit of morphological stability. In the case of dendrite growth, use of this criterion leads to better agreement between theory and experiment.

4.1 Constrained and Unconstrained Growth

The situation in which the heat flow is opposite to the growth direction (i.e. directional or columnar solidification - figures 1.7a,c and 4.1a) is often referred to as being constrained growth. That is, the rate of advance of the isotherms constrains the dendrites (which in this situation are only found in alloy solidification) to grow at a given velocity. This forces them to adopt the corresponding tip undercooling. The grain boundaries are parallel to the primary dendrite axes (trunks) and are continuous along the length of the solid. Each dendrite forms low-angle boundaries with its neighbours and many trunks, formed by repeated branching, together make up one grain (figure 4.2).

When the heat flows from the crystal into the melt (equiaxed solidification - figure 1.7b,d and 4.1c), the dendrites can grow freely, in pure materials and alloys, as rapidly as the imposed undercooling permits. The dendrites grow in a radial fashion until they impinge upon dendrites originating from other nuclei, and the grain boundaries form a continuous network throughout the solid (figure 1.9).

In the case of directional growth, most of the dendrites are ar ed parallel to each other and a characteristic trunk spacing (λ_1) can be defined. In the case of equiaxed solidification, each dendrite forms a grain and the primary spacing, λ_1, is usually equal to the grain diameter. A secondary arm spacing, λ_2, can be defined for both columnar and equiaxed dendrites.

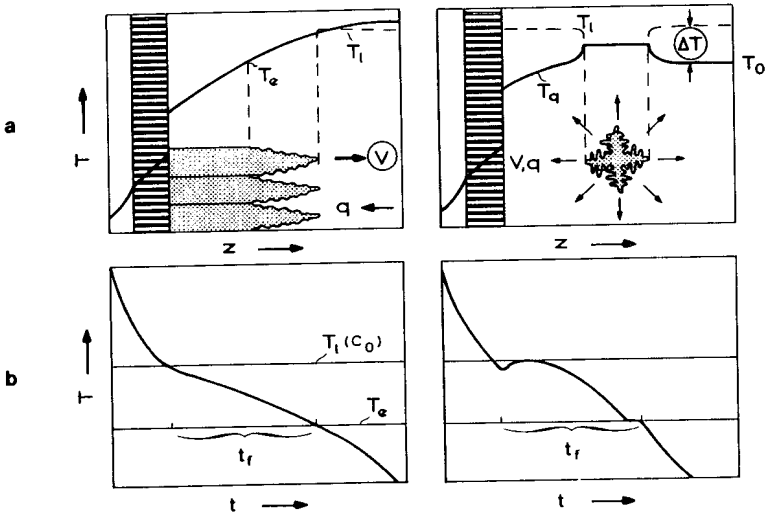

Figure 4.1: THERMAL FIELDS AND COOLING CURVES OF ALLOY DENDRITES. The upper part of the figure corresponds to the lower part of figure 1.7 with superimposed liquidus temperatures (broken lines). The case of directional (columnar) growth is indicated in diagram (a) and that of equiaxed growth in diagram (c). If a thermocouple is placed at a fixed position in the melt and overgrown by the dendrites, different cooling curves will be recorded for directional growth (b) and equiaxed growth (d). This difference is essentially due to nucleation in the case of equiaxed solidification. Due to microsegregation (chapter 6) some eutectic will usually form in the last stages of solidification (i.e. at T_e). Note that, in the case of directional growth, the crystals are in contact with the mould and heat will be conducted through them in a direction which is parallel and opposite to that of their growth. Therefore, the melt is the hottest part of the system. In the case of equiaxed growth, the heat produced by solidification must be transported through the melt. Thus, in this case, the crystals are the hottest part and the heat flux, q, is radial and in the same direction as that of growth. The local solidification time, t_f, is the elapsed time between the beginning and the end of solidification at a fixed point in the system i.e. from the tip to the root of the dendrite.

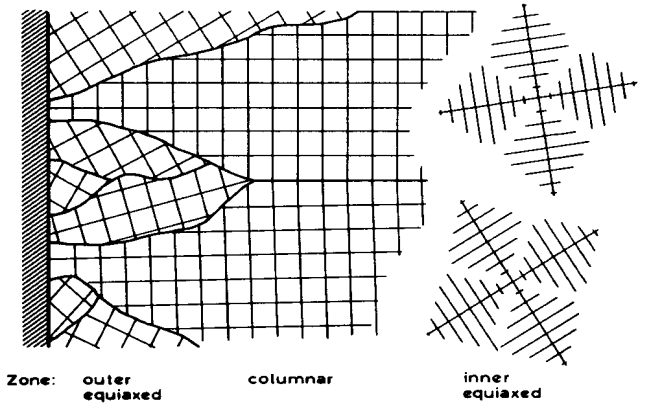

Figure 4.2: FORMATION OF COLUMNAR AND EQUIAXED DENDRITIC MICROSTRUCTURES. Initial competition of crystals nucleated at random at the mould wall, and their growth into the liquid, leads to grain selection. In cubic metals, columnar grains having one [001] axis close to the heat flux direction ultimately overgrow the others. Note that, in this section, differences in the rotation of the columnar grains about their growth axis is not visible. Large orientation differences are accommodated at high-angle grain boundaries. Branching of the dendrites leads to the creation of new trunks which are crystallographically related to the initial primary trunk and form a grain. The transition from columnar to equiaxed growth occurs when the melt has lost its superheat, becoming slightly undercooled, and detached dendrite arms growing in the melt form a barrier ahead of the columnar zone. (Compare with figure 1.6.)

4.2 Morphology and Crystallography of Dendrites

The formation of a dendrite begins with the breakdown of an unstable planar solid/liquid interface. Perturbations are amplified until a marked difference in growth of the tips and depressions of the perturbed interface has occurred. As the tip can also reject solute in the lateral direction, it will tend to grow more rapidly than a depression, which tends to accumulate the excess solute rejected by the tips. Therefore, the form of the perturbation is no longer sinusoidal, but adopts the form of cells (figure 4.3). If the growth conditions are such as to lead to dendrite formation, the cells will rapidly change to dendrites, which exhibit secondary arms and crystallographically governed growth directions. Cell and primary dendrite

spacings are much larger than the wavelength of the original perturbation which initiates the corresponding growth morphology (figure 4.3). It is important to note that cells can only appear during the directional growth of alloys. For instance, cells can grow under conditions such as those indicated in figure 1.7c. In other cases (figures 1.7b,d), only dendrites will be observed. Figure 4.4 summarises the

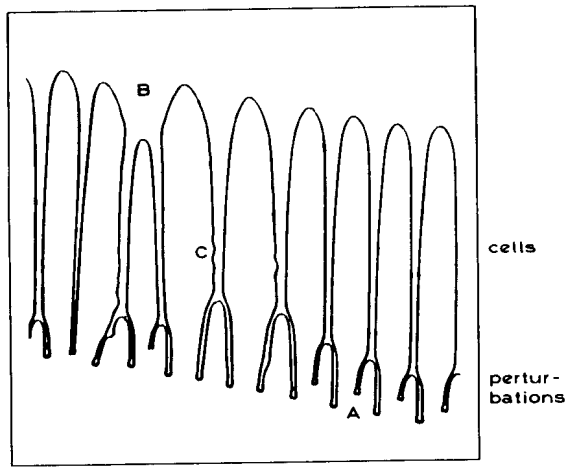

Figure 4.3: BREAKDOWN OF A PLANE SOLID/LIQUID INTERFACE TO GIVE CELLS. The development of perturbations at the constitutionally undercooled solid/liquid interface is only a transient phenomenon. The tips of the perturbations can readily reject solute while the depressed parts of the interface accumulate solute and advance much more slowly. (The effect is rather like pushing ones flattened hand through a layer of sand in a direction which is parallel to the line of the fingers - the sand piles up more rapidly between the splayed fingers than at the finger tips.) The initial wavelength is too small for further rapid growth to occur, and the final result is the formation of a cellular structure. Note that the wavelength has approximately doubled between the initial perturbation and the final cells. Also, the spacing between the cells is not constant. The initial cellular morphology can adjust itself to give a more optimum growth form via the cessation of growth of some cells (B) in order to decrease their number or by the division of cells in order to increase the number present. The division of cells is not shown here, but it resembles the change at point A, with two branches continuing to grow. Furthermore, the larger centre cells(C) have slightly perturbed surfaces and this suggests that, in the intercellular liquid, some driving force remains for further morphological change which might possibly lead to dendrite formation. When the driving force due to the temperature gradient difference is large, i.e. large constitutional undercooling, dendrites form instead of the cells shown.

differences between cells, dendritic cells, and dendrites. Cells are usually ellipsoid-like crystals which grow anti-parallel to the heat flux direction. They grow under conditions which are close to the limit of constitutional undercooling of the corresponding planar interface. On the other hand, dendrites are crystalline forms which grow far from the limit of stability of the plane front and adopt an orientation which is as close as possible to the heat flux direction or opposite to it, but follows one of the preferred growth axes. These directions are crystallographically determined (table 4.1). Equiaxed dendrites grow along all of the available preferred directions when the heat extraction is isotropic. In cubic crystals, the six [001] axes form the trunks and therefore the crystal orientation can easily be determined. In the case of a directionally solidified dendritic monocrystal (e.g. a turbine blade), all of the dendrites composing the monograin are aligned (figure 4.5), leading to improved properties.

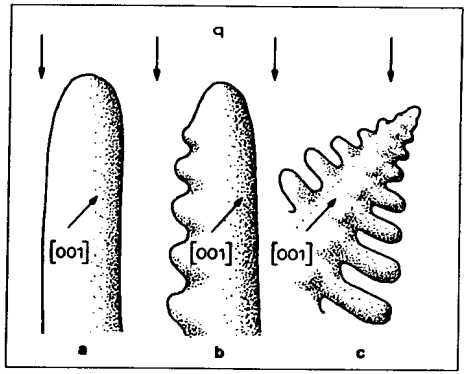

Figure 4.4: CELLS, DENDRITIC CELLS, AND DENDRITES. During directional growth in a positive temperature gradient, and only under those conditions, cells can exist as a stable growth form (a). However, intercellular instability such as that visible in figure 4.3 may lead to dendritic cell formation (b). The asymmetry of the form may be caused by an asymmetry of the thermal field. Dendrites will be particularly common in conventional castings and are characterised by growth of the trunks and branches along preferred crystal orientations such as [001] in cubic crystals (c). Due to the anisotropy of properties such as the solid/liquid interface energy and the growth kinetics, dendrites will grow in that preferred crystallographic direction which is closest to the heat flow direction, whereas cells grow with their axes parallel to the heat flow direction without regard to the crystal orientation. In the above figure, all three of the morphologies have the same crystallographic orientation.

Table 4.1: PREFERRED GROWTH DIRECTIONS OF DENDRITES OF VARIOUS MATERIALS

Structure	Dendrite Orientation	Example
face-centred cubic	<100>	Al
body-centred cubic	<100>	delta-Fe
body-centred tetragonal	<110>	Sn
hexagonal close-packed	<10$\bar{1}$0>	H_2O (snow)
"	<0001>	$Co_{17}Sm_2$

Figure 4.5: TRANSVERSE SECTION OF A MONOCRYSTALLINE GAS-TURBINE BLADE. In an alloy, the last (interdendritic) liquid to solidify always has a different composition compared to that of the first crystals (dendrite trunks) to form. Therefore, the dendritic structure can be revealed in a casting due to variations in etching behaviour. This is seen in the above transverse section of a directionally solidified monocrystalline turbine blade. The orientation of the dendrite trunks is parallel to the blade axis (and perpendicular to the plane of this section). The absence of high-angle grain boundaries improves the high-temperature strength and fatigue behaviour of superalloy castings used in jet-aircraft. The formation of such a monocrystal can be understood with the aid of figure 4.2. During the initial stages of growth, when a columnar zone has progressed to some distance from a chill plate, the grains enter a restriction placed in the path of the growing crystals. As a result, only one grain can continue to grow and form the blade. This is the principle used in alloy single-crystal casting. (Photograph - Pratt and Whitney).

If a single dendrite could be extracted from the columnar zone of a casting during growth, it would resemble the one depicted schematically in figure 4.6. Behind a short paraboloid tip region, which often constitutes less than 1% of the length of the whole dendrite, perturbations appear on the initially smooth needle as in the case of the breakdown of a planar interface. These perturbations grow and form branches in the

four [001] directions which are perpendicular to the trunk. If the primary spacing is sufficiently great, these cell-like secondary branches will develop into dendritic-type branches and lead to the formation of tertiary and higher-order arms. When the tips of the branches encounter the diffusion field of the branches of the neighbouring dendrite, they will stop growing and begin to ripen and thicken. Thus, the final secondary spacing will be very different to the initial one. Compare the upper and lower parts of figure 4.6. The final value of λ_2 is largely determined by the contact time between the branches and the liquid. This period is known as the local solidification time, t_f, and is given by the time required for a thermocouple placed at a fixed point to pass from the tip to the root of the growing dendrite (figure 4.1).

4.3 Diffusion Field at the Tip of a Needle-Like Crystal

The growth rate, as well as the dendrite morphology or spacing, are all largely dependent upon the behaviour of the tip region. During the growth of the tip, either heat (in the case of pure metals) or heat and solute (in alloys) are rejected (figure 4.7). These diffusion processes are driven by gradients in the liquid, and the latter are in turn due to differences in temperature (ΔT_t) and concentration (ΔT_c) ahead of the growing crystal. The concentration difference can be converted into a liquidus temperature difference via the phase diagram, as shown in figure 3.4. After adding the temperature difference, at the solid/liquid interface, caused by the curvature of the tip (ΔT_r), the coupling condition (see figure A7.1) can be written:

$$\Delta T = \Delta T_c + \Delta T_t + \Delta T_r \qquad [4.1]$$

In this equation, the possibility of kinetic undercooling has been neglected. This is a reasonable assumption in the case of materials, such as metals, which exhibit a low entropy of melting.

The current state of knowledge concerning the equiaxed dendritic growth of pure substances has been reviewed by Huang and Glicksman (1981). On the other hand, in the theory of the equiaxed dendritic growth of alloys, the problem of coupled heat- and mass-transport must be solved (Lipton et al, 1984 - appendix 8). In the case of the directional growth of alloy dendrites, the situation is somewhat simpler because, due to the imposed temperature gradient, the latent heat is transported through the solid while solute is rejected ahead of the tips. In this case, only mass diffusion need be considered. This permits an approximate solution of the problem of alloy dendrite growth in the columnar zone. This case is of great practical importance and will be considered here in greater detail.

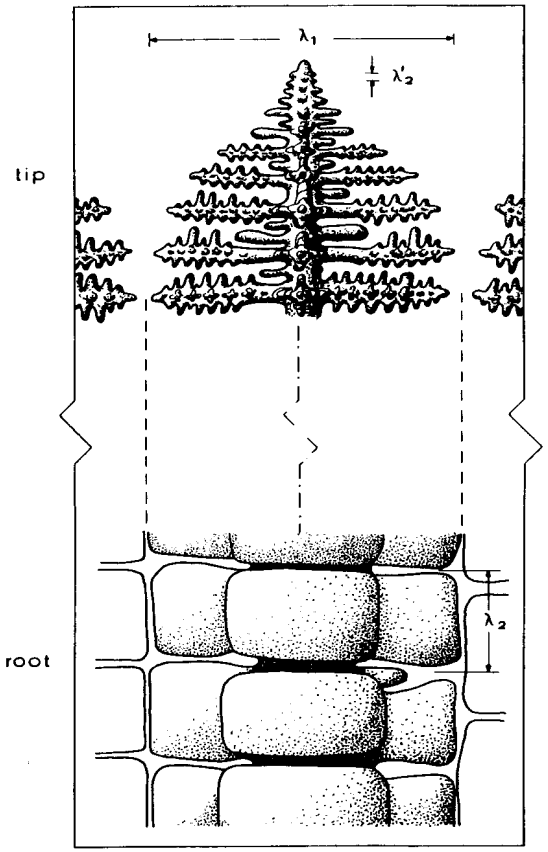

Figure 4.6: GROWING DENDRITE TIP AND DENDRITE ROOT IN COLUMNAR GROWTH. Depending upon the directional growth conditions, the dendrite (from the Greek, dendros = tree) will develop arms of various orders. A dendritic form is usually characterised in terms of the primary (dendrite trunk) spacing, λ_1, and the secondary (dendrite arm) spacing, λ_2. Tertiary arms are also often observed close to the tip of the dendrite. It is important to note that the value of λ_1 measured in the solidified microstructure is the same as that existing during growth, whereas the secondary spacing is enormously increased due to the long contact time between the highly-curved, branched structure and the melt. The ripening process not only modifies the initial wavelength of the secondary perturbations, λ_2', to give the spacing which is finally observed, λ_2, but also often causes dissolution of the tertiary or higher order arms. The two figures are drawn at the same scale, refer to the same dendrite, and illustrate morphologies which exist at the same time but which are widely separated along the trunk length (by about $100\lambda_1$).

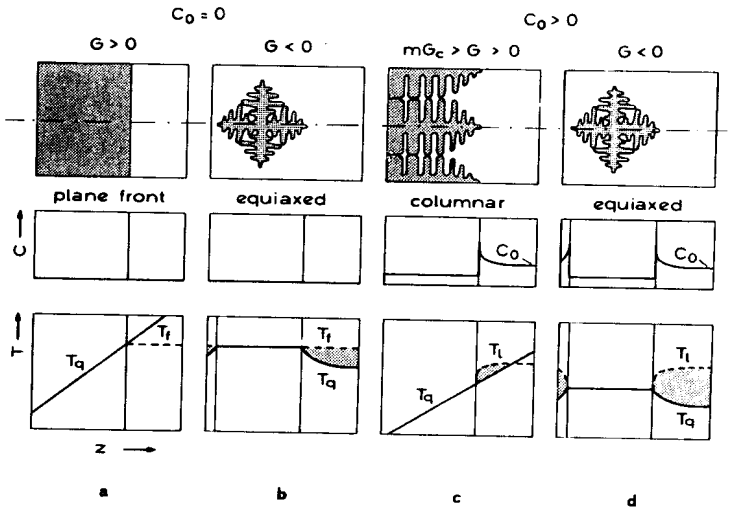

Figure 4.7: CONCENTRATION AND TEMPERATURE FIELDS OF DENDRITES. These diagrams illustrate the heat and mass diffusion fields existing along the dendrite axis, and correspond to various possible cases (figure 1.7 and table 3.1). In pure substances (a,b), there is no solute rejection and dendrites can form only in an undercooled melt. In the latter case (b), the heat rejection occurring during growth sets up a negative temperature gradient ahead of the interface. This leads to the establishment of the necessary conditions for the instability of thermal dendrites. In the case of alloys (c,d), dendrites can form irrespective of the temperature gradient if the interface is constitutionally unstable. If G is greater than zero (c), the latent heat is transported, together with the unidirectional heat flux, into the solid. To a first approximation, therefore, solute rejection alone needs to be considered in the case of directionally solidified (solutal) dendrites. Equiaxed dendrites in alloys (d) reject both solute and heat.

The rejection of solute changes the temperature of the solid/liquid interface at the tip (figure 4.8). The ratio of the change in concentration at the tip, ΔC, to the equilibrium concentration difference, ΔC^* ($= C_l^*$ [1 - k]: length of the tie-line at the temperature of the tip) is known as the supersaturation, Ω. This supersaturation (or the related undercooling, ΔT_c) represents the driving force for the diffusion of solute at the dendrite tip in an alloy. In principal, when the supersaturation is equal to zero the transformation rate will be zero. With increasing supersaturation, the growth rate of the new phase (the solid) will increase (§). The rejection rate is

§ Similar arguments apply to thermal dendrites, as shown in appendix 7.

influenced by the shape of the tip and, at the same time, the form of the tip is affected by the distribution of the rejected heat or solute. This interaction makes the development of an exact theory extremely complex. However, to a first

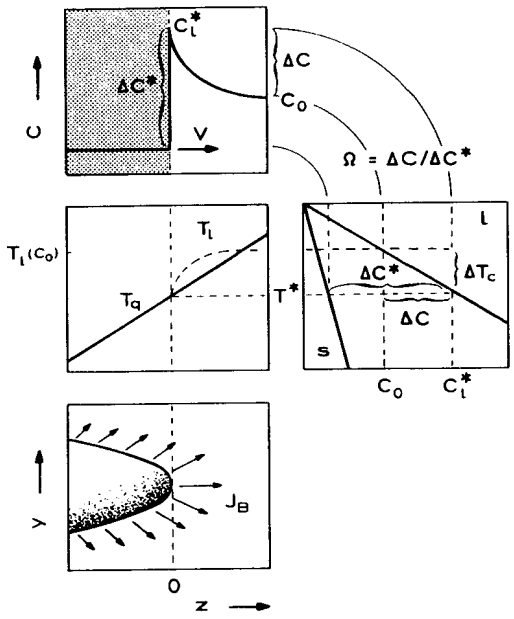

Figure 4.8: SOLUTE REJECTION AT THE TIP OF AN ISOLATED CELL OR DENDRITE. During directional solidification, where the isotherms move due to the imposed heat flux, a needle-like crystal can grow more quickly than a flat interface due to the more efficient solute redistribution: B-atoms rejected at the interface of a thin needle can diffuse outwards into a large volume of liquid. Thus, the solutal diffusion boundary layer, δ_c, of the needle is smaller than that of a planar interface ($\delta_c \propto$ tip radius). Also, because the interface is not planar, the solid formed does not have the same composition as the original liquid (as it does in the case of steady-state plane-front growth - figure 3.4). When a positive gradient is imposed, as in directional solidification, heat is extracted through the solid. If, furthermore, thermal diffusion is rapid (as in metals) the form of the isotherms will be affected only slightly by the interface morphology. Thus, in the case of directionally solidifying dendrites, only solute diffusion will be the limiting factor. The growth temperature, T*, of the tip will define a solute undercooling, ΔT_c, or, via the phase diagram, the degree of supersaturation, $\Omega = \Delta C/\Delta C^*$. The determination of Ω as a function of the other parameters requires the solution of the differential equation which describes the solute distribution. The simplest solution is obtained when the tip morphology is supposed to be hemispherical. Instead, the real form of the dendrite tip is closely represented by a paraboloid of revolution.

approximation the dendritic shape can be described satisfactorily as being a paraboloid of revolution as was suggested originally by Papapetrou (1935). The mathematical solution of the diffusion problem for a paraboloid was derived by Ivantsov (1947) who deduced the following relationship between the supersaturation, Ω, the dendrite tip radius, R, and the growth rate, V:

$$\Omega = I(P) \qquad [4.2]$$

where:

$$I(P) = P\exp(P)E_1(P) \qquad [4.3]$$

and the Péclet number, $P = VR/2D = R/\delta_c$. Here, E_1 is the exponential integral function (equation A7.13b, figure A1.2). The form of the Ivantsov function, I(P), is shown in figure A7.4. It is interesting to note that equation 4.3 can be approximated by a continued fraction of the type (Abramowitz & Stegun, 1965):

$$I(P) = \cfrac{P}{P + \cfrac{1}{1 + \cfrac{1}{P + \cfrac{2}{1 + \cfrac{2}{P + \ldots}}}}}$$

If only the first term is taken, one obtains:

$$I(P) \simeq P \qquad [4.4]$$

and insertion of this approximation into equation 4.2 gives:

$$\Omega \simeq P \qquad [4.5]$$

This is the simple solution obtained for the diffusion field existing around a hemispherical cap (equation A7.11), and will be used in the following discussion because it permits a clearer insight into the physics of dendrite growth than does the more complicated relationship of equation 4.3. Nevertheless, it should be kept in mind that equation 4.3 or more complicated ones (Trivedi, 1970) can easily be used in numerical calculations and this will then lead to more exact solutions. Equation 4.5 simply states that the response of the system characterised by the Péclet number is proportional to the driving force defined by the supersaturation. Since P is the ratio of the tip radius, R, to the diffusion length, 2D/V (figure A2.5), a large value of Ω leads to a diffusion length which is small in comparison with R.

The solution to the diffusion problem, described by equation 4.5, is seen i ure 4.9, for an alloy dendrite (Al-2wt%Cu under directional solidification conditions), as a straight line at an angle of 45° in logarithmic coordinates. This indicates that, for a given Ω-value, R and V are not defined unambiguously. Thus, solution of the diffusion problem does not indicate whether the dendrite will grow quickly or slowly, but merely relates the sharpness of the tip to its rate of propagation.

In this respect, it is often useful to use the analogy of a body moving through a fluid, where blunt shapes have a higher hydrodynamic resistance. The diffusion boundary layer around the tip is proportional to the tip radius. Because the gradient of C is inversely proportional to the boundary layer thickness, a sharper tip has a steeper gradient. A sharper tip can grow more rapidly because it can reject solute (or heat in the case of a thermal dendrite) more efficiently; the flux being proportional to the gradient. However, there is a limit, to the possible sharpness of the dendrite tip, which is represented by the critical radius of nucleation, $R^o = r^o$ (table 2.1). At r^o, the growth rate is zero and therefore all of the supersaturation is used to create curvature and none remains to drive diffusive processes (figure 4.9).

4.4 Operating Point of the Needle Crystal - Tip Radius

The overall growth curve of a needle-like crystal, which reflects the sum of the capillarity and diffusion effects, follows the solid curve in figure 4.9, and exhibits a maximum close to R^o. Until recently, this maximum, R_e, was considered to be the radius at which the dendrite would actually grow. This so-called extremum criterion permitted the establishment of an unique solution, to the otherwise indeterminate growth problem, by setting the first derivative of the equation of growth equal to zero.

Recently, Langer and Müller-Krumbhaar (1977) have argued that a dendrite tip having a small radius tends to increase its radius due to the development of side-branches which interact with the tip. On the other hand, a large tip radius will tend to decrease due to the development of instabilities. The result is a growth rate which is associated with a tip having a size at the limit of stability. Thus, one can then immediately determine the expected tip radius by setting:

$$R_s = \lambda_i \qquad [4.6]$$

where λ_i is the shortest wavelength perturbation which would cause the dendrite tip to undergo morphological instability. To a first approximation, the wavelength of the favoured perturbation at a planar interface can be used. It is described by

equation 3.22 and, for the condition $G \ll mG_c$ (which is true for dendrites) it is given by equation 3.25:

$$\lambda_i = 2\pi\sqrt{\delta \cdot s} \qquad [4.7]$$

This wavelength is the geometric mean of a diffusion length, δ (= D/V) and a capillary length, s (= $\Gamma/\Delta T_o$). In figure 4.9, the value at which R is at the limit of morphological stability is also indicated. It can be seen that this operating point is situated some distance from the extremum, and leads to the prediction of larger R-values. This prediction is consistent with experimental measurements. Since R_s is considerably greater than R_e, the effect of curvature on the growth curve can be neglected. (The point, $R = \lambda_i$, is situated upon the fully diffusion-limited curve, therefore ΔT_r in equation 4.1 is almost zero.) The curvature then exerts its influence only through the λ_i-value, via the capillary length. Figure 4.10 illustrates how one obtains an unique solution by using the extremum criterion (dash-dot line) or with the aid of equations 4.5 and 4.6 (solid line). In this way, Ω is eliminated from the V-R-relationship. The final result for constrained growth is given in figure 4.11 for growth rates, $V > V_c$, i.e. above the limit of constitutional undercooling of the plane front.

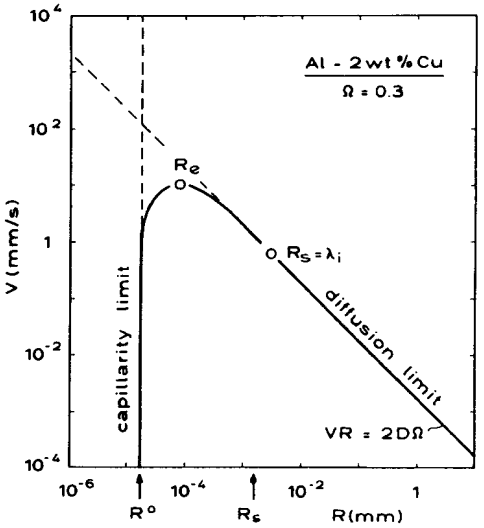

Figure 4.9: UNOPTIMISED GROWTH RATE OF A HEMISPHERICAL NEEDLE FOR Ω = CONSTANT. For a hemispherical needle crystal, the solution of the diffusion equation shows that the supersaturation, Ω, is equal to the ratio of the tip radius to the diffusion boundary layer. This dimensionless ratio is known as the Péclet number, P(=RV/2D). For a given supersaturation, the product, RV, is therefore constant and means that either a dendrite with a small radius will grow rapidly or one with a large radius will grow slowly (line at 45° in the figure). At small R-values, the diffusion limit is cut by the capillarity limit. The minimum radius, R^o, is given by the critical radius of nucleation, r^o (table 2.1). A maximum value of V therefore exists. Because it was reasoned that the fastest-growing dendrites would dominate steady-state growth, it was previously assumed that the radius chosen by the real substance would be the one which gave the highest growth rate (value at extremum, $R = R_e$). However, experiment indicates that the radius of curvature of the dendrite is approximately equal to the lowest wavelength perturbation of the tip, which is close to λ_i (figure 3.7). This is referred to as growth at the limit of stability ($R = R_s$).

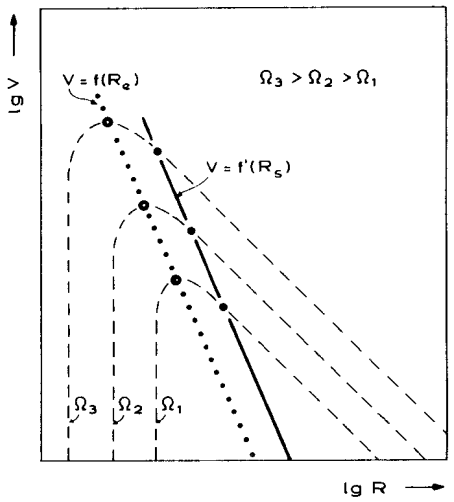

Figure 4.10: GROWTH RATE AS A FUNCTION OF TIP RADIUS FOR OPTIMUM GROWTH. In this figure, it is demonstrated how, using the optimisation criterion, $V = f'(R_s)$, the observed V-R-values are obtained as a function of Ω. That is, for a given value of V, a given value of R is found. The unoptimised growth rate, V, of figure 4.9 is here shown as a function of the tip radius, R, for various supersaturations, $\Omega_3 > \Omega_2 > \Omega_1$. Two optimisation criteria are used here. One is that tip growth occurs at the extremum (dotted line) and the other is that it occurs at the limit of stability (solid line). The optimised curve deduced from the stability criterion (solid line) corresponds to a portion of the solid lines in figure 4.11, where the coordinates have been inverted.

In order to understand these relationships more fully, the calculation (Kurz & Fisher 1981) of the tip radius of a dendrite growing under conditions of

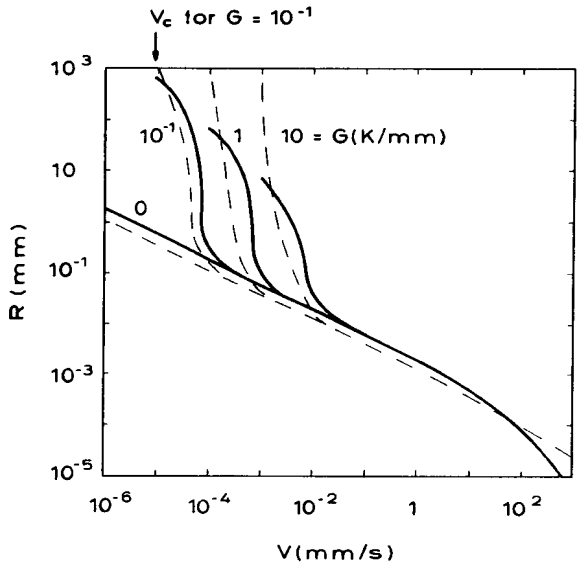

Figure 4.11: OPTIMISED DENDRITE TIP RADIUS AS A FUNCTION OF GROWTH RATE. If it is assumed that, in directional solidification, growth occurs with a tip radius which is equal to the minimum instability wavelength, λ_i, curves such as those above can be generated. They indicate the magnitude of the dendrite tip radius for a given growth rate. Here, the ..eavy lines are given by the simple model described in the text (equation 4.11), while the dotted lines are predicted by a more detailed analysis (Trivedi, 1980). Note the marked effect of the temperature gradient upon the radius of curvature at low growth rates (constrained growth regime or cellular regime e.g. for G = 0.1K/mm between $V = 10^{-4}$ and $V = 10^{-5}$mm/s). A sufficiently high gradient, or a sufficiently low growth rate ($V_c = GD/\Delta T_o$) will lead to the re-establishment of a planar interface (i.e. a 'dendrite' with an infinite radius of curvature). The approximate analysis does not quite succeed in showing this, because of the simplified assumptions made. When the temperature gradient is less than, or equal to zero, no cells are formed and the steep curves usually observed at low values of V do not occur.

directional solidification (§) will be developed in more detail. This is the solutal case with an imposed temperature field, as in figures 4.7 and 4.8. The minimum wavelength of the instability of a planar interface is approximated by equation 3.22:

$$\lambda_i = 2\pi \sqrt{\frac{\Gamma}{\phi}}$$

Using equation 4.6 gives:

$$R = 2\pi \sqrt{\frac{\Gamma}{\phi}} \qquad [4.8]$$

where $\phi = mG_c - G$. From a flux balance, in the z-axis direction at the dendrite tip (equation 3.6), and knowing that, from the phase diagram (figure 4.8):

$$C_l^* = \frac{C_o}{1 - \Omega p} \qquad [4.9]$$

(p = 1-k), one obtains for G_c:

$$G_c = \frac{C_o}{\frac{R}{2} - \frac{D}{Vp}} \qquad [4.10]$$

This leads, together with equation 4.8, to:

$$V = \frac{2DGR^2 + 8\pi^2 D\Gamma}{R^3 pG - 2R^2 pC_o m + 4\pi^2 \Gamma Rp} \qquad [4.11]$$

This cubic equation, which relates R to V and G for various alloys, is valid only for an isolated hemispherical-tip needle growing into supersaturated liquid. It is plotted in figure 4.11 for various values of G, and indicates the existence of two different regimes when G>0. At growth rates close to V_c (steep part of the curves) where mainly cellular growth is found. Equation 4.11 can be simplified to give:

$$R = \frac{2D}{Vp} + \frac{2mC_o}{G} \qquad [4.12]$$

while, at medium to high growth rates (dendritic regime), the corresponding

§ Note that directional solidification can be obtained by using a Bridgman-type furnace (G and V independent) or by directional casting (G and V coupled) - see exercise 1.9

approximation to equation 4.11 is:

$$R = 2\pi \sqrt{\frac{D\Gamma}{Vk\,\Delta T_o}} \qquad [4.13]$$

The degree of agreement with the more exact analysis (Trivedi [1980]) is reasonable (figure 4.11).

The R-V relationship for isolated cells is therefore very different to that for isolated dendrites. The tip concentration, which is important with regard to segregation, or the tip temperature can easily be determined from the value of R (table 4.2). It is seen (figures 4.12 and 4.13) that cells grow with much higher tip concentrations, and consequently lower tip temperatures, than those usually encountered for dendrites (when V<10mm/s). This is easily understood if it is realised that growth at the limit of stability infers that the condition proposed by Burden and Hunt (1974) is valid. That is:

$$\Delta T_t = \frac{GD}{V}$$

This equation expresses the fact that the cell tip, where ΔT_t is used instead of the ΔT_o-value of a planar interface, is growing with a concentration gradient which corresponds to equality between G and mG_c, i.e. at the limit of constitutional undercooling (equation 3.15).

Table 4.2: DENDRITE GROWTH VARIABLES ACCORDING TO THE APPROXIMATE SOLUTION OF EQUATION 4.11 ($p.P < 1$)

$$R \simeq 2\pi\sqrt{\frac{D\Gamma}{\Delta T_o k V}}$$

$$P \simeq \pi\sqrt{\frac{V\Gamma}{D\,\Delta T_o k}}$$

$$\frac{C_i^*}{C_o} \simeq \frac{1}{1 - pP}$$

$$\Delta T = \Delta T_c = mC_o\left(1 - \frac{1}{1 - pP}\right)$$

The rapidly increasing tip concentration or decreasing tip temperature of dendrites at very high growth rates is due to the dominant capillarity term at small values of R. The error involved in using equation 4.5 is quite large in this case since P is greater than unity. Use of the more exact solution (figure 4.13) indicates a less rapid decrease in tip temperature at high growth rates. In table 4.2, some related variables for the approximate solution of problems arising in the directional growth of dendrites are given.

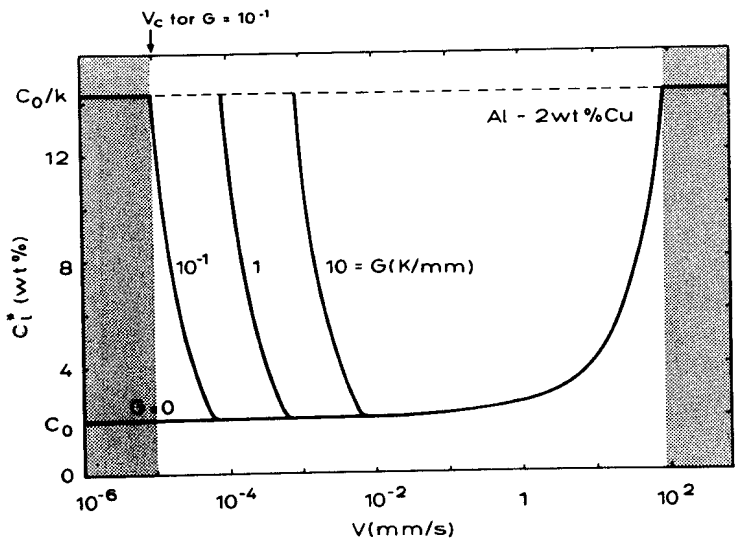

Figure 4.12: INTERFACE CONCENTRATION OF A HEMISPHERICAL NEEDLE IN DIRECTIONAL GROWTH. From the radius of curvature predicted by figure 4.11, the associated interface concentration can be derived. The blunt cell tips existing close to the limit of constitutional undercooling, V_c, cannot easily dissipate the solute rejected there and the tip concentration will therefore be higher than that ahead of a sharp dendrite tip. If the temperature gradient is zero, this will not occur as no cells are formed in this case. At very high growth rates, the interface concentration in the liquid will again increase to high values due to the increase in supersaturation necessary to drive the process. Again, at very high growth rates a crystal with a supersaturation of unity will grow which has the same composition, C_o, as the alloy (the composition of the liquid is equal to C_o/k). Under these conditions, a planar solid/liquid interface will result as in growth at low rates in a positive temperature gradient (grey regions). Note that the composition of the solid is related to C_i^* via the distribution coefficient, k. The latter becomes a function of V at growth rates of the order of 100mm/s or above.

The tip radius would not be so important if it did not influence other morphological parameters of the cell or dendrite. The theory presented here is a useful approximation in the case of isolated needles. Dendrites can be regarded as being isolated crystals, at least at their tips, but the applicability of this assumption to cellular growth is limited since cells always grow with their tips close together ($R \simeq \lambda_1$) and their diffusion fields overlap.

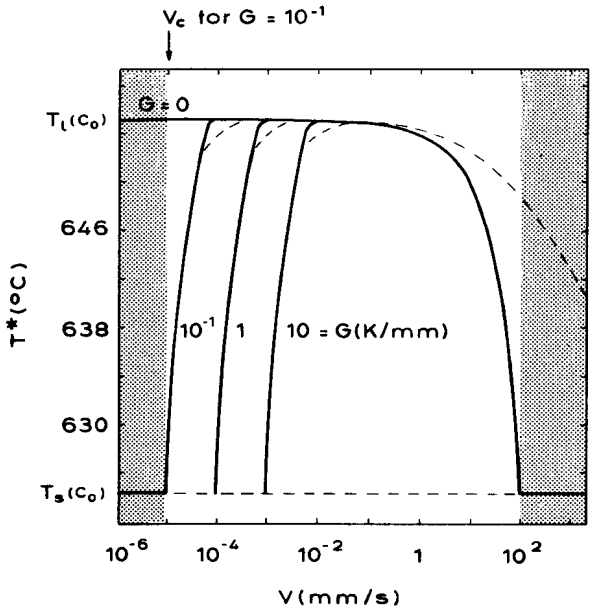

Figure 4.13: INTERFACE TEMPERATURE OF A HEMISPHERICAL NEEDLE IN DIRECTIONAL GROWTH. Use of the phase diagram and the assumption of the existence of local equilibrium at the solid/liquid interface permit the calculation of the temperature associated with the interface concentration (figure 4.12). At high and low growth rates, the tip temperature reaches the solidus temperature. In the low growth rate range, below the critical rate where the dendrite tip temperature and solidus temperature are equal (grey area on the left-hand side), the planar front is the more stable since it can grow at a higher temperature. (This is another way of regarding the limit of constitutional undercooling). A similar argument applies at high growth rates. As in figure 4.11, the broken curves again indicate the more exact behaviour described by the relationship of Trivedi (1980).

4.5 Primary Spacing of Dendrites after Directional Growth

The primary arm spacing is an important characteristic of columnar dendrites and has a marked effect on the mechanical properties. On the other hand, in equiaxed growth the primary spacing does not play the same role and a more important parameter is the distance between the nuclei, or the grain size.

Returning to the primary spacing in the columnar (directional) growth situation, it is assumed that the cell or the dendrite envelope, representing the mean cross-section of the trunk and branches, can be described approximately by an ellipse (figure 4.14). The radius of curvature of the ellipse is given by:

$$R = \frac{b^2}{a} \qquad [4.14]$$

The semi-axis, b, is proportional to λ_1, where the proportionality constant depends upon the geometrical arrangement of the dendrites. A hexagonal arrangement is assumed in figure 4.14, where the last liquid is assumed to solidify at the centre of

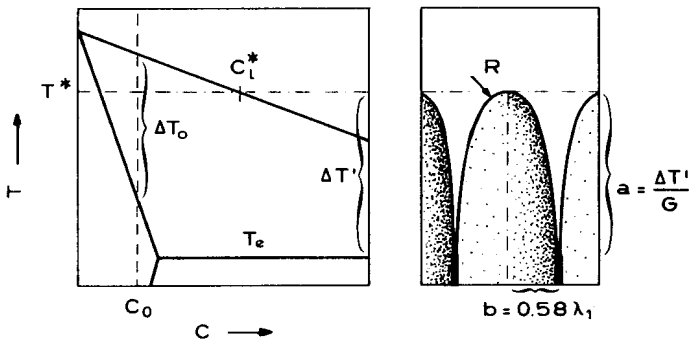

Figure 4.14: ESTIMATION OF THE PRIMARY SPACING IN DIRECTIONAL SOLIDIFICATION. In practical applications, the dendrite tip radius is not as important a parameter as the primary spacing since it is almost impossible to measure it directly. In order to estimate the primary spacing, the dendrites are imagined to be elliptical in shape. The length of the major half-axis, a, of the ellipse is equal to $\Delta T'/G$. Here, $\Delta T'$ is the difference between the tip temperature and the melting point of the last interdendritic liquid. The primary spacing, λ_1, which is proportional to the minor half-axis, b, can be determined from simple geometrical considerations. The factor, 0.58, arises from the assumption that the dendrite trunk arrangement is hexagonal.

gravity of the equilateral triangle formed by three densely packed dendrites. This assumption leads to $b = 0.58\lambda_1$.

The semi-axis length, a, is given by the difference between the tip temperature and the root temperature, divided by the mean temperature gradient in the mushy zone:

$$a = \frac{\Delta T'}{G} = \frac{T^* - T_s'}{G}$$

where, due to microsegregation, T_s' is often equal to the eutectic temperature if an eutectic exists in the system (chapter 6). Therefore, it can be assumed that the tip radius and the length of the interdendritic liquid zone together determine the primary spacing, due to purely geometrical requirements. From equation 4.14, one has $\lambda_1 \propto \sqrt{(Ra)}$, and:

$$\lambda_1 = \sqrt{\frac{3\,\Delta T' R}{G}} \qquad [4.15]$$

Substituting for R from equation 4.12 or 4.13 into equation 4.15 leads to two different spacing equations for cells or dendrites, where λ_1 is always directly related to $\Delta T'$ (equation 4.15). Knowing that $\Delta T'$ is strongly dependent upon the tip temperature, T*, a sharp decrease in T* at low and high V (figure 4.13) should cause λ_1 to decrease sharply as shown in figure 4.15. However, no firm experimental evidence exists to show that this does in fact occur. Between these two limiting growth rates, cells will follow a different relationship to that of dendrites. For the most important range of dendritic growth, at medium to high V, the following equation can be obtained by substituting equation 4.13 into equation 4.15 and assuming that, in this range, $\Delta T' \simeq \Delta T_o$:

$$\lambda_1 = \frac{4.3(\Delta T_o D \Gamma)^{0.25}}{k^{0.25} V^{0.25} \sqrt{G}} \qquad [4.16]$$

This equation indicates that a variation in the growth rate has a smaller effect upon λ_1 than does a change in the temperature gradient. As in directional growth, the cooling rate, $\dot{T}$, is given by:

$$\dot{T} = -GV \qquad [4.17]$$

It can be seen that λ_1 for dendrites will not obey a simple relationship such as the ones often proposed in the literature e.g.:

$$\lambda_1 = K\dot{T}^n$$

Although equation 4.16 gives only a qualitative description of λ_1, due to the simplified model used, it nevertheless indicates that G and V have a different functional relationship to λ_1; a conclusion which is also borne out by Hunt's analysis (1979). Another interesting aspect of the present elliptic dendrite model is that it permits the description of a planar, flattened cellular, elongated cellular, or dendritic growth morphology (figure 4.15) with the use of only two geometrical

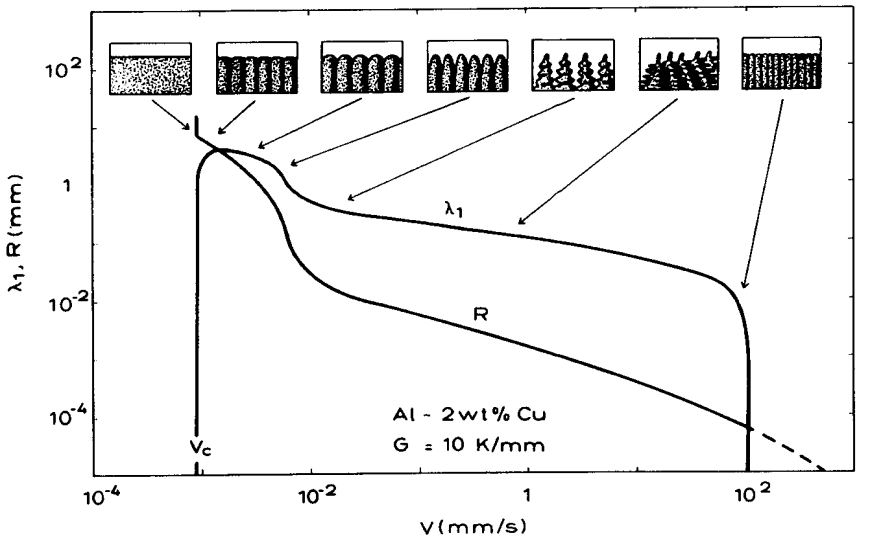

Figure 4.15: MORPHOLOGY, TIP RADIUS, AND SPACING OF CELLS AND DENDRITES. According to the simple dendrite model, the tip radius decreases from very large values at the limit of constitutional undercooling, V_c, to small values at high growth rates (as in figure 4.11). Over the same range, the primary spacing starts at zero (plane interface) crosses the R-V curve, and reaches zero again at high growth rates. The corresponding interface structures are also shown and vary from planar at growth rates less than V_c to blunt cells ($R \geq \lambda_1/2$) or well-developed cells ($R \leq \lambda_1/2$) and to dendrites which become finer and finer until they disappear at very high growth rates to give a planar interface again. Note that this behaviour of λ_1 has been derived for isolated cells and dendrites. In reality, the interaction of the diffusion fields at the tips will change the relationship for cells at low growth rates.

parameters, a and b (§).

Once the primary spacing is established, it will not change during, or after, solidification. This is not so for the secondary arms, which undergo a ripening process.

4.6 Secondary Spacing after Directional or Equiaxed Growth

As seen from figure 4.6, the secondary arms start very close to the tips. They appear initially as a sinusoidal perturbation of the paraboloid. As in the case of a planar solid/liquid interface which becomes unstable (figure 4.3), these perturbations grow, become cell-like, are sometimes eliminated by their neighbours, and a number of them finally become real secondary dendrites growing perpendicularly to the primary trunk (in the case of a cubic crystal). These secondary arms, with their higher-order branches, grow and eliminate each other as long as their length is less than $\lambda_1/2$. Once the diffusion fields of their tips come into contact with those of the branches growing from the neighbouring dendrites, they stop growing. A ripening process causes the highly-branched arms to change with time into coarser, less branched, and more widely-spaced ones (figures 4.6 and 4.16).

Careful inspection of the photographs in figure 4.16 suggests that one possible mechanism for the coarsening process is the melting of thinner secondary arms and an increase in the diameter of the thicker branches. This process is analogous to Ostwald ripening of precipitates. The process is depicted schematically in the upper diagram of figure 4.16. Each time that a thin secondary arm melts, the local spacing is doubled. The driving force for the ripening process is the difference in chemical potential of two crystals with different interfacial energies (i.e. different curvatures). As in the ripening of precipitates, the spacing of the branches, λ_2, is proportional to the cube root of time (equation A8.34):

$$\lambda_2 = 5.5\,(Mt_f)^{1/3} \qquad [4.18]$$

with

$$M = \frac{\Gamma D \ln\left(\frac{C_t^m}{C_o}\right)}{m(1-k)(C_o - C_t^m)} \qquad [4.19]$$

§ Very recently, Trivedi (1984) has published another model for λ_1 and compared the predictions of the latter with measurements made by Somboonsok et al (1984).

where C_t^m is often equal to C_e.

The value of M can easily vary between 1 and 10. However, because its effect on λ_2 is only proportional to the cube root, the differences will be relatively small when compared with the inevitable scatter to be expected in the measurements. Such

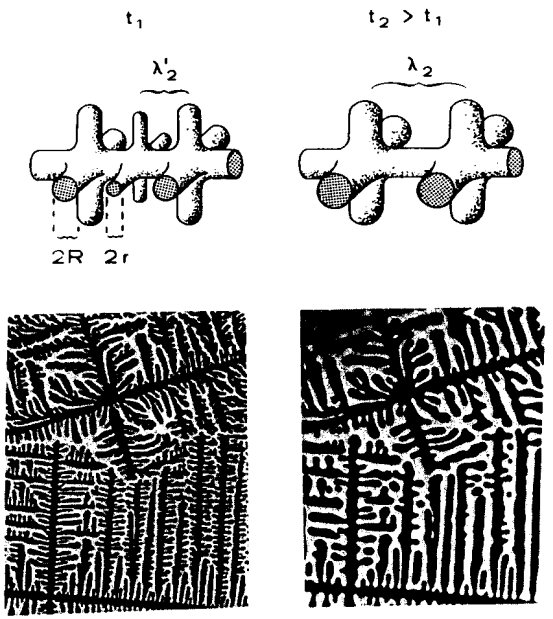

Figure 4.16: ESTABLISHMENT OF THE SECONDARY DENDRITE ARM SPACING IN EQUIAXED SOLIDIFICATION. In contrast to the primary spacing, the secondary dendrite arm spacing, as measured in the solidified metal, is largely determined by annealing processes occurring during growth of the dendrites (figure 4.6). Due to a ripening phenomenon, smaller (higher curvature) features disappear and 'feed' the growth of the already larger features. The upper figures illustrate the model assumed in calculating the effect of these changes, while the lower photographs show equiaxed cyclohexane dendrites (a) just after solidification, and (b) 20min later. In these photographs, the black areas correspond to the solid phase and the white areas to the liquid phase. Note that the primary spacing in an equiaxed structure is not well-defined and usually corresponds to the mean grain diameter. [Photographs: K.A.Jackson, J.D.Hunt, D.R.Uhlmann, T.P.Seward: Transactions of the Metallurgical Society of AIME 236 (1966) 149]

experimental results are presented (figure 4.17) for the secondary spacing in an Al-4.5wt% Cu alloy.

Measurements of the secondary spacing observed in directionally solidified or equiaxed structures give some indication of the local solidification conditions, and can be helpful when cooling curves are unavailable.

In the case of directional solidification, the local solidification time is given by:

$$t_f = \frac{\Delta T'}{|\dot{T}|} = \frac{\Delta T'}{GV} \qquad [4.20]$$

When there is no eutectic reaction in the system, the determination of $\Delta T'$ might be difficult. In chapter 6, it is shown that one can obtain an approximate value in this situation.

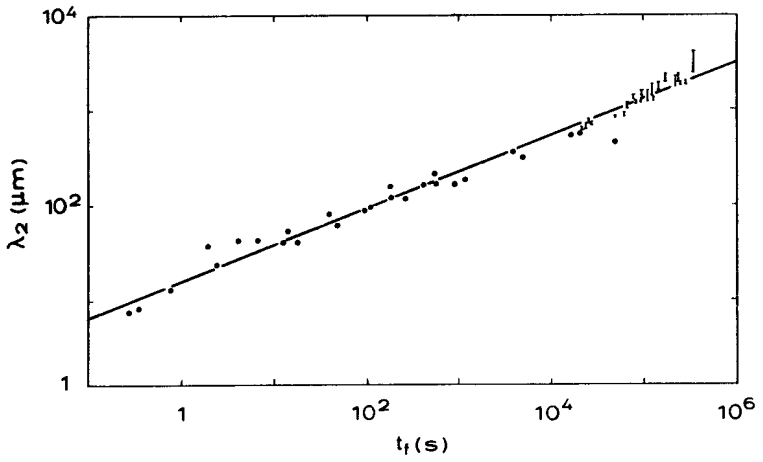

Figure 4.17: SECONDARY SPACING AS A FUNCTION OF SOLIDIFICATION TIME. The best-fit curve to the experimental points for Al-4.5wt% Cu alloy over a wide range of solidification conditions shows that the secondary spacing varies approximately as the cube root of the local solidification time. The latter is defined as the time during which each arm is in contact with liquid (figure 4.1), and is therefore a function of the growth rate, the temperature gradient, and the alloy composition. The secondary spacing is important since, together with λ_1, this determines the spacing of precipitates or porosity and thus has a considerable effect on the mechanical properties of as-solidified alloys (figure 1.2). [T.F.Bower, H.D.Brody, M.C.Flemings: Transactions of the Metallurgical Society of AIME 236 (1966) 624].

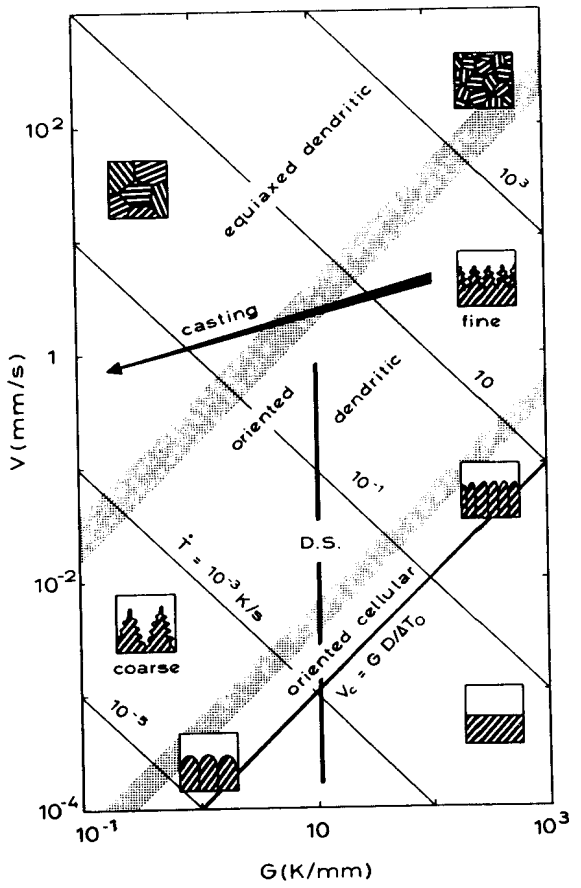

Figure 4.18: SCHEMATIC SUMMARY OF SINGLE-PHASE SOLIDIFICATION MORPHOLOGIES. This diagram summarises the various microstructures which can be obtained using a typical alloy, with a melting range (ΔT_o) of 50K, when the imposed temperature gradient, G, or growth rate, V, are varied. Provided that a unidirectional heat flow is imposed, the product, GV, is equivalent to the cooling rate, $\dot{T}$, which controls the scale of the microstructures formed. The ratio, G/V, largely determines the growth morphology. Moving from the lower left to the upper right along the lines at 45° leads to a refinement of the structure without changing the morphology (G/V = constant). Crossing these lines by passing from the lower right to the upper left leads to changes in morphology (from planar, to cellular, to dendritic growth), and the scale of the microstructure remains essentially the same ($\dot{T}$ = constant). The grey bands define the regions over which one structure changes into another. The conditions required to produce single-crystal turbine blades (figure 4.5) are those at the upper end of the thick vertical line (DS = directional solidification). Processes which produce perfect single crystals, such as those required for semiconductor-grade silicon preparation are found at the bottom of the same vertical line. (For single crystal growth, all but one of the crystals initially present must be eliminated.) In a conventional casting, the growth conditions change with time approximately in the manner indicated upon following the inclined arrow from right to left. Splat-cooling conditions are found in the far upper-right region. At these rates, k will begin to approach unity.

Figure 4.18 summarises the main points considered in this chapter. Thus, for one alloy, G and V are the main variables which determine the form and scale of the microstructures found after solidification of a given alloy. Specific G/V values (lines and bands running from the bottom left to the upper right) represent a constancy of microstructure (planar, cellular, columnar, and equiaxed dendritic). On the other hand, the various G.V ($= \dot{T}$) values (lines running from upper left to lower right) indicate a constant scale for these structures (e.g. λ_2). Thus, fine or coarse dendrites can be produced when G and V can be changed independently (see the insets in figure 4.18). Herein lays the value of the directional solidification (DS) method. That is, structures can be tailored to some extent so as to have optimum properties, as in the case of a turbine blade (figure 4.5). In a normal casting, G and V tend to be interrelated via the heat flux and the thermal properties of the metal. In a casting, therefore, only conditions close to the arrow in figure 4.18 can be exploited. When the growth rate is below the limit of constitutional undercooling, V_c (equation 3.15), plane front solidification is obtained and no solidification microstructure will develop. Note, however, that solidification with a planar interface does not alone ensure that a monocrystal will be obtained. To achieve this, elimination of all but one grain is necessary.

In castings there arises another important factor which will not be considered here. This is convective flow, which can markedly influence the transition from columnar to equiaxed dendritic growth. Generally, the presence of strong convection will decrease the length of the columnar dendritic zone and enhance equiaxed grain formation. This is mainly due to the breaking-off of parts of dendrites, and has a beneficial effect upon the internal quality of castings. In the continuous casting of steel, in particular, electromagnetic stirring has become a technologically important means of controlling the solidification structures.

BIBLIOGRAPHY

- Diffusion Field around Dendrite Tip

A.Papapetrou: Zeitschrift für Kristallographie 92 (1935) 89
G.P.Ivantsov: Doklady Akademii Nauk SSSR 58 (1947) 567
G.P.Ivantsov: Growth of Crystals, Consultants Bureau, New York, 1958, Vol. 1, p.76
G.Horvay, J.W.Cahn: Acta Metallurgica 9 (1961) 695

- Dendrite Tip Growth Theory (Free Growth)

R.Trivedi: Acta Metallurgica 18 (1970) 287
R.Trivedi: Metallurgical Transactions 1 (1970) 921
R.D.Doherty in: Crystal Growth (Edited by B.R.Pamplin), Pergamon, Oxford, 1975, p576.
M.E.Glicksman, R.J.Schaeffer, and J.D.Ayers: Metallurgical Transactions 7A (1976) 1747
J.S.Langer, H.Müller-Krumbhaar: Journal of Crystal Growth 42 (1977) 11
J.S.Langer: Reviews of Modern Physics 52 (1980) 1
S.C.Huang, M.E.Glicksman: Acta Metallurgica 29 (1981) 701, 717
M.E.Glicksman, N.B.Singh, M.Choppra in: Materials Processing in the Reduced Gravity Environment of Space (Edited by G.E.Rindone), Elsevier, 1982, p461.
B.Cantor, A.Vogel: Journal of Crystal Growth 41 (1977) 109
J.Lipton, M.E.Glicksman, W.Kurz: Materials Science and Engineering (1984), special issue on, "Solidification Microstructures" (Edited by H.Jones, W.Kurz)

- Dendrite Tip Growth Theory (Constrained Growth)

M.H.Burden, J.D.Hunt: Journal of Crystal Growth 22 (1974) 109
R.Trivedi: Journal of Crystal Growth 49 (1980) 219
W.Kurz, D.J.Fisher: Acta Metallurgica 29 (1981) 11

- Theory of Primary Dendrite Spacing

J.D.Hunt in: Solidification and Casting of Metals, The Metals Society, London, 1979, p1.
W.Kurz, D.J.Fisher: Acta Metallurgica 29 (1981) 11
R.Trivedi: to be published in Metallurgical Transactions 15A (1984)

- Theory of Secondary Dendrite Spacing

T.Z.Kattamis, M.C.Fleming: Transactions of the Metallurgical Society of AIME 233 (1965) 992
T.Z.Kattamis, J.C.Coughlin, M.C.Fleming: Transactions of the Metallurgical Society of AIME 239 (1967) 1504
U.Feurer, R.Wunderlin: Einfluss der Zusammensetzung und der Erstarrungs bedingungen auf die Dendritenmorphologie binärer Al-Legierungen, Fachbericht der Deutschen Gesellschaft für Metallkunde, Oberursel, FRG, 1977.
P.W.Voorhees, M.E.Glicksman in: Rapidly Solidified Amorphous and Crystalline Alloys (Edited by B.H.Kear, B.C.Giessen, M.Cohen), Elsevier, 1982, p.33

- Dendrite Spacing Measurements

K.P.Young, D.H.Kirkwood: Metallurgical Transactions 6A (1975) 197
T.Okamoto, K.Kishitake, I.Bessho: Journal of Crystal Growth 29 (1975) 131
T.Edvardsson, H.Fredriksson, I.Svensson: Metal Science 10 (1976) 298
H.Jacobi, K.Schwerdtfeger: Metallurgical Transactions 7A (1976) 811
G.M.Klaren, J.D.Verhoeven, R.Trivedi: Metallurgical Transactions 11A (1980) 1853
D.G.McCartney, J.D.Hunt: Acta Metallurgica 29 (1981) 1851
M.A.Taha, H.Jacobi, M.Imagumbai, K.Schwerdtfeger: Metallurgical Transactions 13A (1982) 2131
K.Somboonsok, J.T.Mason, R.Trivedi: to be published in Metallurgical Transactions 15A (1984)

- Mathematical Functions

M.Abramowitz, I.A.Stegun: Handbook of Mathematical Functions, Dover, New York, 1965.

EXERCISES

4.1 What will happen when the angle of the dendrite trunk axis in figure 4.4c is at exactly 45° to the heat flow direction? Sketch a portion of such a dendrite growing under these conditions.

4.2 A microstructure such as that in figure 4.3 is being formed by directional solidification. The material is cubic and the cube axis is 20° away from the axis of the cells. What will happen when the growth rate is markedly increased? (Consider the transition from cells to dendrites depicted in figure 4.4)

4.3 What does monocrystalline mean in the case of figure 4.5 (no concentration variation in the solid, absence of low-angle boundaries, absence of high-angle boundaries)? Compare with the columnar zone of a casting (figure 4.2).

4.4 Design a mould which is suitable for the production of a dendritic monocrystalline casting, e.g. a gas-turbine blade.

4.5 Sketch a sequence of transverse sections of a dendrite which illustrates the region between the tip and the root of the dendrite in figure 4.6.

4.6 In appendix 7, the solution (equation A7.10) for solute diffusion around a hemispherical needle crystal is developed. Derive the equivalent solution for the case of heat diffusion (equation A7.12).

4.7 Imagine a dendrite tip which changes its radius during growth. What will happen to the concentration field of this dendrite (figure 4.8 where $\Delta T = \Delta T_c$) as the tip becomes sharper and sharper at a given growth rate. Note that $\Delta T = \Delta T_c + \Delta T_r$ in directional solidification. Sketch the concentration profile for the case where (a) $\Delta T > \Delta T_r$, (b) $\Delta T = \Delta T_r$, (c) $\Delta T < \Delta T_r$. Which situation corresponds to the critical nucleation radius? Which dendrite grows and which melts?

4.8 Calculate the undercooling for the case of figure 4.9 which represents an Al-2wt%Cu under directional solidification conditions. From the value of R_o determine the Gibbs-Thomson parameter, Γ, used.

4.9 The unoptimised dendrite growth behaviour can be expressed as, $V = f(R)$ (as in figure 4.10) or as $\Delta T = g(R)$. Derive an equation for $\Delta T(R)$ on the basis of equation A8.3. Indicate the range of R values within which diffusion or capillarity is governing growth.

4.10 In figure 4.11, the results of Trivedi's more exact model, based upon the Ivantsov solution, for directionally solidifying dendrites are compared with those of the simple model derived in the present text. The discrepancy between them is large at low and high growth rates. At both extremes, the Péclet number becomes large (P greater than unity). Discover which of the simplifications made is responsible for the unrealistic predictions of the simple model. (Consider the low-V part of the curve, where the dendrite tip changes to a plane front, and make use of figure A7.4).

4.11 Calculate the tip temperature (table 4.2) of a dendritic growth front in Al-2%Cu alloy when $V = 0.1$mm/s and $G = 10$K/mm. Determine λ_1, λ_2, and the length of the mushy zone, assuming that G is constant in that region and the melting point of the last liquid is T_e. What is the value of the ratio, $\Delta T' / \Delta T_o$?

4.12 By using the lower limit, C_o/k, instead of C_l^m in equation 4.19, show how λ_2 varies with C_o in a given alloy system. For many systems, this simplification is realistic.

4.13 In an Al-5wt%Si alloy casting, measurements of temperature and microstructure gave the results below. Compare these values to the theoretical ones and estimate the cooling rate.

t_f(s)	$\lambda_2(\mu m)$
43	41 ± 3
330	81 ± 13
615	93 ± 3

4.14 In experiments involving strong, uniform flow of the melt across the solid/liquid interface (for example the electromagnetic stirring of steel during continuous casting), it is observed that columnar dendrites are inclined in a direction which is opposite to the flow direction. How would you explain this

observation? Consider the way in which the boundary layers around the dendrite tip are changed. Would the same effect occur in pure metals?

4.15 Stirring of the melt during solidification is an efficient method of promoting the columnar-to-equiaxed transition in a casting. The reason for this transition in stirred castings is that the melt becomes more rapidly cooled and, at the same time, many dendrite branches are detached from the interface. With the aid of figure 4.1, indicate the two limiting temperatures at which the melt must be in order to make this transition possible.

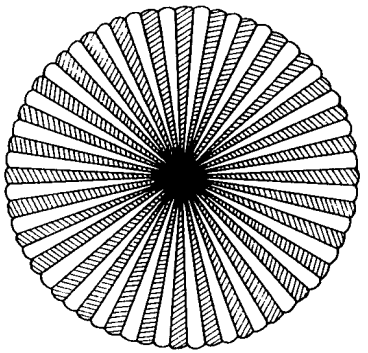

CHAPTER FIVE

SOLIDIFICATION MICROSTRUCTURE: EUTECTIC AND PERITECTIC

As shown in chapter 4, the solid which forms during solidification can adopt various morphological forms, and these can be present in a wide range of sizes. Dendrites make up the bulk of the microstructure of most alloys, but a number of important eutectic alloys are also used in practice. Eutectic morphologies are characterised by the simultaneous growth of two (or more) phases from the liquid. Due to their excellent casting behaviour, which is often similar to that of a pure metal, and the advantageous composite properties exhibited by the solid, casting alloys are often of near-eutectic composition.

5.1 Regular and Irregular Eutectics

Due to the fact that they are composed of more than one phase, eutectics can exhibit a wide variety of geometrical arrangements. With regard to the number of phases present, as many as four phases have been observed to grow simultaneously. However, the vast majority of technologically useful eutectic alloys are composed of two phases. For this reason, only the latter type of eutectic will be considered here (figure 5.1).

At high volume fractions of both phases ($f \simeq 0.5$), a situation which is encouraged by a symmetrical phase diagram, there is a marked preference for the formation of lamellar structures (e.g. Pb-Sn). On the other hand, if one phase is present in a small volume fraction, there is a tendency to the formation of fibres of that phase (e.g. Cr in NiAl-Cr). As a rule of thumb, one can suppose that when the volume fraction of one phase is between zero and 0.25, the eutectic will probably be fibrous, especially if both phases are of non-faceted type. If it is between 0.25 and 0.50, the eutectic will tend to be lamellar. If both phases possess a low entropy of fusion, the eutectic will exhibit a regular morphology. Fibres will become faceted if one phase has a high entropy of fusion or when interfaces having a minimum energy exist between the two phases. When faceting occurs, the eutectic morphology often becomes irregular and this is particularly true of the two eutectic alloys of greatest practical importance: Fe-C (cast iron) and Al-Si (§).

The regularity of an eutectic has a marked effect upon its mechanical properties, and this becomes especially important when it is required to control the orientation of the phases in order to obtain what are known as in situ composites. These are alloys where, using a controlled heat flux (figure 1.4), the eutectic phases can be caused to grow in a well-aligned manner. When the fibres are strong, as in the case of TaC in Ni-TaC eutectic, a marked increase in the creep strength of the alloy is found.

Because eutectic alloys exhibit small interphase spacings which are typically one tenth of the size of those of dendrite trunks under similar conditions of growth, a large interfacial area exists between the two solid phases. For a 1cm cube, this area is of the order of $1 m^2$. Moreover, the specific energy of the interface is usually high and increases with increasing dissimilarity of the phases. As a result, there is a tendency for certain, lowest-energy, crystallographic orientations to develop between

§ Nodular graphite in cast iron is an exception in non-faceted/faceted growth. In this case, the graphite grows as a primary faceted phase, together with austenite dendrites, and there is no eutectic-like growth of both phases. Such a behaviour has been called divorced growth. If both phases are faceted, the types of coupled growth described in the present chapter are not observed.

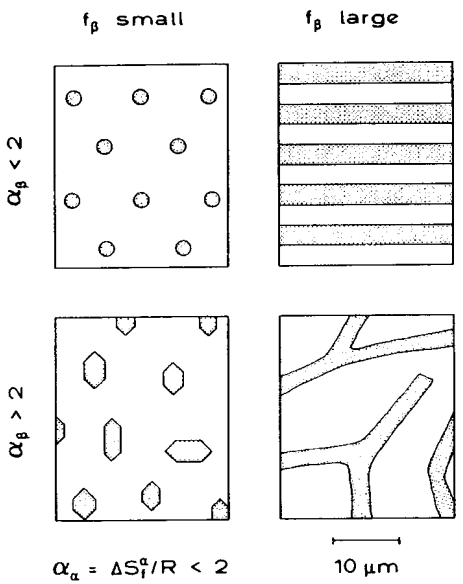

Figure 5.1: TYPES OF BINARY EUTECTIC MORPHOLOGY. Seen in transverse cross-section, eutectic microstructures can be fibrous or lamellar, regular or irregular. The condition is that one phase (here the white alpha-phase) must always have a low entropy of fusion, so that $\alpha_\alpha < 2$. If both phases possess a low entropy of fusion, their growth is easy on all crystallographic planes (chapter 2.3) and the resultant structures are regular (non-faceted/non-faceted eutectic - upper part of the above figure). When the low volume fraction phase possesses a high entropy of melting, as do semiconductors and intermetallic compounds for instance, the eutectics are of non-faceted/faceted type and the microstructures are usually irregular. The important eutectic casting alloys, Fe-C and Al-Si, belong to the latter class (lower right of the figure). In general, fibres are the preferred growth form when a small volume fraction of one phase is present, especially in the case of non-faceted/non-faceted eutectics. This is so because, for λ = constant, the interface area, A, and therefore the total interface energy attributed to the surfaces between the phases decreases with decreasing volume fraction of the fibres ($A \propto \sqrt{f_\beta}$), while the interface area is constant for lamellae. The interface area of fibres is lower than that for lamellae at volume fractions which are smaller than about 0.25. However, if the specific interface energy between the two phases is very anisotropic, lamellae may also be formed at a much lower volume fraction (as in Fe-C where $f_C = 0.07$).

the phases and thereby minimise the interfacial energy. This is also the reason why graphite exposes a maximum extent of its (0001) planes to the iron in cast iron. This can be done by the preferential formation of lamellae, even at a volume fraction as low as 0.05. Extensive experimental studies have been made of the crystallography of eutectic alloys and the results have been reviewed by Hogan, Kraft and Lemkey (1971). Table 5.1 indicates the results for a number of systems. A list of most of the eutectics studied by means of directional solidification as well as their properties can be found in Kurz and Sahm (1975).

Table 5.1: CRYSTALLOGRAPHY OF EUTECTIC ALLOYS

Eutectic	Growth Directions	Parallel Interfaces
Ag-Cu	$[110]_{Ag}$, $[110]_{Cu}$	$(211)_{Ag}$, $(211)_{Cu}$
Ni-NiMo	$[1\bar{1}2]_{Ni}$, $[001]_{NiMo}$	$(110)_{Ni}$, $(100)_{NiMo}$
Pb-Sn	$[211]_{Pb}$, $[211]_{Sn}$	$(1\bar{1}\bar{1})_{Pb}$, $(0\bar{1}\bar{1})_{Sn}$
Ni-NiBe	$[112]_{Ni}$, $[110]_{NiBe}$	$(111)_{Ni}$, $(110)_{NiBe}$
Al-AlSb	$[110]_{Al}$, $[211]_{AlSb}$	$(111)_{Al}$, $(111)_{AlSb}$

5.2 Diffusion-Coupled Growth

In order to determine the growth behaviour of the two eutectic phases, the simplest morphology for the solid/liquid interface will be assumed, i.e. that which exists during the growth of a regular, lamellar eutectic. For this simple case, the problem can be treated in two dimensions and, for reasons of symmetry (appendix 2), only half of a lamellae of each phase need be considered (figure 5.2). In this figure, the alloy is imagined to be growing in a crucible which is being moved vertically downwards at the rate, V'. In a steady-state thermal environment, this is equivalent to moving the solid/liquid interface upwards at a rate, $V = V'$. The alloy of eutectic composition is growing with its essentially isothermal interface at a small temperature difference (ΔT = constant) below the equilibrium eutectic temperature, T_e. The alpha- and beta-phase interfaces are perpendicular to the solid/liquid interface and parallel to the growth direction. In order to proceed further, it is necessary to know more about the mass transport involved. It can be seen from the phase diagram that the two solid

phases are of very different composition, while the melt composition, C_e, is situated in between. Obviously, the mean composition of the solid is equal to the composition of the melt. This makes it clear that eutectic growth is largely a question of diffusive mass transport. Firstly, imagine that the two eutectic phases are growing separately from the eutectic melt with a plane solid/liquid interface (left-hand side of figure 5.3). During growth, the solid phases reject solute into the liquid. Thus, the alpha-phase will reject B-atoms into the melt, while the beta-phase will reject A-atoms. Note here that, expressed as atomic fractions, $C_B = (1 - C_A)$. When the phases are supposed to be growing separately with a plane front, solute transport must occur in the direction of growth. This involves long-range diffusion and, in the steady-state, the solute distribution is described by the exponential decay discussed in chapter 3, with a boundary layer, $\delta_c = 2D/V$. Such a long-range diffusion field will involve a very large solute build-up and a correspondingly low (much lower than T_e) growth temperature at the interface. During steady-state growth, each phase would have the interface temperature indicated by the corresponding metastable solidus line when extended as far as the eutectic composition (see figure 3.4).

Imagining now that both phases are placed side-by-side and that the solid/liquid

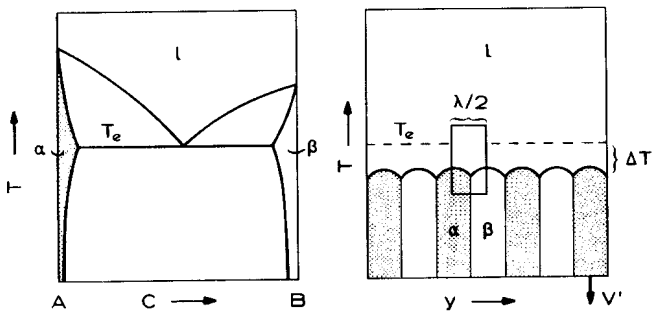

Figure 5.2: PHASE DIAGRAM AND REGULAR EUTECTIC STRUCTURE. The figure shows an eutectic phase diagram and a regular lamellar two-phase eutectic morphology growing unidirectionally in a positive temperature gradient. The alpha and beta lamellae grow side by side and are perpendicular to the solid/liquid interface. The form of the junctions where the three phases (alpha, beta, liquid) meet is determined by the condition of mechanical equilibrium. In order to drive the growth front at a given rate, V, an undercooling, ΔT, is necessary. Due to the perfection and symmetry of the regular structures, only a small volume element of width, $\lambda/2$, need be considered in order to characterise the behaviour of the whole interface under steady-state conditions.

interfaces are at the same level (figure 5.3b). This situation is much more favourable since the solute which is rejected by one phase is needed for the growth of the other. Therefore, lateral diffusion along the solid/liquid interface, at right-angles to the lamellae, will become dominant and lead to a huge decrease in the maximum solute build-up at both phases. A periodic diffusion field will be established. The varying melt composition at the interface will cause the liquidus temperature to vary along

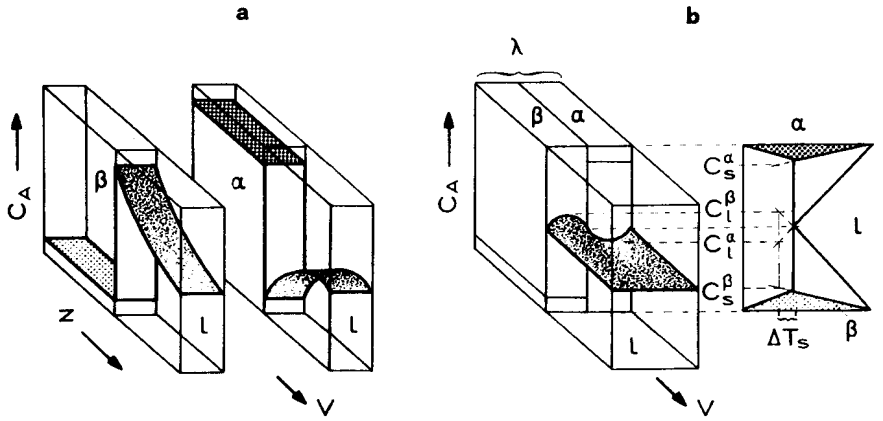

Figure 5.3: EUTECTIC DIFFUSION FIELD. If it is imagined that the two eutectic phases are growing from a melt of eutectic composition in separate, adjacent containers (a), very large boundary layers, like that in figure 3.4, will be created. If both phases are constitutionally undercooled, their solid/liquid interfaces will break down to give dendrites, making solute rejection easier. If the two containers are now brought together and the intervening wall is removed (b), extensive lateral mixing will take place because of the concentration jump at the α/β interface. The large boundary layers of the planar interfaces of 'a' (approximately equal to 2D/V) are replaced by a very limited layer whose thickness is approximately equal to the phase separation, λ. This marked change in the extent of the boundary layer is due to the diffusion flux which is established at, and parallel to, the eutectic solid/liquid interface and permits the rejection of solute by one phase to be balanced by incorporation of the solute into the other phase (diffusion coupling). The interface composition in the boundary layer oscillates, by a very small amount, about the eutectic composition, and the amplitude of the oscillation will decrease as λ decreases, when V is constant. The lateral concentration gradients create free energy gradients which exert a 'compressive' force perpendicular to the alpha/beta interface and tend to decrease λ. The corresponding phase diagram has been placed next to the solid/liquid interface in such a way that the local phase equilibria can be determined. It can be seen that the amplitude of the concentration variation at the solid/liquid interface is proportional to a solute undercooling, ΔT_s.

the solid/liquid interface of the corresponding phase. Because the maximum concentration differences at the interface (compared to the eutectic composition) are much smaller than in the case of single-phase growth, the temperature of the growing interface will be close to the equilibrium eutectic temperature. The proximity of the lamellae, while making diffusion easier, also causes a departure, from the equilibrium described by the phase diagram, due to capillarity effects (figure 5.4).

Both effects, diffusion and capillarity, are considered together in figure 5.5. In figure 5.5a, the diffusion paths at the interface are shown schematically. These are most densely packed (higher flux) at points near to the interface. They rapidly become less significant as the distance from the interface increases. The characteristic decay distance for the lateral diffusion is of the order of one interphase spacing, λ. Note that the diffusion paths for the other species, in the

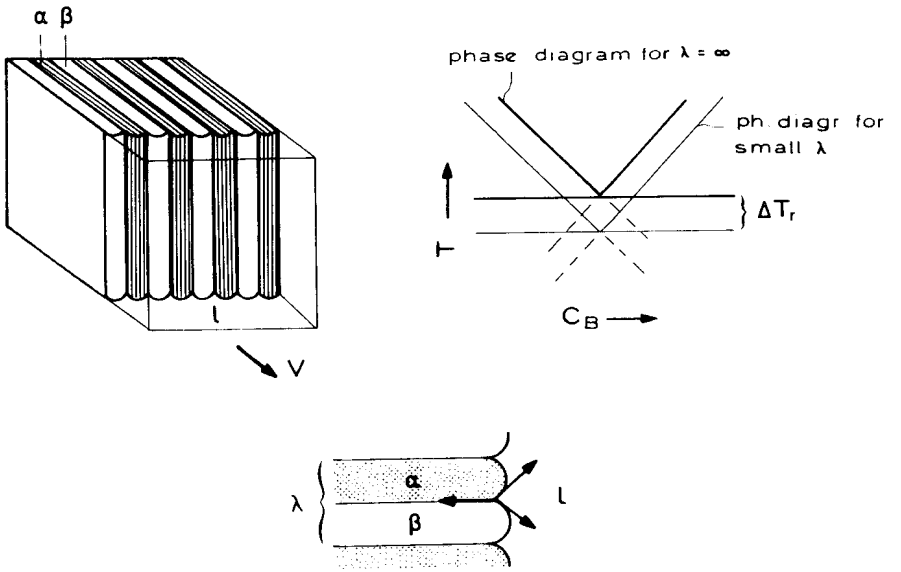

Figure 5.4: CURVATURE EFFECTS AT THE EUTECTIC INTERFACE. The diffusion field causes the λ-value of the structure to be minimised, and this leads to more rapid growth. There is an opposing effect which arises from the increased energy associated with the increased curvature of the solid/liquid interface as λ decreases. The latter can be expressed in terms of a curvature undercooling, ΔT_r, which depresses the liquidus lines of the equilibrium phase diagram as shown. The positive curvature of the solid phases in contact with the liquid arises from the condition of mechanical equilibrium of the interface forces at the three-phase junction (lower figure, see also appendix 3).

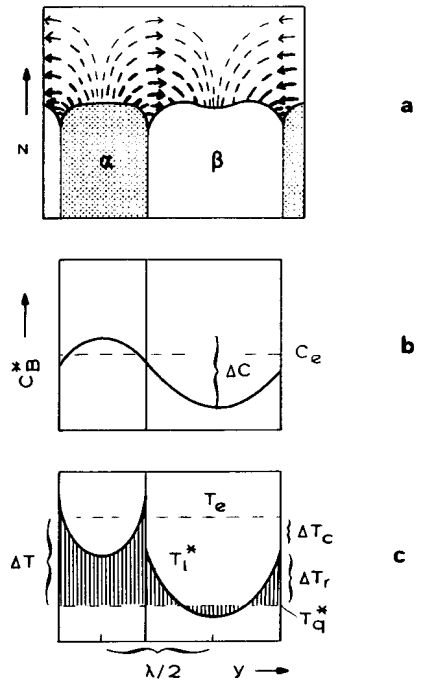

Figure 5.5: EUTECTIC INTERFACE CONCENTRATION AND TEMPERATURE. If one considers the concentration field shown on the right-hand-side of figure 5.3 more closely, it can be seen that the diffusion paths of component B will be as shown in diagram (a). The concentration in the liquid at the interface will vary as in diagram (b). (Note that the eutectic composition is not necessarily found at the junction of the two phases, and that $C_B = 1 - C_A$). This sinusoidal concentration variation decays rapidly over one interphase spacing, in the direction perpendicular to the solid/liquid interface, as shown in figure 5.3. The equilibrium between an attractive force arising from the diffusion field, and a repulsive force between the eutectic lamellae arising from capillarity effects at small λ determines the eutectic spacing. The growing interface can be regarded as being in a state of local thermodynamic equilibrium. This means that the measurable temperature, T_q^*, of the interface which is constant along the solid/liquid interface (over $\lambda/2$) corresponds to equilibrium at all points of the interface. The latter is a function of the local concentration and curvature (c). The sum of the solute (ΔT_c) and curvature (ΔT_r) undercoolings must therefore equal the interface undercooling, ΔT. A negative curvature, as shown here at the centre of the beta lamella, is required when the solute undercooling, ΔT_c, is higher than ΔT. The discontinuity in the solute undercooling, as the alpha/beta interface is crossed, is only a discontinuity in equilibrium temperature and not a real temperature discontinuity.

opposite direction, are analogous. According to the phase diagram, the sinusoidal concentration variation at the solid/liquid interface (figure 5.5b) leads to a change in the liquidus temperature of the melt in contact with the phases (figure 5.5c). The points where the liquid composition, C_B^* is equal to C_e are exactly at the eutectic temperature, while those points of the alpha-phase close to the alpha/beta interface are at a higher liquidus temperature because the liquid in these regions has a lower content of B, as determined by the lateral diffusion field. On the other hand, the melt ahead of the beta-phase is always richer in A than is the equilibrium eutectic composition. Therefore, its liquidus temperature is lower, compared to the equilibrium eutectic temperature, and decreases with increasing values of C_A. (These relationships can be understood with the aid of the phase diagram - see exercises 5.7 and 5.8).

In order to determine the solute distribution, the flux condition (appendix 2) must first be applied. In the present calculation, it is assumed that the interface is planar and that the sinusoidal concentration variation of figure 5.5b can be approximated by using a saw-tooth waveform with amplitude, $\Delta C = (C_l^\alpha - C_l^\beta)$, and diffusion distance, $\lambda/2$. In this way, the concentration gradient in the liquid at the solid/liquid interface is found to be: $(dC/dy)_{z=0} = \Delta C/(\lambda/2)$ and the flux transporting atoms from one solid phase to the other via the liquid is:

$$J_t = -\frac{2D\Delta C}{\lambda} \qquad [5.1]$$

The rejected flux per unit solid/liquid interface area is equal to $V(C_l^* - C_s^*)$, giving:

$$J_r \simeq VC_e(1 - k) \qquad [5.2]$$

This relationship holds for deviations of the melt concentration, ΔC, which are small compared to C_e, and $C_l^* \simeq C_e$. This is the case for many eutectics, where ΔC is typically of the order of 1%, and C_e is of the order of 50%.

Under steady-state conditions, the flux balance, $J_t = J_r$, can then be written:

$$\frac{\Delta C}{C_e(k - 1)} = \frac{\lambda V}{2D} \qquad [5.3]$$

which is, in fact, entirely analogous to the previously presented equation for the diffusional growth of a hemispherical needle. The left-hand-side of equation 5.3 corresponds to a supersaturation, while the right-hand-side is the Péclet number for eutectic growth. Therefore, one can also write equation 5.3 in the form:

$$\Omega_e = P_e \qquad [5.4]$$

The concentration difference, ΔC, required to drive solute diffusion in eutectic growth can be used to determine a temperature difference (undercooling) from the phase diagram, via the constant liquidus slopes, $\Delta C = \Delta T_c[1/(-m_\alpha) + 1/m_\beta]$, leading, via equation 5.3, to a relationship of the form:

$$\Delta T_c = K_c \lambda V \qquad [5.5]$$

From equation 5.4 or 5.5, it can be seen that this problem is not completely solved because, as in the case of dendritic growth, the above equations apply equally well to a fine eutectic growing at high rates or a coarse eutectic growing at low rates.

5.3 Capillarity Effects

Returning to the periodic concentration variation existing ahead of the solid/liquid interface (figure 5.5), it can be seen that the corresponding liquidus temperature varies from values greater than T_e, for certain regions of the alpha-phase, to values below the actual interface temperature, T_q^*. The difference (hatched region in figure 5.5c) has to be compensated by the local curvature in order to maintain local equilibrium at the interface. Thus, since T_q^* is constant due to the high thermal conductivity and small dimensions of the phases:

$$\Delta T = \Delta T_c + \Delta T_r = T_e - T_q^* = \text{constant } (\S) \qquad [5.6]$$

A negative curvature (depression) may appear at the center of a lamella in order to compensate for a very high local solute concentration which is often associated with a large spacing, λ.

At points close to the alpha/beta interface, another condition must be imposed. That is, the alpha/beta interface energy, $\sigma_{\alpha\beta}$, at the three-phase junction, has to be balanced by the sum of components of the α/ι- and β/ι-interface energies (figure 5.4). The angles at the three-phase junction are thereby determined by considerations of mechanical equilibrium (appendix 3).

The curvature of the alpha/liquid or beta/liquid interface, necessary to match the angles at the three-phase junction, changes the equilibrium temperature by an amount, ΔT_r, which is a function of y (figure 5.5c). By calculating the mean curvature over the alpha/liquid and beta/liquid interfaces (appendix 9), the effect of capillarity can be related to a mean change in the liquidus temperature by (equation 1.4):

$$\Delta T_r = \Gamma K$$

Because the curvature, K, is proportional to $1/\lambda$:

$$K = \frac{K'}{\lambda} \qquad [5.7]$$

where K' is a constant. Use of equations 5.5 to 5.7 leads to the following relationships for the solid/liquid interface undercooling:

$$\Delta T = K_c \lambda V + \frac{K_r}{\lambda} \qquad [5.8]$$

Thus, a relationship is obtained which exhibits a maximum in the growth temperature (equivalent to a minimum in ΔT) as a function of λ (figure 5.6), where the growth rate is imposed and constant and ΔT is the dependent variable. Constant values of the growth rate are typical of directional solidification. On the other hand, the undercooling is imposed and constant in the initial stages of equiaxed solidification and results in a maximum in the V-λ-curve (figure 5.7).

5.4 Operating Range of Eutectics

Upon considering equation 5.8, it becomes clear that it is not uniquely determined since ΔT is a function of the product, λV. Therefore, another equation is required in order to determine the growth behaviour of an eutectic. This situation is analogous to that existing in dendrite growth. In the case of dendrite growth, the assumption of growth at the limit of morphological stability as the operating point has been found to correspond well with the experimental results. In the case of eutectic growth, both a point analogous to this one, and the extremum point, have been found to explain various experimental results. Eutectic alloys which grow in a regular manner (e.g. Pb-Sn) can be described well by the use of the extremum criterion. Using this assumption, the first derivative of equation 5.8 is determined and set equal to zero:

$$\frac{d(\Delta T)}{d\lambda} = 0 \qquad [5.9]$$

§ As in the case of directional dendrite growth, the thermal undercooling is zero during directional eutectic growth because heat is flowing into the solid (G>0).

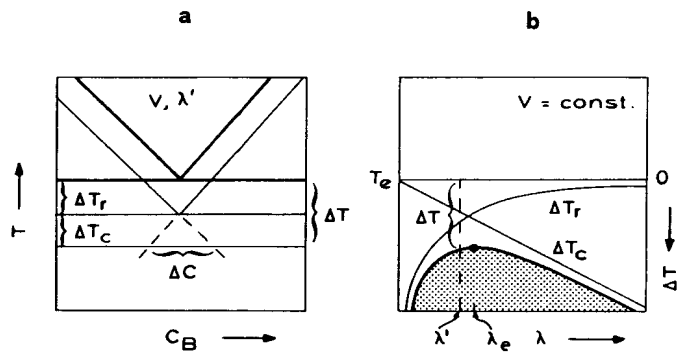

Figure 5.6: CONTRIBUTIONS TO THE TOTAL UNDERCOOLING IN EUTECTIC GROWTH. Using figure 5.5c, a mean solute undercooling and a mean curvature undercooling can be defined. Both undercoolings vary in opposite senses when the spacing is changed; ΔT_c increases linearly while ΔT_r decreases with increasing spacing (b). Note that ΔT is measured downwards with respect to T_e. The sum of the contributions exhibits a minimum in ΔT or a maximum in T with respect to λ. At smaller spacings, eutectic growth is controlled by capillarity effects ($\Delta T_r > \Delta T_c$). At larger spacings, diffusion is the limiting process. Generally, it is assumed (ad hoc) that growth will occur at the extremum, λ_e. An increase in the growth rate increases the absolute value of the slope of the ΔT_c line, without influencing the ΔT_r curve, and displaces the maximum of the T-λ curve to smaller spacings.

The condition that ΔT be a minimum implies, since $\Delta T = \Delta G/\Delta S_f$, that $d(\Delta G)/d\lambda = 0$ and means that the driving force for spacing changes is zero. Insertion of the corresponding value of the spacing leads to the final result for growth at the extremum:

$$\lambda^2 V = \frac{K_r}{K_c} \qquad [5.10]$$

$$\frac{\Delta T}{\sqrt{V}} = 2\sqrt{K_r K_c} \qquad [5.11]$$

$$\Delta T \lambda = 2K_r \qquad [5.12]$$

Equation 5.10 is illustrated in figure 5.8.

The situation is more complex when irregular eutectics are considered. In this case, the local spacing corresponding to the extremum values can be found, but the mean spacing is much larger (figure 5.8). Such large spacings can be explained by the difficulty which this class of eutectic experiences in branching. The latter is an essential mechanism which permits the eutectic to adapt its scale to the local growth conditions and to approach the extremum point. If one of the phases does not easily change direction during growth, and instead grows in a highly anisotropic manner (e.g. the faceted phases, C and Si, in Fe- and Al-alloys respectively), due to its atomic structure or planar defect growth mechanism, the lamellae of the phase must diverge until one of them can branch. This behaviour can be understood with the aid

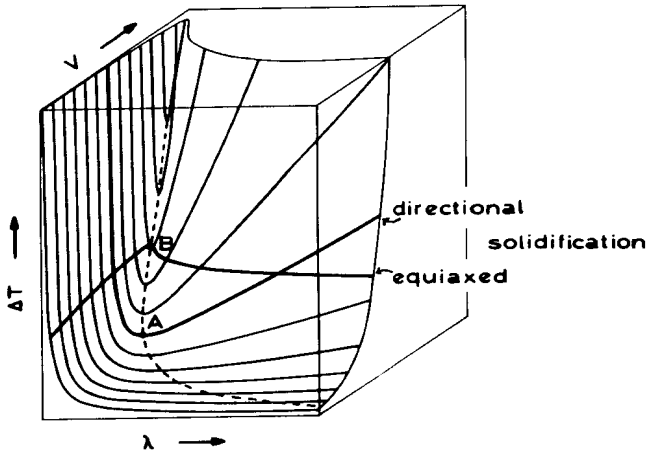

Figure 5.7: OPTIMISATION OF THE EUTECTIC SPACING. A range of possible spacings exists, each of which satisfies local equilibrium requirements. This situation is described by the ΔT-V-λ surface of this figure which form a valley running from the left rear to the front right of the diagram. (The ΔT axis is reversed here with respect to the equivalent diagram in figure 5.6b). It is seen that if the growth rate is constrained (V = constant), as in directional solidification, a minimum in the ΔT-λ curve (e.g. at point A) is obtained, corresponding to the maximum in the T-λ of figure 5.6b. If ΔT is maintained constant, as in equiaxed (isothermal) growth, the V-λ curve exhibits a maximum at point B for example. This curve for the plane-front growth of an eutectic is analogous to that in figure 4.9 for dendrites, where R replaces λ. The spacings corresponding to A or to B are called 'extremum' or 'optimum' spacings and, in regular eutectics, correspond closely to experimentally determined values.

of figure 5.9. When two adjacent lamellae are growing with the extremum spacing and begin to diverge, the interface of the matrix will first become depressed because of the consequent increase in solute concentration at its centre (lower middle of figure 5.9). As the solute builds up more and more at the interface of the diverging phases, the growth temperature must decrease because ΔT_c increases. Finally, the diverging phases will reach a spacing which is so large that even the low volume fraction phase will exhibit depressions at its solid/liquid interface. Under these conditions, the single lamella may branch into two. When a new lamella has been created, it will usually diverge from the other one of the pair and tend to converge towards other lamellae at the interface (figure 5.10). In this case, since the phase separation is decreasing, the interface temperature will increase, due to the decreasing solute build-up, and eventually reach the maximum in temperature (or minimum in undercooling). As the faceted phase cannot easily change its growth direction, its growth will decrease the local spacing to a value below the extremum value. However, smaller values will soon decrease the temperature appreciably due to the steep slope of the curve in this region. As a result, any spacing smaller than the extremum value will tend to be increased by the cessation of growth of one of the neighbouring lamellae (a termination appears).

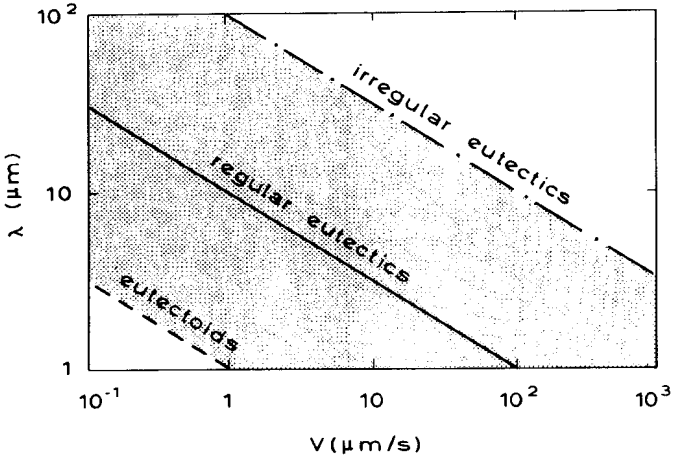

Figure 5.8: EUTECTIC AND EUTECTOID SPACINGS AS A FUNCTION OF GROWTH RATE. If the optimum spacings (figure 5.7) are determined for a range of growth rates (projection of the broken line on the λ-V surface in figure 5.7), curves such as the centre one above are found, where the spacing versus growth rate relationship can be described by $\lambda^2 V$ = constant. The eutectoid microstructure resembles that of the eutectic, as does its growth law, but diffusion occurs only through solid phases. Thus, there is a tendency to decrease the diffusion distances by decreasing the spacing, and the values of the latter are therefore smaller than those of regular eutectics. Also, because of the relative inefficiency of solid-state diffusion, interface diffusion can be very important in eutectoid growth. In this case, the growth law is no longer the same as that for eutectic growth. Irregular eutectics, such as Fe-C and Al-Si, do not appear to grow at the extremum, but rather at larger values of λ.

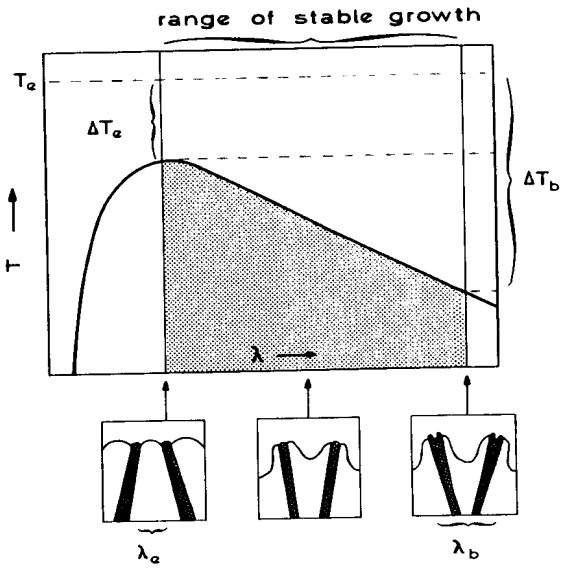

Figure 5.9: SPACING-CONTROLLING MECHANISMS IN IRREGULAR EUTECTICS. This figure illustrates the interface morphologies obtained with convergent and divergent growth of the minor faceted phase of an irregular eutectic. In this case, the faceted phase can grow only along a planar growth defect (figure 2.10), making changes in the growth direction of the faceted phase, and therefore in the spacing, very difficult. In convergent growth, the spacing will decrease during growth, thereby increasing the curvature of both phases. This will lead to the cessation of growth in that region because the interface temperature drops at the left of the extremum, λ_e, due to an increasing ΔT_r value. In divergent growth, the spacing becomes larger during growth, leading to increased solute pile-up ahead of both phases. This leads to the formation of depressions in the major phase at first (figure 5.5), and later in the minor phase. When the minor phase becomes depressed at λ_b, branching (formation of two lamellae from one) is possible and the spacing will be decreased again. This leads to zig-zag growth of the faceted phase between λ_e and λ_b.

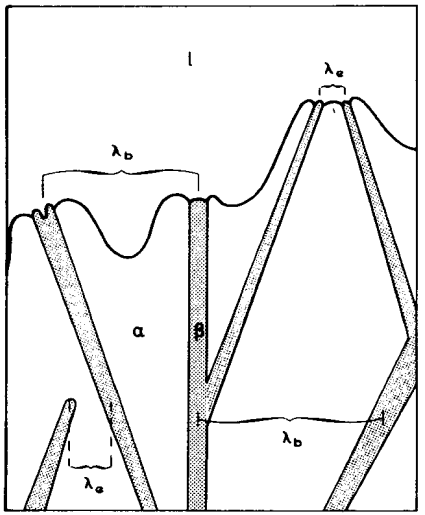

Figure 5.10: GROWTH OF IRREGULAR EUTECTICS. Difficulty in smoothly changing the growth direction (stiffness) of certain faceted phases results in the zig-zag growth structure described in figure 5.9. Here, the corresponding spacings are defined as well as the non-isothermal character of the solid/liquid interface. The resultant microstructures are irregular, and common examples are the two eutectics, Fe-C and Al-Si, upon which most commercial casting alloys are based.

Thus, the range of stable eutectic growth is located between the extremum value, λ_e, and the branching spacing, λ_b. Only those eutectics with branching difficulties will exploit the whole range and this explains their coarse spacing (figure 5.8), large undercoolings, large spacing variations (= irregularity), and sensitivity to temperature gradient variations.

The branching point can be calculated by using a stability analysis which is analogous to the criterion used in the case of dendritic growth. The main difficulty involved in using this approach is the estimation of the concentration gradient at the non-isothermal interface. This has been done by the use of numerical methods (Fisher & Kurz, 1980).

5.5 Competitive Growth of Dendritic and Eutectic Phases

As shown in figure 5.11, binary eutectics can undergo two types of morphological instability; single-phase or two-phase. The latter is analogous to the morphological instability of a planar single-phase interface (chapter 3) but, due to the very complex behaviour involved, quantitative analysis is difficult. In general, it can be said that a third alloying element which is similarly partitioned between both solid phases will lead to two-phase instability and the appearance of cells or even eutectic dendrites (figure 5.11b).

When the third element is incorporated preferentially into one phase, or during off-eutectic growth of a pure binary eutectic, single-phase instability can occur and result in the appearance of mixed structures, that is, dendrites of one phase and

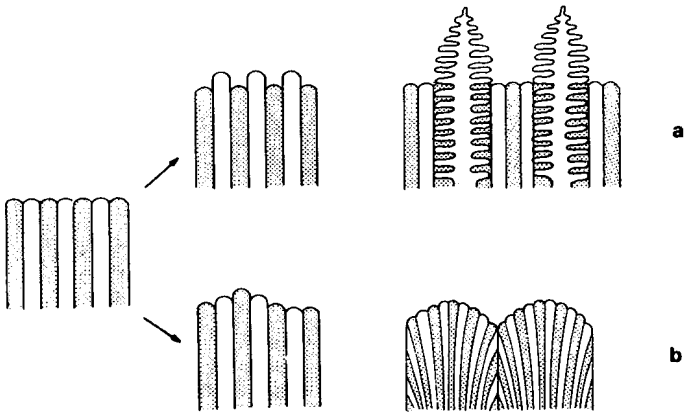

Figure 5.11: TYPES OF EUTECTIC INTERFACE INSTABILITY. The planar eutectic solid/liquid interface can become unstable just as in the case of a single-phase interface. Here, there are two different ways in which an instability can develop; instability of one phase (a), or instability of both phases (b). The former leads to the appearance of dendrites of one phase (plus interdendritic eutectic) and is mainly seen in off-eutectic alloys in binary systems. Alternatively, a third (impurity) element may destabilise the morphology as a whole because a long-range diffusion boundary layer is established ahead of the composite solid/liquid interface. (Recall that the eutectic tie-line of a binary system degenerates to an eutectic three-phase ($\iota + \alpha + \beta$) region in a ternary system). This can lead to the appearance of two-phase eutectic cells or dendrites (b).

interdendritic two-phase eutectic (figure 5.11a). The reason for the latter effect is that, due to the long-range boundary layer built up ahead of the solid/liquid interface in this case, one phase becomes heavily constitutionally undercooled. This can be appreciated from the fact that, in an off-eutectic composition, the alloy liquidus is always higher than the eutectic temperature (figure 5.12). That is, the corresponding

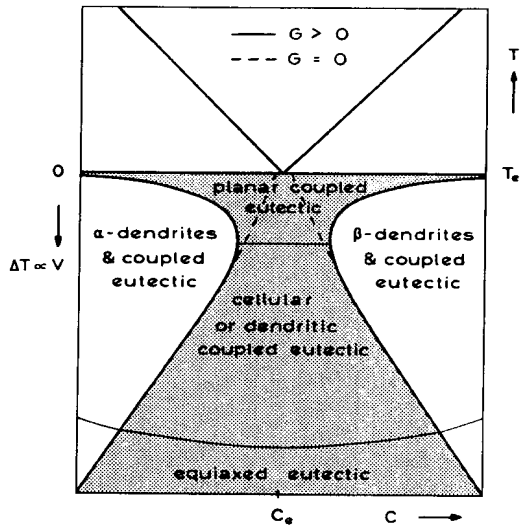

Figure 5.12: COUPLED ZONE OF EUTECTICS. From consideration of the equilibrium eutectic-type phase diagram alone, it might be thought that microstructures consisting entirely of the eutectic can only be obtained at the exact eutectic composition. In fact, due to the growth characteristics of dendrites and eutectics, the latter can often grow more rapidly than the dendrites and therefore outgrow them over a range of growth conditions. This occurs during directional growth, in a Bridgman furnace for instance (figure 1.4a), when the dendrite tip temperature is low. This can happen at both low and high growth rates (figure 4.13). The coupled zone (grey region) represents the growth temperature/composition region where the eutectic grows more rapidly (or at a lower undercooling) than dendrites of the alpha or beta phases. This zone, corresponding to an entirely eutectic microstructure, may take the form of an anvil, where the upper widening is detected in experiments carried out at low growth rates and high temperature gradients, and the lower widening is found for growth at high growth rates, corresponding to high undercoolings. Within the coupled zone, an increased growth rate (decreased temperature) will destabilise the solid/liquid interface due to the presence of impurities. This leads firstly to the formation of two-phase cells and later to the formation of two-phase dendrites (figure 5.11b). Outside of the coupled zone, primary dendrites and interdendritic eutectic will grow simultaneously (figure 5.11a).

primary phase will be more highly undercooled and tend to grow faster than the eutectic. This case is of considerable importance because the properties of a casting can be appreciably impaired or enhanced when single-phase dendrites appear. Under some circumstances, dendrites can be observed in alloys having an exactly eutectic composition if the growth rate is sufficiently high. The reason for this behaviour is qualitatively explained by figure 5.13. The undercooling of the eutectic interface as a function of V is described by equation 5.11, while the undercooling of the dendrite tips obeys an analogous relationship when the temperature gradient is equal to zero. When growth occurs in a positive temperature gradient, the temperature-velocity curve exhibits a maximum (figure 4.13) and the eutectic curve (which is usually unaffected by G) may be cut at both high and low growth rates. When the dendrite curve is below the eutectic curve, only eutectic will be observed. When the dendrite curve is higher, both dendrites and eutectic are observed. If the undercoolings which lead to entirely eutectic growth are determined for a range of compositions, they make up what is known as the coupled zone. When the coupled zone is symmetrical (figure 5.12), the eutectic morphology will obviously be obtained for eutectic

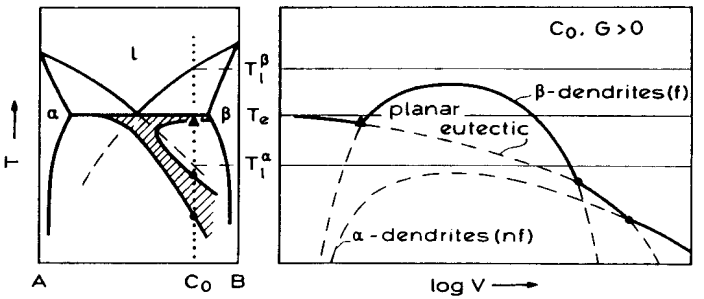

Figure 5.13: ORIGIN OF SKEWED COUPLED ZONES. Symmetrical coupled zones (figure 5.12) are associated with regular eutectics and reflect the similar undercoolings of the two primary dendrite types. When the eutectic is irregular, the associated high undercoolings at high growth rates of the eutectic and the faceted(f) primary β-phase, compared to that of the non-faceted (nf) α-phase, lead to the establishment of a skewed zone. The most important practical effect of this is that a fully eutectic microstructure may not be obtained when an alloy of eutectic composition is rapidly solidified. Because the zone is skewed towards the phase which has growth problems (such as Si in the Al-Si system), it is necessary to use a starting composition which is richer than C_e in the faceted element in order to obtain dendrite-free eutectic microstructures.

compositions at all growth rates (undercoolings). However, in the case of skewed coupled zones, high growth rates may lead to the formation of alpha-dendrites even on the beta-rich side of the eutectic composition. Such skewed zones are usually associated with eutectics which contain one phase having anisotropic growth characteristics. Thus, a skewed zone is normally associated with irregularity of the eutectic morphology (e.g. Al-Si or Fe-C). These assumptions hold only for normal growth conditions. In the case of rapid solidification processing (for example: fibre-spinning, strip-casting, laser surface remelting), new phenomena may occur due to the extremely high undercooling reached. These have been summarised in an interesting paper by Boettinger (1982).

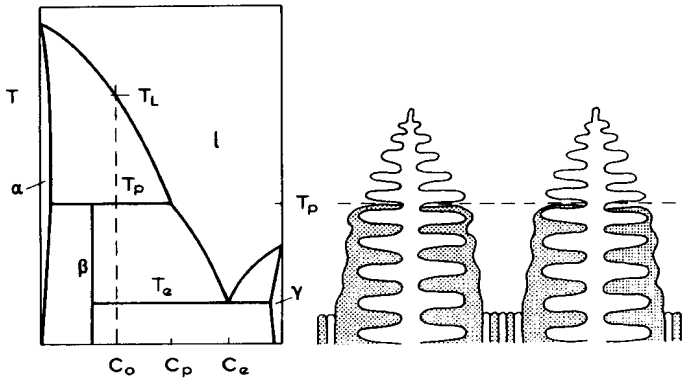

Figure 5.14: DIRECTIONAL PERITECTIC GROWTH. This is an important reaction which occurs in steels, bronzes, and other alloys. It has been suggested that conditions similar to those used in off-eutectic solidification might suppress primary dendrite growth and lead to the formation of an eutectic-like microstructure, at least over short distances. This has not been clearly demonstrated, and the usual sequence of events is that primary dendrite trunks form close to T_l and begin to react with the liquid to form β-phase close to T_p. Because this involves diffusion through the solid β-phase, the reaction is very slow and is rarely completed before the remaining, un-reacted liquid disappears or undergoes an eutectic reaction at T_e (if there is an eutectic in the phase diagram). Normal solidification conditions will tend to produce a microstructure which consists of primary α-dendrites, with a surface layer of β-phase, separated by interdendritic $\alpha + \beta$ eutectic. Dissolution of the interdendritic peritectic phase by preferential chemical etching reveals the form of the dendrites (as on the cover of this book).

5.6 Peritectic Growth

In peritectic alloys, steady-state coupled growth, analogous to that of eutectics, is theoretically impossible and hence similar, uniform, fine microstructures are unknown. Some evidence exists which suggests that coupled growth may be possible over short distances but, in general, dendrites of one phase are formed. At a point behind the dendrite tip, partial reaction with the interdendritic liquid begins and gives the peritectic phase (figure 5.14). The microstructure of these alloys is therefore dendritic, with the peritectic phase, and possibly an eutectic phase, forming the interdendritic precipitate (Glardon & Kurz, [1981]).

BIBLIOGRAPHY

BIBLIOGRAPHY

- Theory of Eutectic Growth

C.Zener: Transactions of the Metallurgical Society of AIME 167 (1946) 550
M.Hillert: Jernkontorets Annaler 141 (1957) 757
W.A.Tiller in: Liquid Metals and Solidification, American Society for Metals, Cleveland, Ohio, 1958, p276
K.A.Jackson, J.D.Hunt: Transactions of the Metallurgical Society of AIME 236 (1966) 1129
T.Sato, Y.Sayama: Journal of Crystal Growth 22 (1974) 259
D.J.Fisher, W.Kurz: Acta Metallurgica 28 (1980) 777
I.Minkoff: The Physical Metallurgy of Cast Iron, Wiley, New York, 1983

- Eutectic Growth Experiments

B.Lux, W.Kurz, M.Grages: Praktische Metallographie 6 (1969) 464
J.D.Livingston, H.E.Cline, E.F.Koch, R.R.Russell: Acta Metallurgica 18 (1970) 399
A.Hellawell in: Progress in Materials Science 15 (1970) 1
H.A.H.Steen, A.Hellawell: Acta Metallurgica 20 (1972) 363
Y.Sayama, T.Sato, G.Ohira: Journal of Crystal Growth 22 (1974) 272
B.Lux, A.Vendl, H.Hahn: Radex Rundschau (1980) No.1/2 30
H.Jones, W.Kurz: Metallurgical Transactions 11A (1980) 1265
H.Jones, W.Kurz: Zeitschrift für Metallkunde 72 (1981) 792

- Coupled Zone

G.Tammann, A.A.Botschwar: Zeitschrift für Anorganische Chemie 157 (1926) 26
A.Kofler: Zeitschrift für Metallkunde 41 (1950) 221
E.Schiel: Giesserei, technisch-wissenschaftliche Beihefte 24 (1959) 1313
W.Kurz, D.J.Fisher: International Metals Reviews 5/6 (1979) 177

- Directionally Solidified Eutectics

L.M.Hogan, R.W.Kraft, F.D.Lemkey in: Advances in Materials Research, (Edited by H.Hermann), 5 (1971) 83.
E.R.Thompson, F.D.Lemkey in: Composite Materials, Volume 4, (Edited by K.G.Kreider), Academic Press, New York, 1974.
W.Kurz, P.R.Sahm: Gerichtet erstarrte eutektische Werkstoffe, Springer, Berlin, 1975.

- Rapid Solidification of Eutectics

W.Boettinger in: Rapidly Solidified Amorphous and Crystalline Alloys (edited by B.H.Kear, B.C.Giessen), Elsevier, New York, 1982.
R.Elliott: Eutectic Solidification Processing - Crystalline and Glassy Alloys, Butterworth, London, 1983

- Peritectics

W.Boettinger: Metallurgical Transactions 5 (1974) 2023
R.Glardon, W.Kurz: Journal of Crystal Growth 51 (1981) 283
D.H.St John, L.M.Hogan: Acta Metallurgica 25 (1977) 77

- Spheroidal Graphite Cast Iron

B.Lux: Cast Metal Research Journal 18 (1972) 25, 49

EXERCISES

5.1 Calculate the equilibrium volume fraction of carbon at T_e in an Fe-C alloy of eutectic composition.

5.2 Calculate, on purely geometrical grounds, the volume fraction at which fibrous or lamellar structures have the lower total α/β interface energy. Assume that the α/β interface energy is isotropic and that the phase separation, λ, is equal and constant in both cases.

5.3 In figure 5.5b, the solute concentration in the liquid at the eutectic solid/liquid interface ($z = 0$) is given. Draw an approximate C-y diagram for $z = \lambda$.

5.4 In order to demonstrate the potential value of producing 'in-situ' composites via directional eutectic solidification, calculate the total length of fibres contained in a composite cube of side 1cm when $\lambda = 1\mu m$.

5.5 An eutectic stores part of the transformation energy in the form of α/β interfaces (figure 5.4). By what amount, ΔT, will the melting point of a lamellar eutectic with $\lambda = 1\mu m$ and $\sigma_{\alpha\beta} = 5 \times 10^{-8} J/mm^2$ be lowered? As shown in appendix 12, the magnitude of Δs_f is typically of the order of $10^6 J/m^3 K$.

5.6 Find expressions for K_c and K_r (equation 5.8) for the simple case shown in the main text, and derive the solutions for extremum growth.

5.7 Using the phase diagram, explain the apparent discontinuity of the liquidus temperature, T_l^*, at the α/β-junction shown in figure 5.5c.

5.8 Draw analogous diagrams to those in figure 5.5 for the case where both phases have a positive curvature, and for the case where both phases have depressions at their centers.

5.9 It can be easily shown that, at least over one half-spacing of the eutectic (figure 5.2), the solid/liquid interface of the eutectic must be very close to isothermal: an enormous heat flux in the y-direction would be required in order to change, even slightly, the interface temperature of the two phases. Using the properties of Al (appendix 12), calculate this lateral heat flux, assuming that $\Delta T_y = 0.1K$ and that $\lambda = 1\mu m$.

5.10 Experiments performed on eutectic Fe-C alloys reveal the following relationship for the mean lamellar spacing, $\bar{\lambda}$: $\bar{\lambda}^2 V = 4 \times 10^{-7} mm^3/s$. Does this support the extremum criterion? Use equation A9.30.

5.11 Is an effect of G upon the spacing of regular eutectic microstructures at a given growth rate to be expected? Explain your answer.

5.12 Draw a T-V diagram, similar to that in figure 5.13, for a symmetrical coupled zone under conditions where $G > 0$.

5.13 Repeat exercise 5.12 for the case when $G \leq 0$. Compare your results with figure 5.12. (First study figure 4.13 in detail).

5.14 Under constrained growth conditions ($G>0$) at low growth rates, coupled eutectic growth without the appearance of dendrites is possible at off-eutectic compositions (figure 5.12). Calculate the limit of stability of a hypereutectic Al-Al_2Cu(θ) alloy containing 36wt%Cu at which θ-dendrites plus eutectic will appear as in figure 5.11a. (Hint: use the simple constitutional undercooling criterion and replace ΔT_o by $T_l - T_e$). To what line in figure 5.12 does this situation correspond? What will happen if G is doubled?

5.15 From the growth equations for dendrites (when $G \leq 0$) and eutectic: $\Delta T_d = K_d \sqrt{V}$ and $\Delta T_e = K_e \sqrt{V}$, determine the limiting growth rate and temperature of the coupled zone as a function of the composition. (Note that both growth morphologies must grow at the same rate in order to exist side-by-side under steady-state conditions. Assume that the constants, K_d and K_e, are independent of the composition and that ΔT_d and ΔT_e are defined as shown in the figure below.

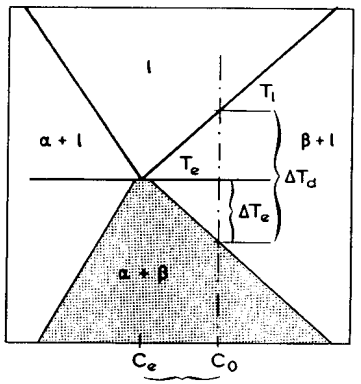

5.16 Sketch the solid/liquid interface of a unidirectionally and dendritically solidifying steel containing 0.2wt%C. Note that, due to the rapid solid-state diffusion of carbon in δ-Fe and γ-Fe, the liquid/solid and solid/solid transformations closely follow the behaviour to be expected on the basis of the equilibrium diagram.

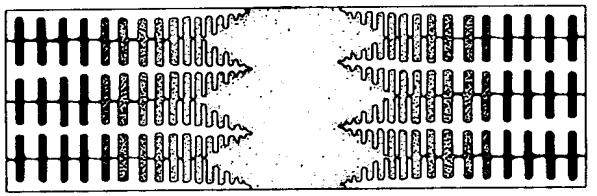

CHAPTER SIX

SOLUTE REDISTRIBUTION

It has been explained in some detail in chapter 3 that the solid/liquid interface rejects solute into the liquid when the solubility of the solute element in the solid is smaller than that in the liquid. In this case, the liquidus slope, m, is negative and the distribution coefficient, k, is smaller than 1. On the other hand, m is positive and k is greater than unity when the solubility is greater in the solid than in the liquid. In this case, solute will diffuse from the liquid to the solid. This leads to the creation of a depleted zone ahead of the solid/liquid interface.

As far as metals growing under normal solidification conditions are concerned, local equilibrium is assumed to hold at the solid/liquid interface. Then, at the interface, the solid concentration is related to the liquid concentration by the equilibrium distribution coefficient (equation 1.8):

$$C_s^* = k\, C_l^*$$

This compos. al difference will always lead to concentration variations, in the solidified alloy, which are known as segregation. Note that the solute distribution in the liquid ahead of the solid/liquid interface leads to the appearance of the various growth morphologies and the latter in turn determine the solute distribution in the solid. Concentration differences over microscopic distances, interdendritic precipitates and porosity are the result.

Because solute can be transported by diffusion or by convection (or both), the segregation pattern will be quite different depending upon the process involved. Convection can lead to the transport of mass over very large distances, compared to those involved in diffusional processes, and may result in macrosegregation, that is, compositional differences over distances equal to the size of a large casting. As convection will not be treated in this book, for reasons outlined in the foreword, attention will here be limited to microsegregation (§). The latter depends upon solute diffusion in the liquid and solid and is related to the dendrite shape and size. Understanding of this phenomenon is the key to interpreting the influence of solidification on the mechanical properties of cast products or welds. Furthermore, microsegregation reveals the original microstructure of any solidified alloy via the differences in etching tendency of regions of varying local composition.

In order to understand the segregation occurring at the scale of the dendrites, which is complicated due to the morphology of these crystals, it is useful to begin with a description of the solute distribution existing during directional solidification of a rod of constant cross-section with a planar solid/liquid interface (figure 1.4). In this special case, all of the changes occur in one dimension only and are therefore easier to analyse. Once this case is fully understood, it will be possible to use the results to study in a qualitative manner more complicated cases by imagining the changes occurring in small volume elements to be the same as those occurring during directional solidification (figure 1.5).

6.1 Mass-Balance in Directional Solidification

In chapter 3, the mass balance was treated only with respect to steady-state conditions. In order to understand microsegregation it is also essential to consider the initial and final transients. The first is required in order to establish the steady-state

§ For an introduction to convection effects in solidification, the reader is referred to the bibliography at the end of the chapter.

boundary layer, and the second arises from the interaction of the bound. ayer at the solid/liquid interface with the end of the specimen (figure 6.1). The diffusion boundary layer in the liquid ahead of a planar solid/liquid interface can be regarded as a limited region of the system which transports the solute missing from the initial transient in the solid where the concentration is below C_o, and maintains constant the overall composition of the system. This moving boundary layer disappears at the end of solidification by 'depositing' its solute content in the final transient. Thus, the mean composition of the solid is always the same as that of the liquid from which it is formed. Account is not taken here of reactions with the crucible or vaporisation of the alloy.

6.2 The Initial Transient

Figure 6.1 depicts in a schematic manner, the mechanism leading to the formation of the boundary layer and the initial transient. The process is shown for a bar of constant cross-section, A (appendix 10). When the first volume element, Adz', has solidified (where dz' is vanishingly small), the solute which has not been incorporated into the solid is equal to the incremental volume of the solid (Adz), multiplied by the difference in composition between the liquid and the solid (C_l^*-C_s^*), which at $z' = 0$ is equal to C_o-kC_o. This mass, divided by the time necessary for the advance of the interface by dz', leads to a solute flow at the interface where $V = dz'/dt$ (equation 3.4):

$$J_1 = AVC_l^*(1 - k)$$

This flow leads to the creation of a pile-up at the interface and leads to the establishment of a concentration gradient, and diffusional flow into the liquid adjacent to the interface:

$$J_2 = -ADG_c = AV(C_l^* - C_o) \qquad [6.1]$$

Note that $G_c = (C_l^* - C_o)V/D$ (appendix 2). The difference between the two flows, J_1, due to the creation of solid and J_2, due to diffusion in the liquid, gives the approximate variation in mean solute accumulation in a boundary layer of thickness, δ_c:

$$J_1 - J_2 = \left(\frac{d\bar{C}}{dt}\right)\delta_c \qquad [6.2]$$

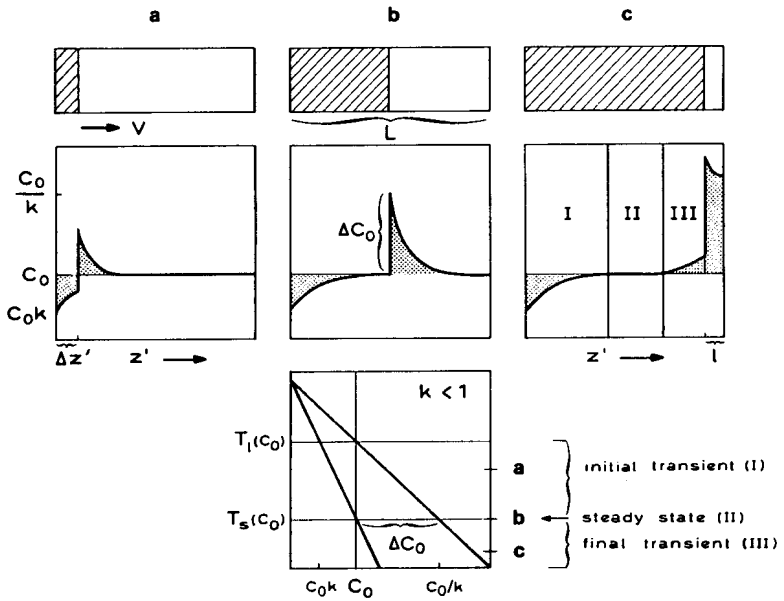

Figure 6.1: INITIAL AND TERMINAL TRANSIENTS. During directional solidification with a planar solid/liquid interface, in an apparatus such as the Bridgman furnace (figure 1.4), the establishment of a steady-state boundary layer requires a distance of growth which corresponds to the length of the initial transient. This distance increases with decreasing growth rate. Within this transient, the concentration of the liquid at the interface increases from C_0 to C_0/k. With respect to the phase diagram (assuming the existence of local equilibrium), this means that the first solid to freeze has the composition, kC_0, and reaches the composition, C_0, and the interface temperature, T_S, corresponding to composition, C_0, at the steady-state. At the steady-state, the flux due to the interface advance (which arises from the difference in liquid and solid solubilities) is equal to the diffusional flux due to the concentration gradient at the solid/liquid boundary. In this case, the exponential decay described in chapter 3 is the exact solution. Finally, when the boundary layer becomes equal to the length of the remaining liquid region, diffusion into the liquid phase is hindered by the system boundary (the concentration gradient must be zero at the end of the crucible). Thus, the concentration in the liquid at the solid/liquid interface begins to increase to a value which is greater than C_0/k, and the solid concentration therefore becomes greater than C_0 and a terminal transient is created. In order to maintain the conservation of mass, the surface area of the grey region below C_0 must be equal to the grey area above C_0. Note that the lengths of the initial and terminal transients are unequal. These concentration variations can be a major problem in solidification processes and are known as segregation. The same phenomenon is usefully exploited in 'zone-refining', where the depleted (purer) part of the rod of used.

This leads to a differential equation which, upon integration, gives (appendix 10):

$$C_l^* \simeq \left(\frac{C_0}{k}\right)\left[1 - (1 - k)\exp\left(-\frac{kz'V}{D}\right)\right] \qquad [6.3]$$

As shown in figure 6.1, the initial transient exists until the increasing flow, J_1 (proportional to C_l^*) becomes equal to the initially smaller, but more rapidly increasing flow, J_2 (proportional to G_c). Figure 6.2 shows equation 6.3, for the solid composition, plotted as a function of the dimensionless distance. This permits an estimation of the length which must solidify before the steady-state is reached. Note that in alloys with small values of k, solidifying at low rates, a large distance may be required. For example, if k is equal to 0.1, V is equal to 10^{-3}mm/s, and D is 5×10^{-3}mm^2/s, the characteristic distance required to establish a steady-state planar interface having 82% of the theoretical concentration is of the order of 100mm!

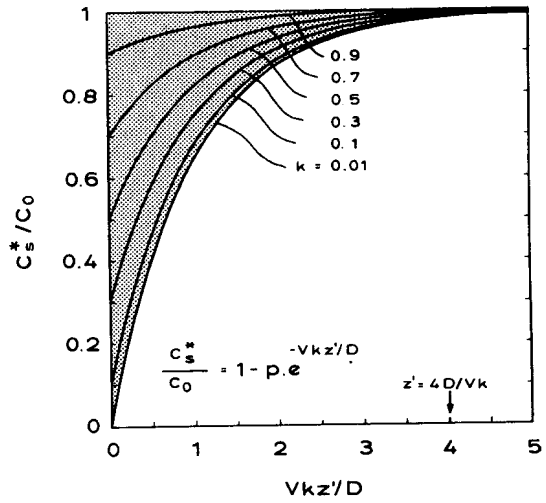

Figure 6.2: LENGTH OF THE INITIAL TRANSIENT FOR A PLANAR SOLID/LIQUID INTERFACE. In many solidification experiments, it is important to ensure that the steady-state has been reached. This is because nearly all of the theoretical analyses of the microstructures formed assume time-independent conditions in order to simplify the analysis. The diagram illustrates the length of the initial transient of figure 6.1 for typical values, of distribution coefficients, less than unity. A safe rule-of-thumb is that the distance of interface travel required for the establishment of the steady-state is 4D/Vk.

This is an important factor to bear in mind when applying steady-state theory to experiments involving a plane interface. Equation 6.3 is only an approximate, but useful, solution for the initial transient. The exact relationship can be found in Smith et al (1955). In the case of dendritic growth, the steady-state is reached much faster. A practical indication of the establishment of the steady-state in this case is the appearance of a uniform microstructure in longitudinal sections of the solidified ingot.

6.3 The Steady State

The steady state is established when $dC_l^*/dt = 0$. Then:

$$J_1 = J_2 \qquad [6.4]$$

and:

$$\frac{C_l^* - C_o}{C_l^*(1 - k)} = 1 \qquad [6.5]$$

which is equivalent to $\Omega_c = 1$. In other words, the planar solid/liquid interface grows at the solidus temperature corresponding to the alloy composition. The concentration of the melt then decreases exponentially as a function of distance, z (equation 3.2):

$$C_l - C_o = \Delta C_o \exp[-\frac{Vz}{D}]$$

forming a diffusion boundary layer with the characteristic length, $\delta_c = 2D/V$ and a concentration gradient at the interface, $G_c = \Delta C_o V/D$.

6.4 The Final Transient

When the boundary layer becomes comparable to the length of the remaining liquid zone, interaction with the boundary of the system begins to occur (figure 6.1). The end of the liquid zone can be regarded as being a perfectly impermeable wall which imposes a zero flux condition at that point:

$$(\frac{dC}{dz})_{z'=L} = 0 \qquad [6.6]$$

This is equivalent to saying that the flow into the liquid decreases and therefore the concentration increases as shown in figure 6.1. If it is imagined that the end of the specimen is acting as a source with a strength equal to the flow which would leave this boundary if it were permeable, equation 6.6 is satisfied and the final concentration profile can be found by superposition of symmetric sources. This method leads to a series giving C_l^* as a function of the final liquid length, l (appendix 10).

6.5 Rapid Diffusion in the Liquid - Small Systems

The analysis of the solute distribution becomes much simpler when it is assumed that diffusion in the liquid is sufficiently rapid to avoid the establishment of any concentration gradient ahead of the solid/liquid interface. This is a reasonable assumption to make in the case of very high diffusion coefficients in the liquid, strong convection, and/or a very small system size, L, compared to the boundary layer thickness. Considering only the case of diffusion, no concentration gradient will exist in the liquid when the diffusion boundary layer is much greater than the system size:

$$\delta_c = \frac{2Dt}{V} \gg L \qquad [6.7]$$

This is so because then the insulating effect of the end of the specimen will smooth out any concentration gradient. Under these conditions, the most general treatment involves a combined approach (appendix 11). Figure 6.3 shows the corresponding concentration profile. Here, the boundary layer in the solid, δ_s, due to back diffusion, will take a value between zero and infinity depending upon the value of the diffusion coefficient in the solid. With the relative interface position, $s/L = f_s = (1 - f_l)$, the mass balance, $A_1 = A_2 + A_3$, can be written, to a first-order approximation:

$$(C_l - C_s^*)df_s = f_l dC_l + \frac{\delta_s}{2} dC_s^* \qquad [6.8]$$

where $C_l = C_l^*$. Assuming that the interface position, s, is a parabolic function of time (§), and integrating (appendix 11) gives:

§ This function gives a consistent solution to the problem. This is not the case when one assumes a linear relationship between s and t.

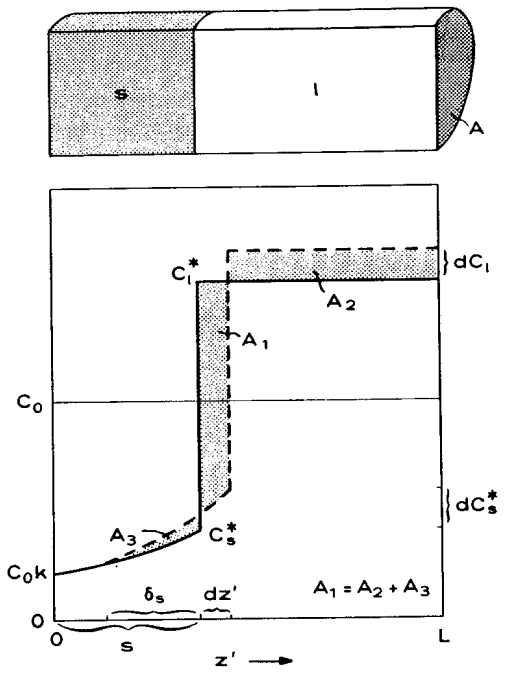

Figure 6.3: SEGREGATION WITH COMPLETE LIQUID MIXING AND SOME SOLID-STATE DIFFUSION. When mass transport in the liquid is very rapid, due to the effect of convection, the diffusion boundary layer will be greatly reduced and contain only a small amount of excess solute, the difference being redistributed evenly over the entire volume of liquid. In this case, there will be an interaction with the far end of the crucible during the whole solidification process, and the entire solute distribution will essentially be a long terminal transient beginning at the solid concentration, C_0k. This behaviour is described by the 'Scheil' equation and predicts an infinite concentration at the end of solidification. In practice, eutectic solidification usually intervenes. In order to obtain a more realistic description of the concentration profile at this point, solid-state back diffusion must be taken into account, especially in the final stages of solidification where z' approaches L. Here, the concentration gradient in the solid becomes very large. This can be done by using a simple mass balance. Thus, the solute rejected from the solid (represented by surface A_1) over the distance, dz', will partially increase the uniform liquid concentration by dC_l (surface A_2), and this in turn will increase the interface concentration and the associated concentration gradient in the solid, and therefore the flux into the solid (surface A_3). Mass conservation requires that the sum of the quantities described by the three surfaces must be zero. If diffusion in the solid is very rapid (e.g. C in delta-Fe), the boundary layer, δ_S, in the solid will be very large. In the limit, due to interaction with the initial boundary of the system ($z' = 0$), the concentration gradient in the solid will be decreased, leading, for the extreme case of infinitely rapid back-diffusion, to equilibrium solidification (lever-rule). In this case, an homogeneous solid, with composition C_o, will result after the completion of solidification. The extent of back diffusion will depend on a dimensionless parameter, α, which can be regarded as describing the ratio of the diffusion boundary layer in the solid, δ_S, to the size of the system, L.

$$\frac{C_l}{C_o} = (1 - uf_s)^{-p/u} \qquad [6.9]$$

where $u = 1 - 2\alpha'k$, $p = 1 - k$, and C_s^* can be obtained directly from $C_s^* = kC_l$. The parameter, α', can be calculated from:

$$\alpha' = \alpha[1 - \exp(-\frac{1}{\alpha})] - 0.5 \exp(-\frac{1}{2\alpha}) \qquad [6.10]$$

where the dimensionless diffusion time (Fourier number) is:

$$\alpha = \frac{D_s t_f}{L^2} \qquad [6.11]$$

The behaviour of α' is such that, at small α-values (less than 0.1), $\alpha' = \alpha$, and at large α-values (greater than 50), $\alpha' = 0.5$ (figure A11.3).

Substituting these limiting values of α' into equation 6.9 leads to two well-known equations. When α is equal to zero, α' is also equal to zero (no solid-state diffusion takes place) and:

$$\frac{C_l}{C_o} = \frac{1}{(1 - f_s)^p} = \frac{1}{f_l^p} \qquad [6.12]$$

This is known as the 'Scheil equation'.

On the other hand, when α approches infinity, α' becomes equal to 0.5 and this implies that solidification will occur under equilibrium conditions. That is, solid-state back-diffusion is so rapid or the solid-state diffusion boundary layer, δ_s, is much greater than L that, as in the case of the liquid, the insulating effect of the solid specimen end also smoothes out any concentration gradient in the solid. This case is described by the 'lever rule':

$$\frac{C_l}{C_o} = \frac{1}{1 - pf_s} \qquad [6.13]$$

Figure 6.4 illustrates the behaviour of equation 6.9 for an Al-2%Cu alloy, including the limiting cases described by equations 6.12 and 6.13. It is evident that the Scheil equation is a very poor approximation with regard to the final liquid composition, since the maximum liquid concentration, C_l^m, is infinite. On the other hand, equilibrium solidification according to the lever-rule case, which leads to a final liquid concentration, $C_l^m = C_o/k$, is again unrealistic for most solutes because of their low solid-state diffusivity. However, there are very important exceptions such as those of interstitial solutes, especially in open crystal structures and small systems (e.g. interdendritic segregation of C in delta-Fe). The latter diffusion coefficient is

so high that α-values greater than 100 are found. Knowledge of the value of C_l^m also permits the temperature of the remaining liquid to be calculated from the phase diagram (figure 6.5).

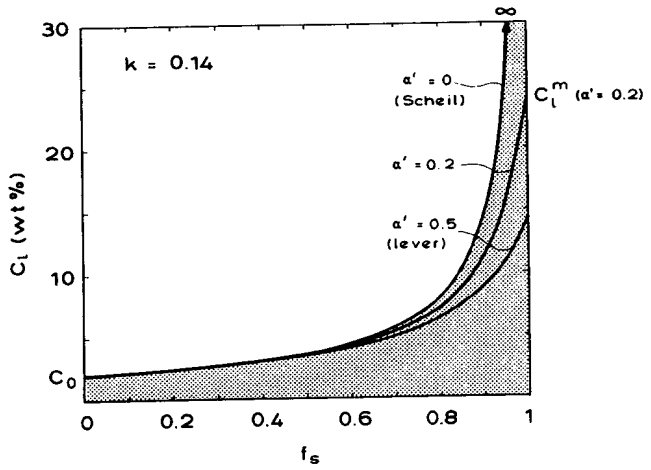

Figure 6.4: SEGREGATION CURVES IN THE PRESENCE OF BACK DIFFUSION. The composition of the liquid (assumed to be homogeneous as in figure 6.3) increases at the end of the specimen. Under lever-rule conditions, the increase is from C_0 to C_0/k, while the Scheil equation predicts an increase from C_0 to infinity. All of the intermediate cases can be described by one relationship (equation 6.9) which contains a modified α-parameter, α', which can take values between 0 and 0.5. Note that the curve represents the path of the interface concentration, C_l^*, as a function of f_S. The final solute distribution profile in the solid cannot be determined in this way because it changes with time when $\alpha > 0$. Therefore, only the end concentration ($f_S = 1$) represents a measurable value.

6.6 Microsegregation

So far, solute distributions have only been considered for the case of relatively large systems under directional solidification involving planar solid/liquid interfaces (figure 6.3). Because of the simplicity of such a unidirectional system and the approximations made, the equations derived are simple. The situation becomes extremely complex when the previously used approaches are applied to dendritic

solidification. Large simplifications must therefore be made in order to make such problems tractable.

Firstly, the case of dendritic solidification in the columnar zone of a casting is considered (figure 6.6). The mushy zone, of length a, is defined as the region within which liquid and solid coexist at various temperatures corresponding to the different concentrations due to solute redistribution. The zone length, a, is proportional to the non-equilibrium solidification range, $\Delta T'$, which is usually larger than the equilibrium melting range, ΔT_0 (figure 6.5).

In order to apply a mass balance, it is necessary to simplify the dendrite form in two respects. Firstly, it is assumed that there are no side-branches and, secondly, that the dendrite is plate-like rather than needle-like. It is now assumed that 'directional

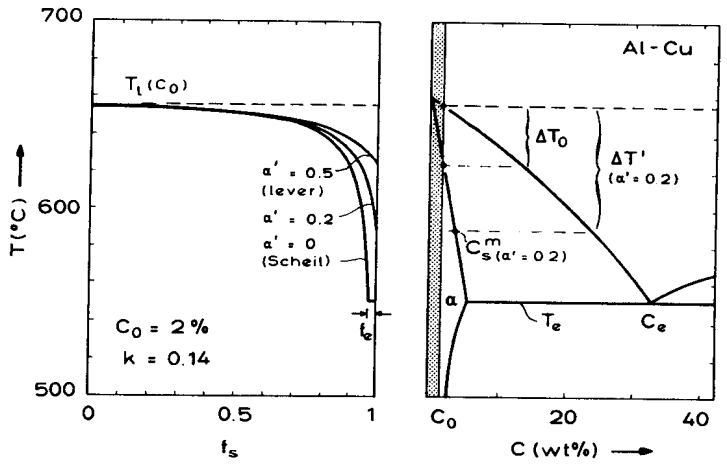

Figure 6.5: RELATIONSHIP OF THE SEGREGATE FREEZING POINT TO THE PHASE DIAGRAM. An increasing concentration (for distribution coefficients less than unity) is associated with a decreasing liquidus temperature since the slope, m, is then less than zero. Using the curves of figure 6.4, the temperature of the liquid as a function of volume fraction solidified can be derived. The use of realistic diffusion coefficients shows that, for small systems (such as interdendritic regions - figure 6.6) interstitial C in delta- and gamma-Fe will behave according to the lever-rule. Hence, the last liquid of a binary Fe-C melt will solidify at a temperature close to the solidus while substitutional alloys, such as Al-Cu, which typically have much smaller solid-state diffusion coefficients will usually contain eutectic material in the last (interdendritic) regions to solidify even when the overall composition is less than the solubility limit at T_e.

solidification' is occurring in an infinitesimally narrow volume element between, and perpendicular to, two dendrites (figure 6.6). All of the relations which were developed before can now be applied in an approximate manner to the interdendritic region, where the solidification time, t_f, is (equation 4.20):

$$t_f = -\frac{\Delta T'}{\dot{T}}$$

where the negative sign arises due to the negative value of $\dot{T}$, the cooling rate. The length of the volume element is then, $L = \lambda_1/2$, and $\Delta T' = m(C_l^* - C_l^m)$, where C_l^m corresponds to the composition of the last liquid. Substituting these values into equation 6.11 gives:

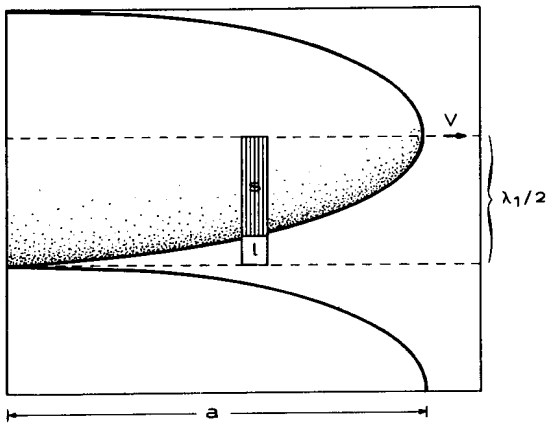

Figure 6.6: CHARACTERISTICS OF THE MUSHY ZONE IN COLUMNAR GROWTH. Applying the macroscopic directional solidification system of figure 6.3 to the cellular structure of a casting, it becomes a small volume element which solidifies at right-angles to the growth axis of the alloy. An increase in the concentration or a decrease in the liquidus temperature of the remaining liquid shown before can thus also be applied qualitatively to the mushy zone of a casting. Here, f_s is now the local volume fraction of solid in the two-phase region with $z' = 0$ at the centre of the cell trunk (corresponding to the position of the infinitely narrow volume element at the cell tip where $f_s = 0$) and $z' = L = \lambda_1/2$ at the last interdendritic liquid (corresponding to the position of the volume element at the cell root with $f_s = 1$). In the case of dendrite growth with secondary branching, the characteristic back-diffusion distance is not $\lambda_1/2$ as in cells, but instead, $\lambda_2/2$.

$$\alpha = -\frac{4D_s m(C_l^* - C_l^m)}{\lambda_1^2 \dot{T}} \qquad [6.14]$$

Under most conditions the dendrite tip concentration, C_l^* is very close to C_o while C_l^m depends markedly on α, and can be obtained from equation 6.9 with $f_s = 1$. Thus:

$$C_l^m = C_o(2\alpha' k)^{-p/u} \qquad [6.15]$$

Considering now the dendrite form of figure 6.7, the back diffusion process, which is most marked at the end, will occur principally between the secondary arms and not between the primary trunks. Therefore, except in the case of cellular growth, where λ_1 is the characteristic spacing, λ_2 would be the appropriate dimension for most castings. This dimension is also important in equiaxed solidification, which is always dendritic in nature. It is known that (equation 4.18):

$$\lambda_2 = 5.5\,(Mt_f)^{1/3}$$

So that the α-value for dendrites is deduced to be:

$$\alpha = 0.13\, D_s \Delta T'^{1/3} M^{-2/3} |\dot{T}|^{-1/3} \qquad [6.16]$$

where M is defined by equation 4.19. Because $\Delta T'$ depends on α, and this in turn depends on $\Delta T'$, the calculations have to be performed in an iterative manner, substituting for the initial $\Delta T' = \Delta T_o$. To a first approximation, one can also substitute for $\Delta T' = \Delta T_o$, leading to a constant value for the ripening parameter:

$$M \simeq \frac{-2\Gamma D \ln [k]}{\Delta T_o p} \qquad [6.17]$$

When C_l^m is greater than C_e, precipitation of the eutectic will generally occur and its volume fraction, f_e, can be calculated using equation 6.9, knowing that $f_e = 1 - f_s$ (for $C_l = C_e$). This shows that:

$$f_e = \left(\frac{1}{u}\right)\left[u - 1 + \left(\frac{C_o}{C_e}\right)^{u/p}\right] \qquad [6.18]$$

In multicomponent systems, the 'path of solidification' is more complicated due to the greater number of variables. In appendix 11, an example of such a situation is given for a ternary system. Futhermore, the practically important case of post-diffusion

homogenisation of interdendritic segregation is also treated. These equations permit an estimation of the degree of microsegregation existing after cooling a casting to room temperature and also of the time required to reach a certain degree of homogenisation during a given heat-treatment process.

Therefore, given the temperature gradient and the growth rate, the most important characteristics (C_l^m, f_e, $\Delta T'$, λ_1, and λ_2) of the solidified structure can be obtained approximately. That is, the solidification microstructure as well as the microscopic inhomogeneities in chemical composition can be determined.

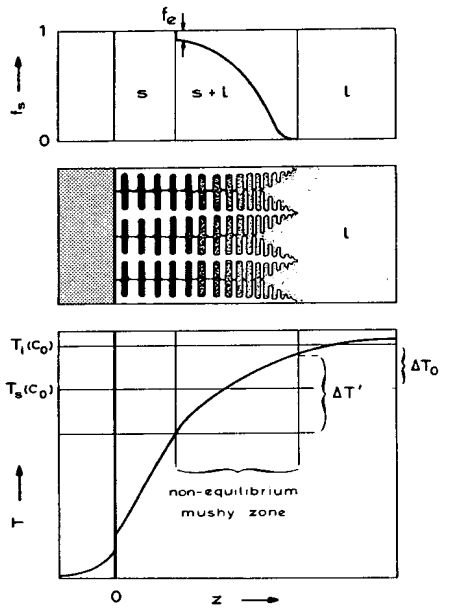

Figure 6.7: MICROSEGREGATION. The equilibrium melting range, ΔT_0 does not, except for the lever rule case, correspond to the range, $\Delta T'$, over which the mushy zone develops. The dendrite tips need a certain undercooling which is determined by the stability of the tip. The dendrite roots will usually have much higher concentrations than C_0/k, due to non-equilibrium solidification. This often leads to interdendritic precipitation of eutectic phases of volume fraction, f_e, even if the composition is not on the eutectic tie-line. In the columnar zone of a casting, as shown here, the volume fraction of solid, f_S, will follow an S-shaped curve like that in the uppermost diagram.

BIBLIOGRAPHY

- Mass Balance

G.H.Gulliver: Metallic Alloys, Griffin, London, 1922.
E.Scheil: Zeitschrift für Metallkunde 34 (1942) 70
W.G.Pfann: Zone Melting, 2nd Edition, Wiley, New York, 1966.
H.D.Brody, M.C.Flemings: Transactions of the Metallurgical Society of AIME 236 (1966) 615
T.W.Clyne, W.Kurz: Metallurgical Transactions 12A (1981) 965

- Transients

V.G.Smith, W.A.Tiller, J.W.Rutter: Canadian Journal of Physics 33 (1955) 723

- Microsegregation

D.H.Kirkwood, D.J.Evans in: The Solidification of Metals, Iron and Steel Institute Publication 110, 1968.
T.F.Bower, H.D.Brody, M.C.Flemings: Transactions of the Metallurgical Society of AIME 236 (1966) 624
K.Schwerdtfeger: Archiv für das Eisenhüttenwesen 41 (1970) 923
E.A.Feest, R.D.Doherty: Metallurgical Transactions 4 (1973) 125
S.N.Singh, B.P.Bardes, M.C.Flemings: Metallurgical Transactions 1 (1970) 1383

- Numerical Heat Flow Calculations with Segregation

P.N.Hansen in: Solidification and Casting of Metals, The Metals Society, London, 1979.
T.W.Caldwell et al: Metallurgical Transactions 8B (1977) 261
T.W.Clyne: Metal Science 16 (1982) 441
T.W.Clyne, M.Wolf, W.Kurz: Metallurgical Transactions 13B (1982) 259
M.Wolf, T.W.Clyne, W.Kurz: Archiv für das Eisenhüttenwesen 53 (1982) 91

- Convection

G.S.Cole in: Solidification, American Society for Metals, Metals Park, Ohio, 1971, chapter 7.
G.H.Geiger, D.R.Poirier: Transport Phenomena in Metallurgy, Addison Wesley, 1973

- Macrosegregation

R.Mehrabian, M.C.Flemings: Metallurgical Transactions 1 (1970) 455
M.C.Flemings: Scandinavian Journal of Metallurgy 5 (1976) 1

EXERCISES

6.1 Write an equation for the T_l^*-f_s relationship for the Lever rule and Scheil equation cases.

6.2 Determine α' values for Al-2wt%Cu and α-Fe-0.09wt%C alloys when $t_f = 10s$. Which system exhibits the greater tendency to segregate? (To obtain an estimate for λ_2 use figure 4.17 for both alloys)

6.3 It is desired to purify part of a cylindrical metal ingot by directional solidification. What conditions are most favourable: a short initial transient or Scheil-type solidification? What interface morphology is required in order to accomplish this? Give the maximum growth rate which can be used.

6.4 Devise a method for estimating part of the phase diagram (m,k values) of a transparent organic alloy by solidifying it under planar interface conditions at the limit of stability and observing it with a microscope. Indicate how one might perform the experiment (see figure 6.2). It is assumed that the values of C_o and D are known.

6.5 What will happen if the rod in figure 6.1 is solidified under conditions of strong convection? Sketch the solute profile and indicate which equation applies to this situation.

6.6 In what respect is equation 6.3 an approximation to the initial transient? Examine the assumptions made concerning the boundary layer for the transient (see appendix 10 and figure A2.4)

6.7 Describe a method for the production of a control sample of a given composition for use in microprobe measurements. Such a standard should present a composition to the electron beam which is homogeneous at a scale of the order of 1 μm.

6.8 Write the equation, given in this chapter, which describes approximately the concentration variation along the curved interface of figure 6.6 under growth conditions where the tip concentration in the liquid, C_l^*, is approximately equal to C_o. In what region would one expect the concentration gradient, perpendicular to the solid/liquid interface, in the liquid to be (a) close to zero and (b) not zero?

6.9 Indicate, with the aid of figure 4.12, the growth rates for which, in an Al-2wt%Cu alloy, no intercellular or interdendritic enrichment (segregation) will occur for (a) $G \leq 0$ and for (b) $G = 1K/mm$.

6.10 Why is equation 6.9 incorrect (under the original assumption that $u = 1 - 2\alpha k$) if $\alpha > 1$? What happens in this case? Sketch the solute profiles present in the solid and liquid under these conditions. Compare with figure A11.2.

6.11 Compare the fractions of eutectic predicted by the Scheil equation, by the Lever rule, and by equation 6.9, in the case of Fe-0.6wt%C and Al-2wt%Cu. Discuss the differences. For α', use the same conditions as those assumed in exercise 6.2.

6.12 Zone melting is a process in which the tendency to segregation is exploited in order to produce a solid having a high purity. In practice, this is done by causing a molten zone with planar solid/liquid interfaces to pass many times through the material (figure). The equation for the impurity distribution after the first pass with strong mixing occurring in the liquid zone (C_l = constant) is: $C_l/C_o = (1/k)[1-(1-k)\exp(-kz/L)]$, where L is the zone length. Discuss this equation with regard to the equation for the initial transient (equation 6.3)

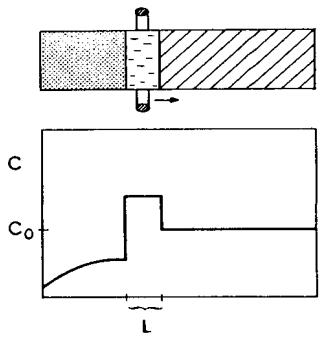

SUMMARY

As outlined at the beginning of this book, the study of solidification microstructures is of increasing importance in the field of engineering since the properties of most alloys, whether cast, forged, or welded, will depend to a large extent upon the degree of control which can be exercised during solidification. Furthermore, various new solidification processes are currently offering signs of great future potential. These include the enlargement of the equiaxed zone by means of the electromagnetic stirring of castings, surface remelting and alloying by high-energy beams such as lasers, directional monocrystalline casting, and other techniques. Therefore, there is a need for a better understanding of the common mechanisms associated with this important phase transformation.

It has been the aim of the authors to describe, from an engineering point of view, and via the use of simple physical models, some of the most important solidification phenomena which occur. The latter range from atomistic to macroscopic in scale.

In the introduction, the importance of heat flow phenomena has been pointed out. Currently, the range of cooling rates employed is from 10^{-5} to 10^{10}K/s and corresponds to 'castings' ranging in size from several metres to a few micrometres. These various cooling rates produce differing microstructures which can be divided into four categories, i.e.: (a) columnar and (b) equiaxed grains of (c) dendrites or (d) eutectic.

In each of these cases, capillarity effects and the diffusion of solute and/or heat determine the microstructure which results from the solidification conditions.

As far as solidification at the atomic level is concerned, two phenomena: nucleation and interface structure, have been described. Nucleation is a predominantly interface-controlled process involving an activation energy which is strongly affected by the presence of a catalyst. The nucleation rate, and therefore the equiaxed grain size, is very sensitive to the existence of heterogeneous particles. From the well-known laws of nucleation, the time-temperature-transformation (TTT) diagram for the solidification of a substance can be derived. This permits, among other things, an explanation of the amorphous phases which can be produced by rapid solidification processes.

The interfacial atomic attachment kinetics determine the crystal morphology. Substances such as metals, which have a low entropy of melting, grow in a non-faceted manner. Some organic substances which behave like metals in this respect are especially useful for the in situ observation of solidification using an optical microscope. On the basis of such observations, the likely behaviour of a metallic system can be deduced without the difficulties posed by the opacity,

reactivity, and high melting point of metals. In substances having a high entropy of melting, the crystal growth behaviour is largely determined by growth defects. These play a decisive role in the growth of irregular eutectics, such as the most important casting alloys (Al-Si, cast iron).

On a larger scale, the first phenomenon which becomes apparent is the morphological instability of solid/liquid interfaces, which occurs on a scale of the order of micrometres. This is associated with a characteristic range of wavelengths and is only a transient stage in the development of the steady-state growth forms of cells, dendrites or eutectics.

Equiaxed grains of pure or alloyed materials are inherently unstable when their diameter exceeds a critical value (of the order of some micrometres). On the other hand, columnar grains are always stable (plane front growth) in pure samples and can be stable in the case of alloys if the temperature gradient is sufficiently high. At very high growth rates, the onset of so-called absolute stability will lead to the occurrence of solidification involving a structureless solid/liquid interface.

The most frequently observed solidification microstructure is the dendrite. This steady-state growth morphology is characterised by its paraboloid-like tip and by the formation of branches only along simple low-index orientations. The growth of these crystals is determined by the following diffusion phenomena: thermal (equiaxed growth of pure substances), solutal (columnar growth of alloys), and thermal/solutal (equiaxed growth in alloys). The solution of the diffusion equation, combined with a stability criterion, leads to a unique description of dendrite tip growth.

In the case of columnar growth, the imposed positive temperature gradient constrains the dendrites to grow in the form of arrays having a characteristic primary spacing, λ_1. During growth, the length of contact time which the initially fine branches have with their melt causes ripening to occur to such a degree that the final branch spacing, λ_2, is very much greater than the initial one at the tip.

As far as eutectics are concerned, there are two types of microstructure: regular and irregular, whose occurrence depends upon the entropy of melting of one of the phases. Regular structures are typically exhibited by phases having a low entropy of melting, and grow in a steady-state manner, whereas irregular structures (in which one phase is faceted) oscillate between two operating points. As in the case of dendrites, the combination of the diffusion solution with a criterion which decides the operating point of the system leads to the deduction of the growth law. Eutectic microstructures store an appreciable fraction of their transformation energy in the form of α/β interfaces (which are usually those having the minimum energy).

The competitive growth of eutectic and dendrites will lead to mixed microstructures which can be summarised with the aid of the so-called coupled zone.

Peritectic reactions develop around dendrites in the form of interdendritic precipitates.

Any local equilibrium between two phases will result in concentration differences which are necessary in order to satisfy thermodynamic requirements. These differences create local concentration variations which are known as segregation. In the case of a dendritic interface, solute concentrations are built into the interdendritic regions. Back-diffusion into the solid dendrite plays an important role in governing the magnitude of the composition of the last liquid to solidify.

The coupling of microstructural models with segregation models, and their incorporation into heat-flux calculations, today permits a semi-quantitative description and understanding of diverse solidification processes occurring over a wide range of conditions. In the future, it will be possible to relate the microstructural models presented here, together with others yet to be developed, to multidimensional, macroscopic heat flow calculations. In this way, the much-needed superior control of solidification processes will be made feasible.

FOR FURTHER READING - BOOKS AND ARTICLES OF GENERAL INTEREST

- Nucleation Phenomena, American Chemical Society, Washington DC, 1966.
- R.L.Parker: 'Crystal Growth Mechanisms', in Solid State Physics (Eds. H.Ehrenreich, F.Seitz, D.Turnbull), 25 (1970) 151-299.
- B.R.Pamplin: Crystal Growth, Pergamon, Oxford, 1975.
- W.G.Pfann: Zone Melting, 2nd Edition, Wiley, New York, 1966.
- M.Glicksman, R.F.Sekerka: 'Solidification Kinetics', in Problems in Materials Science, Volume 1, (Ed. H.D.Merchant), Gordon & Breach, New York, 1972.
- H.I.Aaronson (Ed): Lectures on the Theory of Phase Transformations, Metallurgical Society of AIME, New York, 1975
- J.W.Christian: The Theory of Transformations in Metals and Alloys, 2nd Edition, Pergamon, Oxford, 1975.
- Solidification, American Society for Metals, Metals Park, Ohio, 1971.
- M.C.Flemings: Solidification Processing, McGraw-Hill, New York, 1974.
- H.Jones, W.Kurz (Eds): Solidification Microstructures, 30 years after Constitutional Supercooling, Materials Science and Engineering, Special Issue, 1984.

- W.Kurz, P.R.Sahm: Gerichtet erstarrte eutektische Werkstoffe, Springer, Berlin, 1975.
- R.Elliott: Eutectic Solidification Processing - Crystalline and Glassy Alloys, Butterworths, London, 1983.
- M.McLean: Directionally Solidified Materials for High Temperature Service, The Metals Society, London, 1983.
- A Guide to the Solidification of Steels, Jernkontorets, Stockholm, 1977.
- B.Lux, I.Minkoff, F.Mollard (Eds): The Metallurgy of Cast Iron, Georgi, St Saphorin, Switzerland, 1975.
- I.Minkoff: The Physical Metallurgy of Cast Iron, Wiley, New York, 1983.
- The Solidification of Metals, ISI Publication 110, London, 1968.
- Solidification and Casting of Metals, The Metals Society, London, 1979.
- Solidification Technology in the Foundry and Casthouse, The Metals Society, London, 1983.
- H.Nieswaag, J.W.Schut (Eds): Quality Control of Engineering Alloys and the Role of Metal Science, Delft, 1978.
- H.D.Brody, D.Apelian (Eds): Modelling of Casting and Welding Processes, Metallurgical Society of AIME, New York, 1981.
- H.Hermann (Ed): Ultrarapid Quenching of Liquid Alloys, Academic Press, New York, 1981 (Treatise on Materials Science and Technology, Volume 20).
- B.H.Kear et al (Eds): Rapidly Solidified Amorphous and Crystalline Alloys, Elsevier North-Holland, 1982.
- H.Jones: Rapid Solidification of Metals and Alloys, The Institution of Metallurgists, London, 1982.

APPENDIX 1

MATHEMATICAL MODELLING OF THE MACROSCOPIC HEAT FLUX

Differential Equation

The equation describing heat flow can be obtained by considering the heat balance in an infinitesimal element (figure A1.1). In Cartesian coordinates, the balance can be written [1 - 3] (§):

$$\frac{\partial}{\partial x}(\kappa_x \frac{\partial T}{\partial x}) + \frac{\partial}{\partial y}(\kappa_y \frac{\partial T}{\partial y}) + \frac{\partial}{\partial z}(\kappa_z \frac{\partial T}{\partial z}) - q'(x,y,z) = \frac{\partial (cT)}{\partial t}$$

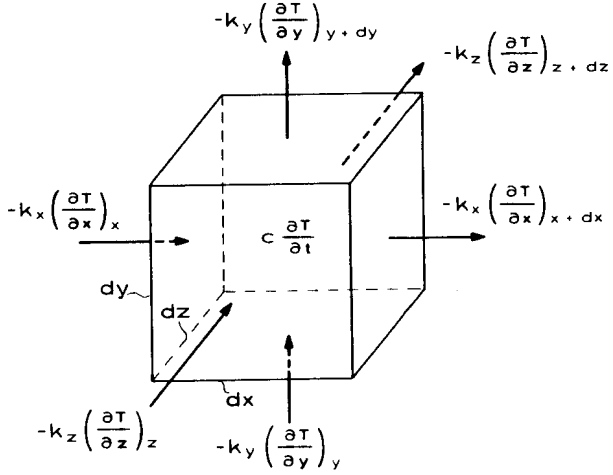

Figure A1.1

§ Here z is a system coordinate which, in the main text and in appendix 2, is denoted by z'. The un-primed symbol is used here in order to improve readability.

where q' is an internal heat source term (W/m^3) and c is the volumetric specific heat ($c = c_p \rho$). Using the Laplacian operator:

$$\nabla(\kappa \nabla T) - q' = \frac{\partial(cT)}{\partial t} \qquad [A1.1]$$

The negative sign on the left-hand side of equation A1.1 arises because q' is proportional to Δh_f and the latter is negative for solidification. When the thermal conductivity, κ, and the specific heat, c, are constant:

$$a\nabla^2 T - \frac{q'}{c} = \frac{\partial T}{\partial t}$$

where $a = \kappa/c$. Only unidirectional heat flow conditions are considered in the present appendix, and in this case:

$$a\frac{\partial^2 T}{\partial z^2} - \frac{q'}{c} = \frac{\partial T}{\partial t} \qquad [A1.2]$$

Analogous equations can be written for cylindrical and spherical coordinates, and, in the absence of tangential heat flow, the problem reduces to the consideration of one direction:

$$a\left[\frac{\partial^2 T}{\partial r^2} + \left(\frac{n}{r}\right)\frac{\partial T}{\partial r}\right] - \frac{q'(r)}{c} = \frac{\partial T}{\partial t} \qquad [A1.3]$$

where n is equal to 2 for spherical coordinates, to 1 for cylindrical coordinates, and to 0 for a plate geometry. The latter case leads to equation A1.2.

General Solutions for Semi-Infinite Systems

Neglecting heat generation for the moment, equation A1.2 can be written:

$$a\frac{\partial^2 T}{\partial z^2} = \frac{\partial T}{\partial t} \qquad 0 \leqslant z \leqslant \infty \qquad [A1.4]$$

(When a is replaced by D and T is replaced by C one obtains the equation for mass diffusion.) One possible general solution of equation A1.4 is:

$$T(z,t) = A + B\,\mathrm{erf}(Z) \qquad [A1.5]$$

where A and B are constants and

$$Z = \frac{z}{2(at)0.5} \qquad [A1.6]$$

The error function, erf, and its complement, erfc (which may be a better choice for problems involving heating), have the properties (figure A1.2)§:

$$\mathrm{erf}[0] = 0$$

$$\mathrm{erf}[\infty] = 1$$

$$\mathrm{erf}[-Z] = -\mathrm{erf}[Z]$$

$$\mathrm{erfc}[Z] = 1 - \mathrm{erf}[Z]$$

$$\mathrm{erfc}[-Z] = 1 + \mathrm{erf}[Z]$$

$$\frac{d(\mathrm{erf}[Z])}{dZ} = \frac{2}{\sqrt{\pi}}\exp[-Z^2] \qquad [A1.7]$$

With the aid of a programable calculator, the error function can easily be determined by using the series [4]:

$$\mathrm{erf}(Z) = \frac{2}{\sqrt{\pi}}\sum_{n=0}^{\infty}\frac{(-1)^n Z^{(2n+1)}}{n!\,(2n+1)} \qquad [A1.8]$$

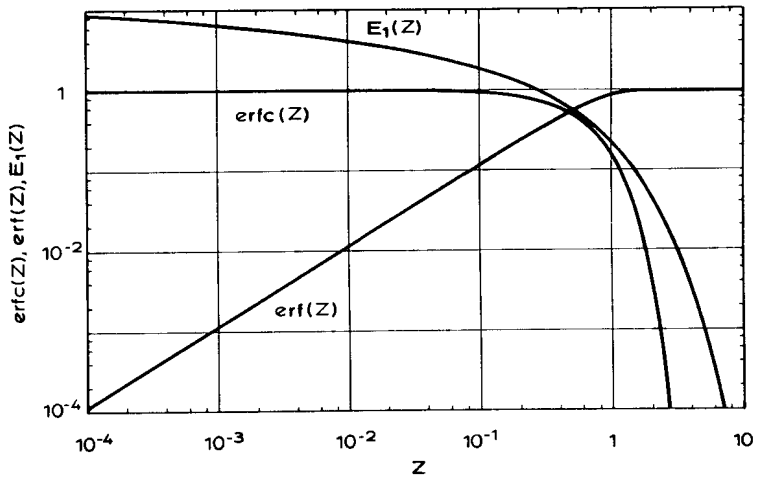

Figure A1.2

§ The exponential integral, E_1, which is also plotted in figure A1.2 will be used in appendix 7 (equation A7.16)

Exact values of erf(Z) are given in table A1.1. Some useful approximations are:

$$\text{erf}(Z) \simeq \sqrt{1 - \exp(-\frac{4Z^2}{\pi})}$$

$$\text{erf}(Z) \simeq 1 \qquad Z > 2$$

$$\text{erf}(Z) \simeq \frac{2Z}{\sqrt{\pi}} \qquad Z < 0.2$$

In order to demonstrate that equation A1.5 is a general solution of equation A1.4, one can use equation A1.7, so that:

$$\frac{\partial T}{\partial z} = \frac{B\exp[-Z^2]}{(\pi at)^{0.5}}$$

Table A1.1: VALUES OF THE ERROR FUNCTION [4]

Z	erf(Z)	Z	erf(Z)	Z	erf(Z)	Z	erf(Z)
0.00	0.0000	0.26	0.2869	0.52	0.5379	0.78	0.7300
0.01	0.0113	0.27	0.2974	0.53	0.5465	0.79	0.7361
0.02	0.0226	0.28	0.3079	0.54	0.5549	0.80	0.7421
0.03	0.0338	0.29	0.3183	0.55	0.5633	0.81	0.7480
0.04	0.0451	0.30	0.3286	0.56	0.5716	0.82	0.7538
0.05	0.0564	0.31	0.3389	0.57	0.5798	0.83	0.7595
0.06	0.0676	0.32	0.3491	0.58	0.5879	0.84	0.7651
0.07	0.0789	0.33	0.3593	0.59	0.5959	0.85	0.7707
0.08	0.0901	0.34	0.3694	0.60	0.6039	0.86	0.7761
0.09	0.1013	0.35	0.3794	0.61	0.6117	0.87	0.7814
0.10	0.1125	0.36	0.3893	0.62	0.6194	0.88	0.7867
0.11	0.1236	0.37	0.3992	0.63	0.6270	0.89	0.7918
0.12	0.1348	0.38	0.4090	0.64	0.6346	0.90	0.7969
0.13	0.1459	0.39	0.4187	0.65	0.6420	0.91	0.8019
0.14	0.1569	0.40	0.4284	0.66	0.6494	0.92	0.8068
0.15	0.1680	0.41	0.4380	0.67	0.6566	0.93	0.8116
0.16	0.1790	0.42	0.4475	0.68	0.6638	0.94	0.8163
0.17	0.1900	0.43	0.4569	0.69	0.6708	0.95	0.8209
0.18	0.2009	0.44	0.4662	0.70	0.6778	0.96	0.8254
0.19	0.2118	0.45	0.4755	0.71	0.6847	0.97	0.8299
0.20	0.2227	0.46	0.4847	0.72	0.6914	0.98	0.8342
0.21	0.2335	0.47	0.4937	0.73	0.6981	0.99	0.8385
0.22	0.2443	0.48	0.5027	0.74	0.7047	1.00	0.8427
0.23	0.2550	0.49	0.5117	0.75	0.7112	1.30	0.9340
0.24	0.2657	0.50	0.5205	0.76	0.7175	1.80	0.9891
0.25	0.2763	0.51	0.5292	0.77	0.7238	2.00	0.9953

and

$$\frac{\partial^2 T}{\partial z^2} = -\frac{Bz\exp[-Z^2]}{2(\pi a^3 t^3)0.5}$$

The time derivative is:

$$\frac{\partial T}{\partial t} = -\frac{Bz\exp[-Z^2]}{2(\pi at^3)0.5}$$

Substituting the latter two expressions into the differential equation (A1.4) shows that the error function is indeed a solution. Other solutions might be $T = A + B\,\text{erfc}[Z]$ or $T = (1/\sqrt{t})\exp[-Z^2]$. The choice of the solution (assuming that one exists) will depend upon the boundary conditions.

The Moving Boundary Problem

As figure A1.3 indicates, several regions exist in a casting; each of which exhibits a specific thermal behaviour. These include the mould, the air-gap, the solid, the mushy (solid plus liquid) zone, and the liquid. The solution of the general problem is therefore very complex. For this reason, attention will here be restricted to one simple case only.

Simple Analytic Solution

Under the simplifying assumptions of highly-cooled mould, planar solid/liquid interface, and zero superheat, the boundary conditions (figure A1.4) are:

$$T_m = T_o = \text{constant} \qquad 0 > z > -\infty$$

$$T_l = T_f = \text{constant} \qquad z > s$$

where the interface position on the z-axis is given by the function, s(t). The temperature in the solid can be determined with the aid of equations A1.5 and A1.6, giving:

$$T_s = A_s + B_s\text{erf}[\frac{z}{2(a_s t)0.5}] \qquad \text{[A1.9]}$$

$$z = 0 \qquad A_s = T_o$$

$$z = s \qquad B_s = \frac{T_f - T_o}{\text{erf}[\Phi]} \qquad \text{[A1.10]}$$

where

$$\Phi = \frac{s}{2(a_s t)0.5} \qquad \text{[A1.11]}$$

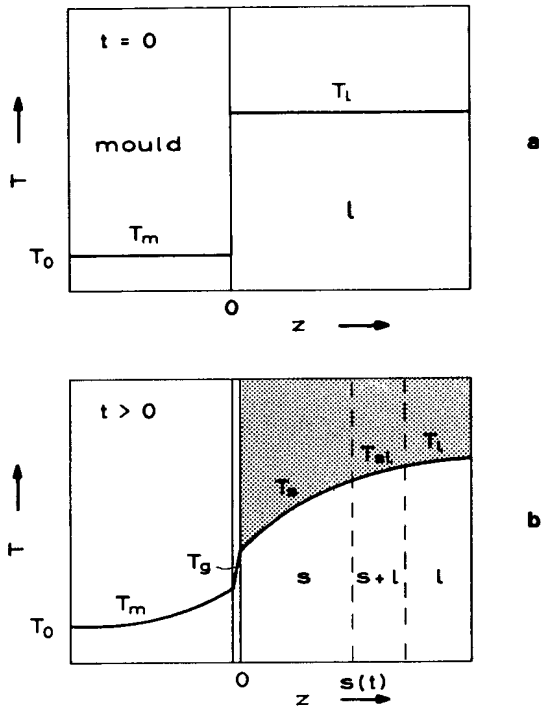

Figure A1.3

Since T_f and T_0 are constant (figure A1.4), Φ is constant and

$$s = 2\Phi(a_s t)^{0.5} \qquad \text{or} \qquad t = \frac{s^2}{4a_s\Phi^2} \qquad [A1.12]$$

In order to determine the value of Φ, it is necessary to consider the (Neumann) boundary condition (appendix 2) which reflects the heat flow at the solid/liquid interface: the latent heat generated during interface advance must be conducted away through the solid, giving the flux balance:

$$\Delta h_f \frac{ds}{dt} = \kappa_s \left(\frac{\partial T_s}{\partial z}\right)_{z=s} \qquad [A1.13]$$

From equation A1.12:

$$V = \frac{ds}{dt} = \sqrt{\frac{a_s}{t}} \cdot \Phi \qquad [A1.14]$$

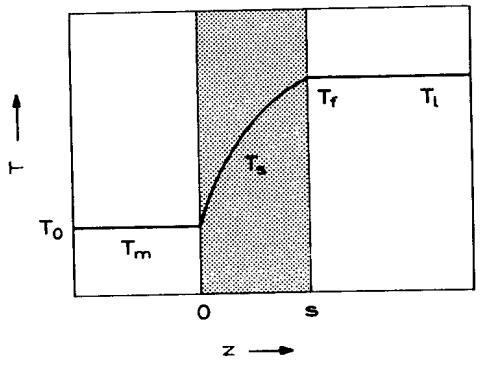

Figure A1.4

while from equation A1.9 at z = s,

$$G = \left(\frac{\partial T_s}{\partial z}\right)_{z=s} = \frac{B_s \exp[-\Phi^2]}{(\pi a_s t)^{0.5}}$$

Combining with equations A1.12, A1.13, A1.14 :

$$\Delta T_s^\circ = \sqrt{\pi}\,\Phi \,\mathrm{erf}(\Phi)\exp(\Phi^2) \qquad [A1.15]$$

where the dimensionless temperature, ΔT_s°, is equal to $(T_f - T_0)c_s/\Delta h_f$. Evaluation of ΔT_s° permits the calculation of Φ by iteration and, using equation A1.12, the position of the interface as a function of time can be found to obey a square-root law. For typical values of ΔT_s°, ranging from 0 to 4, equation A1.16 can be approximated quite well by (figure A1.5):

$$\Delta T_s^\circ \simeq 2\Phi^2(\Phi^2 + 1) \qquad [A1.16]$$

A more general solution, which permits a better description of the real situation shown in figure A1.3, has been given by Garcia et al[5,6]. An analytical treatment which takes account of the mushy zone has been developed by Lipton et al[7].

Numerical Method with Mushy Zone

When describing such complex cases, analytical methods lose their main advantage of simplicity. Instead, numerical calculations are of greater value. In fact, the calculation of the moving (mushy zone) boundary, which varies in width with time,

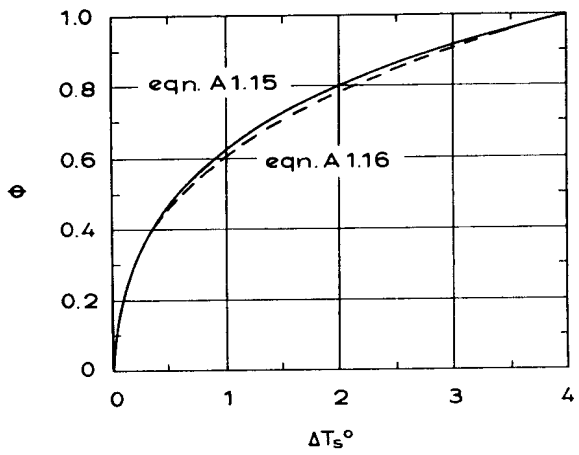

Figure A1.5

has only been published for the one-dimensional case [8,9]. A summary of that method is given here. Thus, substituting the rate of latent heat release:

$$q' = \Delta h_f \frac{\partial f_s}{\partial t} \qquad [A1.18]$$

into equation A1.2 gives:

$$a\frac{\partial^2 T}{\partial z^2} = \frac{\partial T}{\partial t} + \left(\frac{\Delta h_f}{c}\right).\frac{\partial f_s}{\partial t} \qquad [A1.19]$$

For alloys, the volume fraction solidified, f_s, is a function of the temperature. Therefore:

$$\frac{\partial f_s}{\partial t} = \left(\frac{\partial f_s}{\partial T}\right)\left(\frac{\partial T}{\partial t}\right) = f'_s\dot{T} \qquad [A1.20]$$

One can thus write for the cooling rate (after substituting equation A1.20 into equation A1.19):

$$\dot{T} = \frac{a\left(\frac{\partial^2 T}{\partial z^2}\right)}{1 + f'_s\left(\frac{\Delta h_f}{c}\right)} \qquad [A1.21]$$

Compare this equation with equation 1.2. Putting equation A1.21 into finite difference form (appendix 2):

$$\delta T = F_o \frac{T_{j+1} + T_{j-1} - 2T_j}{1 + f_s'\left(\frac{\Delta h_f}{\bar{c}}\right)} \qquad [A1.22]$$

where $F_o = \delta t\bar{a}/\delta z^2$ is a dimensionless constant known as the Fourier number, $\bar{a} = a_s f_s + a_l f_l$, and $\bar{c} = c_s f_s + c_l f_l$. The latter two terms are the weighted values of these properties in the mushy zone. Here, both Δh_f and f_s' are negative. For reasons of computational stability, the Fourier number (in the one-dimensional case) must always satisfy the condition:

$$F_o \leqslant 0.5$$

This can be achieved by the correct choice of the time and space steps. The derivative of f_s with respect to T can be obtained from the segregation equation (6.9) by using temperature ratios rather than concentration ratios. This leads to:

$$f'_s = \frac{\partial f_s}{\partial T} = \left(-\frac{1}{p}\right)(T_f - T_l)^{(u/p)}(T_f - T)^{-[(u+p)/p]} \qquad [A1.23]$$

where $p = 1 - k$, $u = 1 - 2\alpha' k$, $\alpha' = \alpha\{1 - \exp[-1/\alpha]\} - 0.5\exp[-1/2\alpha]$ and $\alpha = 4D_s t_f/\lambda^2$.

Equation A1.22 is very general in form and can be used in all of the regions (l, l+s, s, gap, mould). In the case of solidification of a pure metal or of an eutectic alloy, $f_s' = \infty$. This singularity can be avoided by increasing the specific heat of the interface volume element accordingly or by delaying solidification of the interface elements until the heat evolved during solidification has been transferred away.

The existence of convection in the liquid will often make some modification necessary; for example, the use of a convective boundary layer, δ. This leads to the boundary condition at the dendrite tips:

$$\frac{\partial T}{\partial z} = \frac{T_l^{\infty} - T^*}{\delta} \qquad [A1.24]$$

where T_l^{∞} is the melt temperature far from the tip and T^* is the tip temperature. Furthermore, heat transfer across the gap between the mould and the solidified metal is usually treated by assuming a heat transfer coefficient:

$$q = h\,\Delta T_g \qquad [A1.25]$$

where ΔT_g is the temperature difference across the gap.

REFERENCES

[1] H.S.Carslaw, J.C.Jaeger: Conduction of Heat in Solids, 2nd Edition, Oxford University Press, London, 1959

[2] G.H.Geiger, D.R.Poirier: Transport Phenomena in Metallurgy, Addison Wesley, Reading, 1973

[3] J.Szekely, N.J.Themelis: Rate Phenomena in Process Metallurgy, Wiley Interscience, New York, 1971

[4] M.Abramowitz, I.A.Stegun (Eds.): Handbook of Mathematical Functions, Dover, New York, 1965

[5] A.Garcia, T.W.Clyne, M.Prates: Metallurgical Transactions, 10B (1979) 85

[6] T.W.Clyne, A.Garcia: International Journal of Heat & Mass Transfer, 23 (1980) 773

[7] J.Lipton, A.Garcia, W.Heinemann: Archiv für Eisenhüttenwesen, 53 (1982) 469

[8] T.W.Clyne, A.Garcia, P.Ackermann, W.Kurz, in 'Modelling of Casting and Welding Processes', (Eds. H.D.Brody, D.Apelian). TMS AIME Conference Proceedings, Rindge, 1980.

[9] T.W.Clyne: Metal Science, 16 (1982) 441

APPENDIX 2

SOLUTE AND HEAT FLUX CALCULATIONS RELATED TO MICROSTRUCTURE FORMATION

The literature of solidification microstructure theory, especially in recent times, has become highly complex and different mathematical methods have been used in developing the various models. However, it is the point of view of this book that a reasonably accurate result, which reveals the principles involved and the influence of the physical variables, can be obtained for any problem by using a coherent approach. In fact, exactly the same general principles apply to all solidification problems and the various published analyses differ only with respect to the approximations which are made, and to the weight which is given to various aspects of the problem in question.

The most common approximation which is made is that solidification is occurring under steady-state conditions and that, therefore, the concentrations and solid/liquid interface morphology are independent of time. The principal disadvantage of this assumption is that no evolution of the interface shape can occur. The result of this constraint is that the solution to the basic diffusion problem is indeterminate and a whole range of morphologies is permissible from the mathematical point of view. In order to distinguish the solution which is the most likely to correspond to reality, it is necessary to find some additional criterion. Examination of the stabilities of a slightly perturbed growth form is probably the most reasonable manner in which to treat this situation.

In the present appendix, one aim is to supply the reader with mathematical techniques which are sufficient to attack the problems of microscopic heat and mass transfer which are treated elsewhere in the book. Another aim is to provide the reader with a general and systematic method for approaching steady-state solidification problems.

The general features of a solidification problem can be described as follows: a solid/liquid interface whose form is defined by a given mathematical function containing one or more variable parameters, is assumed to be advancing without change into the melt. As it advances, heat and/or solute are evolved at each point of the interface and diffuse into the solid and the melt. The diffusing solute will build up ahead of the interface when $k < 1$ and form a boundary layer, while a uniform level, C_o, of the solute is supposed to exist at a sufficiently large distance from the interface. The boundary layer can be characterised by the ratio of the diffusion coefficient to the growth rate. Typical orders of magnitude of the equivalent boundary layers for a planar interface are shown in table A2.1. From this, it is seen that the boundary layer thickness for mass transfer of substitutional elements in the solid is so small as to be negligible(§), while the boundary layer thicknesses for heat

§ An exception is the case of microsegregation where, even for substitutional solutes, solid-state diffusion plays an important role due to the very high concentration gradients existing in the last stages of solidification (appendix 11).

Table A2.1: EQUIVALENT BOUNDARY LAYERS FOR A PLANAR INTERFACE

Type of Diffusion	Diffusing Species	Matrix	Layer Thickness (mm) at V = 0.01mm/s
solutal: $\delta_c = 2D/V$	substitutional atom	crystal	10^{-4}
	interstitial atom	crystal	10^{-1}
	either	liquid	10^{0}
thermal: $\delta_t = 2a/V$	heat	crystal	$>10^{3}$
		liquid	$>10^{3}$

transfer (at low growth rates) in the solid or liquid are much larger than the scale of most castings. Convection must also be considered since the presence of a hydrodynamic boundary layer will reduce the thickness of the thermal boundary layer.

Differential Equation for Diffusion

In view of the previous arguments, attention will be restricted here to solute diffusion occurring in the liquid. For simplicity, the suffix, ι, will be dropped from the concentrations since these always refer to the liquid in the present appendix, that is $C_\iota \equiv C$. The equation governing any diffusion process is:

$$\frac{\partial^2 C}{\partial x^2} + \frac{\partial^2 C}{\partial y^2} + \frac{\partial^2 C}{\partial z^2} = \frac{1}{D} \cdot \frac{\partial C}{\partial t} \qquad [A2.1]$$

In physics texts this is usually written:

$$\nabla^2 C = \frac{1}{D} \cdot \frac{\partial C}{\partial t}$$

while, in mathematical texts, it is often written in the suffix notation:

$$C_{xx} + C_{yy} + C_{zz} = \frac{1}{D} C_t$$

Equation A2.1, which is analogous to equation A1.1 but with a zero heat source term, applies to three dimensional space, but the problems treated in the present book require the consideration of no more than two space dimensions:

$$\frac{\partial^2 C}{\partial y^2} + \frac{\partial^2 C}{\partial z^2} = \frac{1}{D} \cdot \frac{\partial C}{\partial t} \qquad [A2.2]$$

A problem can often be simplified by using a suitable coordinate system. For example, in spherical polar coordinates (§) equation A2.1 becomes [1 - 3]:

$$C_{rr} + \frac{2}{r} C_r + \frac{1}{r^2} C_{\theta\theta} + \frac{\cot[\theta]}{r^2} C_\theta + \frac{1}{r^2 \sin^2[\theta]} C_{\psi\psi} = \frac{1}{D} C_t$$

where θ, ψ, and r are the equatorial and azimuthal angles, and radial distance, respectively, and the suffix notation has been used for greater clarity. When the diffusional behaviour is independent of the angular orientations, θ and ψ, this equation becomes:

$$\frac{\partial C}{\partial t} = D\left(\frac{\partial^2 C}{\partial r^2} + \frac{2}{r} \frac{\partial C}{\partial r} \right)$$

More generally, one can write:

$$\frac{\partial C}{\partial t} = D\left(\frac{\partial^2 C}{\partial r^2} + \frac{n}{r} \cdot \frac{\partial C}{\partial r} \right)$$

where n = 2. Further reductions to the equation for a cylindrical or plate geometry can be obtained by replacing n in the above expression by unity or zero respectively. Thus, the steady-state growth of a sphere is governed by:

$$\frac{\partial^2 C}{\partial r^2} + \frac{2}{r} \cdot \frac{\partial C}{\partial r} = 0$$

The principal characteristic of the diffusion equation is its conservative nature; i.e. it acts so as to even out any irregularities. This can be seen firstly by considering the one-dimensional equation for rectangular coordinates:

$$\frac{\partial^2 C}{\partial z^2} = \frac{1}{D} \cdot \frac{\partial C}{\partial t} \qquad [A2.3]$$

Note that the left-hand-side is the expression which defines the sense of the curvature of a function. Thus, when the second derivative is positive it denotes a concave-upwards part of a function. In the present case, it would correspond to a local minimum in the concentration distribution. However, from equation A2.3, the local change in concentration with time is also positive and therefore the depression

§ For other coordinate systems, see reference 3. In principle, any interface shape can be given a suitable system of coordinates. However, this would be pointless unless the resultant transformed differential equation could be separated. This can only be achieved in some eleven systems, including the cylindrical, spherical, and parabolic. The latter system is very useful for treating dendrite tip problems.

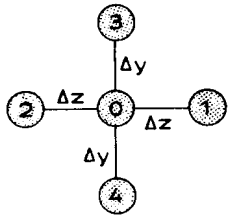

$$\frac{\partial^2 C}{\partial y^2} + \frac{\partial^2 C}{\partial z^2} = 0$$

$$\frac{(C_3 - C_0) - (C_0 - C_4)}{\Delta y^2} + \frac{(C_1 - C_0) - (C_0 - C_2)}{\Delta z^2} = 0$$

$$\boxed{C_0 = \frac{C_1 + C_2 + C_3 + C_4}{4}} \qquad \Delta y = \Delta z$$

Figure A2.1

in the concentration distribution will tend to be removed. The reverse is true for negative values of the left-hand-side. The conservative nature of the two-dimensional, time-independent (Laplace) equation can also be seen clearly from the finite-difference scheme (figure A2.1) where each cell must take a value which is the average of the values of the four surrounding cells. A little reflection will show that the only 'bumps' which can persist, in this steady-state situation, are those imposed by the boundary conditions. Finally, it can be proved that the direction of flow of heat or mass at any point is at right-angles to the isotherms or isoconcentrates. It is less well known that both the isotherms and flux lines can be drawn by inspection, without ever solving the diffusion equation. Unfortunately, this 'flux-plotting' technique [4] does not work well for solidification problems because of the complicated boundary conditions which are usually imposed.

Directional Growth Equation

Equation A2.3, which is known as Fick's second law, would be of little use in treating moving boundary problems because the interface movement would have to be accounted for. Instead, an equation expressed in a coordinate system which moves with the interface can be used. In figure A2.2, the coordinates of the point, P, with respect to axes moving with the interface are (y,z). Its coordinates with respect to a stationary observer are (y',z'). From the diagram, it is evident that:

$$z = z' - Vt \qquad [A2.4]$$

Since $\partial z/\partial z' = 1$, $\partial C/\partial z' = (\partial C/\partial z)(\partial z/\partial z') = \partial C/\partial z$, and similarly, $\partial^2 C/\partial z'^2 = \partial^2 C/\partial z^2$, the left-hand-side of equation A2.3 is unchanged.

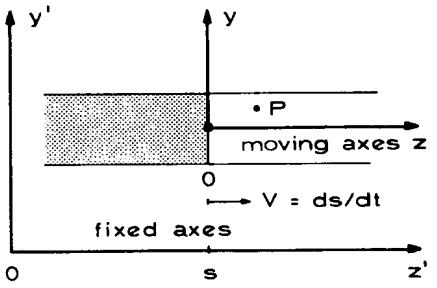

Figure A2.2

The concentration is a function of z' and t, but must be transformed so as to become a function of z(t) and t. Therefore, using the 'chain rule' for differentiation,

$$\frac{dC}{dt} = \frac{\partial C}{\partial z} \cdot \frac{dz}{dt} + \frac{\partial C}{\partial t}$$

From equation A2.4, $\partial z/\partial t = -V$ and equation A2.3 becomes:

$$D \frac{\partial^2 C}{\partial z^2} = -V \frac{\partial C}{\partial z} + \frac{\partial C}{\partial t} \qquad [A2.5]$$

Re-introducing a second space coordinate (which is unaffected by the above transformation of coordinates) in order to describe lateral diffusion, and rearranging gives:

$$\frac{\partial^2 C}{\partial y^2} + \frac{\partial^2 C}{\partial z^2} + \frac{V}{D} \cdot \frac{\partial C}{\partial z} = \frac{1}{D} \cdot \frac{\partial C}{\partial t}$$

or, in its time-independent form (steady-state growth):

$$\frac{\partial^2 C}{\partial y^2} + \frac{\partial^2 C}{\partial z^2} + \frac{V}{D} \cdot \frac{\partial C}{\partial z} = 0 \qquad [A2.6]$$

This equation, which is known as the directional growth equation, will be used in order to solve most of the problems in this book.

Solutions of the Directional Growth Equation

The first step in solving a directional growth problem is to discover what functions satisfy equation A2.6. These functions can then be used as the starting point in solving any problem (in rectangular coordinates), and an exact solution would be obtained if all of the boundary conditions could be satisfied everywhere.
It is assumed firstly that the solution of equation A2.6 can be expressed as the product of separate functions of y and z alone [1 - 3]:

$$C(y,z) = Y(y)\,Z(z) \qquad [A2.7]$$

Inserting the relevant derivatives of this expression into equation A2.6 gives:

$$\frac{d^2Y}{dy^2}\,Z + \frac{d^2Z}{dz^2}\,Y + \frac{V}{D}\cdot\frac{dZ}{dz}\,Y = 0$$

and dividing throughout by C(y,z) gives:

$$\frac{1}{Y}\cdot\frac{d^2Y}{dy^2} + \frac{1}{Z}\cdot\frac{d^2Z}{dz^2} + \frac{V}{D}\cdot\frac{1}{Z}\cdot\frac{dZ}{dz} = 0 \qquad [A2.8]$$

Each term which involves y or z alone must be equal to a constant known as the separation constant. This can be seen by considering the term in Z for instance: either it is a constant or it is a function of z. In the latter case, the other terms in equation A2.8 must be functions of z in order to satisfy the equation. However, this contradicts the assumption that the functions each depend on only one variable. Hence, each term is equal to a constant, a, and the sum of the constants must be zero (from equation A2.8). The sign of the separation constant is determined by inspection after considering the properties which the solution must have in order to reflect the characteristics of the physical model. Thus, one can write:

$$\frac{1}{Z}\cdot\frac{d^2Z}{dz^2} + \frac{V}{D}\cdot\frac{1}{Z}\cdot\frac{dZ}{dz} = a$$

$$\frac{d^2Z}{dz^2} + \frac{V}{D}\cdot\frac{dZ}{dz} - aZ = 0 \qquad [A2.9]$$

In the overall direction of advance of the interface (z axis), one expects the existence of a boundary layer which is theoretically of infinite extent. This fact, together with the form of equation A2.9 (i.e. a weighted sum of successive differentials) makes the exponential function a likely candidate. Therefore, setting:

$$Z = \exp[bz] \qquad [A2.10]$$

and performing the differentiations indicated by equation A2.9 gives:

$$b^2\exp[bz] + \frac{Vb}{D}\exp[bz] - a\exp[bz] = 0$$

The factor, exp[bz], cancels to leave:

$$b^2 + \frac{Vb}{D} - a = 0$$

This quadratic algebraic equation is solved by elementary means to give:

$$b = -\frac{V}{2D} - \sqrt{\left(\frac{V}{2D}\right)^2 + a}$$

The positive root is not considered because the solution to the problem might then predict infinite values of concentration. The general solution to equation A2.9 is thus:

$$Z = \exp\left[\left[-\frac{V}{2D} - \sqrt{\left(\frac{V}{2D}\right)^2 + a}\right] z\right] \qquad [A2.11]$$

Considering now the term in Y (equation A2.8), one can set:

$$\frac{1}{Y}\cdot\frac{d^2Y}{dy^2} = -a$$

or:

$$\frac{d^2Y}{dy^2} + aY = 0 \qquad [A2.12]$$

The form of this equation suggests that the function to be substituted should be such that its second derivative is of the same form as the original function. Both the exponential and circular functions exhibit this characteristic, but it should be remembered that the Y function must describe the concentration variation along the interface. Due to the uniform or repetitive nature of the interface morphology (figures 3.1, 4.14, 5.2), this concentration is not expected to deviate to a large extent. Thus, an exponential function would not be suitable and a circular function can be assumed to be more correct. Thus:

$$Y = \cos[cy] \text{ or } Y = \sin[cy] \qquad [A2.13]$$

Substitution of this expression into equation A2.12 gives:

$$c = \sqrt{a}$$

and

$$Y = \cos[a^{0.5}y] \text{ or } Y = \sin[a^{0.5}y] \qquad [A2.14]$$

Finally, substituting equations A2.14 and A2.11 into equation A2.7 gives:

$$C = \cos[a^{0.5}y]\exp\left[\left[-\frac{V}{2D} - \sqrt{\left(\frac{V}{2D}\right)^2 + a}\right] z\right] \qquad [A2.15a]$$

or

$$C = \sin[a^{0.5}y]\exp\left[\left[-\frac{V}{2D} - \sqrt{\left(\frac{V}{2D}\right)^2 + a}\right] z\right] \qquad [A2.15\ b]$$

Examination of the form of this equation shows that, overall, the lateral distribution will be cyclic in form, and that the concentration will decrease exponentially away from the interface in the growth direction (figure A2.3). Using the theory of Fourier series, any number of cosine (or sine) functions can be added together in order to satisfy the boundary conditions. Note that when the constant, a, is very large it will dominate the exponential decrease of the boundary layer. When it is very small, the boundary layer will be the same as that for a uniform plane interface. These two cases correspond to a frequently varying lateral concentration, and a slowly varying lateral concentration respectively, since the value of a is inversely proportional to the wavelength of the interface morphology. This is seen in the case of eutectic growth where the rate of exponential decrease is dominated by the wavelength, and the thickness of the boundary layer becomes proportional to the eutectic spacing (appendix 9). When the scale of the interface morphology can vary over a wide range, the full solution (equation A2.15) must be used. This situation arises when carrying out stability analyses (equation A2.32, appendix 6).

Boundary Conditions

Three types of mathematical boundary condition are generally imposed on the solution of a differential equation. These are the Dirichlet condition, which defines the absolute value of the solution at a boundary point, the Neumann condition, which defines the normal gradient of the solution at the boundary, and the Robin (mixed) condition which establishes a relationship between the absolute value and the gradient of the solution at the boundary. The latter condition is the main source of difficulty in solidification problems because the interface concentrations and their gradients are usually not given explicitly but must be found as part of the solution. This condition, since it arises from the balance between solute rejection and diffusion at the interface, will be called the flux condition. The other conditions will also be given names which reflect their significance in solidification problems (figure A2.3).

Flux Condition

As a solid/liquid interface advances at the local normal growth rate, V_n, with an interface concentration in the liquid, C*, and solid concentration, kC*, the quantity of solute rejected per unit time will be $V_n(1-k)C^*$. This must be balanced by the creation of a concentration gradient in the liquid, normal to the isoconcentration contours, which permits solute removal at the same rate via diffusion. Thus:

$$V_n(1-k)C^* = -D\frac{\partial C}{\partial m} \qquad [A2.16]$$

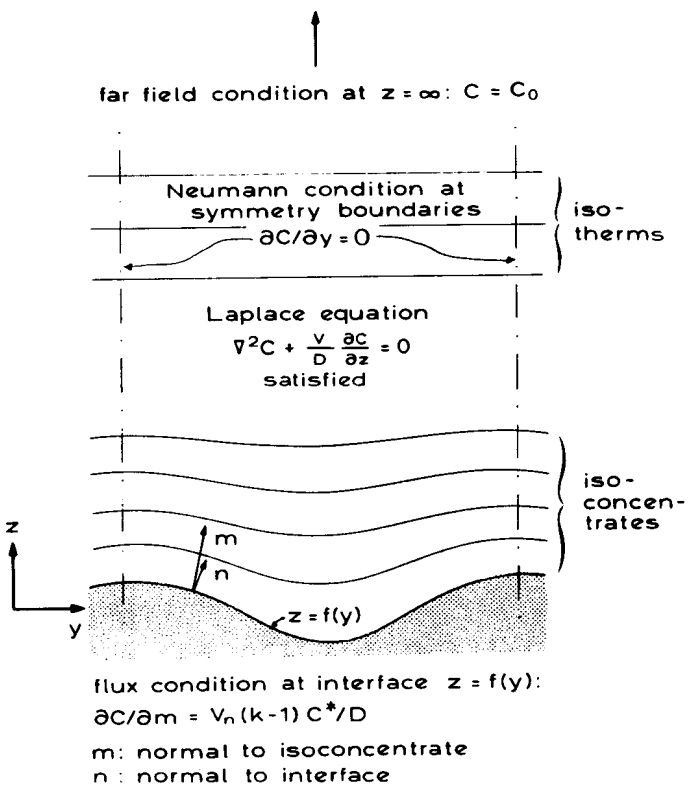

Figure A2.3

One complication is that the normal to the interface, n, along which the interface advances locally, is not generally the same as the normal, m, to the isoconcentration contours in the liquid. Thus, in order to simplify the problem, the interface should be assumed to be of uniform concentration (or isothermal). Otherwise, the flux condition can only be applied on an axis of symmetry, where the two normals are bound to be aligned. Such a point would be the tip of the perturbation shown in figure A2.3.

Far-Field Condition

A Dirichlet condition can be imposed far ahead of the interface because here the original composition is expected to be unaffected by the advance of the interface, i.e.:

$$C = C_o \qquad z = \infty \qquad [A2.17]$$

Symmetry Condition

Most interface morphologies consist of arrays of similar shapes. Advantage can be taken of this fact by studying just one half-period of the shape along the y-axis. If the shapes are presumed to be identical, there can be no mass transfer between them. Hence, zero concentration gradient (Neumann) conditions can be imposed at the boundaries of a typical interface 'motif', i.e.:

$$\frac{\partial C}{\partial y} = 0 \qquad y = \frac{n\lambda}{2} \qquad [A2.18]$$

where n = 0, 1, 2, ...

Coupling Condition

Under the normal solidification conditions for metals ($V \prec 100$mm/s), each location along the interface will have a local freezing point which is a function of the local concentration and the local curvature. In steady-state growth, each point of the interface must lie on the corresponding isotherm of the temperature field:

$$T^* = T + m\Delta C - \Gamma K \qquad [A2.19]$$

Satisfaction of Boundary Conditions

In the last section, a general solution to the Laplace equation was obtained in terms of elementary functions. It would be overly optimistic to expect any real situation to involve boundary conditions which permitted such a solution to be used without any further effort. Unfortunately, the greater part of the problem still lies ahead. Indeed, the requirement that the basic solution (or its derivatives) should have certain values at the boundaries of the region studied accounts for most of the effort expended by applied mathematicians. Their researches over the past two hundred years have produced an enormous range of methods for attacking the problem [2]. A number of these methods, which are used elsewhere in the text, will be described below.
Firstly, two cases will be considered in which the boundary conditions can be satisfied exactly.

i) Steady-State Diffusion Field ahead of a Moving Planar Interface

As shown above, the diffusion equation in a coordinate system with its origin fixed at the solid/liquid interface takes the steady-state form for unidirectional diffusion (figure A2.4a) obtained from equation A2.6:

$$\frac{\partial^2 C}{\partial z^2} + \frac{V}{D}\cdot\frac{\partial C}{\partial z} = 0$$

Noting the similarity of the above expression to equation A2.9, setting the separation constant, a, equal to zero, and repeating the steps after equation A2.10 above, gives:

$$Db^2 + Vb = 0$$

The solutions of this so-called 'auxiliary' equation are b = 0 and b = -V/D. Therefore, the general solution is:

$$C = A + B\exp[-\frac{Vz}{D}] \qquad [A2.20]$$

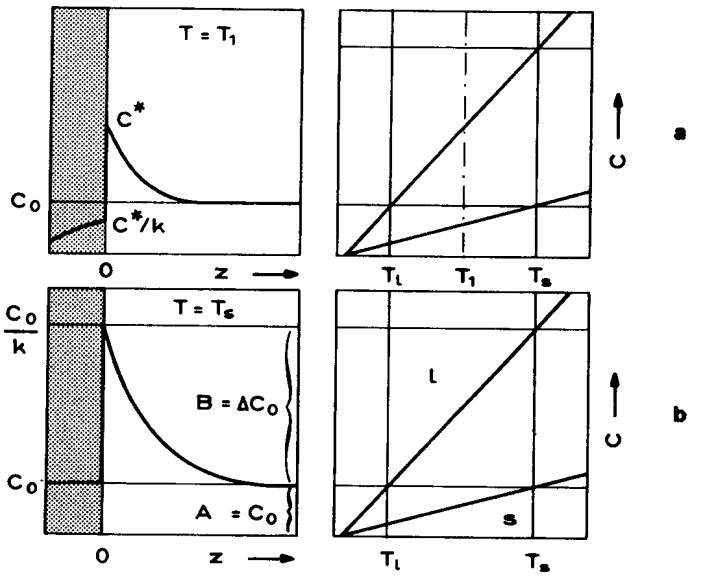

Figure A2.4

Again, following the principles described above, a far-field condition is applied. That is, far from the interface the concentration must be equal to the original composition, C_o. Letting $C = C_o$ when z tends to infinity shows that $A = C_o$. Therefore:

$$C = C_o + B \exp[-\frac{Vz}{D}]$$

Next, one can apply the flux (Robin) condition at the solid/liquid interface. Here, the rate of solute rejection must be equal to the diffusional flux in the liquid at the interface:

$$C^*(1 - k)V = -D(\frac{dC}{dz})_{z=0}$$

Therefore, when z = 0:

$$C^* = C_o + B$$

and

$$(\frac{dC}{dz})_{z=0} = -\frac{VB}{D}$$

Substituting these expressions into the above shows that:

$$B = C_o\frac{1 - k}{k} = \Delta C_o$$

Therefore, the complete solution for the solute distribution ahead of a planar solid/liquid interface, advancing under steady-state conditions, is [5]:

$$C = C_o + (\frac{C_o}{k} - C_o) \exp[-\frac{Vz}{D}] \qquad [A2.21]$$

The boundary layer shown in figure A2.5 is of infinite extent. In order to obtain a convenient practical estimate of its thickness, an equivalent boundary layer, δ_c, is often defined. This equivalent layer is chosen so as to contain the same total solute content as the infinite layer, and has a constant concentration gradient across its thickness. Thus, the surface area of the triangle, OMN, must be equal to the cross-hatched surface. That is:

$$\frac{C_o\delta_c}{2} = \Delta C_o\int_o^\infty \exp[-\frac{Vz}{D}]\,dz$$

and:

$$\delta_c = \frac{2D}{V}$$

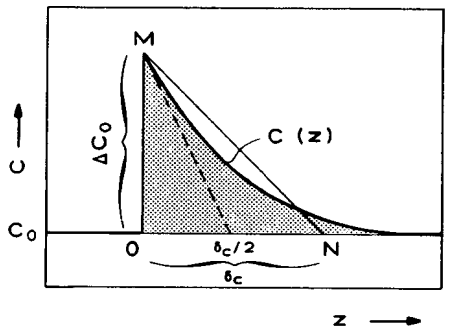

Figure A2.5

Differentiating equation A2.21 at z = 0 gives:

$$G_c = (\frac{dC}{dz})_{z=0} = -\frac{\Delta C_o V}{D} \qquad [A2.22]$$

From this, it can be seen that the absolute value of the concentration gradient at the interface is equal to twice the absolute mean concentration gradient of the equivalent boundary layer. Such relationships are very useful in understanding the constitutional undercooling criterion (chapter 3.3).

ii) Diffusion Field Around a Growing Sphere

When no tangential diffusion is occurring, the diffusion equation can be written in terms of the radial coordinate alone [6,7]:

$$\frac{\partial C}{\partial t} = D(\frac{\partial^2 C}{\partial r^2} + \frac{2}{r}\cdot\frac{\partial C}{\partial r}) \qquad [A2.23]$$

where r is the radius. Under steady-state conditions,

$$\frac{d}{dr}(r^2\frac{dC}{dr}) = 0$$

the general solution of this equation is:

$$C = A + \frac{B}{r} \qquad [A2.24]$$

For the situation described in figure A2.6, the boundary conditions are:

$C = C_o$ $\qquad r = \infty$

$C = C^*$ $\qquad r = R$

Use of these conditions shows that $A = C_o$ and $B = R(C^* - C_o)$. Thus, equation A2.24 becomes:

$$C = C_o + \frac{R}{r}(C^* - C_o) \qquad [A2.25]$$

The concentration gradient in the liquid becomes:

$$\frac{dC}{dr} = -\frac{R}{r^2}(C^* - C_o)$$

and, at the interface

$$(\frac{dC}{dr})_R = -\frac{C^* - C_o}{R} \qquad [A2.26]$$

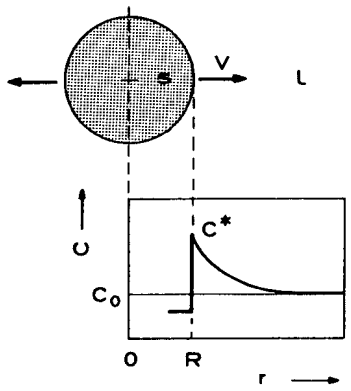

Figure A2.6

This shows that, to a first approximation, the thickness of the boundary layer around a growing sphere is equal to the radius and increases with increasing size of the sphere. For other solutions see references 8 and 9.
Some methods which are available for the treatment of more difficult cases can now be considered:

Classical Method

When using this method, advantage is taken of the linearity of equation A2.6. That is, the sum of any series of terms having the same form as the basic solution (such as the sine and cosine functions found previously) will also be a solution. This means that, although the basic solution (often called an eigenfunction) is unlikely to satisfy the boundary conditions, 'adjustment' using terms of the same form will allow the conditions to be approximated more closely. For example, if the basic solution is of the form, $\cos[2\pi y/\lambda]$, one can consider adding terms such as $\cos[4\pi y/\lambda]$, e.g.:

$$C(y) = A_1\cos[\frac{2\pi y}{\lambda}] + A_2\cos[\frac{4\pi y}{\lambda}] + \ldots + A_i\cos[\frac{2\pi iy}{\lambda}] \qquad [A2.27]$$

where the A_i are constants. Because the oscillation of the cosine functions increases in frequency with increasing value of i, finer and finer adjustments can be made to the basic solution. In order to carry this out in practice, the constants before each term in a series such as the one above are suitably chosen. Many methods have been devised in order to find the required values of these constants. The best method, but one which is rarely feasible, is to take advantage of the orthogonality of functions such as the circular ones (sine, cosine). In this method, each term in the above series would be multiplied by $\cos[2\pi jy/\lambda]$:

$$C(y)\cos[\frac{2\pi jy}{\lambda}] = A_1\cos[\frac{2\pi y}{\lambda}]\cos[\frac{2\pi jy}{\lambda}] + A_2\cos[\frac{4\pi y}{\lambda}]\cos[\frac{2\pi jy}{\lambda}]$$

$$+ A_i\cos[\frac{2\pi iy}{\lambda}]\cos[\frac{2\pi jy}{\lambda}]$$

When both sides are integrated over one wavelength:

$$\int_0^{2\pi} C(y)\cos[\frac{2\pi jy}{\lambda}]dy = A_1\int_0^{2\pi}\cos[\frac{2\pi y}{\lambda}]\cos[\frac{2\pi jy}{\lambda}]dy$$

$$+ A_2\int_0^{2\pi}\cos[\frac{4\pi y}{\lambda}]\cos[\frac{2\pi jy}{\lambda}]dy + \ldots$$

$$\ldots + A_i\int_0^{2\pi}\cos[\frac{2\pi iy}{\lambda}]\cos[\frac{2\pi jy}{\lambda}]dy \qquad [A2.28]$$

all of the terms on the right-hand side will disappear unless $j = i$. Therefore, by setting j equal successively to 1, 2, 3, etc, the value of any A_i can be 'singled out'. A general expression is usually obtained for all of the adjustable constants of the series.

The reader should satisfy himself that if this 'trick' were not available, the A-values (Fourier coefficients) could only be determined exactly by solving an infinite set of simultaneous algebraic equations. Unfortunately, this is usually the case since the above method can only be employed when the boundary coincides with a coordinate line over which the functions are also orthogonal.
In response to this common difficulty, approximate methods have been developed and will be described in the next section. Meanwhile, a relatively little-known technique for obtaining the Fourier coefficients without integration will be described. However, this technique is only applicable when the boundary conditions are discontinuous in some way. For example, see figure A11.4 where the first and higher derivatives of the concentration distribution are discontinuous at regular intervals.
In the case of a cosine series, the Fourier coefficients are given directly by:

$$A_i = \frac{1}{i\pi}[-\sum_{s=1}^{m} J_s \sin(iy_s) - \frac{1}{i}\sum_{s=1}^{m} J_s' \cos(iy_s) + \ldots$$

$$\ldots + \frac{1}{i^2}\sum_{s=1}^{m} J_s'' \sin(iy_s) + \ldots] \qquad [A2.29]$$

where the J, J', J", etc are 'jumps' in the function, first derivative, second derivative, etc. The definition of such a jump will be described in later appendices where the technique is applied to various problems. The derivation of equation A2.29 is quite simple [10] but is beyond the scope of the present book.

Method of Weighted Residuals

In effect, this technique [11] sets out to satisfy the boundary conditions of the problem in the same way as does the classical method. Thus, a series consisting of functions having adjustable multiplying constants is used. However, in this case, the functions are rarely orthogonal and the constants can only be found by solving a set of simultaneous algebraic equations. The number of terms in the series is chosen so as to be equal to the number of adjustable constants. The method is approximate in nature and the higher-order approximations can only be handled by using numerical analysis techniques and a computer. Nevertheless, surprisingly accurate analytical results can often be obtained using just a few terms, and sometimes only one [12]. Such an analytical solution has the advantage that it will reveal the influence of the various experimental and physical parameters directly whereas a more accurate but numerical method will not. The method is extremely flexible and can be applied to any problem. As an example, it will be used to find a solution to the dendritic growth problem in two dimensions:

Simple Dendrite Analysis

A function will be chosen which satisfies the boundary conditions. This is known as the external method. The trial solution can also be such that, alone, it does not satisfy either the differential equation, or the boundary conditions. The reader will doubtless appreciate the flexibility of the method, but on the other hand he must also have a firm grasp of the physics of the real situation in order to be able to use it properly.

In the present case, a Dirichlet condition will be applied at the interface, assuming that the concentration is constant over the parabolic surface of the dendrite (figure 2.8). Thus:

$$C = C^* \qquad z = -\beta y^2$$

Also, applying the far-field condition,

$$C = C_o \qquad z = \infty$$

One can easily construct an expression which satisfies these conditions. Firstly, take the basic solution for a planar interface which was derived above:

$$C = C_o + (C^* - C_o)\exp[-bz] \qquad [A2.30]$$

This describes a solute distribution in which the value at infinity is C_o. Thus, the far-field condition is satisfied. It is also required that the concentration be equal to C* when the value of the exponential term is unity. In the case of the planar interface, this only occurs when z is equal to zero. Therefore, it is necessary to replace z by an expression which is equal to zero whenever a coordinate pair, (y,z), corresponds to the surface of the parabolic plate dendrite. This is true when $z = -\beta y^2$, so that the required expression is:

$$C = C_o + (C^* - C_o)\exp[-b(\beta y^2 + z)] \qquad [A2.31]$$

The reader should prove for himself that this satisfies the boundary conditions and that the concentration decreases exponentially with y^2 and z. The value of b can be determined by means of the flux condition, applied at the tip:

$$V(k - 1)C^* = D\left(\frac{\partial C}{\partial z}\right)_{y=z=0} \qquad [A2.32]$$

Substituting the z-derivative of equation A2.31 into equation A2.32 gives:

$$b = \frac{V}{D} \cdot \frac{(k - 1)C^*}{C_o - C^*}$$

so that:

$$C = C_o + (C^* - C_o)\exp[-\frac{V(k - 1)C^*(\beta y^2 + z)}{D(C_o - C^*)}] \qquad [A2.33]$$

The differential equation (equation A2.6) is:

$$\frac{\partial^2 C}{\partial y^2} + \frac{\partial^2 C}{\partial z^2} + \frac{V}{D} \cdot \frac{\partial C}{\partial z} = 0$$

Substituting equation A2.33 into A2.6 and simplifying gives:

$$\frac{V}{D} \cdot \frac{4y^2\beta^2(k - 1)C^*}{(C_o - C^*)} - 2\beta + \frac{V}{D} \cdot \frac{(k - 1)C^*}{(C_o - C^*)} - \frac{V}{D} = 0$$

The first term in the above equation (the 'residual' which gives the method its name) will be made equal to zero at the point, y = 0 so that:

$$\frac{V}{D}\cdot\frac{(k-1)C^*}{C_o - C^*} = \frac{V}{D} + 2\beta \qquad [A2.34]$$

The curvature at the tip of the parabola, $y = -\beta y^2$, is given by the second derivative of z with respect to y. Thus, the curvature is 2β and the radius of curvature is:

$$R = \frac{1}{2\beta} \qquad [A2.35]$$

Substituting this value into equation A2.34 gives:

$$\frac{V}{D}\cdot\frac{(k-1)C^*}{C_o - C^*} = \frac{V}{D} + \frac{1}{R}$$

and:

$$\frac{(k-1)C^*}{C_o - C^*} = 1 + \frac{D}{VR}$$

but VR/2D is the Péclet number, so that:

$$\frac{(k-1)C^*}{C_o - C^*} = 1 + \frac{1}{2P}$$

Now, $(C^*-C_o)/(C^*-kC^*)$ is the dimensionless supersaturation, Ω, so that:

$$\Omega = \frac{2P}{2P+1} \qquad [A2.36]$$

which is the same as the Zener/Hillert [9] solution (appendix 7).

Perturbation Method

If the geometry of the problem is such that the interface form corresponds closely to some simple shape, any exact solution which is available for the simple shape can be assumed to be similar to that for the slightly different morphology. This principle will be illustrated by treating an almost planar solid/liquid interface growing under steady-state conditions. A related problem will be studied in appendix 6.

Slightly-Perturbed Interface

The form of the planar solid/liquid interface, described by the equation, z = 0, is assumed to be changed so that it is then represented by the expression:

$$z = \epsilon\sin[\omega y] \qquad [A2.37]$$

where ϵ is assumed to be a very small amplitude, and ω is the wave number $(= 2\pi/\lambda)$ of the perturbation.
Recall that the exact solution for a planar solid/liquid interface under steady-state conditions (equation A2.21) is:

$$C = C_o + (\frac{C_o}{k} - C_o)\exp[-\frac{Vz}{D}]$$

where C_o/k is the concentration in the liquid at the interface and C_o is the original composition. Now, using the perturbation technique, a term having the same form as the perturbation (equation A2.37) is added to the exact solution for the unperturbed interface, i.e.:

$$C = C_o + (\frac{C_o}{k} - C_o)\exp[-\frac{Vz}{D}] + A\,\epsilon\sin[\omega y]\exp[-bz] \qquad [A2.38]$$

where b has to be equal to $(V/2D) + \sqrt{(V/2D)^2 + \omega^2}$ in order that the added term should satisfy equation A2.6 (see equation A2.11), and A is a constant whose value is to be determined by forcing equation A2.38 to satisfy the boundary conditions. These are, for $z = \epsilon\sin[\omega y]$:

$$C = C^* \qquad [A2.39]$$

$$V(1-k)C^* = -D\frac{\partial C}{\partial z} \qquad [A2.40]$$

Note that equation A2.38 already satisfies the far-field condition, $C = C_o$ when $z = \infty$, since the unknown constant, A, disappears. Rather more work is required to make it satisfy the other boundary conditions (e.g. equation A2.39). The first step is to substitute C* for C and $\epsilon\sin[\omega y]$ for z:

$$C^* = C_o + (\frac{C_o}{k} - C_o)\exp[-\frac{VS}{D}] + A\,S\exp[-bS] \qquad [A2.41]$$

where, for clarity, S has been used to represent $\epsilon\sin[\omega y]$. The above expression can only be evaluated because of the assumption that ϵ (and S) are small. In this case, an exponential function, exp[-x], can be approximated by 1 - x. Again, because ϵ is small, terms involving ϵ^2 (and S^2) can be neglected. This leads to:

$$C^* = C_o + (\frac{C_o}{k} - C_o)(1 - \frac{VS}{D}) + A(1 - bS)$$

By differentiating equation A2.21 with respect to z and then setting z equal to zero, the concentration gradient, G_c, at the plane interface is found to be (equation A2.22):

$$G_c = -\frac{V}{D}\left(\frac{C_o}{k} - C_o\right)$$

Substituting this into the previous equation and dropping terms in S^2 gives:

$$C^* = \frac{C_o}{k} + G_c S + AS \qquad [A2.42]$$

Thus far, no real progress has been made since the value of C* is also unknown. It is necessary to find another equation which links C* and A, i.e. the flux condition (equation A2.40). Thus, differentiating equation A2.38 gives:

$$\frac{dC}{dz} = -\frac{V}{D}\left(\frac{C_o}{k} - C_o\right)\exp\left[-\frac{Vz}{D}\right] - bAS\exp[-bz]$$

At the interface this becomes:

$$\left(\frac{dC}{dz}\right)_{z=S} = -\frac{V}{D}\left(\frac{C_o}{k} - C_o\right)\left(1 - \frac{VS}{D}\right) - bAS(1 - bS)$$

Substituting G_c for $-(V/D)(C_o/k - C_o)$ gives:

$$\left(\frac{dC}{dz}\right)_{z=S} = G_c\left(1 - \frac{VS}{D}\right) - bAS \qquad [A2.43]$$

Substituting equations A2.42 and A2.43 into equation A2.40 and cancelling S throughout leads to:

$$A = \frac{kVG_c}{Vp - Db}$$

where $p = 1-k$. Thus, the original expression becomes:

$$C = C_o + \left(\frac{C_o}{k} - C_o\right)\exp\left[-\frac{Vz}{D}\right] + \left(\frac{kVG_c\,\epsilon\sin[\omega y]}{Vp - Db}\right)\exp[-bz] \qquad [A2.44]$$

This expression describes the solute distribution ahead of the slightly perturbed solid/liquid interface. Further use is made of it in appendix 6, where the stability of a planar solid/liquid interface is considered.

REFERENCES

[1] H.S.Carslaw, J.C.Jaeger: Conduction of Heat of Solids, 2nd Edition, Oxford University, London, 1959

[2] J.Crank: The Mathematics of Diffusion, Oxford University Press, London, 1956

[3] P.Moon, D.E.Spencer: Field Theory Handbook, Springer-Verlag, Heidelberg, 1961

[4] L.F.Richardson: Philosophical Magazine, 15 (1908) 237

[5] W.A.Tiller, K.A.Jackson, J.W.Rutter, B.Chalmers: Acta Metallurgica, 1 (1953) 428

[6] C.Zener: Journal of Applied Physics, 20 (1949) 950

[7] R.L.Parker: Solid State Physics, 25 (1970) 151

[8] F.C.Frank: Proceedings of the Royal Society of London, A201 (1950) 586

[9] G.Engberg, M.Hillert, A.Oden: Scandinavian Journal of Metallurgy, 4 (1975) 93

[10] E.Kreyszig: Advanced Engineering Mathematics, Wiley, New York, 1968

[11] B.A.Finlayson: The Method of Weighted Residuals and Variational Principles, Academic Press, New York, 1972

[12] R.Aris: Mathematical Modelling Techniques, Pitman, London, 1978

APPENDIX 3

LOCAL EQUILIBRIUM AT THE SOLID/LIQUID INTERFACE

The Phase Diagram

In most analyses of alloy solidification, and in all of the cases considered in this book, it is assumed that the solid/liquid interface behaves locally as if it were in a state of equilibrium. This means that the reaction rates in the small volume making up the very thin but finite interface layer, are expected to be rapid in comparison with the rate of interface advance. As a result, the transfer of atoms and changes in arrangement, which are required in order to maintain constancy of the chemical potentials in both phases, are rapid and can therefore be neglected. Such a simplification is permissible in the case of metals solidifying at the rates encountered in normal casting and welding operations (§). The assumption of local equilibrium means that, if the interface temperature is known, then one can obtain the liquid and solid compositions at the interface by reference to the equilibrium phase diagram. This does not mean that the system as a whole is at equilibrium, as gradients of temperature and composition are present.
In order to avoid non-essential variables which would complicate the analysis without revealing any new principles, it is usually assumed that both the liquidus and the solidus lines of the relevant part of the phase diagram are straight. In solidification, the liquidus line is most important and represents the point where the liquid 'first' transforms to solid, i.e., the liquidus is the freezing point of an alloy. Thus, only the slope, m, of the liquidus is used in calculations. The liquidus slope is defined as:

$$T_l[C] = T_f + mC \qquad [A3.1]$$

The solidus composition can be determined at any time from the definition of the distribution coefficient:

$$k = \left(\frac{C_s}{C_l}\right)_{T,P} \qquad [A3.2]$$

The constants, m and k, are always defined in the present book in such a way that the product, m(k-1) is positive. In general, m can be positive or negative and k can be greater or less than unity respectively.

§ At very high growth rates (V>100mm/s), such as those which occur in rapid solidification processing, conditions of local equilibrium no longer exist. Therefore, the value of k changes [1].

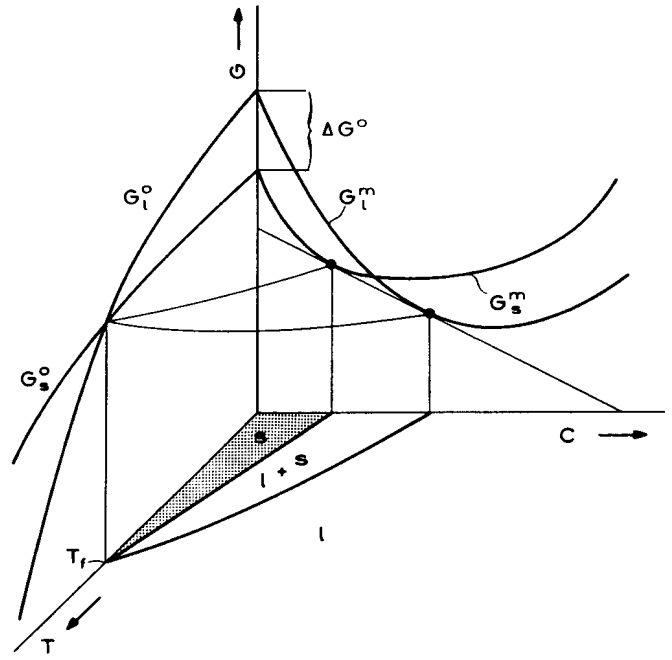

Figure A3.1

Two important properties characterise the range of coexistence of solid and liquid for a given alloy:

$$\Delta T_o = -m\Delta C_o \qquad [A3.3]$$

$$\Delta C_o = \frac{C_o(1-k)}{k} \qquad [A3.4]$$

All of these properties depend upon the Gibbs free energy (free enthalpy) of the alloy system as shown by figure A3.1. The latter relates a free-enthalpy/concentration diagram and a free-enthalpy/temperature diagram to a temperature/concentration (phase) diagram. The form of the curves in the ΔG-C diagram can be described using the regular solution model [2-4] which shows that:

$$G_m = \Delta G^* + \Omega X(1-X) + RT[X\ln(X) + (1-X)\ln(1-X)] \qquad [A3.5]$$

The curves in the ΔG-T diagram depend upon the standard values for the pure components:

$$G^* = H^* - TS^*$$

where the dots indicate values for the pure component. For convenience, G_m and $G^\cdot$ are written as differences. Then,

$$\Delta G^\cdot = \Delta H^\cdot - T\Delta S^\cdot \qquad [A3.6]$$

which is the free enthalpy (Gibbs free energy) difference existing between the pure liquid and pure solid:

$$\Delta H^\cdot = \Delta H_f^\cdot - \int_T^{T_f} \Delta c^\cdot dT$$

$$\Delta S^\cdot = \Delta S_f^\cdot - \int_T^{T_f} \left(\frac{\Delta c^\cdot}{T}\right) dT$$

where $\Delta c^\cdot = c^l - c^s$. For clarity, the dot suffix will be dropped in the remainder of this appendix.
The quantity, ΔG, in equation A3.6 is very important with regard to nucleation and growth processes and can be evaluated when the temperature dependence of Δc is known. At high temperatures, the difference in specific heat of the liquid and solid can be described by:

$$\Delta c = K_1 T + K_2 \qquad [A3.7]$$

For an undercooled melt, $\Delta T \equiv T_f - T$ and [5]:

$$\Delta G = \frac{\Delta H_f \Delta T}{T_f} - \Delta T^2 \left[\frac{K_1}{2} + \frac{K_2}{T_f + T}\right] \qquad [A3.8]$$

If the value of Δc is unknown, the simplest assumption (and one which is quite reasonable for metals) is that $\Delta c = 0$. This leads to:

$$\Delta G = \frac{\Delta H_f \Delta T}{T_f} = \Delta S_f \Delta T \qquad [A3.9]$$

The quantity, ΔS_f, is the difference in slope of the G-T function of two phases (figure A3.1). In the case of solidification, ΔS_f is less than zero.
From equations A3.5 and A3.9, one can now see what parameters influence the magnitude of m and k. These are the interaction parameter, Ω, for the atoms of both species in the alloy, which determines the form of the G_m-X curves, and the melting entropy, ΔS_f, which is the basis of the ΔG_m-X curves. A description of further relationships between k, m, and thermodynamic properties is given by Flemings [6].

Capillarity Effects [7,8]

The total Gibbs free energy of a small solid particle in a melt is inversely proportional to its size. As the free enthalpy of the solid increases with decreasing diameter, while the free enthalpy of the liquid remains constant (if the amount of liquid is much greater than the amount of solid), the melting point decreases for the pure solid as well as for the alloy (figure A3.2). The increase in the free enthalpy of

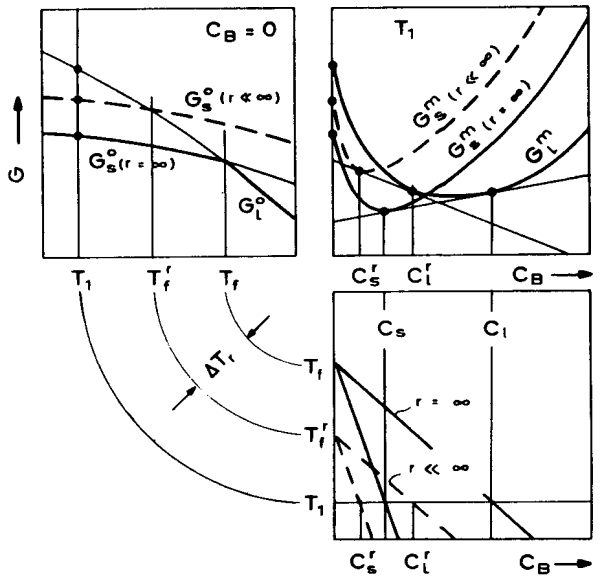

Figure A3.2

the particle due to its curved surface (of radius, r) can be regarded as being an internal pressure increase:

$$\Delta G_r = v_m \Delta P \qquad [A3.10]$$

where v_m is the molar volume (assumed to be constant), and ΔP is given by the specific interface energy and the curvature:

$$\Delta P = \sigma K \qquad [A3.11]$$

Equating equations A3.9, A3.10, and A3.11 leads to a relationship between the equilibrium temperature drop and the curvature:

$$T_f - T_f^r = \Delta T_r = \Gamma K \qquad [A3.12]$$

and

$$\Gamma = \frac{\sigma v_m}{\Delta S_f} = \frac{\sigma}{\Delta s_f} \qquad [A3.13]$$

where ΔS_f is the molar freezing entropy and Δs_f is the volume freezing entropy. In order to use these equations, the parameters σ and K have to be defined:

Specific Interface Energy, σ: It is assumed that the solid/liquid interface (in fact a volume) is a surface across which the properties change discontinuously. The specific surface energy is defined there as being the reversible work, dw, which is required in order to create new surface area, dA. In the case of a solid/liquid interface, the specific interface energy can be set equal to the interfacial tension, γ. According to figure A3.3, the work necessary to extend the surface by dz is:

$$dw = f dz = \sigma l dz = \sigma dA$$

from which one can obtain the definition:

$$\sigma \equiv \left(\frac{dw}{dA}\right)_{T,V,\mu} \qquad [A3.14]$$

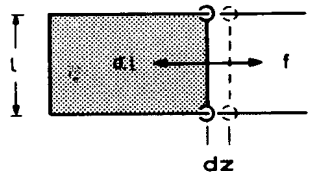

Figure A3.3

Curvature, K: In two dimensions, the curvature of a function is defined as the change in the slope, $\delta\theta$, of that function over a length of arc, δl (figure A3.4a):

$$K = \frac{\delta\theta}{\delta l}$$

and, since $\delta l = r\,\delta\theta$,

$$K = \frac{1}{r}$$

It can be shown that, in general, the curvature at a point ($\delta l \to 0$) can be obtained in Cartesian coordinates as:

$$K = \frac{z''}{[1 + z'^2]^{3/2}} \qquad [A3.15]$$

where z' and z'' are the first and second derivatives, respectively, of the function, z(y).

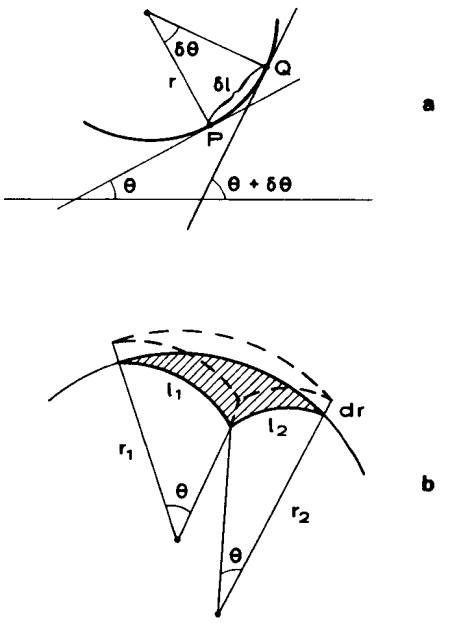

Figure A3.4

The average curvature of a general line depends only upon the gradients of the curves at its end-points, and upon the distance between them (figure A3.5). In the case of surfaces in three dimensions, the curvature can be defined as the variation in surface area divided by the corresponding variation in volume:

$$K = \frac{dA}{dv} \qquad [A3.16]$$

For a general surface with constant principal radii (minimum and maximum at 90° to each other - figure A3.4b) one can define (for small angles):

$$l_1 = r_1\theta$$

$$l_2 = r_2\theta$$

Increasing the radii by dr gives:

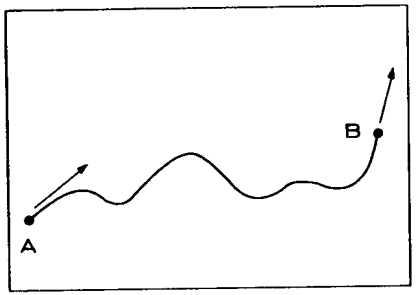

Figure A3.5

$$dA = l_1 dl_2 + l_2 dl_1 = r_1\theta\, dr\theta + r_2\theta\, dr\theta$$

$$dA = (r_1 + r_2) dr\, \theta^2 \qquad [A3.17]$$

$$dv = l_1 l_2 dr = (r_1\theta)(r_2\theta) dr$$

$$dv = r_1 r_2 dr\, \theta^2 \qquad [A3.18]$$

Therefore from equations A3.16, A3.17, and A3.18,

$$K = \left(\frac{1}{r_1} + \frac{1}{r_2}\right) \qquad [A3.19]$$

In the case of a sphere, $r_1 = r_2 = r$ so that $K = 2/r$. In the case of a cylinder, r_1 is infinite and $r_2 = r$ so that $K = 1/r$.
Thus, using equation A3.12, the decrease in melting point due to the curvature of a spherical crystal in a melt can be written:

$$\Delta T_r = \frac{2\Gamma}{r} \qquad [A3.20]$$

It is supposed in the above calculations that the value of σ is isotropic. The effect of anisotropy of the latter is treated by Aaronson [9].

Mechanical Equilibrium at the Three-Phase Junction

A junction between two solid phases at the solid/liquid interface will form a groove. At this point, the surface forces will tend to set up an equilibrium (minimum energy) morphology in which:

$$\Sigma f = 0$$

From figure A3.6, it is evident that this condition will be satisfied when:

$$\sigma_{\alpha\beta} = \sigma_{\alpha l} \cos[\theta_1] + \sigma_{\beta l} \cos[\theta_2]$$

and [A3.21]

$$\sigma_{\alpha l} \sin[\theta_1] = \sigma_{\beta l} \sin[\theta_2]$$

In establishing mechanical equilibrium, it is important to consider the equilibrium of the moments acting on the junction (second equation above) since this affects the angle of eutectic or grain boundaries with respect to the solid/liquid interface. In most cases, it is expected to be close to 90°.

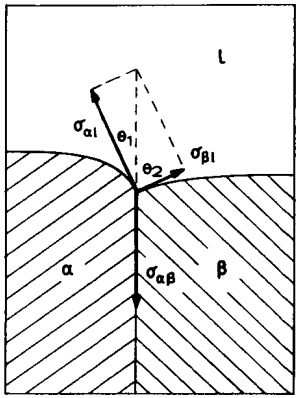

Figure A3.6

Calculation of f[θ] for Heterogeneous Nucleation [4]

Application of equations A3.21 to heterogeneous nucleation shows that real mechanical equilibrium (figure A3.7b) cannot be established and that a surface stress will be built up (figure A3.7a). Due to the presence of foreign crystalline surfaces (crucible, surface oxide, inclusions) in a melt, nucleation may become much easier. The effect of these interfaces can be deduced from the energy balance:

$\Delta G_i =$ interface energy creation due to nucleation - interface energy gained due to the substrate

$$\Delta G_i = (A_{lc}\sigma_{lc} + A_{cs}\sigma_{cs}) - A_{cs}\sigma_{ls}$$

$$\Delta G_i = A_{lc}\sigma_{lc} + \pi R^2(\sigma_{cs} - \sigma_{ls}) \qquad [A3.22]$$

$$\sigma_{ls} = \sigma_{cs} + \sigma_{lc}\cos[\theta]$$

$$\Delta G_i = A_{lc}\sigma_{lc} - \pi R^2\cos[\theta]\sigma_{lc} \qquad [A3.23]$$

$$\Delta G = \Delta G_v + \Delta G_i = v_c\Delta g + (A_{lc} - \pi R^2\cos[\theta])\sigma_{lc} \qquad [A3.24]$$

$$v_c = \frac{\pi r^3(2 - 3\cos[\theta] + \cos^3[\theta])}{3}$$

$$A_{lc} = 2\pi r^2(1 - \cos[\theta])$$

$$R = r\sin[\theta]$$

$$\sin^2[\theta] = 1 - \cos^2[\theta]$$

$$\Delta G = \left(\frac{4\pi r^3\Delta g}{3} + 4\pi r^2\sigma_{lc}\right)\left(\frac{2 - 3\cos[\theta] + \cos^3[\theta]}{4}\right)$$

$$\Delta G_{het} = \Delta G_{hom}\cdot f[\theta] \qquad [A3.25]$$

where:

$$f(\theta) = \frac{2 - 3\cos(\theta) + \cos^3(\theta)}{4} = \frac{[2 + \cos(\theta)][1 - \cos(\theta)]^2}{4}$$

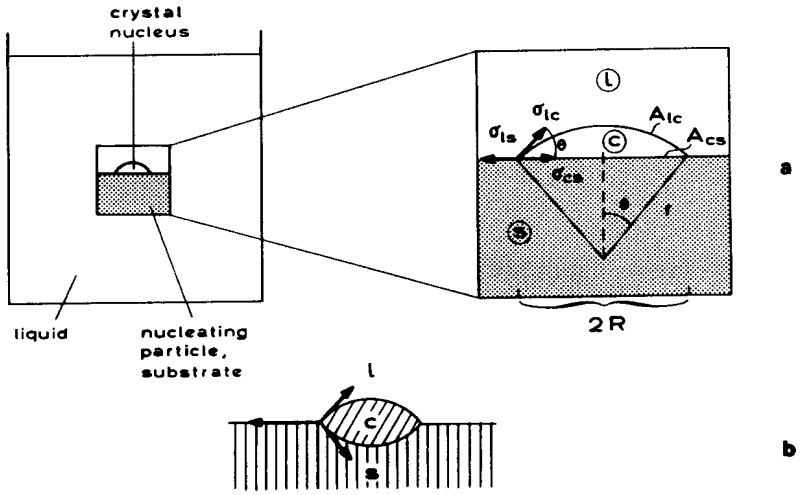

Figure A3.7

REFERENCES

[1] K.Jackson, G.H.Gilmer, H.J.Leamy in: Laser and Electron Beam Processing of Materials (C.W.White, P.S.Peercy, Eds.), Academic Press, New York, 1980, p104
M.J.Aziz: Journal of Applied Physics, 53 (1982) 1158
R.F.Wood: Physical Review, B25 (1982) 2786

[2] D.R.Gaskell: Introduction to Metallurgical Thermodynamics, McGraw-Hill, New York, 1981

[3] M.Hillert in: Lectures on the Theory of Phase Transformations, (H.I.Aaronson Ed.) Transactions of the Metallurgical Society of AIME, New York, 1975, p1

[4] J.S.Kirkaldy in: Energetics in Metallurgical Phenomena, Volume IV (W.M.Mueller, Ed.), Gordon & Breach, New York, 1968, p197

[5] C.V.Thompson, F.Spaepen: Acta Metallurgica, 27 (1979) 1855

[6] M.C.Flemings: Solidification Processing, McGraw-Hill, New York, 1974

[7] W.W.Mullins in: Metal Surfaces - Structure, Energetics, Kinetics, American Society for Metals, Metals Park, 1963, p17

[8] R.Trivedi in: Lectures on the Theory of Phase Transformations, (H.I.Aaronson Ed.) Transactions of the Metallurgical Society of AIME, New York, 1975, p51

[9] H.I.Aaronson in: Lectures on the Theory of Phase Transformations, (H.I.Aaronson Ed.) Transactions of the Metallurgical Society of AIME, New York, 1975, p158

APPENDIX 4

NUCLEATION KINETICS IN A PURE SUBSTANCE

In order to determine the nucleation rate, it is necessary to determine the number of critical nuclei and the rate of arrival of atoms necessary to make up these nuclei [1 - 3].

Equilibrium Distribution of Nuclei in an Undercooled Melt

The system shown in figure A4.1 represents a mixture of N_ℓ atoms in the liquid state and N_n small crystal clusters each of which contains n atoms. The free enthalpy change of such a system compared to another one, at the same temperature, which contains only atoms and no crystal nuclei, is:

$$\Delta G = N_n \Delta G_n - T\Delta S_n \qquad [A4.1]$$

Here ΔG_n is the free enthalpy change due to the formation of one nucleus containing n atoms and ΔS_n is the entropy of mixing of N_n clusters with N_ℓ atoms. (When the existence of an ideal mixture of crystal clusters and atoms of liquid is assumed, the mixing enthalpy, ΔH_n, is equal to zero.)
In the case of sub-critical clusters (known as embryoes), ΔG_n is positive due to the work of interface creation. This is demonstrated in figure A4.2 and corresponds to figure 2.2 where n and r, characterising the difference in size, are related by equation 2.2. The value of ΔG_n can be determined in an analogous manner using equation 2.3 and leads to the relationship:

$$\Delta G_n = n\Delta G' + A_n\sigma \qquad [A4.2]$$

$$A_n = \eta n^{2/3}$$

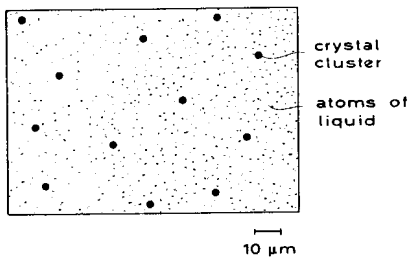

Figure A4.1

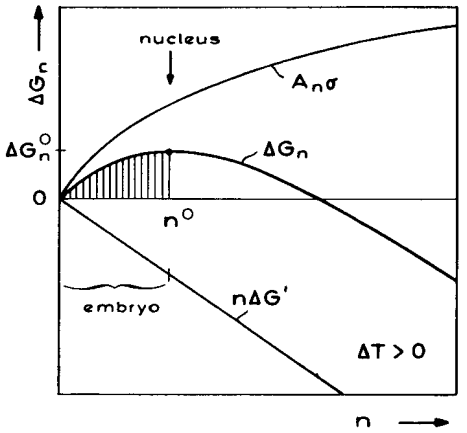

Figure A4.2

where $\Delta G'$ is the atomic free energy difference, A_n is the interface area of the cluster, η is a form factor which depends upon the shape of the cluster, and $n^{1/3}$ is proportional to the cluster diameter.
The mixing entropy of equation A4.1 can be derived using the well-known relationship:

$$\Delta S_n = k_B \ln\left[\frac{(N_\ell + N_n)!}{N_n!N_\ell!}\right] \qquad [A4.3]$$

and therefore

$$\Delta G = N_n \Delta G_n - k_B T \ln[(N_\ell + N_n)!] + k_B T \ln(N_n!) + k_B T \ln(N_\ell!) \qquad [A4.4]$$

where ΔG_n is always positive for critical nuclei. An increase in N_n will first decrease the total free energy of the system, due to the mixing of clusters and atoms (figure A4.3) and then reach a minimum value which represents the equilibrium concentration of clusters for a given undercooling. Applying Stirling's approximation for large values of N, i.e. $\ln(N!) = N\ln(N) - N$, differentiating equation A4.4 with respect to N_n, and setting the result equal to zero gives:

$$\Delta G_n - k_B T[\ln(N_\ell + N_n) - \ln(N_n)] = 0$$

from which:

$$\frac{N_n}{N_\ell + N_n} = \exp\left[-\frac{\Delta G_n}{k_B T}\right] \qquad [A4.5]$$

Since $N_\ell \gg N_n$

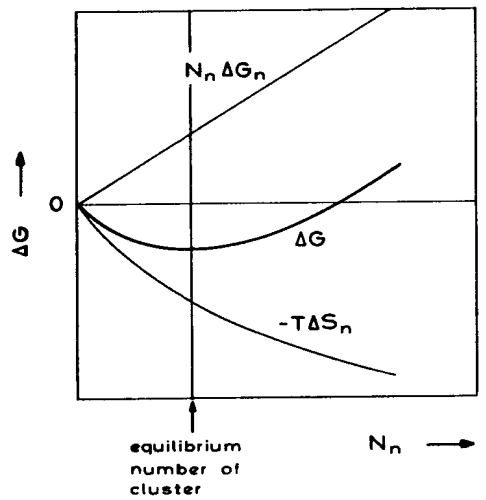

Figure A4.3

$$\frac{N_n}{N_\ell} = \exp[-\frac{\Delta G_n}{k_B T}]$$

The number of nuclei (critical clusters) in equilibrium is therefore:

$$N_n^o = N_\ell \exp[-\frac{\Delta G_n^o}{k_B T}] \qquad [A4.6]$$

where ΔG_n^o is the energy barrier for nucleation as defined in figure A4.2. These relationships are given in figure 2.3 of the main text.

Rate of Formation of Stable Nuclei

The nucleation rate must be proportional to the number of crystals of critical size, N_n^o. However, in order that these crystals should grow the addition of further atoms is required. The system, containing clusters of size, n°, is in an unstable state and can produce smaller or larger clusters (figure A4.2) in order to decrease its energy. Therefore, it is necessary to determine the rate of incorporation, dn/dt, of new atoms into the nuclei. The nucleation rate is then:

$$I = N_n^o \frac{dn}{dt} \qquad [A4.7]$$

where the adsorption rate, dn/dt, is the product of an adsorption frequency, ν, and the density of sites at which the atoms can be adsorbed by the critical nucleus, n_s^o:

$$\frac{dn}{dt} = \nu n_s^o \qquad [A4.8]$$

The adsorption frequency is:

$$\nu = \nu_o \exp[-\frac{\Delta G_d}{k_B T}]p$$

where ν_o is the atomic vibration frequency, $\exp[-\Delta G_d/k_B T]$ is the fraction of atoms in the liquid which are sufficiently activated to surmount the interface addition activation energy, ΔG_d, and p is the adsorption probability.
The site density, n_s^o :

$$n_s^o = A_n^o n_c \qquad [A4.9]$$

where A_n^o is the surface area of the critical nucleus and n_c is the capture site density per unit area.
The nucleation rate is therefore:

$$I = I_o \exp[-\frac{\Delta G_n^o + \Delta G_d}{k_B T}] \qquad [A4.10]$$

and

$$I_o = N_\ell \cdot \nu_o p A_n^o n_c$$

Since the exponential term is extremely sensitive to small variations in the argument (figure 2.5), the exact value of I_o is relatively unimportant and for metals is often approximated by:

$$I_o = N_\ell (\frac{k_B T}{h}) = N_\ell \cdot \nu_o \simeq 10^{42} m^{-3} s^{-1} \qquad [A4.11]$$

All of these relations assume the existence of a steady state and are not of general applicability. Nevertheless, they give a good guide to the principles which are involved. For a more complete treatment of nucleation theory, the reader should consult reference 3.

REFERENCES

[1] D.Turnbull, J.C.Fisher: Journal of Chemical Physics, 17 (1949) 71

[2] D.R.Uhlmann, B.Chalmers: Industrial and Engineering Chemistry, 57 (1965) 19

[3] J.W.Christian, 'The Theory of Transformations in Metals and Alloys' (2nd edition), Pergamon Press, Oxford, (1975).

APPENDIX 5

ATOMIC STRUCTURE OF THE SOLID/LIQUID INTERFACE

In order to explain the principles involved, the simple case of a two-dimensional crystal consisting of 'square atoms' of only one type which interact only with their nearest neighbours and form single layer interfaces will be treated here. It is assumed that there are three different structural elements making up the surface structure (three-site model - figure A5.1). This situation has been treated in detail by Jackson [1]. The model is an improved version of a previous one which was developed by the same author [2]

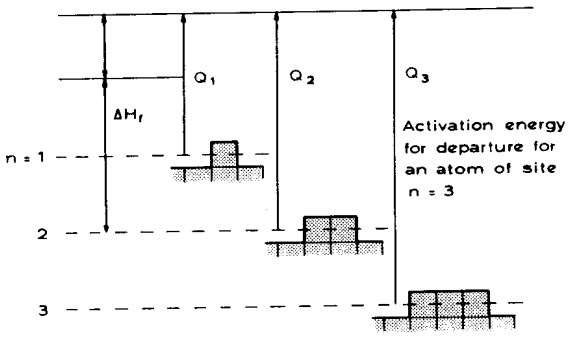

Figure A5.1

There is a continuous interchange of sites due to the thermally activated adsorption or desorption of atoms. For example, a site n = 1 will be transformed into an n = 2 site by adsorption of one neighbouring atom. It is assumed that, after a short time, the interface structure reaches a steady state, i.e., the overall density of the three types of site does not change with time. The rate of adsorption of atoms is independent of the rate of departure. Both are activated processes which are similar to diffusion in the liquid, but the desorption of atoms is more difficult from an undercooled crystal, due to the gain in energy which occurs when an atom is added at the solid/liquid interface. The probability of adsorption will depend upon the roughness of the

interface; the greater the density of steps (and therefore the greater the number of exposed atomic bonds presented to the liquid), the higher is the probability that an atom will be incorporated into the crystal, as a result of the stronger bonding involved.
The rate of atom arrival, J^+, is governed by:

$$J^+ = J_o^+ \exp[-\frac{Q}{RT}] \qquad [A5.1]$$

where Q is the activation energy for diffusion in the liquid. The flux of atoms leaving is determined by:

$$J^- = J_o^- \exp[-\frac{Q}{RT}]\exp[-\frac{2n\Delta H_f}{zRT}] \qquad [A5.2]$$

where ΔH_f is the latent heat of fusion, n is the number of bonds which have to be broken by an atom in leaving the crystal, and z is the coordination number (4 in the case of a two-dimensional crystal). An atom which makes two bonds with the crystal (i.e. half of the maximum possible number of bonds) can be viewed as being half in the solid and half in the liquid. At the melting point, T_f, the rates of arrival and departure from such sites (n = 2) should be equal. Thus,

$$J_o^+ \exp[-\frac{Q}{RT_f}] = J_o^- \exp[-\frac{Q}{RT_f}]\exp[-\frac{\Delta H_f}{RT_f}] \qquad [A5.3]$$

therefore:

$$\frac{J_o^-}{J_o^+} = \exp[\frac{\Delta H_f}{RT_f}] \qquad [A5.4]$$

Combining equations A5.2 and A5.4 and rearranging the exponential terms:

$$J^- = J_o^+ \exp[-\frac{Q}{RT}]\exp[\frac{\Delta H_f}{RT_f} - \frac{n\Delta H_f}{2RT}] \qquad [A5.5]$$

The second exponential term can be regarded as being a measure of the probability that an atom which has n neighbours will leave the site, that is:

$$p_n = \exp[\frac{\Delta H_f}{RT_f} - \frac{n\Delta H_f}{2RT}]$$

The net flux is determined by the difference between equations A5.1 and A5.5:

$$J = J_o^+ \exp[-\frac{Q}{RT}][1 - p_n] \qquad [A5.6]$$

It is now possible to set up balance equations for the arrival and departure of atoms at various types of site. The detailed calculations have been given by Jackson [1].

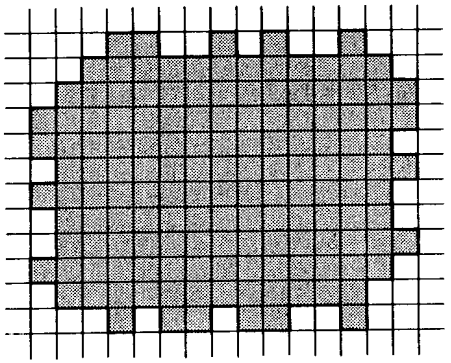

Figure A5.2

Carrying these through and realising that, if $(\Delta H_f/RT_f)(\Delta T/T) \ll 1$,

$$\exp[-\frac{\Delta H_f \Delta T}{RT_f T}] \simeq 1 - \frac{\Delta H_f \Delta T}{RT_f T}$$

the net growth rate, V, of the crystal becomes:

$$V = Jv' = v'J_o^+ \exp[-\frac{Q}{RT}]\alpha(\frac{\Delta T}{T})f[hk] \qquad [A5.7]$$

where $\alpha = \Delta H_f/RT_f = \Delta S_f/R$; the dimensionless melting entropy and v' is the atomic volume.
Therefore, to a first approximation the growth rate is a linear function of the undercooling. It also depends upon the magnitude of the crystallographic factor, f[hk], which is a function of interface structure. It thus depends upon the value of α and upon the Miller indices, (hk), of the crystallographic plane. When α takes on high values (e.g. 10), the fraction of extra atoms or holes in the interface is proportional to $\exp[-\alpha]$.
For (11)-faces of the present square crystal (figure A5.2), f is independent of α but this is not so for the (10)-face (table A5.1). The reason for this is that a 45° edge

Table A5.1: CRYSTALLOGRAPHIC FACTOR, f[hk], OF TWO FACES OF A SQUARE CRYSTAL

α	f[10]	f[11]
1	0.56	0.60
5	0.30	0.60
10	0.039	0.60

exhibits many growth steps which cannot be removed by atom addition. When the value of α is large, the (11)-edges will grow much more quickly and leave the crystal bounded by slow-growing (10)-edges (figure A5.3 - see also figure 2.9). Note also in table A5.1 that for small values of α, the growth is almost isotropic (f[10]~f[11]). This behaviour is typical of metals.

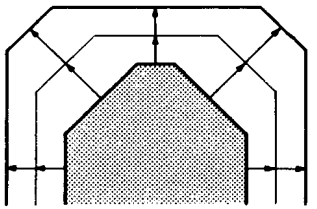

Figure A5.3

REFERENCES

[1] K.A.Jackson: Journal of Crystal Growth, 3/4 (1968) 507

[2] K.A.Jackson in: Liquid Metals and Solidification, American Society for Metals, Cleveland, 1958, p174

APPENDIX 6

THE MULLINS-SEKERKA INTERFACE STABILITY ANALYSIS

The constitutional undercooling criterion provides a useful means of estimating whether a solid/liquid interface will be planar under directional solidification conditions. However, from a theoretical point of view it has several faults. Firstly, it does not take account of the effect of surface tension. It is expected that this will tend to inhibit the formation of perturbations. Secondly, the constitutional undercooling theory does not give any indication of the scale of the perturbations which will develop if an interface becomes unstable. In order to gather more information about the morphological instability of a plane interface than that provided by the constitutional undercooling theory, one must suppose that the interface has already been slightly disturbed and then ask whether the disturbance will grow or disappear (chapter 3). To this end, it is sufficient to consider a sinusoidal interface form having a very small, time-dependent amplitude (figure A6.1). (Provided that the amplitude is small, a sinusoidal form represents the most general disturbance possible; it can be supposed to be one term of the Fourier series describing any disturbance.)
The present appendix is a simplified version of the classic paper by Mullins and Sekerka [1] which first treated the problem in this way.
The object of the calculation is to determine the conditions required for the growth or decay of a perturbation at the solid/liquid interface (figure 3.1) under the type of thermal conditions imposed by directional solidification. The first step is to solve the diffusion equation for the perturbed interface. In fact, a suitable solution (equation A2.43) was derived earlier:

$$C = C_o + (\frac{C_o}{k} - C_o)\exp[-\frac{Vz}{D}] + A S \exp[-bz] \qquad [A6.1]$$

where $A = kVG_c/(Vp - Db)$, $S = \epsilon \sin[\omega y]$, $b = (V/2D) + [(V/2D)^2 + \omega^2]^{0.5}$, and $p = 1 - k$.

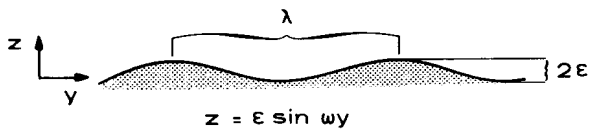

Figure A6.1

In general, neglecting atomic kinetics and convection (for a more complete treatment see reference [2]), it would be necessary to solve four coupled differential equations simultaneously, i.e. for heat and solute diffusion in each phase (solid and liquid). On the other hand, as explained in appendix 2, the effect of solid-state diffusion can be neglected. In order to simplify the calculations even further, the thermal field will be assumed to be linear, to have the gradient, G (figure A6.2), and to be unaffected by the shape of the interface. Assuming steady-state conditions to be applicable, the only equation which remains to be solved is therefore the one which describes the solute field in the liquid phase ahead of the solid/liquid interface.
Equation A6.1 has been shown (appendix 2) to satisfy the far-field condition, and the flux condition. It remains to make the equation satisfy the coupling condition at the interface.

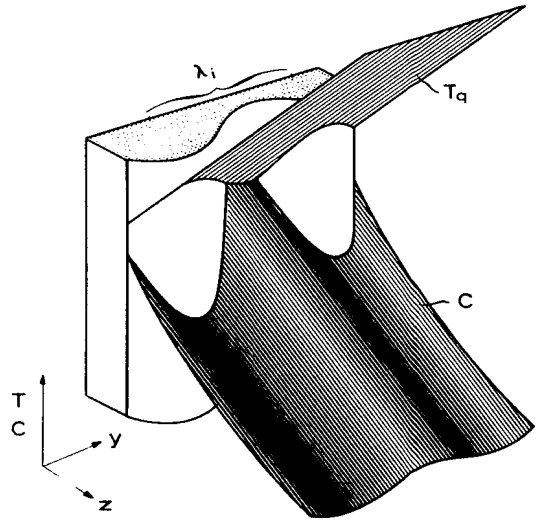

Figure A6.2

Coupling Condition

Because the interface is assumed to be situated in a linear temperature field resulting from the imposed heat flux occurring from the liquid to the solid, the temperature varies over the non-planar interface. In order to maintain local equilibrium conditions, the constitutional undercooling and curvature variations at the interface must be such that their sum results in a local melting point which is the same as the temperature imposed by the growth conditions (equation 3.17). The temperature and concentration fields are thus coupled via the following relationship:

$$T^* = T_q^* \qquad [A6.2]$$

The thermodynamic equilibrium temperature of the interface is affected by the local concentration and the local curvature, according to:

$$T^* = T_f + mC_l^* - \omega^2 S\Gamma \qquad [A6.3]$$

The final term arises from the mathematical definition of curvature (equation A3.15) which is approximately equal to z'' for small values of z' (figure A6.1). Considering now the interface temperature distribution arising from the temperature gradient imposed by the heat flow:

$$T_q^* = T_o + Gz \qquad [A6.4]$$

where T_o ($= T_f + mC_o/k$) is the liquidus temperature of the plane interface under steady-state conditions, and $z = S$. The interface temperature, as a function of y therefore becomes:

$$T_q^* = T_f + \frac{mC_o}{k} + GS \qquad [A6.5]$$

In order to satisfy the coupling condition, equations A6.3 and A6.5 must be set equal to each other, giving:

$$mC_l^* - \omega^2 S\Gamma = \frac{mC_o}{k} + GS$$

Substituting for C_l^* ($= C^*$) from equation A2.41 gives:

$$m\left(\frac{C_o}{k} + G_c S + AS\right) - \omega^2 S\Gamma = \frac{mC_o}{k} + GS$$

that is:

$$mG_c - G + mA - \omega^2\Gamma = 0$$

Substituting for A gives:

$$mG_c - G + \frac{mkVG_c}{Vp - Db} - \omega^2\Gamma = 0$$

Rearrangement of this expression leads very simply to:

$$-\omega^2\Gamma\left(b - \frac{Vp}{D}\right) - G\left(b - \frac{Vp}{D}\right) + mG_c\left(b - \frac{V}{D}\right) = 0 \qquad [A6.6]$$

This expression determines the form (values of ω) which the perturbed interface must assume in order to satisfy all of the conditions of the problem, and is the same (allowing for the different symbols used and the simpler temperature distribution assumed here) as the expression in curly brackets which appears in equation 20 of the paper by Mullins and Sekerka [1]. However, in the present simplified treatment, the time dependence of the amplitude has been lost; the time derivative of ϵ being zero in equation A6.6. Compare this with equation 3.23, where $p = 1$. From equation 3.23, it

is known that the parameter, $F = (\dot{\epsilon}/\epsilon)(mG_c/V)$, should appear on the RHS of equation A6.6. Replacing this term permits the solid/liquid interface stability analysis to be pursued further. If the reader finds this step to be too arbitrary, he should recall that replacing the zero by such a parameter is a standard method of exploring the behaviour of the roots of an algebraic equation. Equation A6.6 will therefore be written as:

$$-\omega^2\Gamma\left(b - \frac{Vp}{D}\right) - G\left(b - \frac{Vp}{D}\right) + mG_c\left(b - \frac{V}{D}\right) = F \qquad [A6.7]$$

If the parameter, F, is positive for any value of ω, the distortion of the interface will increase whereas, if it is negative for all values of ω, the perturbation will disappear and the interface will be stable.

Stability Criterion

The form of F, as a function of ω (the purpose of the other abscissae will be explained later), is shown in figure A6.3 for the stable and unstable situations (compare with figure 3.7). There is a difference between figures 3.7 and A6.3 in that the latter demonstrates the behaviour of the exact solution (equation 20 of Mullins and Sekerka, 1964) where the unstable range is not limited by λ_i and ∞, but rather by λ_i and λ_c. That is, there is also an upper limit, λ_c, to the λ-values of the instabilities. Note that ω in figure A6.3 is related to λ in figure 3.7 by $\omega = 2\pi/\lambda$.

From the signs of the terms in equation A6.7, one can immediately deduce the effects of the parameters involved. For example, $\omega^2\Gamma$ (curvature effect) and G (imposed temperature gradient) tend to decrease the value of F and thus increase the stability, whereas mG_c (liquidus temperature gradient) is always positive (since m and G_c always have the same sign) and therefore decreases stability.

As it stands, equation A6.7 is of little use to the practising metallurgist since numerical analysis techniques would have to be used in order to calculate the stability limits. It is desirable to derive a readily computed stability criterion, analogous to the simple constitutional undercooling criterion (chapter 3). At first sight, this appears to be easy since equation A6.7 is 'only' of the third degree. However, the fact that b is a function of ω complicates the situation. To convince himself of this, the reader is invited to try to write equation A6.7 in terms of ω and at the same time eliminate b, before reading on.

The elimination of b leads to a formidable equation of high order which, even if could be solved algebraically, would be unlikely to yield a simple criterion. The derivation of equation A6.7 is thus only the first step in analysing interface stabilty, and the more difficult step is to deduce a clear stability criterion. That is the main object of this appendix.

Sekerka [3] devoted a paper to the problem and obtained tabular and graphical criteria for the determination of stability in a given system. His results will be discussed later. The alternative technique presented here is felt to be rather more transparent than Sekerka's method.

From figure A6.3, it is evident that, in order to derive a stability criterion, one only needs to know whether equation A6.7 has roots for positive values of ω. If it has no roots, then the interface is stable because the curve never rises above the positive ω-axis and F is therefore negative for all wavelengths.

Now, any good elementary textbook on the theory of equations will describe a number of theorems, such as De Gua's, Descartes', Budan's, and Sturm's, concerning the number of positive roots possessed by an algebraic equation. The latter theorems are listed in the order of increasing precision and increasing complexity. The simplest

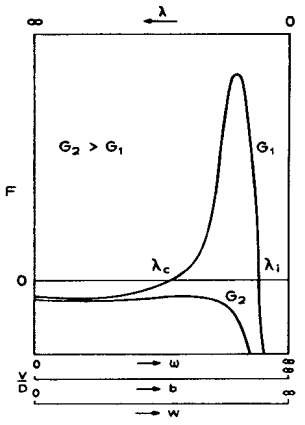

Figure A6.3

one which is applicable to the present case is Descartes' theorem. This states that, "in any algebraic equation, the number of positive roots cannot exceed the number of changes of sign of the coefficients".
In order to test for the situation where there are no positive roots, it is more convenient to express equation A6.7 entirely in terms of b than it is to try to obtain a solution in terms of ω (for the reason mentioned before). Unfortunately, the definition of b means that a ω-value of zero corresponds to a b-value of V/D (figure A6.3). Thus equation A6.8:

$$-\Gamma b^3 + \frac{V\Gamma}{D}(1+p)b^2 + (\frac{p\Gamma V^2}{D^2} + mG_c - G)b + (\frac{mG_cV}{D} - \frac{GVp}{D}) = F \qquad [A6.8]$$

which is obtained by replacing the ω^2 term in equation A6.7 by the definition of b, should be tested for roots between V/D and infinity. This is not possible using Descartes' theorem and a transformation must be introduced so that the independent variable again ranges from zero to infinity. This can be done by replacing b by W + V/D to give:

$$-\Gamma W^3 - \frac{V\Gamma}{D}(1+k)W^2 + (mG_c - G - \frac{k\Gamma V^2}{D^2})W - (\frac{kGV}{D}) = F \qquad [A6.9]$$

where W = b - V/D is a arbitrary variable which is introduced in order to change the origin of the horizontal axis. By now, the reader is probably uneasy about the various modifications which the original equation has suffered and is wondering how the values of the roots of the original equation will be determined. The answer is that they do not have to be. Recall that only the existence of roots is of interest and that their location (provided that they are between zero and infinity) is irrelevant. This is made clear by the parallel scales used in figure A6.3 since the values of the roots differ depending upon the scale used but their existence or non-existence does not.
To continue with the derivation of a stability criterion, the manner in which the signs of the coefficients change as the parameters are varied will be studied. From tables A6.1 and A6.2, it can be seen that stability occurs when:

$$\frac{\Gamma k V^2}{D^2} + G - mG_c \geqslant 0$$

Hence, the criterion for stability becomes:

$$G \geqslant mG_c - \frac{\Gamma k V^2}{D^2}$$

Table A6.1: SIGNS OF THE COEFFICIENTS OF THE STABILITY EQUATION (A6.9)

Term	W^3	W^2	W^1	W^0
Sign	-	-	+ or - (*)	-

* negative if $mG_c - G - kV^2\Gamma/D^2 < 0$

Table A6.2: USE OF DESCARTES' THEOREM TO DETERMINE INTERFACE STABILITY

W^3	W^2	W^1	W^0	Changes in sign	Maximum Number of Roots	Stable
-	-	-	-	0	0	yes
-	-	+	-	2	2	no

Recalling that $G_c = -(V/D)\Delta C_o$ (chapter 3) for plane-front growth, the stability criterion becomes:

$$G \geqslant \frac{V\Delta T_o}{D} - \frac{\Gamma k V^2}{D^2} \qquad [A6.10]$$

where $\Delta T_o = -m\Delta C_o$. The simple constitutional undercooling criterion for stability (chapter 3) can be written:

$$G > mG_c \qquad [A6.11]$$

Thus, an interesting result of the more exact analysis described here (equation 6.10) is to reveal conditions under which stability is obtained even when equation A6.11 predicts instability. This is so because the additional curvature term on the right-hand side of equation A6.10 decreases the value of the liquidus temperature gradient which must be exceeded by the imposed temperature gradient, G, in order to ensure stability.
A more striking fact is that high growth rates will lead to stability, regardless of the value of G, because the $\Gamma kV^2/D^2$ term, which is subtracted from the right hand side of equation A6.10, increases more rapidly than G_c (which depends only linearly upon V/D). This stability at high growth rates was termed, 'absolute stability', by Mullins and Sekerka.
Thus, the use of Descartes' theorem has led, in a rather simple way, to the derivation of a useful stability criterion which reflects the conclusions of previous analyses. However, it must be pointed out that the use of the theorem should only lead to a conservative criterion. This is because the theorem can state definitely whether there are no roots (no change in sign) but does not give an unambiguous answer when there is a change in sign. Instead, it merely gives an upper limit to the number of roots. Pedantically speaking then, the equation could still have no roots and the

system could still be stable. On the other hand, the values of F in table A6.3, when calculated for various values of G, do show that in this specific but typical case the criterion is obeyed. Thus, the positive values of F (underlined) gradually decrease in number as G is increased and finally disappear upon exceeding the critical value for the given system and growth rate.
At the beginning of the present calculations, the temperature field was assumed not to be affected by the presence of the perturbed interface, i.e. the effect of the latent heat of solidification and of the differing thermal conductivities in the solid and liquid were neglected. Mullins and Sekerka allowed for such effects and found that their inclusion simply changed the imposed temperature gradient, G, to an effective value given by:

$$G' \simeq \left(\frac{2\kappa_l}{\kappa_s + \kappa_l}\right)G - \left(\frac{\Delta h_f}{\kappa_s + \kappa_l}\right)V$$

where G is the temperature gradient in the liquid at the interface.
The second term leads to an increase in stability while the first term generally decreases the stability.
For stability, Sekerka [3] predicts:

$$\left(\frac{2\kappa_l}{\kappa_s + \kappa_l}\right)\left(\frac{D}{\Delta T_o}\right)\left(-\frac{\Delta h_f}{2\kappa_l} + \frac{G}{V}\right) > S(A^*,k) \qquad [A6.12]$$

where $S(A^*,k)$ is a function of k and of a dimensionless parameter, A*, which takes into account the interface energy:

$$A^* = \frac{k\Gamma V}{\Delta T_o D} \qquad [A6.13]$$

Figure A6.4 illustrates the relationship between $S(A^*,k)$ and $(k\Gamma V)/\Delta T_o D$. There exist two regimes where the solid/liquid interface will be stable.

Table A6.3: VALUES OF THE STABILITY PARAMETER, F, FOR A TYPICAL SYSTEM (Al-2%Cu)*

ω(/m)	100	1000	10000	100000	1000000
G(K/mm)					
8.0	-10.6	229	2620	17625	-8.7×10^6
9.0	-25.3	125	1616	7620	-8.8×10^6
10.0	-40	20	611	-2384	-8.9×10^6
10.1	-41.5	9.5	510	-3384	-8.9×10^6
10.2	-42.9	-0.94	410	-4385	-8.9×10^6
10.3	-44.4	-11.4	310	-5385	-8.9×10^6
10.4	-45.9	-21.8	209	-6386	-8.9×10^6
10.5	-47.3	-32.3	109	-7386	-8.9×10^6
10.6	-48.8	-42.8	8.2	-8387	-8.9×10^6
10.7	-50.2	-53.3	-92.3	-9387	-9.0×10^6

* data from appendix 12 and an assumed growth rate of 10^{-6}m/s. The critical value of $mG_c - kV^2\Gamma/D^2$ for these conditions is 10.67

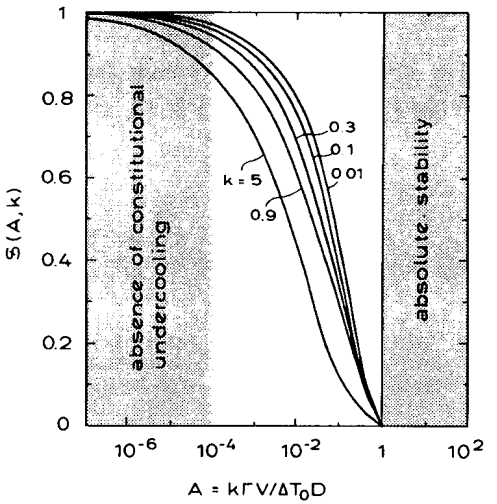

Figure A6.4

Lower Limit of Stability

At small growth rates, such as those encountered under conditions of zero constitutional undercooling, A* will become much smaller than unity.
It is possible to estimate the value of A* by substituting the growth rate of constitutional undercooling, $V_{cs} = GD/\Delta T_o$ (equation 3.15), into equation A6.13:

$$A^* \simeq \frac{k\Gamma G}{\Delta T_o^2}$$

Using typical values for alloys undergoing directional solidification: $k<1$, $\Gamma = 10^{-4}$Kmm, G = 10K/mm, and $\Delta T_o = 10$K, the stability parameter becomes $A^* < 10^{-5}$ indicating (figure A6.4) that $S \simeq 1$ when V is small as in this situation. Since G/V is quite large compared to $|\Delta h_f/2\kappa_l|$, equation A6.12 simplifies to:

$$\left(\frac{2\kappa_l}{\kappa_s + \kappa_l}\right)\left(\frac{DG}{\Delta T_o V}\right) > 1 \qquad [A6.14]$$

for the case of stability. This criterion is very similar to the criterion of constitutional undercooling and becomes the same for equal thermal conductivities. As most metals have lower conductivities in the liquid state than in the solid state, at the melting point, the stability criterion will be shifted to values which are slightly greater than unity. For instance, for the common case where $\kappa_l = \kappa_s/2$:

$$\frac{DG}{\Delta T_o V} > 1.5 \qquad [A6.15]$$

Compare this equation with equation 3.15. Following Sekerka [3], equation A6.12 can also be written as:

$$\frac{G^*}{mG_c} > S \qquad [A6.16]$$

where $G^* = (\kappa_s G_s + \kappa_l G_l)/(\kappa_s + \kappa_l)$. As for the limit of constitutional undercooling, $S \simeq 1$ and $mG_c = \Delta T_o V/D$, one finds for morphological stability:

$$\frac{DG^*}{\Delta T_o V} > 1 \qquad [A6.17]$$

Upper Limit of Stability

This limit, which is called 'absolute stability' arises when A* is greater than unity and the parameter, S(A*,k), becomes equal to zero. In this case, according to equation A6.12, any positive value of the LHS will lead to stable interfaces. Thus, it is possible to estimate the growth rates in this regime by setting A* greater than unity to give:

$$V_{abs} \geqslant \frac{\Delta T_o D}{k\Gamma} \qquad [A6.18]$$

Using typical values for metals: $\Delta T_o = 10K$, $D = 5 \times 10^{-3} mm^2/s$, $k = 0.5$, and $\Gamma = 10^{-4} Kmm$, the limit of absolute stability should be attained when V is greater than 1m/s. Such rates are very high but can be obtained by rapid solidification processes such as laser surface melting. At these rates, account must be taken of the value of the distribution coefficient, which is a function of the growth rate and may approach unity [4].

REFERENCES

[1] W.W.Mullins, R.F.Sekerka: Journal of Applied Physics, 35 (1964) 444

[2] R.T.Delves in: Crystal Growth (Ed. B.R.Pamplin), Pergamon, Oxford, 1975, p40

[3] R.F.Sekerka: Journal of Applied Physics, 36 (1965) 264

[4] K.Jackson, G.H.Gilmer, H.J.Leamy in: Laser and Electron Beam Processing of Materials (Eds. C.W.White, P.S.Peercy), Academic Press, New York, 1980, p104

APPENDIX 7

DIFFUSION AT A DENDRITE TIP

There are three different types of dendrite:

i equiaxed dendrites of pure substances - freely growing and limited by thermal diffusion (figure 4.7b)
ii equiaxed dendrites of alloys - freely growing and limited by solute and thermal diffusion (figure 4.7d)
iii columnar alloy dendrites - constrained in their growth by a positive temperature gradient and controlled by solute diffusion (figure 4.7c)

The first two types of growth form are similar and both lead to the creation of an equiaxed polycrystal in which each grain is made up of six orthogonal primary trunks (in the case of a cubic crystal), arranged in a random manner. The space remaining between the trunks is filled with secondary and possibly higher-order branches (figure 4.16). These crystals grow in an undercooled melt, and this makes them inherently unstable. Therefore, no steady-state cellular morphologies can be observed and the spacing, λ_1, between the trunks corresponds approximately to the grain diameter. The growth of equiaxed dendrites of pure metals occurs under conditions where only heat flows from the interface to the surrounding liquid. That is, the temperature gradient is negative at the interface (left-hand side of figure A7.1) and a thermal undercooling, ΔT_t, exists. In the case of equiaxed alloy growth, there exists not only a negative temperature gradient but also a solute build-up (if k is less than unity) ahead of the dendrite tip. This changes the local liquidus temperature (right-hand side of figure A7.1). When an equiaxed grain of an alloy of composition, C_o, is growing it experiences an undercooling, ΔT, which is the sum of a solute undercooling, ΔT_c, a thermal undercooling, ΔT_t, and a curvature undercooling, ΔT_r. The temperature and solute fields of columnar dendrites growing in alloys have been described in figure 4.8.
In general, it can be said that, due to the large tip radius of the dendrites predicted by the stability criterion (appendix 8), the curvature undercooling is small compared to the other contributions and can be neglected. At the tip one can therefore write, $C_l^*(r) \simeq C_l^*$. One can now evaluate the solutal and thermal undercoolings, ΔT_c and ΔT_t. From the definition of the solutal supersaturation (figure A7.2):

$$\Omega = \frac{C_l^* - C_o}{C_l^* p} \qquad [A7.1]$$

$$C_l^* = \frac{C_o}{1 - \Omega p}$$

$$\Delta T_c = m(C_o - C_l^*) = mC_o\left[1 - \frac{1}{1 - \Omega p}\right] \qquad [A7.2]$$

where $p = 1 - k$. At low supersaturations, where Ω is much smaller than unity

$$\Delta T_c \simeq -mC_o \Omega p$$

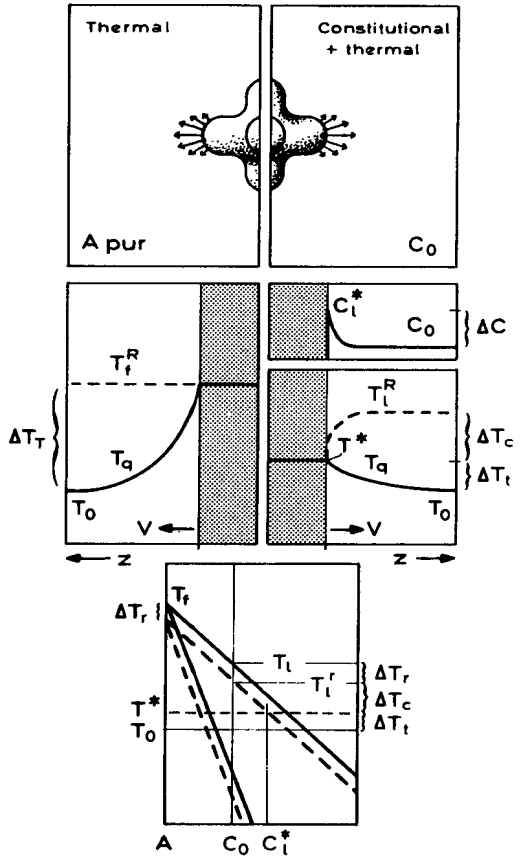

Figure A7.1:

Substituting, $-mC_0p = \Delta T_0k$, one obtains

$$\Delta T_c \simeq \Omega \Delta T_0 k \qquad \Omega \ll 1 \qquad [A7.3]$$

Therefore, the solutal supersaturation, Ω, can be defined as the ratio of two temperature differences

$$\Omega = \frac{\Delta T_c}{\Delta T_0 k} \qquad [A7.4]$$

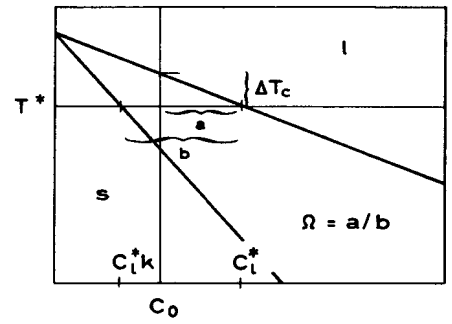

Figure A7.2:

Similarly, the thermal supersaturation, Ω_t, can be defined as the ratio of the thermal undercooling to the unit undercooling ($-\Delta h_f/c$)

$$\Omega_t = \frac{\Delta T_t}{-\Delta h_f/c} \qquad [A7.5]$$

from which is obtained an equation which is analogous to equation A7.3

$$\Delta T_t = \Omega_t \frac{-\Delta h_f}{c} \qquad [A7.6]$$

Hemispherical Needle Approximation

A cylinder with a hemispherical tip, growing along its axis, is the simplest approximation which can be made to the problem of dendrite tip growth [1]. Nevertheless, it permits a rapid comprehension of the important factors involved in dendrite growth to be obtained. The cross-section of the cylinder, $A = \pi R^2$, determines the volume which grows in the time, dt, and which is responsible for the rejection of solute (figure A7.3a). The surface area of the hemispherical cap, $A_h = 2\pi R^2$, determines the amount of radial solute diffusion. Thus, a flux due to solute rejection, J_1, and one due to diffusion in the liquid ahead of the tip, J_2, can be identified:

$$J_1 = AV(C_l^* - C_s^*) \qquad [A7.7]$$

$$J_2 = -DA_h\left(\frac{dC}{dr}\right)_{r=R} \qquad [A7.8]$$

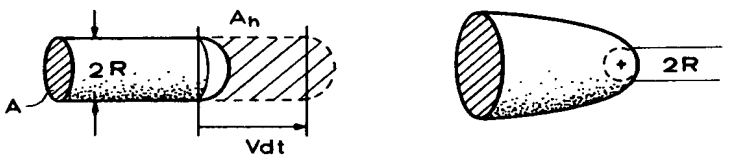

a b

Figure A7.3:

Under steady-state conditions, both of the fluxes must be equal, leading to the relationship:

$$VC_l^*(1 - k) = -2D(\frac{dC}{dr})_R \qquad [A7.9]$$

The concentration gradient at the tip can be approximated by the value which is found for a growing sphere (equation A2.24):

$$(\frac{dC}{dr})_R = - \frac{C_l^* - C_o}{R}$$

Therefore, the diffusion equation reduces to:

$$\frac{VR}{2D} = \frac{C_l^* - C_o}{C_l^*(1 - k)} \qquad [A7.10]$$

which is generally written in the abbreviated form:

$$P_c = \Omega \qquad [A7.11]$$

Here, P_c (= RV/2D) is the solute Péclet number (the ratio of a characteristic dimension, R, of the system to the solute boundary layer thickness at a planar interface). In figure 4.9, this expression is represented by the straight line which runs from the upper left to the lower right.
In the case of thermal diffusion-limited dendrites, a similar flux balance to that above can be made and leads to the same relationship as that of equation A7.11, where the solute Péclet number is replaced by a thermal Péclet number:

$$P_t = \frac{RV}{2a} \qquad [A7.12]$$

and the solute supersaturation is replaced by the thermal supersaturation, as defined by equation A7.5. Therefore, the thermal case is defined by

$$P_t = \Omega_t \qquad [A7.13]$$

Paraboloid of Revolution

As proposed originally by Papapetrou [2], a much better approximate form for the dendrite tip is a paraboloid of revolution (figure A7.3b). Ivantsov [3] was the first to develop a mathematical analysis based on that shape, although it has since been generalised by Horvay and Cahn [4]. They found that, for a needle crystal corresponding to a paraboloid of revolution:

$$I(P) = \Omega \qquad [A7.14]$$

where the Ivantsov function (a function of P) is given by:

$$I(P) = Pexp[P]E_1[P] \qquad [A7.15]$$

and E_1 is the exponential integral function, defined by:

$$E_1(P) = \int_P^{\infty} \frac{\exp(-z)}{z} dz = -Ei(-P) \qquad [A7.16]$$

Its value (figure A1.2) can be determined from the series [5]:

$$E_1(P) = -0.5772157 - \ln(P) - \sum_{n=1}^{\infty} \frac{(-1)^n p^n}{n.n!} \qquad [A7.17]$$

The Ivantsov function, I[P], can also be written as a continued fraction:

$$I[P] = \cfrac{P}{P + \cfrac{1}{1 + \cfrac{1}{P + \cfrac{2}{1 + \cfrac{2}{P + \cfrac{}{\ddots + \cfrac{n}{1 + \cfrac{n}{P + \ddots}}}}}}}} \qquad [A7.18]$$

From the above, it can be seen that truncating the fraction at the zeroth, first, and higher terms will lead to various approximations:

$$I_o = P$$

$$I_1 = \frac{P}{P + 1}$$

$$I_2 = \frac{2P}{2P + 1}$$

$$I_\infty = I(P) = Pexp(P)E_1(P)$$

These approximations are shown graphically in figure A7.4.
Substituting the zeroth approximation into equation A7.14 gives the solution which was obtained for the case of a hemispherical tip (equation A7.11). Furthermore, it is interesting to note that the modification of Zener's analysis made by Hillert [6] for high supersaturations leads to:

$$\frac{VR}{D} = \frac{C_i^* - C_o}{C_o - C_s^*}$$

which is equivalent to $2P = \Omega/(1 - \Omega)$ or $\Omega = 2P/(2P+1)$. This is the second approximation arising from the continued fraction representation when substituted into equation A7.14. The paraboloid of revolution, for which the solution is given by equation A7.15 or A7.18 with n equal to infinity, represents an isothermal dendrite, and closely approximates the real, observed form.
From figure A7.4 it can be seen that I_1 is a much better approximation than is I_o because the latter cannot be used when P is greater than unity. As the series (equation A7.18) converges very slowly, it is usually preferable to use the Ivantsov solution (equation A7.15). More exact, non-isothermal, solutions have been given by Trivedi [7].
Finally, the most recent analytical technique [8] to be used to study dendrite morphology is one in which an equation is derived which describes the movement of an element of the solid/liquid interface. This movement is supposed to be essentially independent of the long-range diffusion and thermal fields, and the evolution of the dendritic form can be computed relatively easily.

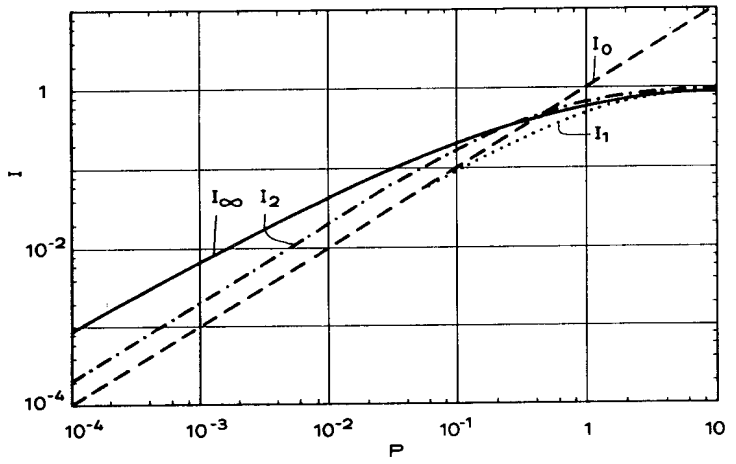

Figure A7.4:

REFERENCES

[1] J.C.Fisher, referred to by B.Chalmers in 'Principles of Solidification', Wiley, New York, 1966, p105

[2] A.Papapetrou: Zeitschrift für Kristallographie, 92, (1935) 89

[3] G.P.Ivantsov: Doklady Akademii Nauk SSSR, 58, (1947) 567

[4] G.Horvay, J.W.Cahn: Acta Metallurgica, 9, (1961) 695

[5] M.Abramowitz, I.A.Stegun (Editors): Handbook of Mathematical Functions, Dover, New York, 1965

[6] M.Hillert: Jernkontorets Annaler, 141 (1957) 757, and Metallurgical Transactions, 6A, (1975) 5

[7] R.Trivedi: Acta Metallurgica, 18 (1970) 287, and Metallurgical Transactions, 1 (1970) 921

[8] E.Ben-Jacob, N.Goldenfeld, J.S.Langer, G.Schön: Physical Review A, 29 (1984) 330

APPENDIX 8

DENDRITE TIP RADIUS AND SPACING

Growth at the Extremum

The relationships defining solutal (or thermal) diffusion at the hemispherical tip of a needle-like crystal (appendix 7):

$$P = \Omega \qquad [A8.1]$$

or for a paraboloid of revolution

$$I[P] = \Omega \qquad [A8.2]$$

do not specify an unique functional dependence between the tip radius and growth conditions (supersaturation, undercooling). They only relate the product, RV, to the supersaturation as shown in figure 4.9. Therefore, another equation relating the variables is required. For many years, this was done by adding a capillarity term to the diffusion equation and determining the extremum of the corresponding equation. This approach will be illustrated by means of the simple solution to equation A8.1:

$$\Omega = P + \frac{2s}{R} \qquad [A8.3]$$

where s is the capillarity length (for the solutal case at low Ω-values, $s_c = \Gamma/\Delta T_0 k$, and for the thermal case, $s_t = -\Gamma c/\Delta h_f$). In figure A8.1, relationships such as equation A8.3 for various models are presented, in terms of dimensionless variables, for free thermal dendrite growth and for a constant undercooling, $\Delta T_t = -0.05\Delta h_f/c$ [1]. These curves indicate that the addition of a capillarity term to equation A8.1 cuts off the straight line of the diffusion solution (see also figure 4.9). The radius at which the cut-off occurs corresponds to the critical radius of nucleation. This can easily be verified by noting that this radius is the one which uses up the total supersaturation indicated by equation A8.3 to satisfy the curvature which makes V (and therefore P) equal to zero. Therefore:

$$\Omega = \frac{2s}{R^\circ} \qquad V = 0$$

where the critical radius, R°, for growth is equal to the critical radius, r°, for nucleation. Substituting ΔT for Ω from equation A7.3 or A7.6 leads to:

$$r^\circ = \frac{2s}{\Omega} = \frac{2\Gamma}{\Delta T} \qquad [A8.4]$$

Examination of equation A8.3 for the thermal or solutal case reveals that

$$\Delta T_t = \frac{RV}{2a}\left(-\frac{\Delta h_f}{c}\right) + \frac{2\Gamma}{R} \qquad [A8.5]$$

$$\Delta T_c = \frac{RV}{2D}\,\Delta T_0 k + \frac{2\Gamma}{R} \qquad [A8.6]$$

The extremum (maximum) value of V defines the radius, R_e, of figure 4.9. It is shown in chapter 5 (figure 5.7) that the maximum value of V in an isothermal environment corresponds to a minimum in ΔT for constant velocity growth. Therefore, minimising ΔT in equation A8.5 or A8.6 will give the extremum radius. This can be done by setting the first derivative of equation A8.5 or A8.6 equal to zero. This leads to

$$R_e^t = 2\sqrt{-\frac{\Gamma ac}{\Delta h_f}} \cdot \frac{1}{\sqrt{V}} \qquad [A8.7]$$

$$\Delta T_t = 2\sqrt{-\frac{\Gamma \Delta h_f}{ac}} \cdot \sqrt{V} \qquad [A8.8]$$

for thermal dendrites and to

$$R_e^c = 2\sqrt{\frac{\Gamma D}{\Delta T_0 k}} \cdot \frac{1}{\sqrt{V}} \qquad [A8.9]$$

$$\Delta T_c = 2\sqrt{-\frac{\Gamma \Delta T_0 k}{D}} \cdot \sqrt{V} \qquad [A8.10]$$

for solutal dendrites when both are growing at the extremum. Equations A8.8 and A8.10 reflect the well-known square-root-of-V relationships obtained for free dendrite growth in a constant supersaturation environment. Others can be found in the review paper by Glicksman et al [1].
Instead of using the extremum method, the recent trend has been to use stability criteria which are analogous to those used in treating the stability of a planar solid/liquid interface [2-4]. The published analyses for the dendrite case are very complicated [5,6,7]. Therefore, some simpler cases will be treated here which demonstrate the essential points of the more complete treatments.

Simple Solution of Equiaxed Dendrite Growth

Langer and Müller-Krumbhaar [3] proposed a criterion which was based on extensive numerical calculations, and the use of which gives results which are close to those found experimentally. See the points on the curve in figure A8.1 where the open circle refers to Langer and Müller-Krumbhaar's theory [3], and the closed circle is due to Glicksman [1]. This criterion supposes that the dendrite tip grows at a constant value of $\sigma \simeq 1/4\pi^2$, where the stability constant, $\sigma (\equiv \delta.s/R^2$: ratio of the product of the diffusion length, δ, and the capillarity length, s, to the square of the tip radius) is also given by the relationship, $\sigma = (\lambda_i/2\pi R)^2$. Therefore, for the dendrite tip radius it can be assumed that:

$$R = \lambda_i \qquad [A8.11]$$

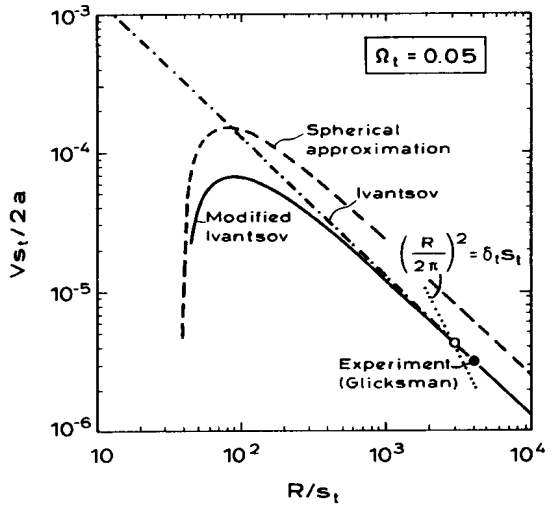

Figure A8.1:

where λ_i is the limiting wavelength for a perturbation which can grow at the solid/liquid interface. Using this value for the wavelength for a planar interface (equation 3.22) as a zeroth approximation gives:

$$\lambda_i = 2\pi\sqrt{\frac{\Gamma}{\phi}} \qquad [A8.12]$$

Thus:

$$R = 2\pi\sqrt{\frac{\Gamma}{mG_c - G}} \qquad [A8.13]$$

The concentration gradient ahead of an advancing dendrite can be found from a simple flux balance (equation A7.9):

$$G_c = -\frac{P_c C_t^* p}{R} \qquad [A8.14]$$

Evaluating C_t^* from equation A7.1 and A7.12 gives:

$$G_c = -\frac{P_c p C_o}{R[1 - pI(P_c)]} \qquad [A8.15]$$

In a similar manner, the temperature gradient is found to be:

$$G = \frac{P_t \Delta h_f}{cR} \qquad [A8.16]$$

Substituting equation A8.15 and A8.16 into equation A8.13 gives:

$$R = \frac{-4\pi^2\Gamma}{\frac{P_c m C_o p}{1 - pI(P_c)} + \frac{P_t \Delta h_f}{c}} \qquad [A8.17]$$

From this R-value (at the limit of morphological stability) one can calculate the solutal and thermal undercoolings required to drive the dendrite tip growth. Using equations A7.2 and A7.6 and the corresponding Ivantsov solutions (equation A7.12) gives:

$$\Delta T_c = mC_o[1 - \frac{1}{1 - pI(P_c)}] \qquad [A8.18]$$

$$\Delta T_t = I(P_t)(-\frac{\Delta h_f}{c})$$

Neglecting the small curvature undercooling for growth at the limit of stability (figure A8.1) and coupling the solutal and thermal fields at the interface by:

$$\Delta T = \Delta T_c + \Delta T_t \qquad [A8.19]$$

leads to:

$$\Delta T = mC_o[1 - \frac{1}{1 - pI(P_c)}] - (\frac{\Delta h_f}{c}) I(P_t) \qquad [A8.20]$$

Equations A8.20 and A8.17 determine the growth rate and tip radius of an equiaxed dendrite as a function of ΔT in pure substances ($C_o = 0$) or in alloys [8]. For a given ΔT-value, the solution of these equations reveals a maximum in V with increasing solute content in a given alloy system (figure A8.2), here succinonitrile-acetone.

Simple Solution of Constrained (Alloy) Dendrite Growth

During the directional growth of dendrites, the heat generated at the growing interface is conducted away into the solid, due to the imposed temperature gradient. Therefore, it can be assumed that the resultant behaviour (e.g. the tip undercooling) is essentially determined by the solute flux around the tip. This flux is created by the moving isotherms, thus forcing the tips to grow at a given rate into the liquid. This case has been treated by Trivedi [9], and in a similar but simpler manner, by the present authors [10]. In the case of constrained growth, G is given by the heat flux in the system, and G_c can be evaluated by equation A8.15. By doing this, one obtains a

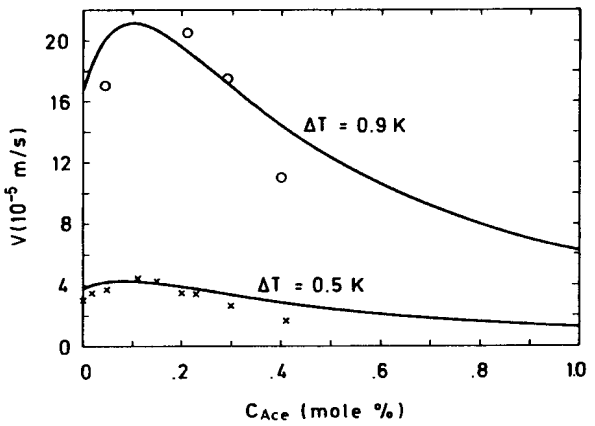

Figure A8.2:

quadratic equation which relates V and R via the Péclet number for solute diffusion ($R = 2P_cD/V$)

$$V^2\left(\frac{\pi^2\Gamma}{P_c^2D^2}\right) + V\frac{C_o m p}{2D[1 - pI(P_c)]} + G = 0 \qquad [A8.21]$$

This solution for a directionally growing dendrite of parabolic form can be simplified by using the hemispheric diffusion solution (equation 4.11). At medium growth rates, equation 4.11 can be further simplified to give equation 4.13 which can be written as:

$$V = \frac{K'}{R^2} \qquad [A8.22]$$

where the constant, K', is equal to $4\pi^2D\Gamma/(k\Delta T_o)$. In figure A8.3, these two simple solutions are compared with each other. When V is greater than V_{tr}, the tips of the dendrites are very small (the primary spacing, λ_1 is much greater than R) and equation A8.22 is a good approximation. This has been confirmed by a paper which compares the present results with those of Trivedi [11].
Note that, in deriving the R-V-G relationships, only equation A8.1 has been used and not equation A8.3. This is possible because the radius for growth at the limit of stability is much larger than the extremum radius (in good agreement with other theories and experimental data - figure A8.1).

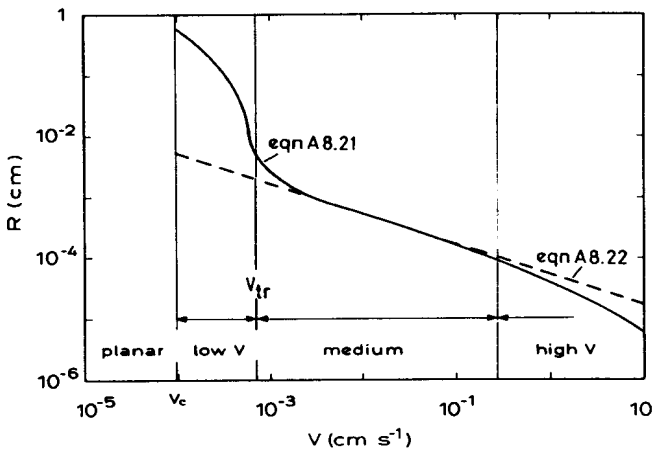

Figure A8.3:

Primary Spacing in Constrained Growth

It is assumed [10] that the shape of a fully developed dendrite, including the mean volume of its branches, can be approximated by an ellipsoid of revolution (figure 4.14). The radius of an ellipse is given by its semi-axes, a and b:

$$R = \frac{b^2}{a} \qquad [A8.23]$$

In the case of an hexagonal array, $b = \lambda_1/\sqrt{3}$ and $a = \Delta T'/G$, where $\Delta T'$ is the non-equilibrium solidification range:

$$\lambda_1 = \frac{\sqrt{3\Delta T'R}}{\sqrt{G}} \qquad [A8.24]$$

Substituting equation A8.27 into equation A8.29 and replacing, to a first approximation, $\Delta T'$ by ΔT_o gives a relationship for the primary trunk spacing:

$$\lambda_1 = 4.3\left(\frac{D\Gamma\Delta T_o}{k}\right)^{1/4}V^{-1/4}G^{-1/2} \qquad [A8.25]$$

Secondary Spacing in Constrained or Unconstrained Growth

In order to simplify the model, it is assumed that only dendrite arms of two diameters need to be considered. In reality, a distribution of arms of various thickness will exist. Following Kattamis and Flemings[12] and Feurer and Wunderlin[13], the situation illustrated in figure A8.4 will be analysed in a very approximate manner. Two arms of radius, R and r, are located in a locally isothermal melt. Since, at the interface between the solid and the liquid, local equilibrium will be established very rapidly, the concentration along the surface of the cylindrical arms will differ; the thinner arms will be in liquid of lower solute concentration. That is:

$$T' = T_f + mC_l^R - \frac{\Gamma}{R}$$

$$T' = T_f + mC_l^r - \frac{\Gamma}{r}$$

$$m(C_l^R - C_l^r) = \Gamma\left(\frac{1}{R} - \frac{1}{r}\right) \qquad [A8.26]$$

Therefore, solute will diffuse along the concentration gradient from thick to thin arms while the solvent will diffuse from the thin to the thick arms. The thin arms therefore tend to dissolve while the thicker arms tend to thicken.

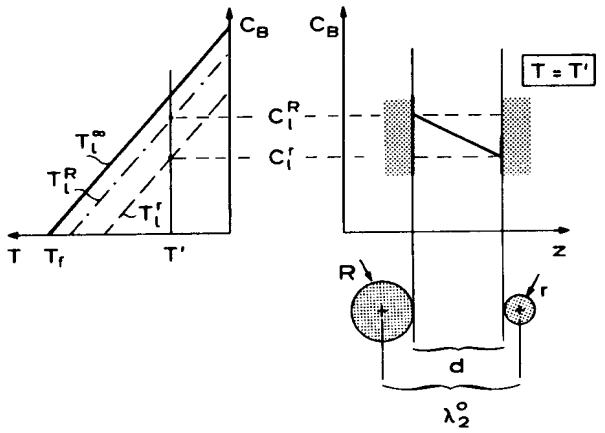

Figure A8.4:

For simplicity, it is assumed that the concentration gradient between two arms is constant and that the diffusion is unidirectional. Now, if R is assumed to be much greater than r, dR/dt can be neglected with respect to dr/dt, and the two fluxes existing between the arms are:

$$J = D\frac{C_l^R - C_l^r}{d} \qquad [A8.27]$$

$$J = -C_l^r(1 - k)\frac{dr}{dt} \qquad [A8.28]$$

Combining equations A8.26 to A8.28:

$$\frac{dr}{dt} = -\frac{\Gamma D}{mC_l^r(1 - k)d} \cdot \left(\frac{1}{R} - \frac{1}{r}\right) \qquad [A8.29]$$

For small compositional differences in the liquid between the arms, C_l^r is approximately equal to C_l, the interdendritic concentration due to segregation. It is further assumed that d is approximately equal to λ_2^o, leading to:

$$\frac{dr}{dt} = \frac{\Gamma D}{mC(1 - k)\lambda_2^o} \cdot \left(\frac{1}{r} - \frac{1}{R}\right) \qquad [A8.30]$$

where λ_2^o is the arm spacing before ripening. All of the parameters except C_l in the first bracket on the right-hand side of equation A8.30 are assumed to be constant. Furthermore, it is assumed that R/λ_2^o and r_o/R are constant and that the interdendritic liquid concentration is a linear function of time, starting with the alloy concentration, C_o, and ending (due to segregation) at the composition, C_l^m:

$$C_l = C_o + (C_l^m - C_o)\frac{t}{t_f} \qquad [A8.31]$$

where t is the time elapsed since the beginning of solidification, and t_f is the local solidification time. If $C_l^m = C_e$, t_f is approximately equal to $(T_l - T_e)/\dot{T}$. Rearranging equation A8.30 and integrating from $t = 0$ to $t = t_f$ and from $r = r_o$ to $r = 0$ gives:

$$\lambda_2^o R^2\left[\frac{r_o}{R} + \ln\left(1 - \frac{r_o}{R}\right)\right] = Mt_f \qquad [A8.32]$$

where:

$$M = \frac{-\Gamma D \ln\left(\frac{C_l^m}{C_o}\right)}{m(1 - k)(C_l^m - C_o)} \qquad [A8.33]$$

Assuming further that $R/\lambda_2^o \simeq 0.5$ and $r_o/R \simeq 0.5$ gives $Mt_f = 0.1(\lambda_2^o)^3$.

Thus, when the arms have melted, $\lambda_2 = 2\lambda_2^o$ and therefore:

$$\lambda_2 = 5.5(Mt_f)^{1/3} \qquad [A8.34]$$

Due to the extreme simplification of the ripening phenomena described, the constant factor of 5.5 in equation A8.34 should not be given too much importance. This applies to both its value and its constancy. Nevertheless, the coarsening parameter, M, has been shown to be of some use in estimating λ_2 values in Al alloys [13].

REFERENCES

[1] M.E.Glicksman, R.J.Schaeffer, J.D.Ayers: Metallurgical Transactions, 7A (1976) 1747

[2] W.Oldfield: Materials Science and Engineering, 11 (1973) 211

[3] J.S.Langer, H.Müller-Krumbhaar: Journal of Crystal Growth, 42 (1977) 11

[4] J.S.Langer: Reviews of Modern Physics, 52 (1980) 1

[5] J.S.Langer, H.Müller-Krumbhaar: Acta Metallurgica, 26 (1978) 1681 and 1689

[6] H.Müller-Krumbhaar, J.S.Langer: Acta Metallurgica, 26 (1978) 1697 and Acta Metallurgica, 29 (1981) 145

[7] J.S.Langer: Physico-Chemical Hydrodynamics, 1 (1980) 41

[8] J.Lipton, M.E.Glicksman, W.Kurz: Materials Science and Engineering, Special Issue on 'Solidification Microstructures' (1984)

[9] R.Trivedi: Journal of Crystal Growth, 49 (1980) 219

[10] W.Kurz, D.J.Fisher: Acta Metallurgica, 29 (1981) 11

[11] H.Esaka, W.Kurz: submitted to Journal of Crystal Growth, (1984)

[12] T.Z.Kattamis, M.C.Flemings: Transactions of the Metallurgical Society of AIME, 233 (1965) 992

[13] U.Feurer, R.Wunderlin: Fachbericht DGM, 1977 (see detailed reference in chapter 4)

APPENDIX 9

EUTECTIC GROWTH

This text follows the treatment of Jackson and Hunt [1], but is a simplified version of the latter paper. Figure 5.2 shows the corresponding phase diagram and interface geometry. Using symmetry arguments (appendix 2), the analysis of a solidifying lamellar eutectic interface can be reduced firstly to the consideration of a pair of lamellae. No net mass transport can occur between this pair and another pair under steady-state conditions because this would cause changes in the morphology and violate the assumption of steady-state behaviour. Thus, the concentration gradient in the y-direction is zero at the mid-point of each lamella (figure A9.1). Secondly, attention can be further restricted to half of each lamella because, again, there can be no net transport of solute in or out of this symmetry element.
The differential equation describing the solute distribution in the melt ahead of a steadily advancing interface is (A2.6):

$$\frac{\partial^2 C}{\partial y^2} + \frac{\partial^2 C}{\partial z^2} + \frac{V}{D}\frac{\partial C}{\partial z} = 0$$

and it has been shown (appendix 2) that the general solution satisfying this equation consists of products of circular and exponential functions. It is logical to associate the exponential function with the z-variation of the solution, since it is known that the boundary layer has this form for a single-phase interface. It is equally logical to associate the circular functions with the alternating pattern of eutectic phases. Thus, to a first approximation, the distribution of component B can be described by:

$$C = C_e + A\exp(-\frac{Vz}{D}) + B\exp(-bz)\cos(gy) \qquad [A9.1]$$

This tentative solution can be seen to be made up of an exponential term which reflects the planarity of the interface as a whole, and another term which reflects the alternating pattern of the two phases. The cosine function is chosen because the expression describing the gradient of the interface concentration in the y-direction must be able to take zero values at the origin of the region considered and at $\lambda/2$ (figure A9.1). Another way of regarding the choice of the function in equation A9.1 is to imagine that it reflects the interface solute distributions depicted in figure 5.3. Thus, equation A9.1 without the third term on the right-hand side could describe the solute distribution ahead of either of the single phases (figure 5.3a). The re-introduction of the third term can then be looked upon as being the expected solution when the originally single phase interface is 'perturbed' by the addition of the second phase.
It is now necessary to determine the constants, A, B, b, and g. The value of g can be immediately determined because, again due to symmetry considerations, the derivative of the solution with respect to y, $\partial C/\partial y$, must be equal to zero when $y = \lambda/2$. Thus:

$$C = C_e + A\exp(-\frac{Vz}{D}) + B\exp(-bz)\cos(\frac{2\pi y}{\lambda}) \qquad [A9.2]$$

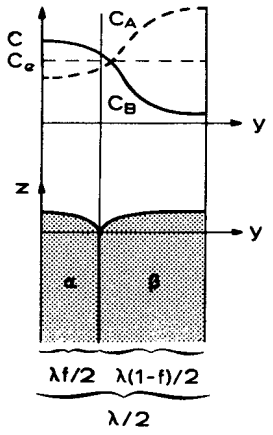

Figure A9.1:

The derivation of b has already been discussed (equations A2.10 and A2.11). It is equal to:

$$b = \frac{V}{2D} + \sqrt{(\frac{V}{2D})^2 + (\frac{2\pi}{\lambda})^2} \qquad [A9.3]$$

This relatively complicated expression can be simplified on the basis of experimental observation. Firstly, it is noted that the term, V/2D, is the inverse of the equivalent solute boundary layer of a planar interface. Its value will be relatively small, whereas $2\pi/\lambda$ is the wave number of the eutectic and will be large, due to the small values of λ which are usually encountered. Therefore:

$$\frac{4\pi^2}{\lambda^2} \gg \frac{V^2}{4D^2}$$

and equation A9.3 can be simplified to:

$$b \simeq \frac{2\pi}{\lambda}$$

by neglecting terms in V/2D. Thus, equation A9.2 can now be written:

$$C = C_e + A\exp(-\frac{Vz}{D}) + B\exp(-\frac{2\pi z}{\lambda})\cos(\frac{2\pi y}{\lambda}) \qquad [A9.4]$$

The values of the constants, A, B, can be found by forcing the above solution to satisfy the flux condition at the interface. The fluxes can be deduced from the phase diagram. The general flux boundary condition is:

$$V(k - 1)C^* = D(\frac{\partial C}{\partial z})_{z=0} \qquad [A9.5]$$

but, because the variation of the interface concentration, with respect to C_e, is relatively small in most cases, it can be supposed that $C^* \simeq C_e$.
Thus, the flux conditions for the two eutectic phases can be written:

$$\text{alpha-phase: } V(k_\alpha - 1)C_e = D(\frac{\partial C}{\partial z})_{z=0} \qquad [A9.6]$$

$$\text{beta-phase: } -V(k_\beta - 1)(100 - C_e) = D(\frac{\partial C}{\partial z})_{z=0} \qquad [A9.7]$$

The negative sign in the case of the beta-phase appears because the interface gradient of C_B in the growth direction is expected to be positive. The concentration gradient at the solid/liquid interface can be found from equation A9.4:

$$(\frac{\partial C}{\partial z})_{z=0} = -\frac{V}{D}A - \frac{2\pi}{\lambda}B\cos(\frac{2\pi y}{\lambda}) \qquad [A9.8]$$

The alpha-phase extends from the origin to the point, $f\lambda/2$, where f is the volume fraction of the alpha-phase.
Using the method of 'weighted residuals' (appendix 2), the values of A and B (the 'weights') can be found by satisfying the flux boundary conditions, equations A9.6 and A9.7, in an average fashion over the alpha and beta interfaces, i.e.:

$$\int_0^{f\lambda/2} V(k_\alpha - 1)C_e dy = \int_0^{f\lambda/2} D(\frac{\partial C}{\partial z})_{z=0}\, dy \qquad [A9.9]$$

$$-\int_{f\lambda/2}^{\lambda/2} V(k_\beta - 1)(100 - C_e)dy = \int_{f\lambda/2}^{\lambda/2} D(\frac{\partial C}{\partial z})_{z=0}\, dy \qquad [A9.10]$$

Inserting the value of $(\partial C/\partial z)_{z=0}$ from equation A9.8, and carrying out the integrations yields the simultaneous algebraic equations:

$$fV\lambda A + 2D\sin(\pi f)B = (1 - k_\alpha)C_e f V\lambda \qquad [A9.11]$$

$$(1 - f)V\lambda A - 2D\sin(\pi f)B = (k_\beta - 1)(100 - C_e)(1 - f)V\lambda \qquad [A9.12]$$

and the values of A and B are easily found to be:

$$A = fC' - C^\beta \qquad [A9.13]$$

$$B = \frac{f(1 - f)V\lambda C'}{2D\sin(\pi f)} \qquad [A9.14]$$

Note that A will be very small in general, and will be equal to zero if the phases have the same density. Here, C' is the difference in composition between the ends of the eutectic tie-line and C^{β} is the difference in composition between the eutectic and the maximum solid solubility in the β-phase (figure A9.2).
Thus, a solution has been obtained which satisfies most of the boundary conditions. The final condition to be satified is the coupling condition, which relates the local melting point to the imposed temperature distribution. This has already been depicted in a qualitative fashion in figure 5.5. If account were to be taken of the detailed shape of the eutectic interface, the problem would rapidly become insoluble because of the need to satisfy the coupling condition at each point(§). Instead, the eutectic interface is assumed to be perfectly planar, in order to make a solution possible, and the quantities involved are treated in an average fashion. The satisfaction of the coupling condition can then be achieved in three steps. These involve calculating the average solute undercooling and the average curvature undercooling for each phase, and then making the two total undercoolings equal. The average concentration differences of the liquid, $\overline{\Delta C} = \overline{C} - C_e$, at the alpha- and beta-phase interfaces, relative to the eutectic composition will first be found. From equation A9.4, they can be shown to be, for z = 0:

$$\overline{\Delta C}_{\alpha} = \frac{2}{f\lambda}\int_{0}^{f\lambda/2} [A + B\cos(\frac{2\pi y}{\lambda})]\, dy$$

$$\overline{\Delta C}_{\beta} = \frac{2}{(1-f)\lambda}\int_{f\lambda/2}^{\lambda/2} [A + B\cos(\frac{2\pi y}{\lambda})]\, dy$$

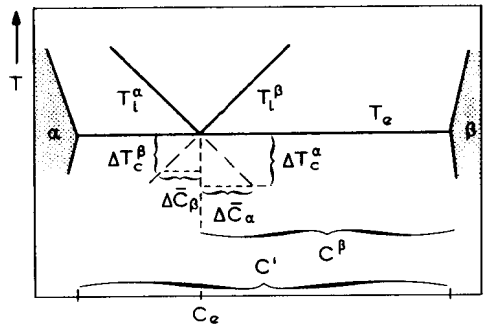

Figure A9.2:

§ Series et al[2] have solved this mathematically intractable problem by using a hybrid method in which an electrical analogue was used to provide a basis for further calculations.

giving:

$$\overline{\Delta C}_{\alpha} = A + B\,\frac{\sin(\pi f)}{\pi f} \qquad [A9.15]$$

$$\overline{\Delta C}_{\beta} = A - B\frac{\sin(\pi f)}{\pi(1-f)} \qquad [A9.16]$$

Since A is usually negligible, it can be seen that the average concentration difference in component B at the α-phase interface is positive, while that at the β-phase is negative. The mean solute undercoolings, ΔT^c, with respect to the eutectic temperature (figure 5.5), can be found by multiplying the above concentration differences by the relevant liquidus slopes, m_{α} (<0) and m_{β} (>0). The solute undercoolings are therefore:

$$\Delta T_c^{\alpha} = -m_{\alpha}[A + B\,\frac{\sin(\pi f)}{\pi f}] \qquad [A9.17]$$

$$\Delta T_c^{\beta} = -m_{\beta}[A - B\,\frac{\sin(\pi f)}{\pi(1-f)}] \qquad [A9.18]$$

The second source of undercooling to be considered is the average undercooling due to the curvature of the interface. First note that the average curvature of a line between two points which are a distance, L, apart can be found by integrating the general expression for the curvature (appendix 3),

$$K = \frac{z''}{(1+z'^2)3/2} \qquad [A9.19]$$

between the two points. Thus:

$$\overline{K} = \frac{1}{L}\int_{0}^{L} \frac{z''}{(1+z'^2)3/2}\, dy$$

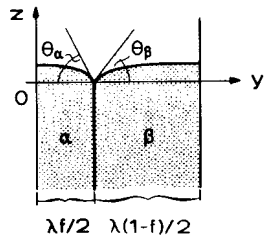

Figure A9.3:

Making the successive substitutions, $Z = z'$ and $\tan(\theta) = Z$ (figure A9.3) leads to:

$$\overline{K} = \frac{1}{L}\,[\sin(\theta)]_0^L$$

Again using the above identities leads to:

$$\overline{K} = \frac{1}{L}\sin[\arctan(z')]_0^L \qquad [A9.20]$$

The form of the eutectic interface is assumed to be as shown in figure A9.3. Thus, the average curvature of the beta-phase can be found by substituting the slopes at $y = f\lambda/2$ and $\lambda/2$ into equation A9.20:

$$\overline{K}_\alpha = -\frac{2\sin(\theta_\alpha)}{f\lambda}$$

$$\overline{K}_\beta = -\frac{2\sin(\theta_\beta)}{(1-f)\lambda}$$

Here, the curvature has been defined to be positive if the solid projects into the melt. Mathematically speaking, it is negative. The curvature is defined in this way so as to give a positive undercooling (for a solid projection) when combined with the (positive) Gibbs-Thomson coefficient. Therefore, using the associated Gibbs-Thomson coefficients, the curvature undercoolings become:

$$\Delta T_r^\alpha = \frac{2\Gamma_\alpha \sin(\theta_\alpha)}{f\lambda} \qquad [A9.21]$$

$$\Delta T_r^\beta = \frac{2\Gamma_\beta \sin(\theta_\beta)}{(1-f)\lambda} \qquad [A9.22]$$

Combining equations A9.17 or A9.18 with equations A9.21 or A9.22 gives the total undercooling of the two phases:

$$\Delta T_\alpha = -m_\alpha\left[A + B\,\frac{\sin(\pi f)}{\pi f}\right] + \frac{2\Gamma_\alpha \sin(\theta_\alpha)}{f\lambda} \qquad [A9.23]$$

$$\Delta T_\beta = -m_\beta\left[A - B\,\frac{\sin(\pi f)}{\pi(1-f)}\right] + \frac{2\Gamma_\beta \sin(\theta_\beta)}{(1-f)\lambda} \qquad [A9.24]$$

Multiplying equation A9.23 by m_β and equation A9.24 by m_α, and subtracting one from the other gives:

$$m_\beta \Delta T_\alpha - m_\alpha \Delta T_\beta = -m_\alpha m_\beta B\,\frac{\sin(\pi f)}{\pi f(1-f)} + \frac{2m_\beta \Gamma_\alpha \sin(\theta_\alpha)}{f\lambda} - \frac{2m_\alpha \Gamma_\beta \sin(\theta_\beta)}{(1-f)\lambda}$$

However, use of the coupling condition (appendix 2) requires that the alpha- and

beta-interfaces should lie on the same isotherm. Due to the very small distances between the phases (typically of the order of a few microns) and their high thermal conductivities, no substantial temperature difference can exist between the α and β phases. Therefore, $\Delta T_\alpha = \Delta T_\beta = \Delta T$ (figure 5.5):

$$\Delta T = -\frac{m_\alpha m_\beta}{m_\beta - m_\alpha} B\,\frac{\sin(\pi f)}{\pi f(1-f)} + \frac{2m_\beta \Gamma_\alpha \sin(\theta_\alpha)}{f(m_\beta - m_\alpha)\lambda} - \frac{2m_\alpha \Gamma_\beta \sin(\theta_\beta)}{(1-f)\lambda(m_\beta - m_\alpha)}$$

Substituting for B from equation 9.14 gives:

$$\Delta T = -\frac{m_\alpha m_\beta}{m_\beta - m_\alpha} V\,\frac{C'}{2\pi D} + \frac{2(1-f)m_\beta \Gamma_\alpha \sin(\theta_\alpha) - 2f m_\alpha \Gamma_\beta \sin(\theta_\beta)}{f(1-f)\lambda(m_\beta - m_\alpha)} \qquad [A9.25]$$

This can be written (see also equation 5.8):

$$\Delta T = K_c V\lambda + \frac{K_r}{\lambda} \qquad [A9.26]$$

where the physical constants of the alloy are:

$$K_c = -\frac{m_\beta m_\alpha}{m_\beta - m_\alpha} \cdot \frac{C'}{2\pi D} \qquad [A9.27]$$

and

$$K_r = \frac{2(1-f)m_\beta \Gamma_\alpha \sin(\theta_\alpha) - 2f m_\alpha \Gamma_\beta \sin(\theta_\beta)}{f(1-f)(m_\beta - m_\alpha)} \qquad [A9.28]$$

Assuming that the λ-value chosen by the eutectic is the one which makes ΔT a minimum, i.e.:

$$\frac{d(\Delta T)}{d\lambda} = K_c V - \frac{K_r}{\lambda^2} = 0$$

it is found that:

$$\lambda^2 V = \frac{K_r}{K_c} = \frac{4\pi D}{f(1-f)} \cdot \frac{f m_\alpha \Gamma_\beta \sin(\theta_\beta) - (1-f)m_\beta \Gamma_\alpha \sin(\theta_\alpha)}{m_\alpha m_\beta C'} \qquad [A9.29]$$

This equation implies that the eutectic spacings will be larger when a small volume fraction, f, of one of the phases is present (although the growth form will probably be fibrous rather than lamellar in this case; chapter 5). The spacings will also be larger when the concentration difference, C', is small. Both of these effects have been observed experimentally.

It is left as an exercise for the reader to develop the other relationships which govern eutectic growth (equations 5.11 and 5.12). Note that the functional relationship between ΔT and V (equation 5.11) is analogous to the dendrite growth equation at the extremum (equations A8.8 or A8.10).

Finally, it will be useful to compare the approximate solution above with the more exact derivation performed by Jackson and Hunt [1]. Writing their expression for $\lambda^2 V$ in terms of the nomenclature used in this book gives:

$$\lambda^2 V = \frac{2D}{P'} \cdot \frac{f m_\alpha \Gamma_\beta \sin(\theta_\beta) - (1-f) m_\beta \Gamma_\alpha \sin(\theta_\alpha)}{m_\alpha m_\beta C'} \qquad [A9.30]$$

where $P' = \sum(1/n^3\pi^3)\sin^2(n\pi f)$ (§).
Equations A9.29 and A9.30 differ only with respect to the first multiplying term on the right-hand side. If the complicated expression, P' (equation A9.30), is compared with the equivalent expression, $f(1-f)/2\pi$, the agreement is found to be quite reasonable (table A9.1) in view of the comparative simplicity of the derivation. As one would expect from the symmetrical form of the approximate solution used, the accuracy is greatest for f-values of about 0.5.

TABLE A9.1: COMPARISON OF TERMS APPEARING IN THE JACKSON-HUNT (JH) AND PRESENT ANALYSES

f	$P' = \sum_1^\infty(1/n^3\pi^3)\sin^2(n\pi f)$ (JH)	$(f-f^2)/2\pi$	Error(%)
0	0	0	0
0.1	0.00626	0.01432	129
0.2	0.01633	0.02546	56
0.3	0.02553	0.03342	31
0.4	0.03174	0.03820	20
0.5	0.03392	0.03820	17

the results for higher f-values are symmetrical about f = 0.5

REFERENCES

[1] K.A.Jackson, J.D.Hunt: Transactions of the Metallurgical Society of AIME, 236 (1966) 1129

[2] R.W.Series, J.D.Hunt, K.A.Jackson: Journal of Crystal Growth, 40 (1977) 221

[3] J.N.Clark, J.T.Edwards, R.Elliott: Metallurgical Transactions, 6A (1975) 232

§ A table of values of this function can be found in reference 3. Note that the form of P' can be deduced immediately by using equation A2.29. This is possible because equations A9.6 and A9.7 define a step function with a 'jump' (at $f\lambda/2$) which has a height equal to the sum of the gradients. These parameters of the jump merely have to be inserted into equation A2.29 in order to give the required series.

APPENDIX 10

TRANSIENTS IN SOLUTE DIFFUSION

Initial Transient

As shown previously (chapter 3), the build-up of solute ahead of a planar solid/liquid interface takes some time - the time required for the saturation of the diffusion boundary layer. It is assumed, to a first approximation, that this process is rapid enough to ensure the existence of a quasi-steady-state solute distribution. In this case, the concentration decreases exponentially from the interface into the liquid, and the equivalent boundary layer is always of the same thickness (appendix 2):

$$\delta_c = \frac{2D}{V}$$

Assuming that the growth rate, V, increases instantaneously to a constant value at the start of solidification, the flux at an interface of unit area, due to the differing solubilities of the solute in the two phases will be:

$$J_1 = VC^*(1-k) \qquad [A10.1]$$

Initially, this flux is greater than the flux created by the concentration gradient in the liquid:

$$J_2 = -DG_c \qquad [A10.2]$$

The difference between the two fluxes will be used to 'fill' the diffusion boundary layer, of thickness δ_c, to a mean concentration, $\bar{C}_l$:

$$J_1 - J_2 = \frac{d\bar{C}_l}{dt}\,\delta_c \qquad [A10.3]$$

Recalling that a steady-state profile is assumed to exist, the concentration gradient at the solid/liquid interface is given directly by the first derivative (at $z=0$) of equation 3.2, with ΔC_o in this transient state being replaced by $\Delta C = (C_l^* - C_o)$ (figure A10.1):

$$G_c = (C_o - C_l^*)\frac{V}{D} \qquad [A10.4]$$

Therefore, for unit area:

$$J_2 = (C_l^* - C_o)V$$

and

$$\frac{2D}{V}\,\frac{d\bar{C}_l}{dt} = V(C_o - kC_l^*) \qquad [A10.5]$$

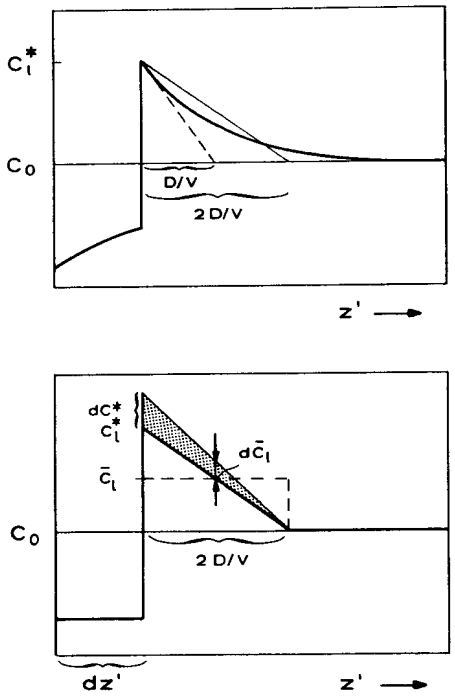

Figure A10.1:

Noting that, for the triangular equivalent boundary layer, the variation in the mean concentration is related to the variation in interface concentration, e.g.:

$$d\bar{C}_i = \frac{dC_i^*}{2}$$

with $V = dz'/dt$:

$$\frac{dC_i^*}{C_o - kC_i^*} = \frac{V}{D}\,dz \qquad [A10.6]$$

Integrating:

$$\int_{C_o}^{C_i^*} \frac{dC_i^*}{C_o - kC_i^*} = \frac{V}{D}\int_0^{z'} dz$$

gives:

$$\ln\left[\frac{C_o(1-k)}{C_o - kC_i^*}\right]^{1/k} = \frac{Vz'}{D}$$

or

$$C_i^* = \frac{C_o}{k}\left[1 - (1-k)\exp\left(-\frac{kz'V}{D}\right)\right] \qquad [A10.7]$$

Figure 6.2 illustrates the behaviour of this expression. It is a good approximation to the exact solution derived by Smith et al [1].

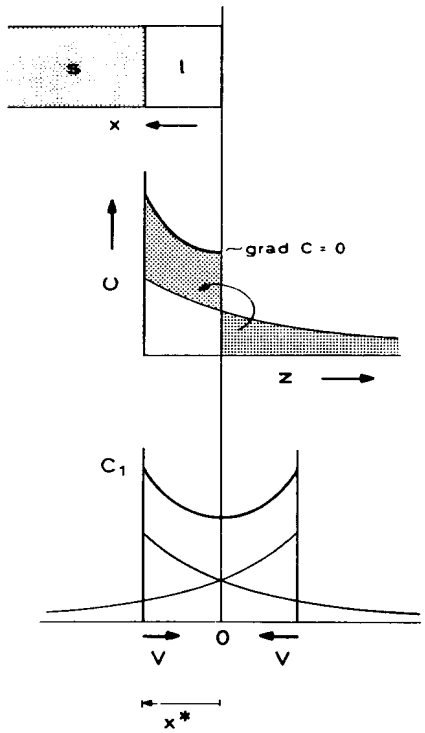

Figure A10.2:

Final Transient

While the initial transient is required to build up a boundary layer, the final transient is the result of the 'collision' of the boundary layer with the end of the specimen (figure A10.2). This problem has been solved by Smith, Tiller, and Rutter [1] in the following way for the special case where the system has reached the steady-state. The origin of the z-axis is placed at the end of the specimen and the diffusion equation becomes, in terms of the new x-coordinate (which does not move with the solid/liquid interface):

$$\frac{d^2C_l}{dx^2} = \frac{1}{D}\frac{dC_l}{dt} \qquad [A10.8]$$

The boundary conditions apply for all values of t. At x = 0 (the end of the specimen) the diffusion flux must be equal to zero and:

$$\frac{dC_l}{dx} = 0 \qquad [A10.9]$$

and at the solid/liquid interface, $x = x^*$:

$$\frac{dC_l}{dx} = \frac{V}{D}C_l^*p \qquad [A10.10]$$

where x^* is the length of the liquid zone.
In order to meet the first boundary condition, an imaginary source placed in a symmetrical position with respect to the real solid/liquid interface is introduced. This is equivalent to a localisation of the mass flux at the end of the specimen (figure A10.2). The steady-state distributions at the two interfaces in an infinite specimen are:

$$C_l = C_o(1 + \frac{p}{k})\exp[-\frac{V(x^* \pm x)}{D}] \qquad [A10.11]$$

where $z = x^* \pm x$. In order to cope with the second boundary condition (equation A10.10) when the sources are close enough to interact, further sources (interfaces) are introduced at distances, nx^*, where n is an integer (figure A10.3). These sources travel at speeds which are ntimes the speed of the real interface. This superposition permits the calculation of the necessary coefficients by constraining the interface to obey the flux balance (equation A10.10):

$$\frac{C_l}{C_o} = 1 + \sum_{n=1}^{\infty} C_n \left\{ \exp[-n\frac{V}{D}(nx^* - x)] + \exp[-n\frac{V}{D}(nx^* + x)] \right\} \qquad [A10.12]$$

This procedure is given in more detail in the original reference and leads to:

$$C_s(x) = 1 + 3\frac{1-k}{1+k}\exp(-\frac{2Vx}{D}) + 5\frac{(1-k)(2-k)}{(1+k)(2+k)}\exp(-\frac{6Vx}{D}) + \ldots$$

$$\ldots + (2n+1)\frac{(1-k)(2-k)\ldots(n-k)}{(1+k)(2+k)\ldots(n+k)}\exp[-\frac{n(n+1)Vx}{D}] \qquad [A10.13]$$

The above equation describes the final transient in the solid for the case where a steady-state solute pile-up has been reached at the solid/liquid interface.

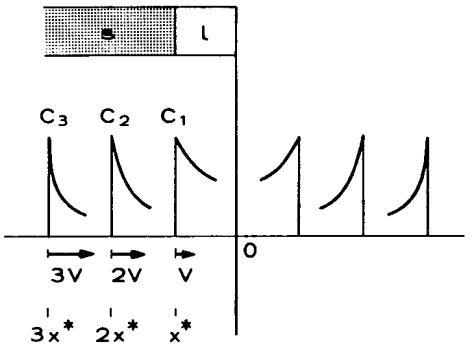

Figure A10.3:

REFERENCES

[1] V.G.Smith, W.A.Tiller, J.W.Rutter: Canadian Journal of Physics, 33 (1955) 723

APPENDIX 11

MASS BALANCE EQUATIONS

The different solubilities of a solute in the liquid and solid phases, together with the differences in mobility, lead to concentration variations known as segregation. Provided that the mass transport in the liquid is infinitely rapid (no concentration gradient in the liquid) the corresponding functions can easily be derived from a mass balance (where C is expressed in per cent):

$$f_S C_S + f_l C_l = 100$$
$$d(f_S C_S) + d(f_l C_l) = 0 \qquad [A11.1]$$

These equations state that all of the solute which cannot be incorporated into the solid must enter the liquid. No account is taken here of all of the other possible reactions which might occur in a practical situation. For instance, solute vaporisation or crucible reaction.

Lever Rule

The simplest case to which a mass balance can be applied is the case of equilibrium solidification (no concentration gradient in the solid or liquid). This can be expressed by the relations:

$$D_l \gg D_S \gg LV \qquad [A11.2]$$

Since L is the length of the solidifying system (figure A11.1), equation A11.2 states that the diffusion boundary layer, $\delta_c = 2D/V$, is much larger than the maximum distance, L, over which either solid or liquid state diffusion can occur. Similarly, it can be supposed that, if the growth rate, V, of the solid is constant and equal to L/t_f, the length of the specimen must be less than the characteristic diffusion length:

$$L \ll \sqrt{D_S t_f} \qquad [A11.3]$$

Under these conditions:

$$\frac{\partial C_l}{\partial z'} = \frac{\partial C_S}{\partial z'} \simeq 0$$

Taking the differential form of equation A11.1, $C_S = kC_l$, $dC_S = kdC_l$, $f_S = 1-f_l$, and $df_S = -df_l$ can be substituted and integrations performed:

$$\int_{C_o}^{C_l} \frac{dC_l}{pC_l} = \int_0^{f_S} \frac{df_S}{1 - f_S p}$$

giving:

$$\frac{C_l}{C_o} = \frac{1}{1 - pf_S} \qquad [A11.4]$$

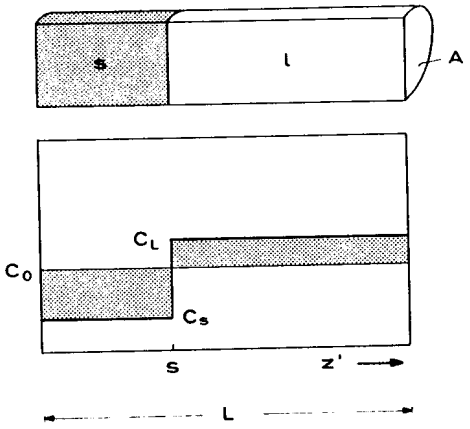

Figure A11.1:

Non-Equilibrium Solidification with Back-Diffusion and Rapid Mixing in the Liquid

The case of a bar having a constant cross-section, A, and a zero concentration gradient, due to rapid mass transport in the liquid ($C_l = C_l^*$) and limited diffusion in the solid, is shown in figure 6.3. For this case, Brody and Flemings [1] have developed a flux balance which, in a slightly modified form (sum of redistributed mass represented by the surfaces, $\bar{A}_1 + \bar{A}_2 + \bar{A}_3 = 0$, in figure 6.3):

$$(C_l - C_S^*)Ads = (L - s)AdC_l + dC_S^* A \frac{\delta_S}{2} \qquad [A11.5]$$

Here, $\bar{A}_3$ represents the surface of the equivalent boundary layer in the solid (appendix 2). Recognising that $f_S = s/L$, $df_S = ds/L$, $\delta_S = 2D_S/V = 2D_S dt/ds$, $C_S^* = kC_l$, and $dC_S^* = kdC_l$, then:

$$C_l(1 - k)df_S L = L(1 - f_S)dC_l + dC_l k D_S \frac{dt}{ds} \qquad [A11.6]$$

Dividing by L, and using a parabolic growth rate relationship (e.g. equation A1.13):

$$\frac{s}{L} = f_s = \sqrt{\frac{t}{t_f}} \qquad [A11.7]$$

Evaluating ds/dt, substituting the results into equation A11.6, and rearranging gives:

$$\frac{dC_l}{pC_l} = \frac{df_s}{(1 - f_s) + 2\alpha k f_s} \qquad [A11.8]$$

where α is a dimensionless solid-state back-diffusion parameter (dimensionless time = Fourier number):

$$\alpha = \frac{D_s}{L^2} t_f \qquad [A11.9]$$

(compare with equation A11.3) from which

$$\frac{1}{p}\int_{C_o}^{C_l} \frac{dC_l}{C_l} = \int_0^{f_s} \frac{df_s}{1 - f_s(1 - 2\alpha k)}$$

and integration leads to:

$$\frac{C_l}{C_o} = [1 - f_s(1 - 2\alpha k)]^{\frac{k-1}{1-2\alpha k}} \qquad [A11.10]$$

This equation is an important one because it includes the two limiting cases (for $\partial C / \partial z' = 0$):

Lever rule: (equation A11.4) when $\alpha = 0.5$

Scheil's equation: when $D_s = 0$ (no solid-state diffusion) $\alpha = 0$. That is:

$$\frac{C_l}{C_o} = f_l^{(k-1)} \qquad [A11.11]$$

It can be seen that, according to equation A11.9, the case $\alpha = 0.5$ (lever rule) does not correspond to the physical characteristics of equilibrium solidification. There, α should approach infinity (equation A11.3). Therefore, a modified back-diffusion parameter, α', has been proposed by Clyne and Kurz [2]. The basis of this calculation is that, in the original Brody-Flemings treatment at high α-values, solute was not conserved in the system. This can be easily understood with the aid of figure 6.3, where the solid diffusion boundary layer, δ_s, still has a small value. If this δ_s-value (proportional to α) becomes comparable in size to, or greater than, the solidified length, s, there is no longer any mass conservation according to equation A11.5 because the end effects are not considered. In reality, the initial specimen end ($z' = 0$) is an isolated system boundary and solute cannot leave the system at that point. In order to find a simple solution to this problem it will be considered that diffusion is semi-infinite and that the tail of the diffusion boundary

layer at z'-values less than zero (outside of the specimen) has to be taken into account.
For the purpose of the analysis, the coordinates are changed: $y = 0$ is fixed at the solid/liquid interface and only the solid concentration profile shown in figure A11.2 is considered. The end of the specimen ($z' = 0$) then corresponds to the cut-off distance on the y-axis (negative z'-axis). The total amount of solute in the boundary layer in the solid is $\bar{A}_T$. The neglected portion of the solute, due to the small cut-off distance, is $\bar{A}_E$. These can be obtained from [2]:

$$\bar{A}_T = \int_0^{\infty} C'dy = C'_o \frac{\delta_s}{2} \qquad [A11.12]$$

$$\bar{A}_E = \int_{y_i}^{\infty} C'dy = C'_o \frac{\delta_s}{2} \exp[-\frac{2y_i}{\delta_s}] \qquad [A11.13]$$

Here, it is assumed to a first approximation that the back-diffusion can be described

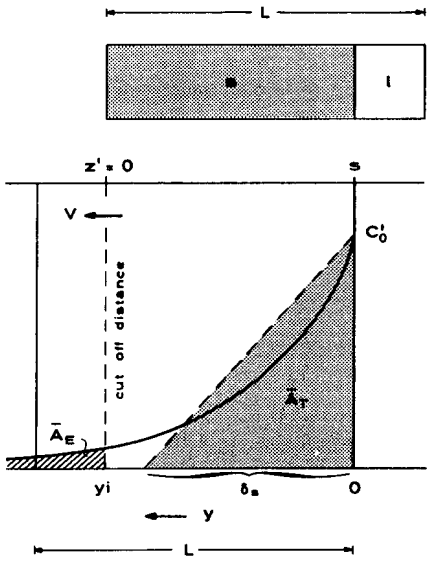

Figure A11.2:

by an exponential function. In order to estimate the correction factor necessary to cope with the cut-off effect, a parameter, Σ, is defined:

$$\Sigma(\alpha) = \frac{1}{t_f}\int_0^{t_f} \frac{A_E}{A_T}\,dt \qquad [A11.14]$$

It will be noted that even if C'_o changes during solidification, the ratio contained in the integral will be independent of such changes. For parabolic growth laws (equation A11.7):

$$y_i = L\sqrt{\frac{t}{t_f}} \qquad [A11.15]$$

Combining equations A11.12 to A11.15 gives:

$$\Sigma(\alpha) = \frac{1}{t_f}\int_0^{t_f} \exp[-\frac{2L}{\delta_s}\sqrt{\frac{t}{t_f}}]dt \qquad [A11.16]$$

Recognising that the exponential term in the integral of equation A11.16 is equal to $(-1/2\alpha)$ leads to:

$$\Sigma(\alpha) = \exp[-\frac{1}{2\alpha}] \qquad [A11.17]$$

Equation A11.17 approaches zero asymptotically at low α-values and unity at high α-values. Therefore, in the low α-range it represents the deviation from α and in the high α-range it represents the deviation from the limiting value, $\alpha' = 0.5$. A spline-like function which connects α' and α must therefore be found which satisfies the two boundary conditions: $\alpha' \to \alpha$ as $\Sigma(\alpha) \to 0$ and $\alpha' \to 0.5$ as $\Sigma(\alpha) \to 1$. An expression which has the required form (figure A11.3) is:

$$\alpha' = \alpha[1 - \exp(-\frac{1}{\alpha})] - \frac{1}{2}\exp(-\frac{1}{2\alpha}) \qquad [A11.18]$$

Substitution of α' (equation A11.18) for α in equation A11.10 permits the calculation of any solute distribution when diffusion in the liquid is very rapid. That is, it is not necessary to decide whether the lever rule or the Scheil case has to be used in a given case. This is of great importance, particularly for alloys which contain interstitial and substitutional solutes. In figure 11.3, typical values of α for P and C in delta-Fe are given. It can be seen that C obeys the lever rule and P is intermediate in behaviour.

The most important application of equation A11.10 is related to the estimation of microsegregation, i.e. the modelling of the behaviour of the mushy zone. Replacing L by the characteristic diffusion distance, $\lambda/2$ ($= \lambda_1/2$ for cells and $\lambda_2/2$ for dendrites; figures 6.6 and 6.7) leads to:

$$\alpha = \frac{4D_s t_f}{\lambda^2} \qquad [A11.19]$$

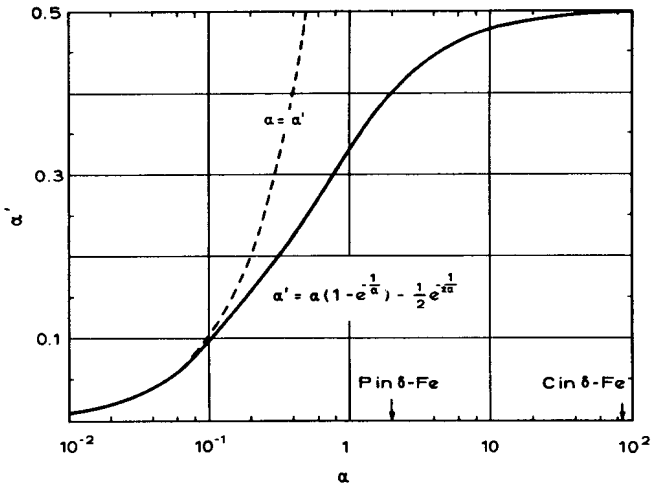

Figure A11.3:

By substituting α' from equation A11.18 into equation A11.10, the fraction solidified can be calculated:

$$f_s = \frac{1}{1 - 2\alpha' k}\left[1 - \frac{T_f - T}{T_f - T_l}\right]^{\frac{1 - 2\alpha' k}{k - 1}} \qquad [A11.20]$$

Here, T_f is the melting point of the pure element, and C has been replaced by T, via the liquidus slope. The first derivative with respect to temperature is:

$$\frac{df_s}{dT} = \frac{1}{k - 1}(T_f - T_l)^{\frac{2\alpha' k - 1}{k - 1}}\,(T_f - T)^{\frac{2 - 2\alpha' k - k}{k - 1}} \qquad [A11.21]$$

This relationship can be used in order to make numerical calculations of the solidification microstructure of cast alloys (appendix 1).

Precipitation in a Ternary System, A-B-C, in the Absence of Solid-State Diffusion

When the effect of back-diffusion is negligible, as in the case of a large volume of precipitating phase at the end of solidification, i.e. the large concentration gradients

close to $f_s = 1$ are avoided, Scheil's equation (A11.11) can be used. For two solute elements, B,C, the corresponding solute profiles (trace of interface concentration as a function of f_s) are:

$$\left(\frac{C_l}{C_o}\right)_B = f_l^{(k_B - 1)}$$
$$\left(\frac{C_l}{C_o}\right)_C = f_l^{(k_C - 1)} \qquad [A11.22]$$

When the solubility product of the phase, B_xC_y, is reached, precipitation will begin (if there is no difficulty of nucleation):

$$(C_l)_B^{\,x}(C_l)_C^{\,y} = K_{B_xC_y} \qquad [A11.23]$$

From equations A11.22 and A11.23:

$$K_{B_xC_y} = (C_o)_B^{\,x}(C_o)_C^{\,y} f_l^{(xk_B + yk_C - x - y)}$$

When precipitation begins, $f_l = f_p$, and the precipitate volume is:

$$f_P = [K_{B_xC_y}(C_o)_B^{-x}(C_o)_C^{-y}]^{\frac{1}{xk_B + yk_C - x - y}} \qquad [A11.24]$$

Solidification Path in Ternary Systems

In general, the path of solidification (trace of liquid or solid composition as a function of f_s) can be obtained in the case of solidification by relating the composition to f_l, which must be the same for all of the elements). Using equation A11.10 and A11.18:

$$\left(\frac{C_l}{C_o}\right)_B = (1 - u_B f_s)^{-\frac{p_B}{u_B}}$$
$$\left(\frac{C_l}{C_o}\right)_C = (1 - u_C f_s)^{-\frac{p_C}{u_C}} \qquad [A11.25]$$

where $u_i = 1 - 2\alpha_i' k_i$ and $p_i = 1 - k_i$. Eliminating f_s:

$$\left(\frac{C_l}{C_o}\right)_B = \left\{1 - \frac{u_B}{u_C}\left[1 - \left(\frac{C_l}{C_o}\right)_C\right]^{-\frac{u_C}{p_C}}\right\}^{-\frac{p_B}{u_B}} \qquad [A11.26]$$

Post-Solidification Homogenisation of Interdendritic Segregation

In order to determine the changes which occur during homogenisation of the cooling solid after solidification, only one dendrite arm need be considered (due to symmetry

- appendix 2). In principle, the form of the solute segregation can be described approximately by the Scheil equation (figure 11.4). Here, it will be shown that all of the possible original distributions can be related to each other by using dimensionless constants.

The changes can be treated approximately using the one-dimensional time-dependent diffusion equation:

$$D_s \frac{\partial^2 C}{\partial x^2} = \frac{\partial C}{\partial t} \qquad [A11.27]$$

It is known (appendix 2) that a likely solution to this equation involves circular and exponential functions. The exponential function is more likely to be associated with the time dependence, and a cosine or sine function is more likely to reflect the characteristics of distributions such as those in figure A11.4. In practice, of course, the solute distribution may take any form at all. However, it will be shown below that analogous changes occur in the distribution, regardless of the initial state. Thus, one can suppose that:

$$C = C_o + \delta C \exp(at)\cos(bx) \qquad [A11.28]$$

where δC is the initial amplitude of the concentration variation (figure A11.4). Substitution of the derivatives of equation 11.28 into equation 11.27 shows that:

$$a = -D_s b^2$$

therefore:

$$C = C_o + \delta C \exp(-D_s b^2 t)\cos(bx) \qquad [A11.29]$$

The value of b can be evaluated by using the boundary conditions. Thus, the gradient of the concentration at the origin must be zero at all times, t, since the origin is a point of symmetry. This can be assumed to be true even though the gradient of distributions such as those illustrated in figure A11.4 is not defined mathematically. The zero gradient condition is already satisfied by equation A11.28 at $\lambda/2$. The gradient of concentration must also be zero at λ (another point of symmetry) for all values of t. This is only true if:

$$\sin(b\lambda) = 0$$

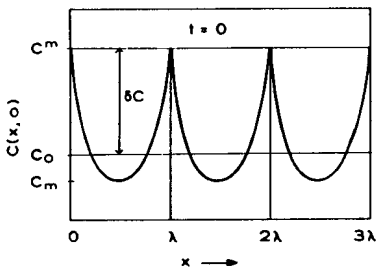

Figure A11.4:

so that:

$$b\lambda = n\pi$$

where n is an integer. The final general solution is:

$$C = C_o + \delta C \exp(-D_s \frac{n^2\pi^2}{\lambda^2} t)\cos(\frac{n\pi x}{\lambda}) \qquad [A11.30]$$

The last condition to be satisfied is that the concentration distribution at the start of homogenisation (figure A11.4) should be described by equation A11.30 (with t equal to zero). Obviously, such a distribution cannot be described by the latter expression unless the initial distribution happens to be sinusoidal. However, because the diffusion equation (A11.27) is linear, any number of similar equations (with different values of n) can be added together. This is simply the technique of Fourier analysis (appendix 2) and leads to a solution, for any initial solute distribution described by f(x), of the form:

$$C = C_o + \frac{2}{\lambda}\sum \exp(-D_s \frac{n^2\pi^2}{\lambda^2} t) \cos(\frac{n\pi x}{\lambda}) \int_o^{\lambda} f(x)\cos(\frac{n\pi x}{\lambda})dx \qquad [A11.31]$$

This solution can be used to determine the concentration distribution at any time. Recall that, using the method described in appendix 2, the result of performing the integration above can be written down immediately when the 'jumps' in the function and its derivatives are known.

Suppose that the measured distribution is parabolic (figure A11.4) with maximum, C^m, minimum, C_m, and average, C_o. There is no jump in the function at 0, λ, 2λ, ... n , but there is a jump of $-(8/\lambda)(C^m - C_m)$ in the first derivative at 0 and at λ. There is no jump in the second and higher derivatives. Thus, using equation A2.29, one can find immediately that the Fourier coefficients are given by:

$$A_n = \frac{16}{n^2\lambda^2} (C^m - C_m)$$

Use of this technique is considerably easier than integrating expressions of the type, $x^2\cos nx$. Note that when assuming an asymmetrical distribution such as the parabolic one (figure A11.4), the maximum and minimum values of the distribution are not independent. Instead, they are related by the requirement that the average concentration should be equal to the original concentration, C_o.

One can introduce the dimensionless value, I, which is defined to be the instantaneous value of the amplitude of the distribution compared with its original value, say $\delta C/(C^m - C_m)$. Another dimensionless constant, $n^2\pi^2 D_s t/\lambda^2$ (compare with equation A11.9), arises naturally in the above calculation. The value, $\lambda^2/n^2\pi^2 D_s$, is usually called the relaxation time, τ_n, of that component.

For the present purpose, the simple sinusoidal concentration variation is quite useful because, as can be seen from equation A11.30, the higher-order terms (short wavelengths) decay much more rapidly than the longer ones, and the homogenisation process will therefore ultimately be determined by the relaxation time of the lowest-order term, i.e. for $\tau_1 = \lambda^2/\pi^2 D_s$. If the initial concentration variation is given approximately by:

$$C(x,0) = C_o + \delta C\cos(\frac{\pi x}{\lambda}) \qquad [A11.32]$$

the solution for the lowest-order term is:

$$C(x,t) = C_o + \delta C\cos(\frac{\pi x}{\lambda})\exp(-\frac{t}{\tau}) \qquad [A11.33]$$

where $\tau = \tau_1$. The maximum concentration at $x = 0$, C^m, changes with time according to

$$C^m(t) = C_o + \delta C\exp(-\frac{t}{\tau}) \qquad [A11.34]$$

giving, after $t = \tau$

$$C^m(\tau) = C_o + \frac{\delta C}{e} = C_o + 0.37\,\delta C \qquad [A11.35]$$

or after $t = 3\tau$

$$C^m(3\tau) = C_o + \frac{\delta C}{e^3} = C_o + 0.05\,\delta C \qquad [A11.36]$$

It can be seen that the secondary dendrite arm spacing will have a significant effect upon the annealing time since the relaxation time is proportional to λ^2. High solidification rates, which reduce λ, will have a marked effect upon the reduction of the annealing time. For example, in order to reduce the amplitude of the concentration variation to 5% of its initial value the annealing time can be obtained by using equations A11.36 and A11.33:

$$t_{0.05} \simeq 0.3\,\frac{\lambda^2}{D_s} \qquad [A11.37]$$

Using equation A11.37, the annealing temperature required to homogenise (to less than 5% variation) an alloy with a given dendrite arm spacing within a given time can be calculated:

$$T_{0.05} = \frac{Q}{R\ln(\frac{tD_o}{0.3\,\lambda^2})} \qquad [A11.38]$$

where Q and D_o are the activation energy and pre-exponential term respectively in the Arrhenius expression for the temperature dependence of the diffusivity.

REFERENCES

[1] H.D.Brody, M.C.Flemings: Transactions of the Metallurgical Society of AIME, 236 (1966) 615

[2] T.W.Clyne, W.Kurz: Metallurgical Transactions, 12A (1981) 965

APPENDIX 12

A GUIDE TO RELEVANT PHYSICAL PROPERTIES FOR SOLIDIFICATION PROBLEMS

olumetric properties such as Δh_f have been calculated on the basis of the density at the elting point

Properties of Pure Materials at the Melting Point

roperty	Units	Al	Cu	δ-Fe (γ-Fe*)	$NC(C_2H_4)CN$**
	°C	660.4	1084.9	1536 (1526)	58.08
f	K	933.6	1358	1809 (1799)	331.23
f	J/m^3	-9.5×10^8	-1.62×10^9	-1.93×10^9	-4.6×10^7
h_f	J/m^3K	1.02×10^6	1.2×10^6	1.07×10^6	1.4×10^5
s_f	W/mK	95	166	35	0.223
$_t$	W/mK	210	244	33	0.225
$_s$	J/m^3K	2.58×10^6	3.96×10^6	5.74×10^6	2.0×10^6
t	J/m^3K	3.0×10^6	3.63×10^6	5.73×10^6	2.0×10^6
s	kg/m^3	2.39×10^3	8.0×10^3	7.0×10^3	0.988×10^3
ρ_t	kg/m^3	2.55×10^3	7.67×10^3	7.25×10^3	1.05×10^3
ρ_s	m^2/s	37×10^{-6}	42×10^{-6}	6.1×10^{-6}	0.116×10^{-6}
t	m^2/s	70×10^{-6}	67×10^{-6}	5.8×10^{-6}	0.112×10^{-6}
s	kg/mol	27×10^{-3}	63.5×10^{-3}	55.8×10^{-3}	80×10^{-3}
l	m^3/mol	11×10^{-6}	8.3×10^{-6}	7.7×10^{-6}	76×10^{-6}
s	K	368	409	336	23
m	J/m^2	93×10^{-3}	177×10^{-3}	204×10^{-3}	9×10^{-3}
$\Delta h_f/c$	mK	0.9×10^{-7}	1.5×10^{-7}	1.9×10^{-7}	0.64×10^{-7}
	m	0.24×10^{-9}	0.37×10^{-9}	0.57×10^{-9}	2.78×10^{-9}
Γ	-	6.5×10^{-2}	4.2×10^{-2}	$3.6(4.1) \times 10^{-2}$	6×10^{-2}
ΔV/V					

* metastable, ** succinonitrile

Properties of Aluminium Alloys

Property	Units	Al-Cu	Al-Cu *	Al-Si	Al-Si *
C_o	wt%	2	33.2	6	12.6
T_l	°C(K)	656 (929)	548 (821)	624 (897)	577 (850)
ΔT_o	K	32	-	240**	-
T_e	°C(K)	-	548 (821)	-	577 (850)
C_e	wt%	-	33.2	-	12.6
C'	wt%	-	46.9	-	98.2
m_α	K/wt%	-2.6	-4.6	-6	-7.5
m_β	K/wt%	-	4.8	-	17.5
k_α	-	0.14	0.17	0.13	0.13
k_β	-	-	0.71	-	2×10^{-4}
f_β	-	-	0.546	-	0.127
D_l	m^2/s	3×10^{-9}	3×10^{-9}	3×10^{-9}	3×10^{-9}
D_s	m^2/s	3×10^{-13}	-	1×10^{-12}	-
Γ_α	mK	0.9×10^{-7}	0.9×10^{-7}	0.9×10^{-7}	0.9×10^{-7}
Γ_β	mK	-	1×10^{-7}	-	2×10^{-7}
s_e	m	20×10^{-9}	-	2.9×10^{-9}	-
P'	-	-	3.35×10^{-2}	-	8.9×10^{-3}

* eutectic, ** metastable

Properties of Iron Alloys

Property	Units	δFe-C	γFe-C	γFe-C *	γFe-Ni
C_o	wt%	0.09	0.6	4.26	10
T_t	°C(K)	1531 (1804)	1490 (1763)	1155 (1428)	1503 (1776)
ΔT_o	K	36	72	-	6
T_e or T_p	°C(K)	1493 (1766 p)	1155 (1428 e)	1155 (1428 e)	-
C_e or C_p	wt%	0.53 [p]	4.26 [e]	4.26 [e]	-
C'	wt%	-	-	97.9	-
m_α	K/wt%	-81	-65	-140	-2.4
m_β	K/wt%	-	-	400	-
k_α	-	0.17	0.35	0.49	0.8
k_β	-	-	-	0.001	-
f_β	-	-	-	0.074	-
D_l	m^2/s	2×10^{-8}	2×10^{-8}	2×10^{-8}	7.5×10^{-9}
D_s	m^2/s	6×10^{-9}	1×10^{-9}	-	3×10^{-13}
Γ_α	mK	1.9×10^{-7}	1.9×10^{-7}	2×10^{-7}	2×10^{-7}
Γ_β	mK	-	-	2×10^{-7}	-
s_c	m	30×10^{-9}	7.5×10^{-9}	-	42×10^{-9}
P'	-	-	-	4×10^{-3}	-

* eutectic

INDEX